THE UNIVERSITY
OF MICHIGAN
OCT 14 1959
LIBRARY

Volume 63A

Number 2

Sept.–Oct. 1959

QC
1
.U56
Vol. 63A
No. 2

# Journal of Research

of the

NATIONAL BUREAU OF STANDARDS

## A. PHYSICS AND CHEMISTRY

Journal of Research
of the
National Bureau of Standards

A. Physics and Chemistry

SEPT.–OCT. • 1959

VOLUME • 63A

NUMBER • 2

Editor: U. Fano

Associate Editors: D. D. Wagman,
I. M. Richardson

Publication Dates:
Aug. 1, Oct. 1, Dec. 1, 1959

JOURNAL OF RESEARCH

The National Bureau of Standards Journal of Research reports research and development in the fields of activity shown at right. Also included from time to time are survey articles and compilations of information on topics closely related to the Bureau's scientific and technical program.

The Journal is published in four separate sections as follows:

**A. Physics and Chemistry**

Contains papers of interest primarily to scientists working in these fields. Issued six times a year. Annual subscriptions: domestic, $4.00; foreign, $4.75.

**B. Mathematics and Mathematical Physics**

Presents studies and compilations designed mainly for the mathematician and the theoretical physicist. Issued quarterly. Annual subscription: domestic, $2.25; foreign, $2.75.

**C. Engineering and Instrumentation**

Reports research and development results of interest chiefly to the engineer and the applied scientist. Issued quarterly. Annual subscription: domestic, $2.25; foreign, $2.75.

**D. Radio Propagation**

Reports work in radio propagation physics and upper atmospheric research. Issued six times a year. Annual subscription: domestic, $4.00; foreign, $4.75.

U.S. DEPARTMENT OF COMMERCE
Frederick H. Mueller, Secretary

NATIONAL BUREAU OF STANDARDS
A. V. Astin, Director

**Functions and Activities**

The functions of the National Bureau of Standards are set forth in the Act of Congress, March 3, 1901, as amended. These include the development and maintenance of the national standards of measurement and the provision of means and methods for making measurements consistent with these standards; the determination of physical constants and properties of materials; the development of methods and instruments for testing materials, devices, and structures; advisory services to government agencies on scientific and technical problems; invention and development of devices to serve special needs of the Government; and the development of standard practices, codes, and specifications. The work includes basic and applied research, development, engineering, instrumentation, testing, evaluation, calibration services, and various consultation and information services. The Bureau also serves as the Federal technical research center in a number of specialized fields. The scope of activities of the National Bureau of Standards is suggested in the following listing of the divisions and sections engaged in technical work.

**Washington, D.C.**

**Electricity and Electronics.** Resistance and Reactance. Electron Devices. Electrical Instruments. Magnetic Measurements. Dielectrics. Engineering Electronics. Electronic Instrumentation. Electrochemistry.

**Optics and Metrology.** Photometry and Colorimetry. Photographic Technology. Length. Engineering Metrology.

**Heat.** Temperature Physics. Thermodynamics. Cryogenic Physics. Rheology. Molecular Kinetics. Free Radicals Research.

**Atomic and Radiation Physics.** Spectroscopy. Radiometry. Mass Spectrometry. Solid State Physics. Electron Physics. Atomic Physics. Neutron Physics. Radiation Theory. Radioactivity. X-rays. High Energy Radiation. Nucleonic Instrumentation. Radiological Equipment.

**Chemistry.** Organic Coatings. Surface Chemistry. Organic Chemistry. Analytical Chemistry. Inorganic Chemistry. Electrodeposition. Molecular Structure and Properties of Gases. Physical Chemistry. Thermochemistry. Spectrochemistry. Pure Substances.

**Mechanics.** Sound. Mechanical Instruments. Fluid Mechanics. Engineering Mechanics. Mass and Scale. Capacity, Density, and Fluid Meters. Combustion Controls.

**Organic and Fibrous Materials.** Rubber. Textiles. Paper. Leather. Testing and Specifications. Polymer Structure. Plastics. Dental Research.

**Metallurgy.** Thermal Metallurgy. Chemical Metallurgy. Mechanical Metallurgy. Corrosion. Metal Physics.

**Mineral Products.** Engineering Ceramics. Glass. Refractories. Enameled Metals. Constitution and Microstructure.

**Building Technology.** Structural Engineering. Fire Protection. Air Conditioning, Heating, and Refrigeration. Floor, Roof, and Wall Coverings. Codes and Safety Standards. Heat Transfer. Concreting Materials.

**Applied Mathematics.** Numerical Analysis. Computation. Statistical Engineering. Mathematical Physics.

**Data Processing Systems.** SEAC Engineering Group. Components and Techniques. Digital Circuitry. Digital Systems. Analog Systems. Application Engineering.

• Office of Basic Instrumentation. • Office of Weights and Measures.

**Boulder, Colorado**

**Cryogenic Engineering.** Cryogenic Equipment. Cryogenic Processes. Properties of Materials. Gas Liquefaction.

**Radio Propagation Physics.** Upper Atmosphere Research. Ionospheric Research. Regular Propagation Services. Sun-Earth Relationships. VHF Research. Radio Warning Services. Airglow and Aurora. Radio Astronomy and Arctic Propagation.

**Radio Propagation Engineering.** Data Reduction Instrumentation. Modulation Research. Radio Noise. Tropospheric Measurements. Tropospheric Analysis. Propagation Obstacles Engineering. Radio-Meteorology. Lower Atmosphere Physics.

**Radio Standards.** High Frequency Electrical Standards. Radio Broadcast Service. High Frequency Impedance Standards. Electronic Calibration Center. Microwave Physics. Microwave Circuit Standards.

**Radio Communication and Systems.** Low Frequency and Very Low Frequency Research. High Frequency and Very High Frequency Research. Ultra High Frequency and Super High Frequency Research. Modulation Research. Antenna Research. Navigation Systems. Systems Analysis. Field Operations.

Order all publications from the Superintendent of Documents
U.S. Government Printing Office, Washington 25, D.C.

Use of funds for printing this publication approved by the Director of the Bureau of the Budget (June 24, 1953).

DEPOSITED BY THE
UNITED STATES OF AMERICA

Journal of Research of the National Bureau of Standards—A. Physics and Chemistry
Vol. 63A, No. 2, September–October 1959

# Reflection of Fast Neutrons from Water[1]

Martin J. Berger and John W. Cooper

(May 28, 1959)

The backscattering of fast (0.3, 1, 3, 6, 9, and 14 Mev) neutrons from a semi-infinite water medium has been calculated by the Monte Carlo method. The information obtained includes the joint angular and spectral distribution of the reflected neutrons, the dependence of the number albedo and energy albedo on the source energy and obliquity, and the contributions to the albedo of successive orders of scattering. The spectra were calculated down to epithermal energies (~0.5 ev). The results for each case are based on the analysis of 3,000 neutron histories, generated with the use of an IBM–704 computer. In the random sampling, elastic scattering from hydrogen and oxygen, inelastic scattering from oxygen, and absorption due to $n$-$\alpha$ and $n$-$p$ processes were taken into account. The cross sections for some of these interactions are not well known. Parallel calculations with different assumptions about the cross sections were made in order to estimate how sensitively the albedo depends on the cross sections. The paper includes a self-contained description of the Monte Carlo method, its application to the calculation of radiation diffusion and in particular to the neutron albedo problem. Emphasis is placed on the technique of correlated sampling which makes possible an accurate estimate of albedo differences resulting from different assumptions about the cross sections. The random sampling computations were supplemented by analytical calculations of the single-scattering albedo. This was useful for an understanding of the Monte Carlo results because a considerable fraction of the reflected neutrons return after only one collision.

## 1. Introduction

### 1.1. Statement of the Problem

Neutrons that are incident on an extended medium make one or more collisions with nuclei in each of which they are deflected and lose a fraction of their energy. Thus they perform a "random walk" until they are either absorbed or re-emerge from the medium with reduced energy. The probability that an individual neutron will eventually re-emerge from a semi-infinite medium (i.e., be reflected) is called the albedo, or the differential albedo if the energy and/or direction of the reflected neutron are specified.

The purpose of this paper is threefold: (1) To calculate the differential albedo and related quantities for neutrons incident on a semi-infinite water medium; (2) to give a self-contained exposition of the methods of calculation used (Monte Carlo, single-scattering analysis); (3) to analyze how the albedo depends on various factors, particularly the cross sections for elastic and inelastic scattering and absorption.

### 1.2. Background

Exact calculations of the neutron albedo have so far been limited to situations in which the slowing down of neutrons could be disregarded. With this limitation, and with further restrictive assumptions, Halpern, Lueneburg, and Clark [1][2] have given an analytic solution based on transport theory. A more general solution of the one-velocity problem is also available from Chandrasekhar's [2] theory of radiative transfer. Fermi [3] and more recently Grosjean [4] have given approximate solutions which are in good agreement with the more rigorous calculations.

When the complicated energy-dependence and directional dependence of the collision processes must be taken into account, an exact analytical treatment becomes all but impossible.

[1] Supported jointly by Armed Forces Special Weapons Project, OCDM, and the Department of the Navy (Bureau of Yards and Docks).
[2] Figures in brackets indicate the literature references at the end of this paper.

Spinney [5] has given an approximate treatment based on age theory which is applicable mainly to energies lower than those considered in the present work.[3] Another possible approach would be to incorporate the exact one-velocity treatment of reference [2] into an energy-group scheme similar to the multigroup diffusion schemes used in reactor calculations. This has not been attempted so far.

The Monte Carlo method recommends itself as the simplest and most promising approach. It has the advantage that the complexity of the calculations is not essentially increased by adding to the number of variables or by introducing complicated cross sections. Increased detail merely creates a data-handling problem which requires a computer with sufficient capacity. A disadvantage of the Monte Carlo method is its purely numerical character which makes necessary a very careful scrutiny of the results before one can understand their significance. We have found that such an analysis is greatly facilitated by parallel analytical calculations of single scattering. In spite of its promise, the Monte Carlo method has not yet been used extensively for albedo calculations. Some results for the backscattering of 0.89-Mev neutrons from water have been given by Foderaro and Obenshain [6], but their work was mainly concerned with transmission through slabs.

One reason for the scarcity of Monte Carlo applications to the albedo problem appears to be the lack of adequate information on neutron collision cross sections, which may have discouraged extensive numerical work.[4] For few if any elements (other than hydrogen) are the cross sections known in the detail and with the accuracy desirable. Only the knowledge of the total collision cross section is in definitive form for most elements. Information about the contributions of different processes to the total cross section is reasonably adequate. Much less is known about differential cross sections. The angular distribution of elastic scattering deflections—which is highly anisotropic at high energies—is not well known for many elements. Even less is known about inelastic scattering. There is uncertainty as to the nuclear levels which are excited, the relative excitation probabilities, and the angular distribution of the inelastic scattering deflections.

We have chosen water as the medium in our calculations because the cross sections for hydrogen and oxygen are known better than those of most other elements. In addition to being of interest in their own right, the results for water will also be typical of those expected with other hydrogeneous substances. Thus the present work should provide guidance for future calculations for media such as concrete which are held up now by lack of cross section data.

## 2. Variables of the Problem

We consider the reflection of neutrons from a semi-infinite medium occupying the region $z \geq 0$. Figure 1 shows a typical trajectory of a neutron which is incident on the medium with obliquity $\theta_0$ and which is reflected with obliquity $\theta$. These obliquities are angles between the direction of motion of the neutron and the positive $z$-axis. Thus $\theta_0$ lies between 0 and $\pi/2$, and $\theta$ lies between $\pi/2$ and $\pi$.

We denote by $A(E,\theta;E_0,\theta_0)\sin\theta d\theta dE$ the probability that a neutron incident with energy $E_0$ and obliquity $\theta_0$ will be reflected from the semi-infinite medium, after one or more scatterings, with an energy between $E$ and $E+dE$ and an obliquity between $\theta$ and $\theta+d\theta$. The function $A(E,\theta;E_0,\theta_0)$ is called the *differential albedo*. Alternatively, instead of regarding the albedo as a probability, we may consider it to be the ratio of the average number of neutrons reflected to the number of neutrons incident. Thus if a beam of $N_0$ neutrons is incident with energy $E_0$ and obliquity $\theta_0$, and if $N(E,\theta)\sin\theta d\theta dE$ neutrons are reflected on the average, then

$$A(E,\theta;E_0,\theta_0)=\frac{N(E,\theta)}{N_0(E_0,\theta_0)}. \tag{2.1}$$

[3] See, however, sec. 7.8.

[4] For a survey of the neutron cross section situation in relation to transport calculations, see the recent book by Goldstein [7].

By integrating the differential albedo one obtains the *number albedo* $A_N$ (ratio of the number of all reflected neutrons to the number of incident neutrons):

$$A_N(E_0,\theta_0)=\int_0^{E_0} dE \int_{\pi/2}^{\pi} \sin\theta d\theta A(E,\theta;E_0,\theta_0). \tag{2.2}$$

Similarly, the *energy albedo* $A_E$ (ratio of the average reflected to the incident energy) is defined as

$$A_E(E_0,\theta_0)=\int_0^{E_0} dE \int_{\pi/2}^{\pi} \sin\theta d\theta \frac{E}{E_0} A(E,\theta;E_0,\theta_0). \tag{2.3}$$

We shall have occasion to consider the probabilities of reflection after exactly 1, 2, . . . $n$ collisions. The corresponding albedos will be indicated as $A^{(n)}(E, \theta;E_0,\theta_0)$, $A_N^{(n)}(E_0,\theta_0)$ and $A_E^{(n)}(E_0,\theta_0)$, $n=1, 2, \ldots$. The case $n=1$ (single-scattering albedo) is particulary important.

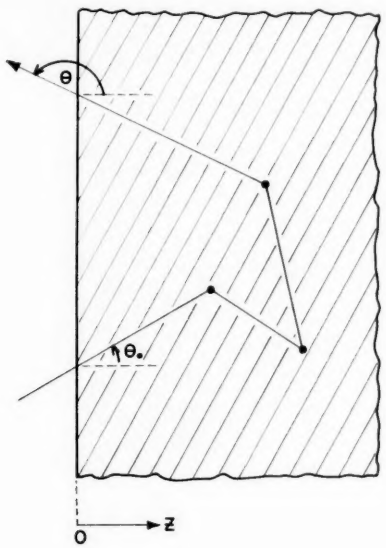


FIGURE 1. *Neutron trajectory.*

## 3. Neutron Cross Sections of Hydrogen and Oxygen

### 3.1. Integral Cross Sections

The most important parameter characterizing the neutron transport process is the mean free path between collisions, $\lambda(E)$. It is inversely proportional to the number $\mathcal{N}$ of target nuclei per unit volume and the total collision cross section $\sigma(E)$,

$$\lambda(E)=\frac{1}{\mathcal{N}\sigma(E)}. \tag{3.1}$$

The reciprocal of the mean-free path (the attenuation coefficient) is additive for a homogeneous mixture of different nuclei. For water,

$$\frac{1}{\lambda_{H_2O}}=\frac{1}{\lambda_H}+\frac{1}{\lambda_{Ox}}=\mathcal{N}_H\sigma_H(E)+\mathcal{N}_{Ox}\sigma_{Ox}(E), \tag{3.2}$$

where $\mathcal{N}_H=6.69\times10^{22}\,\mathrm{cm}^{-3}$ and $\mathcal{N}_{Ox}=3.34\times10^{22}\,\mathrm{cm}^{-3}$.

We have taken the values of $\sigma_H(E)$ and $\sigma_{Ox}(E)$ from the standard Brookhaven compilation [8]. The attenuation coefficients for hydrogen and oxygen thus obtained are shown separately in

figure 2 as functions of the energy. The plots are made in histogram form corresponding to the approximate manner in which the data were used in the machine computations. It can be seen that the energy-dependence for hydrogen is smooth, but that the histogram for oxygen has several sharp peaks and irregularities at high energies.

Next we consider the relative contributions of various processes to the total collision cross section in the energy region of interest (0.5 ev to 14.0 Mev). For hydrogen, only elastic scattering is important in this region. The $(n,\gamma)$ cross section is smaller than 0.1 percent of the total cross section at 0.5 ev, and is even less significant at higher energies.

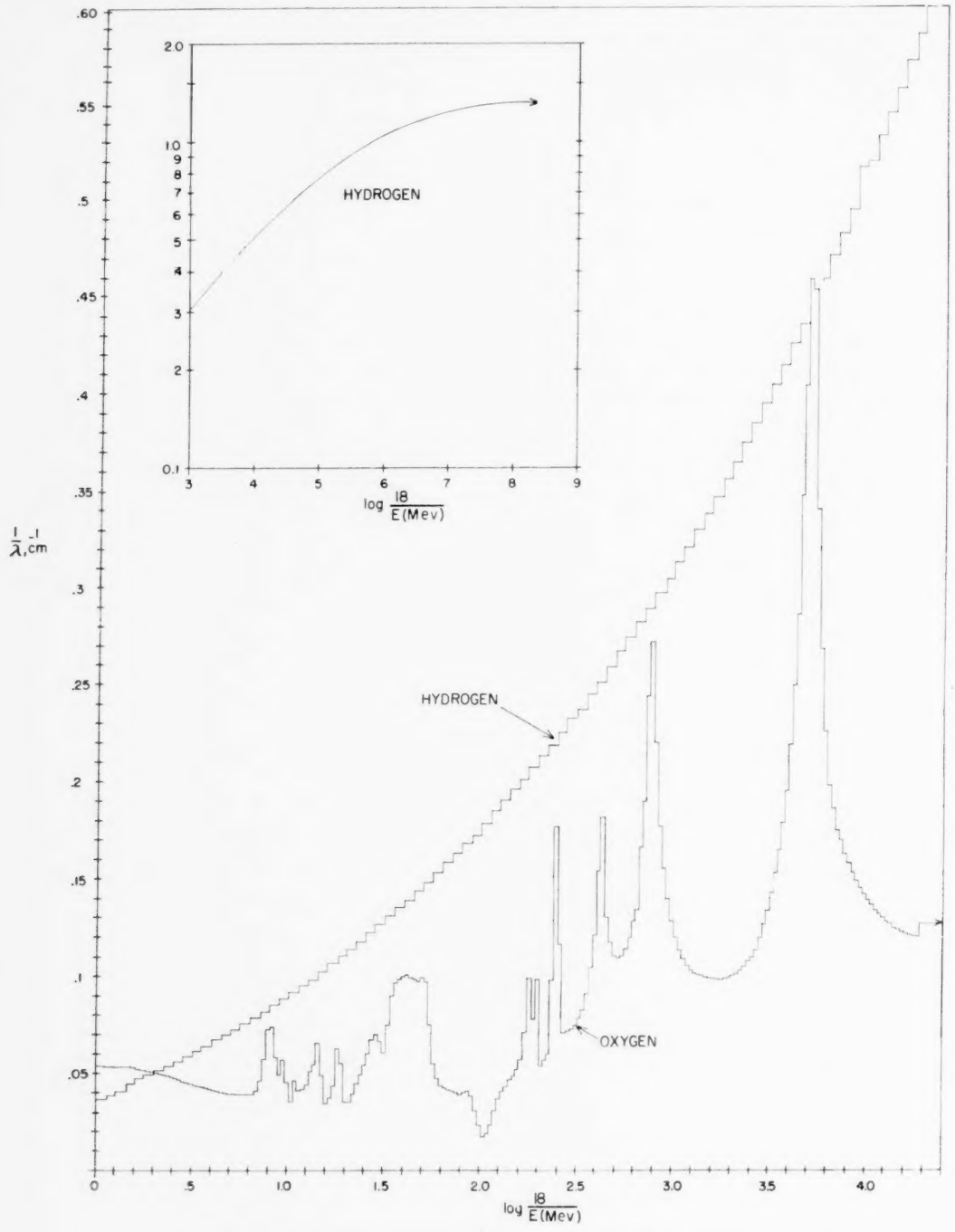


FIGURE 2. *Attenuation coefficients for hydrogen and oxygen.*

For oxygen, the processes that matter are elastic scattering, inelastic scattering (above $\approx$6.4 Mev), and absorption due to $(n,\alpha)$ reactions (above $\approx$4 Mev) and $(n,p)$ reactions (above $\approx$ 10 Mev). Cross sections for these processes, derived from the best experimental evidence and theoretical considerations, have been compiled by Lustig, Kalos, and Goldstein [9].[5] In table 3.1 we list the values of the various cross sections at selected energies to indicate their relative importance. For use in machine calculations, we have fitted cross-section ratios with polynomials in the energy variable. The representations are a smoothed-out version of the data of reference [9] accurate to 5 percent or better, which is sufficient considering the uncertainty in the data.

TABLE 3.1. *Neutron cross sections (barns) for oxygen (from reference [9])*

| Energy *Mev* | $\sigma_{Ox}$ *Total* | $\sigma_{\alpha,Ox}$ $n,\alpha$ | $\sigma_{p,Ox}$ $n,p$ | $\sigma_{n',Ox}$ *Inelastic* |
|---|---|---|---|---|
| 14 | 1.58 | 0.31 | 0.09 | 0.59 |
| 9 | 1.08 | .25 | ..... | .21 |
| 6 | 1.48 | .19 | ..... | ..... |
| 3 | 1.30 | ..... | ..... | ..... |

Ratio of inelastic to total collision cross section:

$$\frac{\sigma_{n',Ox}}{\sigma_{Ox}}=-1.05173+0.24196E-0.013666E^2+0.00024009E^3(6.4\text{ Mev}\leq E\leq 18\text{ Mev})$$

Ratio of absorption to total collision cross section:

$$\frac{\sigma_{\alpha,Ox}+\sigma_{p,Ox}}{\sigma_{Ox}}=-0.40433+0.13254E-0.0085614E^2+0.00017413E^3(4\text{ Mev}\leq E\leq 18\text{ Mev}). \tag{3.3}$$

The probabilities that a given collision will be with a hydrogen or an oxygen nucleus are $\lambda_{H_2O}(E)/\lambda_H(E)$ and $\lambda_{H_2O}(E)/\lambda_{Ox}(E)$, respectively. A collision can have four possible outcomes:

1. With probability

$$p_1=\frac{\lambda_{H_2O}}{\lambda_H}, \tag{3.4}$$

the neutron is scattered elastically by a hydrogen nucleus.

2. With probability

$$p_2=\frac{\lambda_{H_2O}}{\lambda_{Ox}}\frac{\sigma_{Ox}-\sigma_{n',Ox}-\sigma_{\alpha,Ox}-\sigma_{p,Ox}}{\sigma_{Ox}}, \tag{3.5}$$

the neutron is scattered elastically by an oxygen nucleus.

3. With probability

$$p_3=\frac{\lambda_{H_2O}}{\lambda_{Ox}}\frac{\sigma_{n',Ox}}{\sigma_{Ox}}, \tag{3.6}$$

the neutron is scattered inelastically by an oxygen nucleus.

4. With probability

$$p_4=\frac{\lambda_{H_2O}}{\lambda_{Ox}}\frac{\sigma_{\alpha,Ox}+\sigma_{p,Ox}}{\sigma_{Ox}}, \tag{3.7}$$

the neutron is absorbed. Note that $p_1+p_2+p_3+p_4=1$.

[5] Due to theoretical and experimental uncertainties, the cross sections given in this publication are subject to revision. We understand that Dr. Goldstein and his associates are now engaged in making an improved evaluation.

### 3.2. Differential Cross Sections

The outcome of a collision in which a neutron of energy $E$ is scattered can be specified in terms of the probability distribution $f_j(\Theta;E)$ of the scattering deflections $\Theta_c$ in the center-of-mass coordinate system. In conformity with the notation in the preceding subsection, we shall use indices $j=1$, 2, and 3 to indicate the distributions for elastic scattering from hydrogen, elastic scattering from oxygen, and inelastic scattering from oxygen, respectively.

For elastic scattering from hydrogen, the distribution is assumed to be isotropic,[6] i.e.,

$$f_1(\Theta_c;E)=1. \tag{3.8}$$

The angular distribution for elastic scattering from oxygen is also isotropic at energies below about 300 kev, but markedly anisotropic at higher energies, particularly in resonance regions. Above 300 kev we have used the compilation of reference [9] which gives the coefficients $f_{2,l}(E)$ of the Legendre expansion

$$f_2(\Theta_c;E)=\sum_l \frac{2l+1}{2} f_{2,l}(E)P_l(\cos\Theta_c). \tag{3.9}$$

(Note that the normalization is such that $f_{2,0}(E)=1$.) Typical angular distributions at various energies are shown in figure 3.

The angular distribution for inelastic scattering from oxygen depends not only on the energy of the neutron before the collision but also on the excitation energy which the struck nucleus receives. In $O^{16}$, the four lowest levels are 6.06, 6.14, 6.91, and 7.12 Mev above the ground state, the next is at 8.6 Mev and there are numerous levels between 9 and 14 Mev [11]. It appears from the discussion in reference [9] that neither the relative probabilities for the excitation of these levels nor the corresponding angular distributions are known. In order to explore the effect of inelastic scattering on the albedo, we have done three sets of calculations on the basis of the following assumptions:

(1) The nucleus is excited to a level 6.1 Mev above the ground state. The angular distribution is isotropic; i.e.,

$$f_3(\Theta_c;E)=1. \tag{3.10}$$

(2) The neutron loses all its energy in an inelastic scattering, so that it is, in effect, absorbed.

(3) An inelastic scattering is treated as if it were an elastic scattering; i.e., the excitation energy of the nucleus is set equal to zero.

The assumptions of case (1) seem to us to be the most realistic, and may be expected to yield reasonable answers when the neutron source energy is not too much above 9 Mev. The assumptions of case (2) lead to an underestimate of the albedo, and the assumptions of case (3) lead to an overestimate of the energy of the reflected neutrons.

## 4. Single-Scattering Albedo

### 4.1. Formulation

The probability that a neutron, incident on a semi-infinite medium with energy $E_0$ and obliquity $\theta_0$, will be reflected with energy $E$ and obliquity $\theta$ after exactly one collision is

$$\begin{aligned} A^{(1)}(E,\theta;E_0,\theta_0)&=\int_0^\infty e^{-s/\lambda_0}\frac{ds}{\lambda_0}\sum_{j=1}^{3}p_jH_j(E,\theta;E_0,\theta_0)e^{-s'/\lambda} \quad \text{if } \pi/2<\theta\leq\pi,\\ &=0 \quad \text{if } 0\leq\theta\leq\pi/2. \end{aligned} \tag{4.1}$$

[6] This assumption is open to doubt at energies above, say, 5 Mev. See Goldstein, Zweifel and Foster [10].

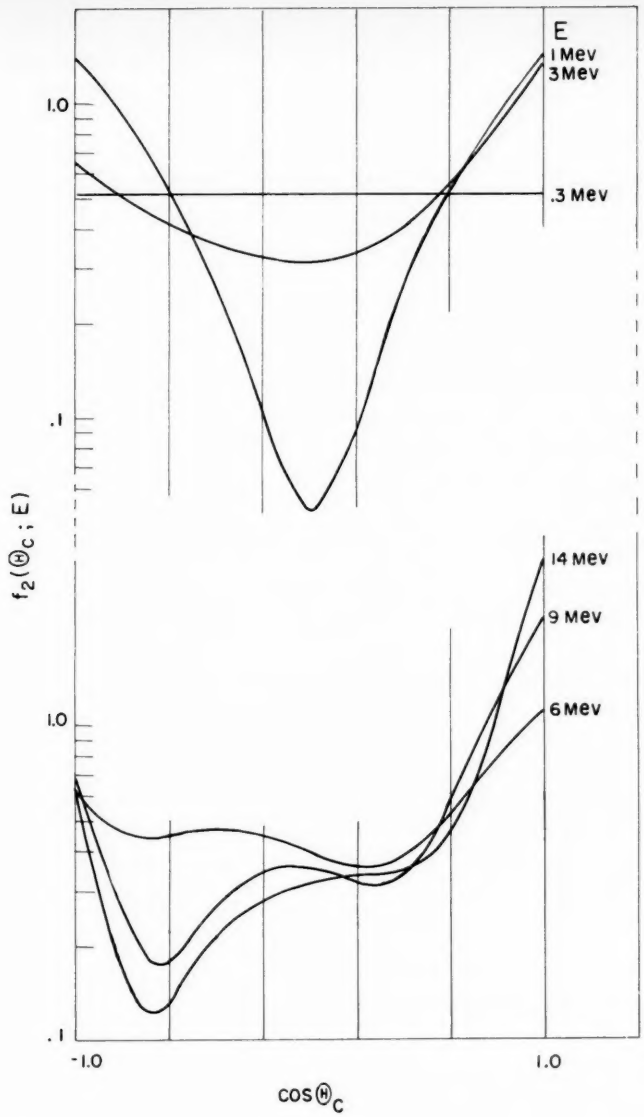


FIGURE 3. *Angular distribution of elastic scattering from oxygen (according to ref. [9]).*

In this expression, the factor $e^{-s/\lambda_0}\frac{ds}{\lambda_0}$ represents the probability that the incident neutron will travel a pathlength $s$ and then undergo its first collision between $s$ and $s+ds$, $\lambda_0=\lambda(E_0)$ being the mean-free path. The collision can be of type 1 (elastic scattering from hydrogen), type 2 (elastic scattering from oxygen), or type 3 (inelastic scattering from oxygen). The fourth type (absorption) need not be considered. The factor $p_j$ (defined by (3.4, 3.5, and 3.6)) represents the probability that the collision will be of type $j$. The function $H_j(E,\theta;E_0,\theta_0)$ is called the *scattering function* and denotes the probability that in a collision of type $j$ the energy of the neutron will change from $E_0$ to $E$ and the obliquity from $\theta_0$ to $\theta$. Finally, $\exp(-s'/\lambda)$ is the probability that the neutron will travel from the point of collision to the boundary without making any more collisions ($\lambda$ is the mean free path at the energy $E$). The pathlength to the boundary is

$$s'=-s\frac{\cos\theta_0}{\cos\theta}. \tag{4.2}$$

Using this relation, and carrying out the integration with respect to $s$ in (4.1), we obtain the equation

$$A^{(1)}(E,\theta;E_0,\theta_0)=\sum_{j=1}^{3}\frac{p_j(E_0)H_j(E,\theta;E_0,\theta_0)\cos\theta}{\cos\theta-(\lambda_0/\lambda)\cos\theta_0}\qquad\text{if }\pi/2<\theta\leq\pi,$$
$$=0\qquad\text{if }0\leq\theta\leq\pi/2. \tag{4.3}$$

## 4.2. Scattering Function

The function $H_j(E,\theta;E_0,\theta_0)$ to be inserted into (4.3) can be derived from the corresponding distribution $f_j(\Theta_c;E_0)$ for the deflections in the center-of-mass coordinate system. To establish the connection, we need the relations between $\Theta_c$, the corresponding deflection angle $\Theta$ in the laboratory coordinate system, and the ratio of energies before and after the collision, $E_0/E$. These relations are a consequence of the conservation of momentum and energy in the collision of a neutron with a nucleus. We state them for the case of inelastic scattering, characterized by the transfer of an amount $Q_j$ of energy to the target nucleus as excitation.[7] The same relations also apply to elastic scattering if we set $Q_j=0$.

The energy of the neutron after the collision is given by

$$E=E_0\frac{1+2M_jK_j\cos\Theta_c+M_j^2K_j^2}{1+2M_j+M_j^2}, \tag{4.4}$$

and the deflection in the laboratory system is

$$\cos\Theta=\sqrt{\frac{E_0}{E}}\frac{1+M_jK_j\cos\Theta_c}{1+M_j}=\frac{M_j+1}{2}\sqrt{\frac{E}{E_0}}-\frac{M_j^2K_j^2-1}{2(M_j+1)}\sqrt{\frac{E_0}{E}}, \tag{4.5}$$

where $M_j$ is the mass of the target nucleus and where

$$K_j=\sqrt{1-\frac{Q_j}{E_0}\frac{1+M_j}{M_j}}. \tag{4.6}$$

Let $F_j(E;E_0)dE$ denote the probability that the energy of the neutron after the collision lies between $E$ and $E+dE$. Using (4.4) we have

$$F_j(E;E_0)=f_j(\Theta_c;E_0)\sin\Theta_c\frac{d\Theta_c}{dE}=\frac{(M_j+1)^2}{2M_jK_jE_0}f_j(\Theta_c;E_0). \tag{4.7}$$

According to (4.5), the deflection $\Theta$ is determined by the value of $E/E_0$. The joint distribution of $E$ and $\Theta$ can, therefore, be expressed formally with the use of a Dirac delta function, as

$$F_j(E;E_0)\delta\left(\cos\Theta-\frac{M_j+1}{2}\sqrt{\frac{E}{E_0}}+\frac{M_j^2K_j^2-1}{2(M_j+1)}\sqrt{\frac{E_0}{E}}\right). \tag{4.8}$$

Let the direction of the neutron before the collision be represented by a unit vector $(\sin\theta_0\cos\varphi_0,\ \sin\theta_0\sin\varphi_0,\ \cos\theta_0)$, and its direction after the collision by a unit vector $(\sin\theta\cos\varphi,\ \sin\theta\sin\varphi,\ \cos\theta)$. Then the cosine of the deflection angle is the inner product of the two vectors,[8]

$$\cos\Theta=\cos\theta_0\cos\theta+\sin\theta_0\sin\theta\cos(\varphi_0-\varphi). \tag{4.9}$$

(The angles $\varphi_0$ and $\varphi$ are azimuths with respect to the $x$-$z$ plane.) If we insert (4.9) into (4.8), introduce the abbreviation

$$\cos\alpha_j\equiv\frac{M_j+1}{2}\sqrt{\frac{E}{E_0}}-\frac{M_j^2K_j^2-1}{2(M_j+1)}\sqrt{\frac{E_0}{E}}, \tag{4.10}$$

[7] For a derivation, see, e.g., Bethe [12].
[8] See also figure 5.

and carry out an azimuthal average with respect to $\varphi' = \varphi_0 - \varphi$, we obtain the scattering function

$$H_j(E,\theta;E_0,\theta_0) = F_j(E;E_0)\,\frac{1}{\pi}\int_0^{\pi} d\varphi'\,\delta(\cos\theta_0\cos\theta + \sin\theta_0\sin\theta\cos\varphi' - \cos\alpha_j)$$

$$= \frac{F_j(E;E_0)}{\pi\{\cos(\alpha_j-\theta_0)-\cos\theta\}^{\frac{1}{2}}\{\cos\theta-\cos(\alpha_j+\theta_0)\}^{\frac{1}{2}}}. \tag{4.11}$$

The square roots in (4.11) must not become imaginary, which requires that

$$\cos(\alpha_j+\theta_0) \leq \cos\theta \leq \cos(\alpha_j-\theta_0). \tag{4.12}$$

In the case of perpendicular incidence ($\theta_0 = 0$), the region (4.12) shrinks to a single value $\cos\alpha_j$, and the scattering function becomes

$$H_j(E,\theta;E_0,0) = F_j(E;E_0)\delta(\cos\theta - \cos\alpha_j). \tag{4.13}$$

In the limiting case of grazing incidence ($\theta_0 = 90°$), the scattering function becomes

$$H_j(E,\theta;E_0,\pi/2) = \frac{F_j(E;E_0)}{\pi\sqrt{\sin^2\theta - \cos^2\alpha_j}}. \tag{4.14}$$

### 4.3. Spectra and Angular Distributions

When using the single-scattering results as a guide for interpreting the Monte Carlo results, it is useful to have the differential albedo with one of the variables integrated out; i.e., the *energy spectrum*

$$A^{(1)}(E;E_0,\theta_0) = \int \sin\theta d\theta A^{(1)}(E,\theta;E_0,\theta_0), \tag{4.15}$$

and the *angular distribution*

$$A^{(1)}(\theta;E_0,\theta_0) = \int dE A^{(1)}(E,\theta;E_0,\theta_0). \tag{4.16}$$

In the evaluation of these expressions the range of integration must include all values of $\theta$ for given $E$ (or of $E$ for given $\theta$) for which the condition (4.12) is satisfied. Moreover, $\cos\theta$ must be negative. The resultant formulas are somewhat complex. We give them in appendix A, confining ourselves here to some qualitative remarks.

The chief characteristic of the energy spectrum is that it is confined to limits which are wide for the case of hydrogen but very narrow for somewhat heavier nuclei such as oxygen. The upper limit of the spectrum follows from the condition that the neutron must be deflected sufficiently to acquire a velocity component in the negative $z$-direction. This implies, as a consequence of (4.12), that $E$ cannot exceed

$$E_{\max} = E_0\left\{\frac{\sqrt{M_j^2K_j^2 - \cos^2\theta_0} + \sin\theta_0}{M_j+1}\right\}^2. \tag{4.17}$$

The lower limit of the spectrum is determined by the conservation of momentum and energy which implies, according to (4.4), that $E$ cannot be smaller than

$$E_{\max} = E_0\left(\frac{M_jK_j-1}{M_j+1}\right)^2. \tag{4.18}$$

The allowed energy regions between $E_{max}$ and $E_{min}$ are indicated in figure 4 as functions of the obliquity of incidence $\theta_0$.

The angular distribution cannot be described by any *one* simple law. For perpendicular incidence, the distribution follows approximately a cosine law; i.e., it peaks in directions corresponding to perpendicular emergence from the medium. As the direction of incidence becomes more oblique, this peak tends to disappear. In the limiting case of grazing incidence the angular distribution becomes flat or may even peak in directions corresponding to emergence parallel to the boundary of the semi-infinite medium. The angular distribution under these circumstances also becomes a sensitive function of the distribution $f(\Theta_c;E_0)$ of scattering deflections. For details, see appendix A.

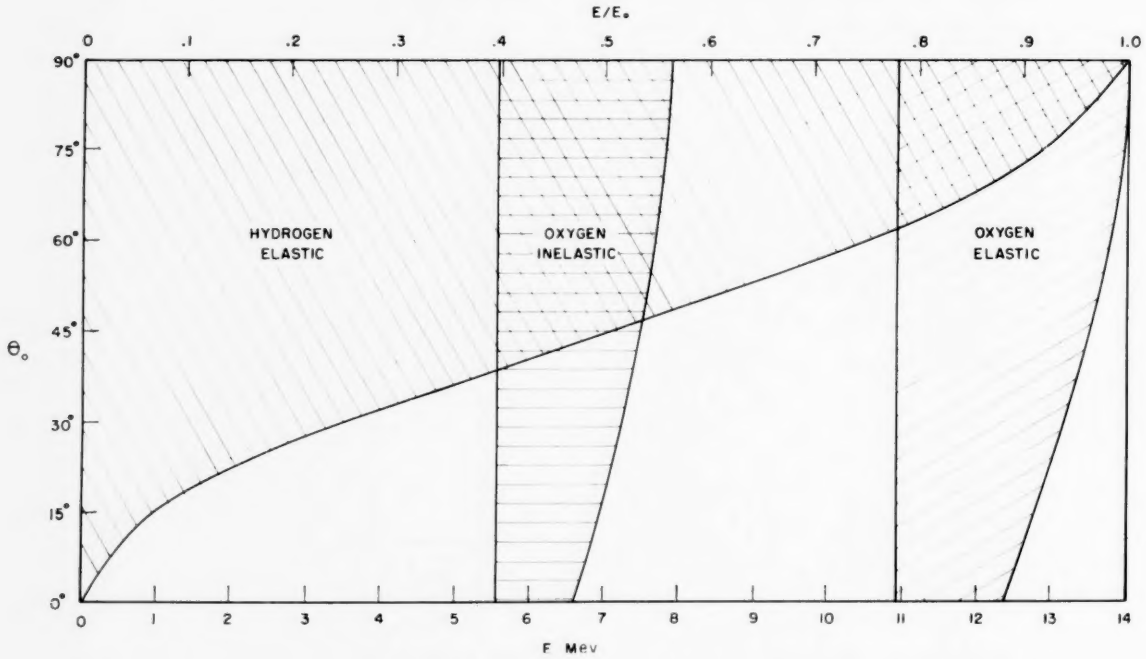


FIGURE 4. *Possible energies which a neutron may have if it is reflected after a single scattering.*

The allowed energy regions for elastic scattering hold for all $E_0$, whereas the indicated region for inelastic scattering applies only to $E_0$=14 Mev and 6.1-Mev excitation.

## 5. Monte Carlo Method

### 5.1. Generalities

Although the general principles of the Monte Carlo method are well known,[9] we give a brief review to make this paper self-contained. The usual assumption is made that a neutron undergoing multiple scattering travels in a straight line until it makes a collision with a nucleus, is then suddenly deflected, travels again in a straight line till the next collision, and so on. The trajectory of a neutron is, therefore, completely described by a specification of the initial conditions and of the energies, obliquities, and positions of the neutron immediately after successive collisions. In the physical process, these characteristics are chance variables whose probability distributions are determined by the neutron cross sections. The Monte Carlo method consists of imitating nature by playing a game of chance. With the use of random numbers, the parameters of model neutron trajectories are calculated according to the appropriate probability distributions. Such a procedure is called random sampling, and a neutron trajectory thus generated is usually called a *neutron history*.

[9] See, e.g., reference [13] for background and bibliography.

By examining a sufficiently large number of neutron histories, one can obtain statistical estimates of various transport phenomena. For example, if $N_0$ histories are generated in each of which the neutron starts at the boundary of a semi-infinite medium, and if in $N$ of these histories the neutron eventually emerges from the medium, then the ratio $N/N_0$ is an estimate of the number albedo $A_N$.

### 5.2. Random Sampling of Neutron Histories

If we let $E_n$, $\theta_n$, and $z_n$ represent the energy, obliquity, and distance from the boundary immediately after the $n$'th collision, the neutron trajectory or history can be described by the array

$$\begin{aligned} &E_0, E_1, \ldots, E_n, \ldots \\ &\theta_0, \ \theta_1, \ \ldots, \theta_n, \ldots \\ &z_0, \ z_1, \ \ldots, z_n, \ldots \end{aligned} \tag{5.1}$$

in which $E_0$, $\theta_0$, and $z_0=0$ indicate the initial conditions. The history ends when the neutron is absorbed or reflected from the semi-infinite medium. We have adopted an additional termination rule in the present work, ending a history when the energy of the neutron drops below 0.5 ev. In order to generate a history, one must proceed from collision to collision, computing $(E_{n+1},\theta_{n+1},z_{n+1})$ from $(E_n,\theta_n,z_n)$ recursively by random sampling.

By "random sampling from a distribution $f(x)$" we mean, in principle, the following procedure. A set of numbers, $x_1$, $x_2$, . . ., is prepared whose frequency distribution is made to approximate $f(x)$ as closely as possible. One of these numbers is then selected at random and is called a *random variate* from the distribution $f(x)$. It is, in fact, sufficient to prepare only a single set of random variates, from a uniform distribution $f(x)=1(0\leq x\leq 1)$. These numbers, distributed uniformly between zero and one, are called *random numbers*. When suitably manipulated they can be made to yield random variates from any distribution, as shown below.

In a machine calculation requiring many random numbers it would be awkward to prepare and store a large set of random numbers. Instead, it is customary to use so-called *pseudorandom numbers* which are generated systematically but have, nevertheless, sufficient randomness for Monte Carlo calculations. We have employed the method of congruential multiplication[10] in order to produce a sequence of pseudorandom numbers

$$\xi_1, \ \xi_2, \ \ldots \ \xi_n \ \ldots \tag{5.2}$$

These numbers are fractions (between zero and one) which are obtained by normalizing a set of integers $x_n$,

$$\xi_n=2^{-35}x_n. \tag{5.3}$$

The integers, in turn, are obtained from the following recursive scheme:

$$\left.\begin{aligned} x_0&=c \\ x_{n+1}&=5^k x_n \bmod 2^{35}, \end{aligned}\right\} \tag{5.4}$$

where $c$ and $k$ are odd integers. The last equation states that $x_{n+1}$ is congruent to $5^k x_n$ modulo $2^{35}$; in other words, that $x_{n+1}$ is the remainder obtained upon division of $5^k x_n$ by $2^{35}$. In the course of our Monte Carlo calculations we have used three pseudorandom number sequences of the type (5.2), with $k=11$, 13, and 15. This will be discussed more fully in section 5.4.

---

[10] See, e.g., the article by J. Todd in reference [13c].

It can be proved (see app. B) that the sequence (5.2) contains $2^{33}$ different numbers which are distributed with uniform density between zero and one. The successive random numbers used in the Monte Carlo calculation have been obtained by picking *successive* numbers in the pseudorandom number sequence (5.2). This is equivalent to a random choice, because the pseudorandom number sequence closely resembles a true random number sequence in the sense that there is no noticeable correlation between successive numbers. This lack of correlation has not been proved, but is an empirical fact that can be demonstrated by statistical tests. In appendix B, section 9, we present the results of such tests for 237,000 pseudorandom numbers actually used in our calculations.

One procedure for selecting a random variate $x$ from a distribution $f(x)$ by the manipulation of random numbers depends on the possibility of finding a random variate $y(x)$ which is distributed uniformly between 0 and 1. We let

$$y(x)=\int_x^\infty f(x')dx', \tag{5.5}$$

i.e., $y(x)$ is the cumulative probability distribution associated with $f(x)$. Note that

$$\text{probability } \{y<y'\}=\text{probability } \{x>x(y')\}=\int_{x(y')}^\infty f(x')dx'=y', \tag{5.6}$$

so that $y$ is equally likely to have any value between 0 and 1. We therefore identify $y$ with a random number $\xi$, and determine a random variate $x$ by inverting the equation

$$\xi=\int_x^\infty f(x')dx. \tag{5.7}$$

A second method, called the "rejection technique" applies to distributions with a finite range, say $0\leq x\leq a$. Let $L$ be the maximum of $f(x)$. The sampling procedure consists of the following steps. First, two random numbers, say $\xi_1$ and $\xi_2$, are selected. If $L\xi_2\leq f(a\xi_1)$ we chose the number $a\xi_1$ as a random variate from $f(x)$. If $L\xi_2>f(a\xi_1)$, we reject the random numbers $\xi_1$ and $\xi_2$ and repeat the testing process with a new pair of random numbers. The justification for this selection procedure is supplied by the observation that

$$\text{probability } \{\text{acceptance of } x=a\xi_1\}=\text{probability } \{L\xi_2\geq f(a\xi_1)\}=\int_0^{f(a\xi_1)/L}d\xi_2=\frac{f(x)}{L}. \tag{5.8}$$

The average number of random number pairs that must be tested before finding an acceptable random variate is given by

$$\frac{1}{\frac{1}{L}\int_0^1 f(a\xi_1)d\xi_1}=aL. \tag{5.9}$$

We shall now describe the actual sampling procedure for generating a neutron history: i.e., the rule for going from $(E_n,\theta_n,z_n)$ to $(E_{n+1},\theta_{n+1},z_{n+1})$.

### a. Location of the Next Collision

The probability distribution of $z_{n+1}$ is

$$\frac{1}{\lambda(E_n)}e^{-s_{n+1}/\lambda(E_n)}=\frac{1}{\lambda(E_n)}e^{-\frac{z_{n+1}-z_n}{\cos\theta_n}\frac{1}{\lambda(E_n)}}, \tag{5.10}$$

where

$$s_{n+1}=\frac{z_{n+1}-z_n}{\cos\theta_n} \tag{5.11}$$

is the pathlength traveled by the neutron between the $n$th and $n+1$st collision. The distribution (5.10) is derived from the assumption that the spatial distribution of target nuclei is random and that the probability of a collision per unit pathlength is $1/\lambda(E_n)$. Applying the cumulative-probability method, we select a random number $\xi_\alpha$, and determine $s_{n+1}$ from the equation

$$\xi_\alpha = \int_{s_{n+1}/\lambda(E_n)}^{\infty} e^{-s/\lambda(E_n)} \frac{ds}{\lambda(E_n)} = e^{-s_{n+1}/\lambda(E_n)}. \tag{5.12}$$

The pathlength determines the position of the next collision, which is given by

$$z_{n+1} = z_n + \cos\theta_n s_{n+1} = z_n - \cos\theta_n \lambda(E_n) \log \xi_\alpha. \tag{5.13}$$

### b. Type of Collision

The probabilities $p_j (j=1, 2, 3, 4)$ for the occurrence of each of the four possible types of collisions are given by (3.4), (3.5), (3.6), and (3.7). To make a random selection, we divide the region between 0 and 1 into four intervals proportional to the probability for each process. A random number $\xi_\beta$ is then picked and the type of collision is determined by the interval into which $\xi_\beta$ falls:

$$\begin{aligned}
0 \le \xi_\beta \le p_1 &\quad : \text{elastic scattering from hydrogen} \\
p_1 < \xi_\beta \le p_1 + p_2 &\quad : \text{elastic scattering from oxygen} \\
p_1 + p_2 < \xi_\beta \le p_1 + p_2 + p_3 &\quad : \text{inelastic scattering from oxygen} \\
p_1 + p_2 + p_3 < \xi_\beta \le p_1 + p_2 + p_3 + p_4 = 1 &\quad : \text{absorption.}
\end{aligned}$$

### c. Energy Loss

If the $n+1$st collision results in a scattering, the energy of the neutron is changed from $E_n$ to $E_{n+1}$ according to the single-scattering law (4.7); i.e., the probability distribution of $E_{n+1}$ is

$$F_j(E_{n+1}; E_n) = \frac{(M_j+1)^2}{2M_j K_j E_0} f_j(\Theta_{c,n+1}; E_n), \tag{5.14}$$

where

$$\cos \Theta_{c,n+1} = \frac{(M_j+1)^2 E_{n+1} - (1+M_j^2 K_j^2) E_n}{2M_j K_j E_n}. \tag{5.15}$$

The choice of the energy loss can be made indirectly through the choice of the center-of-mass deflection $\Theta_{c,n+1}$. When the distribution of deflections is isotropic (for collisions of type 1 and 3), we set

$$\cos \Theta_{c,n+1} = 2\xi_\gamma - 1, \tag{5.16}$$

where $\xi_\gamma$ is a random number. For elastic scattering from oxygen, the angular distribution is anisotropic and is given by the Legendre expansion (3.9). In this case it is convenient to use the rejection technique. Provisionally, a deflection angle is chosen according to (5.16). An additional random number, $\xi_\gamma^{(1)}$, is then selected and a test is made to determine if

$$f_2\{\cos^{-1}(2\xi_\gamma - 1); E_n\} \ge L(E_n)\xi_\gamma^{(1)}, \tag{5.17}$$

where $L(E_n)$ is the largest possible value of $f_2(\Theta_c; E_n)$. If the inequality (5.17) is satisfied, the provisional random variate given by (5.16) is accepted; if not, the selection procedure is repeated with two new random numbers.[11]

---

[11] Using formula (5.9), noting that the range of the angular distribution (in $\cos\Theta_c$) is $a=2$, and using the differential cross sections as shown in figure 3, we find that the average number of random number pairs that must be tested to make a selection has the following values: 6.8 at 14 Mev, 4.3 at 9 Mev, 2.2 at 6 Mev, 2.6 at 3 Mev, 2.8 at 1 Mev, and 1.03 at 0.3 Mev. The sampling efficiency at higher energies could be improved by more elaborate schemes, but we have not considered this worthwhile.

### d. Change of Obliquity

The prescription for selecting the obliquity after the $n+1$st collision can be obtained in two different ways: by a direct geometrical argument, or by an application of the scattering function derived in section 4. Starting with the latter, we note that, according to (4.11) the probability distribution of $\theta_{n+1}$ (for fixed $\Theta_{c,n+1}$ and $\theta_n$) is given by

$$\frac{1}{\pi\{\cos(\alpha_{jn}-\theta_n)-\cos\theta_{n+1}\}^{\frac{1}{2}}\{\cos\theta_{n+1}-\cos(\alpha_{jn}+\theta_n)\}^{\frac{1}{2}}}, \tag{5.18}$$

where

$$\cos\alpha_{jn}=\frac{M_j+1}{2}\sqrt{\frac{E_{n+1}}{E_n}}-\frac{M_j^2K_j^2-1}{2(M_j+1)}\sqrt{\frac{E_n}{E_{n+1}}}, \tag{5.19}$$

and

$$\cos(\alpha_{jn}+\theta_n)\leq\cos\theta_{n+1}\leq\cos(\alpha_{jn}-\theta_n). \tag{5.20}$$

Applying the cumulative-probability method, we pick a random number, $\xi_\delta$, and set

$$\begin{aligned}1-\xi_\delta&=\frac{1}{\pi}\int_{\theta_{n+1}}^{\alpha_{jn}+\theta_n}\frac{\sin\theta d\theta}{\{\cos(\alpha_{jn}-\theta_n)-\cos\theta\}^{\frac{1}{2}}\{\cos\theta-\cos(\alpha_n+\theta_{jn})\}^{\frac{1}{2}}}\\&=1-\frac{1}{\pi}\cos^{-1}\left\{\frac{\cos\theta_{n+1}-\cos\alpha_{jn}\cos\theta_n}{\sin\alpha_{jn}\sin\theta_n}\right\}.\end{aligned} \tag{5.21}$$

The inversion of this equation yields the rule for calculating $\theta_{n+1}$:

$$\cos\theta_{n+1}=\cos\alpha_{jn}\cos\theta_n+\sin\alpha_{jn}\sin\theta_n\cos(\pi\xi_\delta). \tag{5.22}$$

The geometrical derivation goes as follows. Let $\Theta_{n+1}$ be the polar deflection and $\chi_{n+1}$ the associated azimuthal deflection in the laboratory system, resulting from the $n+1$st collision. $\chi_{n+1}$ is assumed to be measured with respect to a plane that contains the $z$-axis and the direction of motion of the neutron before the $n+1$st collision.) The various deflection angles and obliquities form a spherical triangle that is sketched in figure 5. The application of the law of cosines to this triangle yields the relation

$$\cos\theta_{n+1}=\cos\Theta_{n+1}\cos\theta_n+\sin\Theta_{n+1}\sin\theta_n\cos\chi_{n+1}. \tag{5.23}$$

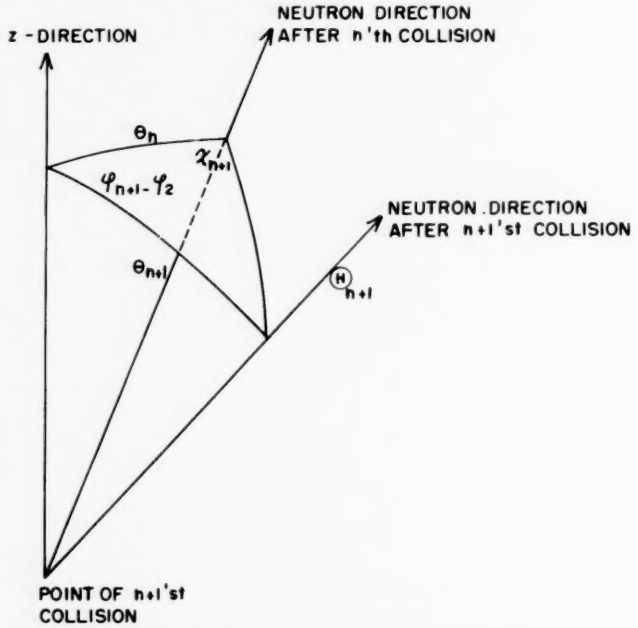


FIGURE 5. *Spherical triangle illustrating the kinematics of a neutron scattering.*

Now, according to (4.5) and (4.10), $\Theta_{n+1}$ is identical with $\alpha_{jn}$. Furthermore, it can be assumed that the azimuthal deflection angle $\chi_{n+1}$ is distributed randomly between 0 and $2\pi$, so that it is legitimate to replace $\cos\chi_{n+1}$ in (5.23) by $\cos\pi\xi\delta$, where $\xi\delta$ is a random number. Thus (5.23) is in fact identical with (5.22).

### 5.3. Albedo Estimates

The estimate of the number albedo $A_N$ involves merely the determination of the fraction $N/N_0$ of the number of histories that end in reflection.[12] To obtain an expression for the statistical error of such an estimate we shall be somewhat formal and assign to each sampled history a "score" $R$, which has the value 1 in case of reflection and is 0 otherwise. Thus, $R$ is a random variable which assumes the value 1 with probability $A_N$ and the value 0 with probability $1-A_N$.

The mean value of $R$ is

$$\overline{R}=A_N\cdot 1+(1-A_N)\cdot 0=A_N \tag{5.24}$$

and its variance (defined as $\overline{R^2}-\overline{R}^2$) is

$$\text{var } R=A_N(1-A_N). \tag{5.25}$$

Suppose now that we sample and examine $N_0$ histories with scores $R_1,R_2,\ldots,R_{N0}$. An estimate of the number albedo is given by the average score

$$A_N^*=\frac{1}{N_0}(R_1+R_2+\ldots+R_{N_0})=\frac{N}{N_0}. \tag{5.26}$$

The variance of this estimate[13] is

$$\text{var } A_N^*=\frac{1}{N_0}\text{var } R=\frac{1}{N_0}A_N(1-A_N). \tag{5.27}$$

An estimate of the energy albedo can be obtained by multiplying the number albedo estimate $N/N_0$ by the quantity $\overline{E}/E_0$, where $\overline{E}$ is the average energy of the reflected neutrons. More formally, we assign to each history a score $T$ which is equal to $E/E_0$ in case of reflection and which vanishes otherwise. The random variable $T$ has the mean value

$$\overline{T}=A_N\frac{\overline{E}}{E_0}, \tag{5.28}$$

and a variance

$$\text{var } T=\overline{T^2}-\overline{T}^2=\frac{1}{E_0^2}(A_N\overline{E^2}-A_N^2\overline{E}^2). \tag{5.29}$$

An estimate of the energy albedo is provided by the average score

$$A_E^*=\frac{1}{N_0}(T_1+T_2+\ldots+T_{N_0})=\frac{N}{N_0}\frac{\overline{E}}{E_0}. \tag{5.30}$$

The variance of this estimate is

$$\begin{aligned}\text{var } A_E^*&=\frac{1}{N_0E_0^2}(A_N\overline{E^2}-A_N^2\overline{E}^2)\\&=\frac{1}{N_0E_0^2}(\overline{E^2}\text{ var } R+A_N\text{ var } E).\end{aligned} \tag{5.31}$$

[12] Crude estimates of the differential albedo can be obtained by counting the neutrons that are reflected with energies and obliquities in specified energy-angle intervals. The statistical accuracy of such estimates is given by formulas analogous to those for the number albedo.

[13] Actually one does not know the exact value of $A_N$, but an estimate of var $(A_N^*)$ is obtained through replacing $A_N$ in (5.27) by $A_N^*$, and $N_0$ by $N_0-1$ in order to make the estimate unbiased.

The two terms contributing to this variance are both non-negative. The first arises from fluctuations of the number of reflected neutrons and the second from variations of the energies of the reflected neutrons.

The significance of the variances var $A_N^*$ and var $A_E^*$ must be interpreted with reference to the probability distributions of $A_N^*$ and $A_E^*$. Both of these quantities are the averages of $N_0$ identically distributed independent random variables. According to the central limit theorem of statistics [14] their distributions approach a Gaussian distribution in the limit of large $N_0$.[14] One can therefore make the following statements about the deviations of the albedo estimates from the true albedo values:

$$\text{Probability}\{|A_N^*-A_N|\geq k\sqrt{\text{var}\,A_N^*}\}=\text{Probability}\{|A_E^*-A_E|\geq k\sqrt{\text{var}\,A_E^*}\}=\sqrt{\frac{2}{\pi}}\int_k^\infty e^{-x^2/2}dx. \tag{5.32}$$

## 5.4. Correlated Random Sampling

To establish the dependence of the albedo on the assumed conditions (source energy and obliquity, collision cross sections, etc.), it is better to use a difference method than to make two or more separate calculations. The difference method can be designed to eliminate irrelevant statistical fluctuations, by keeping constant all random elements in the calculation which are not affected by the change of assumed conditions. Thereby greater accuracy can be achieved with a given amount of computation.

We recall from section 5.2. that the following random numbers specify the nature and outcome of a collision: $\xi_\alpha$ determines the quantity $s_{n+1}/\lambda(E_n)$ which is the distance (in mean free paths) traveled by the neutron between the previous collision and the collision under consideration; $\xi_\beta$ determines the type of collision; $\xi_\gamma$, and, for anisotropic elastic scattering from oxygen, additional numbers $\xi_\gamma^{(1)}$, $\xi_\gamma^{(2)}$, . . . determines the center-of-mass deflection $\Theta_{c,n+1}$; finally, $\xi_\delta$ determines the azimuthal scattering deflection $\chi_{n+1}$. The above characteristics, together with the initial conditions, specify a history completely.

Suppose now that we want to make a direct determination of the difference in the albedo brought about by a change of the obliquity of the incident radiation. We can do this by generating simultaneously two *correlated sets of histories*, one set with one initial obliquity, the second set with another. The sets should be correlated in the sense that for each history in one set there exists a counterpart in the second set in which exactly the same random numbers are used for determining the outcomes of corresponding collisions. Thus two matched histories are alike, except that one of them is "rotated with respect to the other" and may be shorter because of the different initial obliquity. We call this case one of *maximal correlation*.[15]

In order to find out how a change in the assumed cross sections affects the albedo, we may again generate two (or more) correlated sets of histories, using identical random numbers for corresponding choices. Then two matched histories will at least be identical in regard to the distances (in mean free paths) between successive collisions, and in regard to successive azimuthal deflections. However, energy losses in corresponding collisions may be different. Consequently all the parameters of a history which depend on the energy may also be different. We call this case one of *partial correlation*. Even in this case, the use of identical random numbers tends to minimize accidental differences.

It is most economical, but not absolutely necessary, to generate several correlated sets of histories simultaneously. In the present work we wanted to compare the albedo under many different conditions, and used the neutron histories also for the solution of other problems, so that simultaneous computation of all correlated histories was not practicable. We

---

[14] In fact, the distribution of $A_N^*$ is the $N_0$-fold convolution of a binomial distribution with itself, and is very closely approximated by a Gaussian even for $N_0$ as low as 10. The numerical results for the energy albedo indicate that the distribution of $A_E^*$ is a reasonable approximation to a Gaussian for $N_0\approx 100$.

[15] This case also arises in the comparison of the reflection of neutrons after 1, 2, . . . $n$ collisions.

therefore had to devise a technique for doing separate but correlated calculations. This was facilitated by the use of pseudorandom number sequences, which according to (5.3) and (5.4), are completely determined by a "starting value" $c$ and a "multiplier" $5^k$, and can be conveniently regenerated provided we remember these two parameters.

The number of different random numbers required to generate two histories is usually not the same, even when they are correlated. In the first place, even in the case of maximal correlation, the two histories will tend to differ in length. Secondly, in the case of partial correlation there is a statistical variability in the number of random numbers $\xi_\gamma^{(1)}$, $\xi_\gamma^{(2)}$, . . . that may be required to select a scattering deflection by the rejection technique, according to (5.17). Thus it could happen that in spite of the use of the same pseudorandom number sequence (with the same $c$ and $k$), different portions of this sequence would be used for supposedly correlated histories. This difficulty was circumvented by the use of many sequences of pseudorandom numbers instead of just one. A primary sequence was introduced with an arbitrary odd starting value $c$ and a multiplier $5^{k_1}$. Successive members of the primary sequence were then used as the starting values of secondary sequences generated with a multiplier $5^{k_2}$. Successive secondary sequences were used for the calculation of successive histories. When the need arose for random sampling by the rejection technique, the requisite random numbers $\xi_\gamma^{(1)}$, $\xi_\gamma^{(2)}$, . . . were obtained from a tertiary sequence. The tertiary sequence used a multiplier $5^{k_3}$, and a starting value equal to the last member of the secondary sequence currently being used.[16]

We now discuss the effect of correlated sampling on Monte Carlo estimates of $A_N - \tilde{A}_N$ and $A_E - \tilde{A}_E$, where $A_N$ and $A_E$ are albedos under condition 1, and $\tilde{A}_N$ and $\tilde{A}_E$ the albedos under condition 2. Proceeding as in section 5.3, we assign to histories generated under condition 1 the scores $R$ and $T$, and to the histories generated under condition 2 the scores $\tilde{R}$ and $\tilde{T}$. Albedo differences can then be estimated as follows:

$$A_N^* - \tilde{A}_N^* = \frac{1}{N_0}\{(R_1 - \tilde{R}_1) + (R_2 - \tilde{R}_2) + \ldots + (R_{N_0} - \tilde{R}_{N_0})\}, \tag{5.33}$$

$$A_E^* - \tilde{A}_E^* = \frac{1}{N_0}\{(T_1 - \tilde{T}_1) + (T_2 - \tilde{T}_2) + \ldots + (T_{N_0} - \tilde{T}_{N_0})\}. \tag{5.34}$$

The variances of these difference estimates are

$$\text{var}\,(A_N^* - \tilde{A}_N^*) = \frac{1}{N_0}\{\text{var}\,R - 2\rho(R,\tilde{R})\sqrt{\text{var}\,R\,\text{var}\,\tilde{R}} + \text{var}\,\tilde{R}\}, \tag{5.35}$$

$$\text{var}\,(A_E^* - \tilde{A}_E^*) = \frac{1}{N_0}\{\text{var}\,T - 2\rho_E(T,\tilde{T})\sqrt{\text{var}\,T\,\text{var}\,\tilde{T}} + \text{var}\,\tilde{T}\}. \tag{5.36}$$

The quantity

$$\rho(R,\tilde{R}) = \frac{\overline{R\tilde{R}} - \overline{R}\cdot\overline{\tilde{R}}}{\sqrt{\text{var}\,R\,\text{var}\,\tilde{R}}} \tag{5.37}$$

is the correlation coefficient of R and $\tilde{\text{R}}$. Similarly,

$$\rho_E(T,\tilde{T}) = \frac{\overline{T\tilde{T}} - \overline{T}\cdot\overline{\tilde{T}}}{\sqrt{\text{var}\,T\,\text{var}\,\tilde{T}}} \tag{5.38}$$

[16] We have set $k_1 = 11$, $k_2 = 15$, and $k_3 = 13$.

is the correlation coefficient of $T$ and $\tilde{T}$. For uncorrelated pairs of histories, the correlation coefficients vanish. The objective of correlated sampling is to reduce var $(A_N^*-\tilde{A}_N^*)$ and var $(A_E^*-\tilde{A}_E^*)$ by making the correlation coefficients positive and as large as possible.

The magnitude of the actual correlation coefficients must, in general, be estimated from the sampled data, and some typical values will be given in section 7. It is possible, however, to put a theoretical upper limit on $\rho(R,\tilde{R})$. Using (5.25) and (5.37) we find that

$$\rho(R,\tilde{R})=\frac{\overline{R\tilde{R}}-A_N\tilde{A}_N}{\sqrt{A_N(1-A_N)\tilde{A}_N(1-\tilde{A}_N)}}. \tag{5.39}$$

Without loss of generality we may assume that $\tilde{A}_N \leq A_N$.

Therefore

$$\text{probability}\{R=1 \text{ and } \tilde{R}=1\} \leq \text{probability}\{\tilde{R}=1\}=\tilde{A}_N, \tag{5.40}$$

so that

$$\overline{R\tilde{R}} \leq \tilde{A}_N. \tag{5.41}$$

Accordingly the correlation coefficient must obey the inequality

$$\rho(R,\tilde{R}) \leq \sqrt{\frac{\tilde{A}_N(1-A_N)}{A_N(1-\tilde{A}_N)}} \leq 1. \tag{5.42}$$

The greatest possible value of $\rho(R,\tilde{R})$ corresponds to the case of maximal correlation discussed above. It leads to a reduction of var $(A_N^*-\tilde{A}_N^*)$ by a factor

$$1-\frac{2}{\frac{A_N}{\tilde{A}_N}+\frac{1-\tilde{A}_N}{1-A_N}}. \tag{5.43}$$

## 6. Computations and Results

### 6.1. Machine Computations

The Monte Carlo calculations were programed for the IBM–704 computer at the National Bureau of Standards.[17] The neutron histories, generated in order to determine the albedo, were concurrently used for the calculation of the neutron flux in infinite media and in slabs,[18] so that it is difficult to state how much computer memory and computing time were required for the albedo problem alone. Altogether, a little more than 5,000 words of magnetic core memory were required of which not less than one-third were allocated to the albedo problem. For each case treated, 3,000 neutron histories were generated and analyzed. This amount of computation gave the desired accuracy and required approximately 45 min of computer time. Not more than half of this time was required by the albedo problem. The use of magnetic tapes was not necessary, but was an optional device for storing the results of one machine run and combining them with the results of a later run. Intermediate print-outs of the results were made after groups of 1,000 histories had been processed, in order to follow the course of the computations and to have a check on the performance of the computer.

In line with the exploratory nature of the investigation, the machine program was kept flexible. This made possible the exploration of new aspects of the problem as they emerged in

[17] The program was based in part on an earlier code [15] developed at the Westinghouse Atomic Power Division. The authors are indebted to Dr. B. H. Mount and Mrs. Heidi Kuehn who very graciously made their code available to us.

[18] To be reported in a later publication.

the course of the work. In the simplest version of the program only elastic scattering from hydrogen and oxygen was taken into account, and the print-out of results was limited to tables of the differential albedo. In the latest version all relevant collision cross sections were included, and much additional information was printed out that had been found necessary for an understanding of the physical and statistical significance of the Monte Carlo results. This additional information included the mean and mean square energy of the reflected neutrons, the contributions of different orders of scattering to the number albedo and energy albedo, listings of the particular histories in which reflection occurred and of the energies of the reflected neutrons, and a statistical analysis of the pseudorandom numbers used. Intermediate versions of the program yielded only some of this information.

The analytical formulas for the single-scattering albedo, developed in section 4, were used mainly for the interpolation of results, and single-scattering computations were done with the Monte Carlo code. This was simpler to do once the machine program was available but slightly less accurate.

Altogether 38 different cases were treated which are listed in table 6.1. This table contains the source energy and obliquity as well as a brief indication of the assumptions about the cross sections. The computations fall into two groups: 30 cases were done with one set of pseudorandom numbers (analyzed in app. B), and the remaining 8 cases with another set. A high degree of correlation was introduced by the repeated use of the same set of pseudorandom numbers in order to increase the accuracy of intercomparisons. We believed this to be a sound procedure, because the set was large enough (consisting of approximately 237,000 numbers) to be statistically representative.

TABLE 6.1. *Summary of calculations*

The entry in the left column serves as index to the differential-albedo tables in appendix C. Each result for the number albedo $A_N$ and the energy albedo $A_E$ is based on the analysis of 3,000 neutron histories, with $\delta A_N$ and $\delta A_E$ indicating the statistical standard deviations. All runs were done with the same set of pseudorandom numbers (described in app. B), except the runs indicated by an asterisk (*) which were all done with another set of pseudorandom numbers.

| Table | $E_0$(Mev) | $\theta_0$ | $A_N$ | $\delta A_N$ | $A_E$ | $\delta A_E$ | Assumptions |
|---|---|---|---|---|---|---|---|
| 1 | 0.3 | 0° | 0.296 | 0.008 | 0.048 | ---------- | (*). |
| None | 1 | 0° | .370 | .009 | (.135) | ---------- | (*). |
| 2a | 1 | 0° | .361 | .009 | (.115) | ---------- | (*); elastic scattering from oxygen assumed isotropic. |
| 2b | 1 | 0° | .381 | .009 | .148 | 0.005 | |
| 2c | 1 | 0° | .113 | .006 | .091 | ---------- | Single scattering. |
| 3a | 1 | 45° | .450 | .009 | .159 | ---------- | |
| 3b | 1 | 45° | .114 | .006 | .085 | ---------- | Single scattering. |
| 4a | 1 | 60° | .518 | .009 | .183 | ---------- | |
| 4b | 1 | 60° | .142 | .006 | .099 | ---------- | Single scattering. |
| 5a | 1 | 75° | .619 | .009 | .241 | ---------- | |
| 5b | 1 | 75° | .213 | .007 | .144 | ---------- | Single scattering. |
| 6a | 1 | 90° | .767 | .008 | .415 | ---------- | |
| 6b | 1 | 90° | .493 | .009 | .347 | ---------- | Single scattering. |
| 7a | 3 | 0° | .061 | .004 | .023 | ---------- | 2-cm slab; see section 7.9; (*). |
| 7b | 3 | 0° | .131 | .006 | .038 | ---------- | 5-cm slab; see section 7.9; (*). |
| 7c | 3 | 0° | .163 | .007 | .044 | ---------- | 10-cm slab; see section 7.9; (*). |
| None | 3 | 0° | .168 | .007 | (.044) | ---------- | (*). |
| 8a | 3 | 0° | .178 | .007 | (.049) | ---------- | (*); elastic scattering from oxygen assumed isotropic. |
| 8b | 3 | 0° | .167 | .007 | .041 | .003 | |
| 8c | 3 | 0° | .028 | .003 | .023 | ---------- | Single scattering. |
| 9a | 3 | 45° | .232 | .008 | .052 | ---------- | |
| 9b | 3 | 45° | .035 | .003 | .023 | ---------- | Single scattering. |
| 10a | 3 | 60° | .315 | .008 | (.080) | ---------- | |
| 10b | 3 | 60° | .066 | .005 | (.039) | ---------- | Single scattering. |
| 11a | 3 | 75° | .472 | .009 | .144 | ---------- | |
| 11b | 3 | 75° | .143 | .006 | .084 | ---------- | Single scattering. |
| 12a | 3 | 90° | .728 | .008 | (.339) | ---------- | |
| 12b | 3 | 90° | .480 | .009 | (.290) | ---------- | Single scattering. |
| 13 | 3 | (†) | .371 | .009 | (.110) | ---------- | |
| 14a | 6 | 0° | .157 | .007 | .052 | .003 | |
| 14b | 6 | 0° | .171 | .007 | .059 | .004 | Absorption disregarded. |
| 15a | 9 | 0° | .107 | .006 | .027 | .002 | Excitation of 6.1-Mev level in oxygen by inelastic scattering. |
| 15b | 9 | 0° | .138 | .006 | .041 | .003 | Absorption disregarded. |
| 15c | 9 | 0° | .131 | .006 | .047 | ---------- | Absorption disregarded. Inelastic scattering from oxygen treated as elastic. |
| 16a | 14 | 0° | .124 | .006 | .040 | .003 | Excitation of 6.1-Mev level in oxygen by inelastic scattering. |
| 16b | 14 | 0° | .163 | .007 | .038 | .002 | Elastic scattering from oxygen assumed isotropic; excitation of 6.1-Mev level in oxygen by inelastic scattering. |
| 16c | 14 | 0° | .165 | .007 | .079 | .004 | Absorption disregarded. Inelastic scattering from oxygen treated as elastic. |
| 16d | 14 | 0° | .064 | .004 | .023 | .002 | Inelastic scattering treated as absorption. |

(†) Isotropic source.

### 6.2. Differential Albedo

Tables 1 to 16d of appendix C contain the Monte Carlo results for the differential albedo in the form in which they were printed out by the computer. The number of reflected neutrons (for $N_0=3{,}000$ neutrons) is given in a two-way classification according to the spectral energy, $E$, and the cosine of the obliquity of emergence, $\cos\theta$. By normalizing the entries in the tables, i.e., by dividing through by $N_0$, one obtains an estimate of the differential albedo averaged over a small energy-angle interval. Unnormalized numbers are given in the tables in order to preserve their statistical significance, the standard deviation of each entry being proportional to its square root. The energy classification is divided into 10 intervals, labeled $i=1, 2, \ldots 10$, such that the $i$th interval pertains to neutrons with energies between $(11-i)/10E_0$ and $(10-i)/10E_0$. The last interval extends from $E_0/10$ to 0.5 ev rather than to zero energy. The obliquity classification is also divided into 10 intervals, labeled $k=1, 2, \ldots, 10$, such that the $k$th interval pertains to neutrons with obliquity cosines between $(1-k)/10$ and $-k/10$. Two sets of marginal totals are also given which represent the angular distribution integrated over all energies, and the spectral distribution integrated overall directions, respectively.

### 6.3. Number Albedo and Energy Albedo

Table 6.1 contains all the results obtained for the number albedo $A_N$ and the energy albedo $A_E$.[19] The number albedo was obtained by adding the marginal totals in the corresponding differential-albedo tables and dividing the result by $N_0=3{,}000$. The energy albedo was obtained as the product of the number albedo and the average energy $\bar{E}$ of the reflected neutrons. In most of the calculations $A_E$ was computed directly in the course of the machine calculations. In some of the earlier cases, $\bar{E}$ had to be estimated from the differential-albedo tables.[20] Numerical experimentation indicated that such estimates could be made with an accuracy of approximately 1 percent. Values of the energy albedo based on such estimates of $\bar{E}$ are indicated in table 6.1. by being placed in parentheses.

The standard deviations $\delta A_N=\sqrt{\text{var } A_N}$ and $\delta A_E=\sqrt{\text{var } A_E}$ are also shown in table 6.1. They were computed according to (5.27) and (5.31), respectively. The determination of $\delta A_E$ required knowledge of $\bar{E}$ as well as of $\overline{E^2}$. Accordingly, $\delta A_E$ is given only for those cases in which $\overline{E^2}$ was obtained as direct output of the machine program. The relative standard deviation $\delta A_N/A_N$, obtained with 3,000 histories, is of the order of 0.05. The corresponding relative standard deviation $\delta A_E/A_E$, in the cases examined and presumably also in the other cases, is roughly 1½ times greater than $\delta A_N/A_N$.

## 7. Analysis of the Results

### 7.1. Single-Scattering Contribution to the Albedo

Table 7.1 contains a summary of the ratios $A_N^{(1)}/A_N$ and $A_E^{(1)}/A_E$ for various cases. In general, single scattering contributes about 20 percent of the number albedo and more than 50 percent of the energy albedo. The contributions are particularly large at 1 Mev, because at this energy the ratio of the scattering cross section of oxygen to that of hydrogen is large, and the differential oxygen scattering cross section has a peak in the backward direction.

---

[19] In sec. 5.3. the albedo estimates were indicated by $A^*_N$ and $A^*_E$ in order to distinguish them from the true values $A_N$ and $A_E$. In the following, we shall ignore this distinction and simply use $A_N$ and $A_E$ to label the Monte Carlo results.

[20] The most accurate estimation procedure was found to be one based on the "cumulative albedo" $\int_0^E dE' \int_{\pi/2}^{\pi} \sin\theta d\theta A(E',\theta;E_0,\theta_0)$, which can be obtained from the differential-albedo tables for $E_i=i/10E_0$, $i=1, 2, \ldots 10$, and by interpolation for other values of $E$. It was also necessary to take into account the characteristics of the spectrum of the single-scattering albedo, in order to obtain good accuracy.

The estimation of the albedo ratios is a problem with maximal correlation as defined in section 5.4. We have estimated the standard deviations of these ratios in a few typical cases and find, for example, that $A_N^{(1)}/A_N=0.30\pm0.03$ and $A_E^{(1)}/A_E=0.61\pm0.02$ for $E_0=1$ Mev and $\theta_0=0°$.

The ratio $A_E^{(1)}/A_E$ is a relatively slowly varying function of the source energy, whereas $A_E^{(1)}$ and $A_E$ separately vary rapidly. This suggests that the energy albedo for arbitrary energies could be obtained with fair accuracy by combining a single-scattering calculation with an interpolated value of $A_E^{(1)}/A_E$.

TABLE 7.1. *Ratio of single-scattering albedo to total albedo. (The results for 6, 9, and 14 Mev correspond to cases 14a, 15a, and 16a, respectively, as listed in table 6.1).*

| | $\frac{A_N^{(1)}}{A_N}$ | | | | | | $\frac{A_E^{(1)}}{A_E}$ | | | | | |
|---|---|---|---|---|---|---|---|---|---|---|---|---|
| $E_0$ (Mev) \ $\theta_0$ | 0° | 45° | 60° | 75° | 90° | | $E_0$ (Mev) \ $\theta_0$ | 0° | 45° | 60° | 75° | 90° |
| 0.3 | 0.11 | | | | | | 0.3 | 0.54 | | | | |
| 1 | .30 | 0.25 | 0.27 | 0.34 | 0.64 | | 1 | .61 | 0.54 | 0.54 | 0.60 | 0.84 |
| 3 | .17 | .15 | .21 | .30 | .66 | | 3 | .55 | .45 | .48 | .58 | .85 |
| 6 | .22 | | | | | | 6 | .54 | | | | |
| 9 | .17 | | | | | | 9 | .42 | | | | |
| 14 | .27 | | | | | | 14 | .50 | | | | |

## 7.2. Contribution of Higher Orders of Scattering

Figure 6 shows the contributions of successive orders of scattering to the albedo for a few typical cases. As many as twenty orders are shown to contribute to the number albedo,[21] whereas only about five orders contribute significantly to the energy albedo. The relative importance of the first few orders of scattering increases with the source obliquity and energy. In general, an analytical orders-of-scattering approach does not seem to provide a practical alternative to a Monte Carlo calculation. The contribution of the second order of scattering is not sufficient for a precise albedo determination, and calculations for the higher orders would be prohibitively complex.

## 7.3. Energy Spectra of Reflected Neutrons

Figure 7 contains histograms of the energy distribution of reflected neutrons for incident 1-Mev beams with various obliquities. The contributions of single scattering and multiple scattering to the spectra are indicated. The spectra are characterized by two rather sharp peaks: one, primarily due to single scattering, occurs at the upper end of the spectra; the other, due to multiple scattering, at the low-energy end. The single-scattering contribution can in turn be resolved into two components, due to scattering from oxygen and hydrogen. For perpendicular incidence, only single-scattering reflection from oxygen occurs. As the source obliquity is increased, hydrogen scattering becomes possible, and the oxygen contribution is shifted toward higher energies. At 45° and 60° the oxygen and hydrogen components are clearly separated, whereas at 75° and 90° they merge. In the limiting case of grazing incidence there is a hydrogen component distributed uniformly over all energies, and an oxygen component which gives rise to a peak at an energy slightly below the source energy. Further details about the oxygen single-scattering contribution can be obtained from appendix B (fig. 15). The energy spectra for other cases are similar to those shown in figure 7 and can be obtained from the tables in appendix C.

[21] Some contributions from orders beyond the twentieth would have occurred if our calculations had not been cut off at an energy of 0.5 ev.

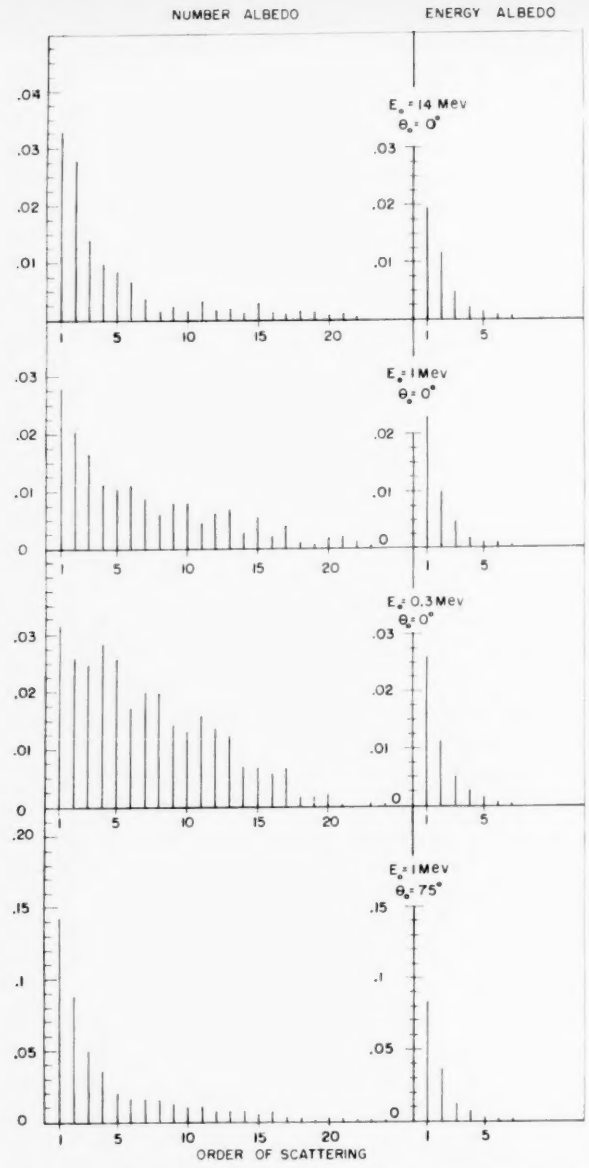


FIGURE 6. *Contributions of successive orders of scattering to the albedo.*

## 7.4. Angular Distribution of Reflected Energy

Figure 8 shows plots, in histogram form, of the quantity

$$A_E(\theta; E_0, \theta_0) = \int_0^{E_0} A(E, \theta; E_0, \theta_0) \frac{E}{E_0} dE, \tag{7.1}$$

for $E_0 = 3$ Mev and various values of $\theta_0$.[22] The angular distribution is dominated by the single-scattering contribution. In particular, it should be noted that for large source obliquities the distribution does not follow the cosine-law which holds for perpendicular incidence and has often been assumed to be universally valid. Rather the emerging radiation tends to peak for $\cos\theta = 0$; i.e., in directions parallel to the boundary of the semi-infinite medium. This is due to

[22] The histograms are a somewhat crude estimate of the angular distribution, because each angular element was obtained by multiplying the differential element of the corresponding table in app. C by the midpoint of the appropriate energy interval and then summing over-all energy intervals.

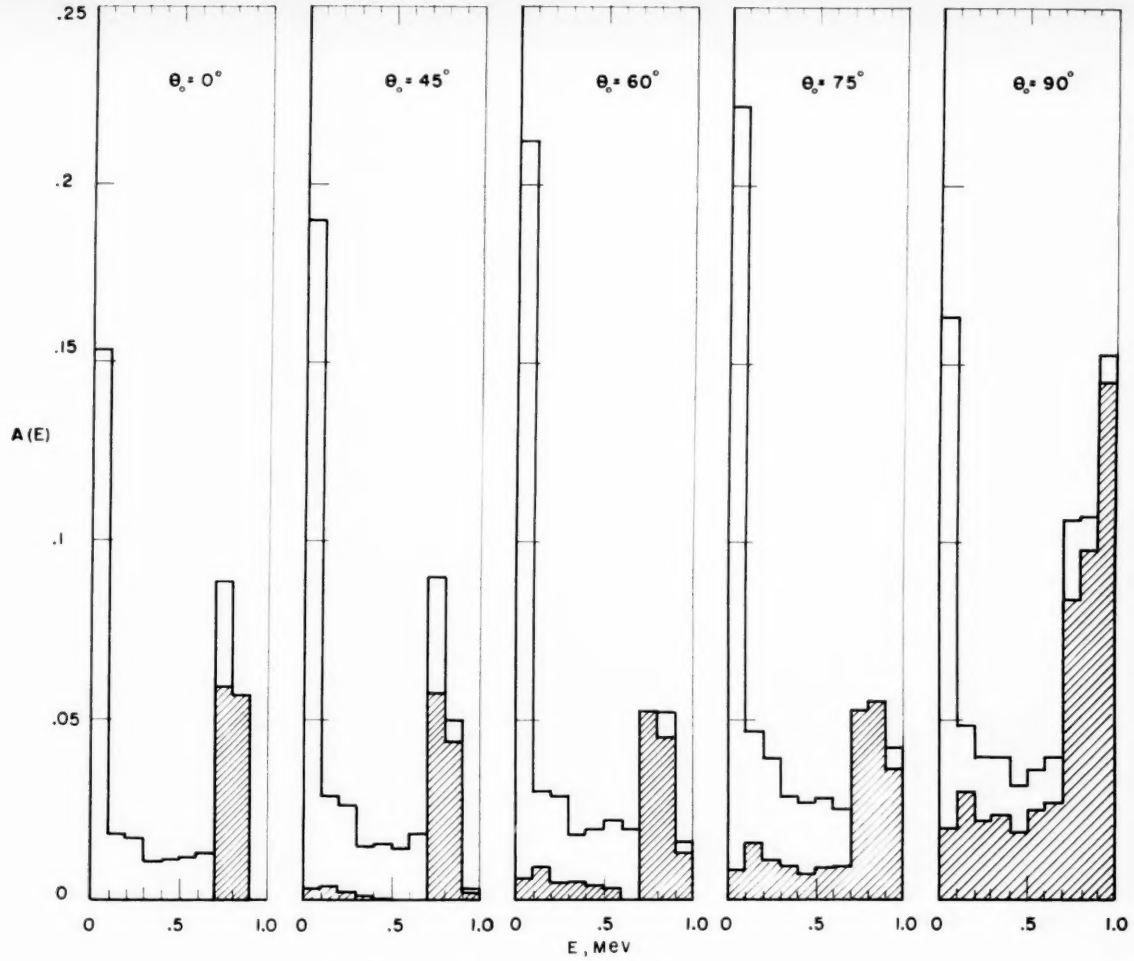


FIGURE 7. *Energy spectra of reflected neutrons.*
The shaded areas indicate the contribution of single-scattering. Source energy 1 Mev.

the behavior of the single-scattering component. For $E_0=3$ Mev and $\theta_0=90°$, we find from eq (A.21), (A.22), and (A.24) of appendix A, and from the cross sections given in figure 2, that

$$A_E^{(1)} \sim 0.049(1.00+1.05 \sin^2\theta+7.14 \sin^3\theta), \tag{7.2}$$

which is in agreement with the Monte Carlo calculations.

### 7.5. Dependence of Albedo on Source Energy and Obliquity

The dependence on the source energy is irregular. It is correlated with the complicated energy-dependence of the attenuation coefficient for water, and is further influenced by the relative probabilities for scattering by hydrogen and oxygen, and by the energy-dependent anisotropy of elastic scattering from oxygen. Just like the attenuation coefficient, the number albedo and energy albedo have a peak at 1 Mev where they are 2 to 3 times larger than at the other energies considered. The correlation between attenuation coefficients and albedo is complicated, however, by the interaction of the various factors, so that interpolation with respect to source energy is not easy, and is perhaps done best by the single-scattering analysis indicated in section 7.1.[23]

[23] For the analysis of an albedo experiment with a broad source spectrum (such as the Po-Be source used by Strickler, Gilbert, and Auxier [16]), it might be preferable to make a Monte Carlo calculation with a realistic source spectrum instead of combining the results of calculations for monoenergetic sources.

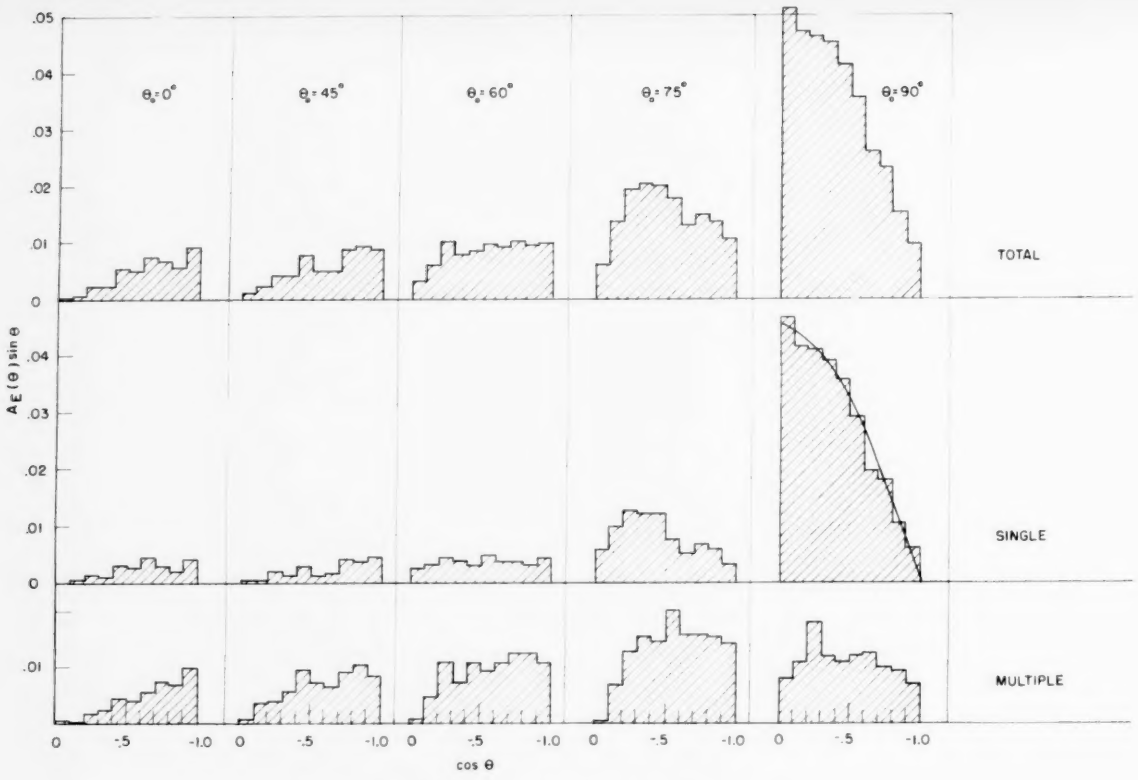


FIGURE 8. *Angular distribution of reflected energy.*
Source energy 3 Mev. A single-scattering curve for $\theta_0=90°$ is shown which corresponds to eq (7.2).

The dependence on the source obliquity is smooth and interpolation should be easy. By way of example, figure 9 contains curves of $A_N$ and $A_E$ as functions of $\theta_0$, for source energies of 1 and 3 Mev. All four curves shown have similar shapes, starting out with a rather flat slope near $\theta_0=0°$ and rising very steeply near $\theta_0=90°$. The closer $\theta_0$ is to grazing incidence, the smaller are the differences of the albedos for different source energies.

## 7.6. Effect of Absorption and Inelastic Scattering

If absorption were disregarded, the number albedo at 6 Mev would be increased by 9 percent and the energy albedo by 13 percent. At 9 Mev, the corresponding increases would be 29 percent and 52 percent, respectively. The effect of absorption is greater on the energy albedo than on the number albedo because the relative probability of absorption is an increasing function of the energy (up to 14 Mev). The effect of absorption on the energy spectrum is shown in figure 10. Although the effect is large, it introduces no large uncertainty into the calculations because the cross section for $n-\alpha$ and $n-p$ processes are reasonably well-known.

The effect of inelastic scattering is more difficult to determine because so little is known about the cross section for this process. We have made computations under three different assumptions: (1) Absorption taken into account, inelastic scattering assumed to excite oxygen to a level 6.1 Mev above the ground state; (2) absorption taken into account, inelastic scattering also treated as absorption; (3) absorption disregarded, inelastic scattering treated as if it were elastic.

As has been discussed in section 3.2, assumption (1) is presumably the most realistic. Assumption (3) is the least realistic and has been included mainly because it has often been made in previous neutron transport calculations. Assumptions (1) and (2) are limiting assumptions in the sense that they allow for the minimum and maximum possible energy loss that a neutron

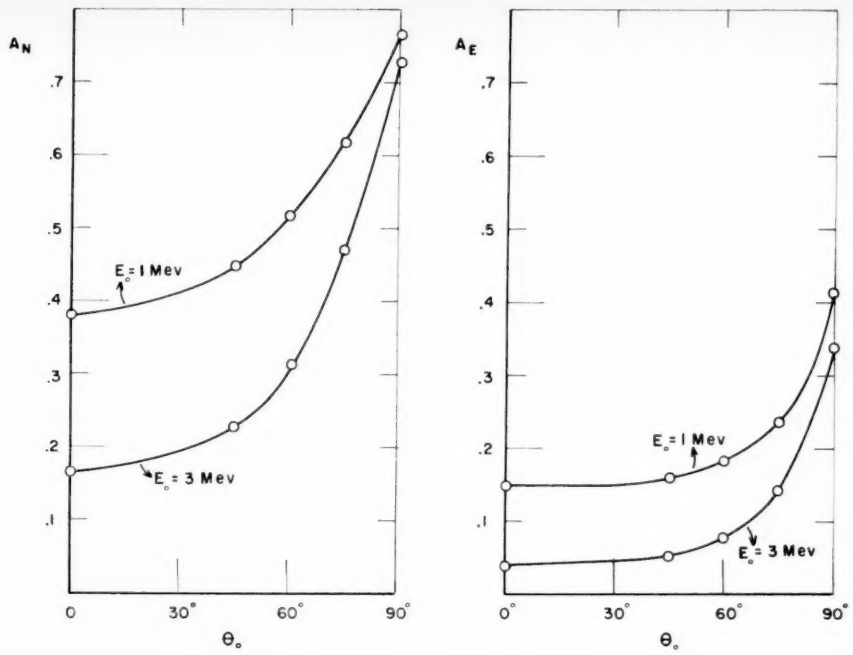


FIGURE 9. *Dependence of albedo on source obliquity.*

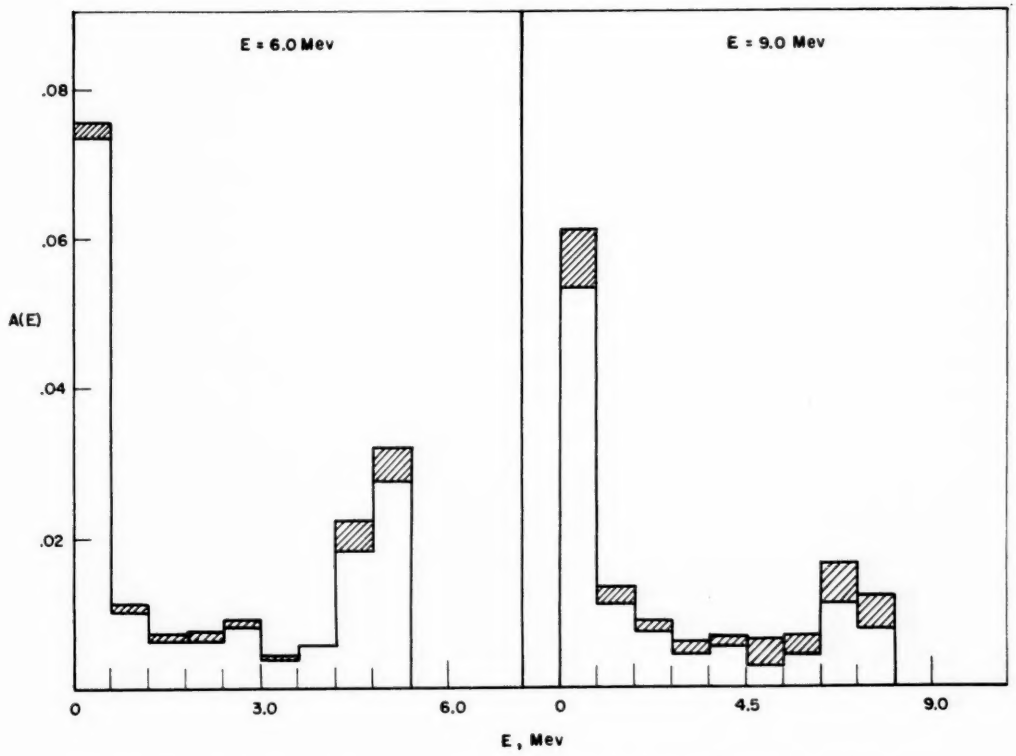


FIGURE 10. *Reduction of energy spectrum due to absorption, indicated by shaded areas.*
Perpendicular incidence.

could suffer in an inelastic collision. The albedo calculated on assumption (3) is almost twice as great as that calculated on the realistic assumption (1), whereas the albedo calculated on assumption (2) is only about half as large. These extreme variations point up the need for accurate knowledge of the inelastic scattering cross section.

The energy spectra obtained with a 14-Mev source under the three assumptions are shown in figure 11. The spectrum in case (1) shows three peaks, due to elastic single scattering, inelastic single scattering, and multiple scattering. The inelastic scattering peak disappears in case (2) and merges with the peak due to elastic single scattering in case (3). More accurate treatment of inelastic scattering would probably give a spectrum similar to that of case (1), but with the middle peak reduced in size and "smeared out" over the lower part of the spectrum.

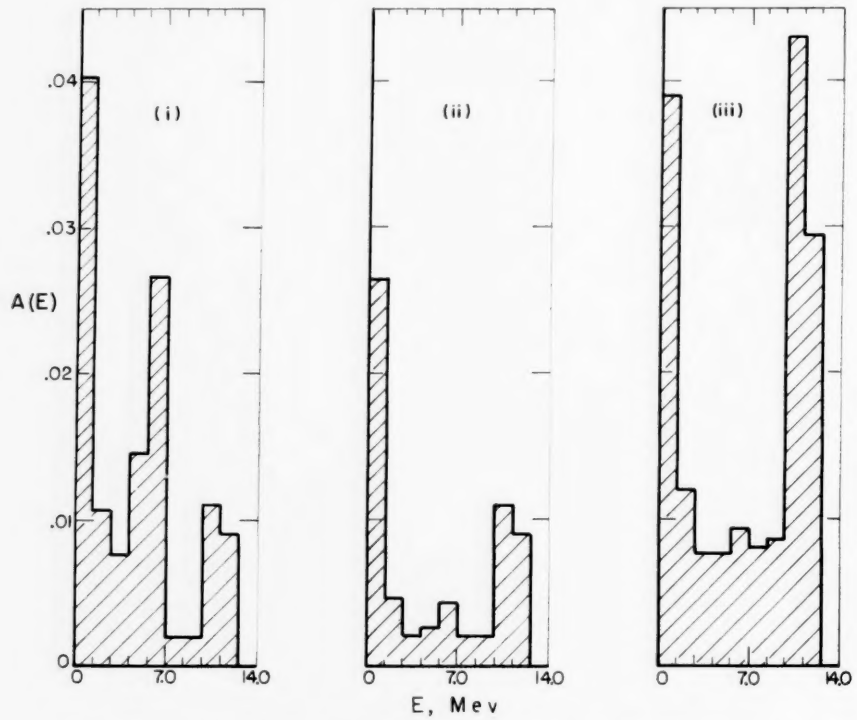


FIGURE 11. *Effect of inelastic scattering on the energy spectrum.*

Source energy 14 Mev. Histograms (i), (ii), and (iii) correspond to the different assumptions in sec. 7.6, and were obtained from tables 16a 16d, and 16e of app. C, respectively. Perpendicular incidence.

### 7.7. Effect of the Anisotropy of Elastic Scattering

The differential elastic scattering cross section is not well-known for most elements. It is therefore of interest to know how much the albedo would be changed by a change of the assumed distribution of elastic scattering deflections. To explore this situation, we have compared the albedo calculated with the best available cross sections for oxygen (reference [9], see also fig. 3) with the albedo calculated on the assumption that the elastic scattering deflections from oxygen are isotropic in the center-of-mass system. The difference between the two assumptions is greater than any expected realistic modification of the oxygen cross sections. Comparisons were made for source energies at 1, 3, and 14 Mev. At 1 Mev, $A_N$ is decreased by 2.5 percent and $A_E$ by 11 percent. Finally, at 14 Mev, $A_N$ is increased by 31 percent, whereas $A_E$ is decreased by 5 percent. In figure 12 the spectra obtained under the two different assumptions

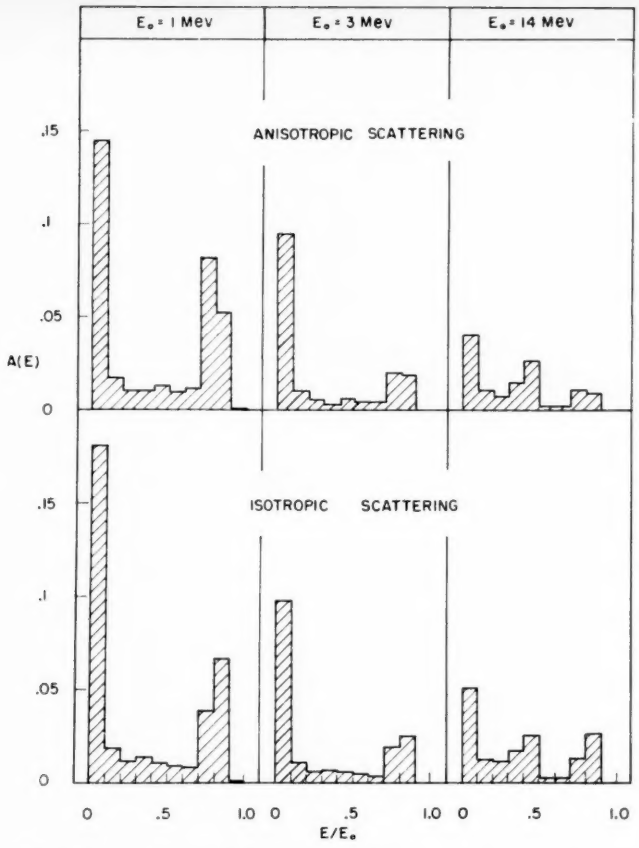


FIGURE 12. *Effect of anisotropy of elastic scattering from oxygen on the energy spectrum.*
Perpendicular incidence.

are compared. There is relatively little change, the main effect being a shift of the single-scattering peak toward higher energies in the case of isotropic scattering.

The albedo differences quoted above were obtained by correlated sampling (case of partial correlation). A listing of all significant statistical parameters for the comparison at 14 Mev is given in table 7.2 from which it appears that by means of correlated sampling an accuracy was achieved that would have required a sample size 3 to 4 times as large with ordinary sampling.

TABLE 7.2. *Estimate of albedo difference by correlated sampling*

Source energy 14 Mev, perpendicular incidence. Elastic scattering from oxygen assumed to be anisotropic in case 16a, isotropic in case 16b.

| *Number albedo:* | *Energy albedo:* |
|---|---|
| $\tilde{A}_N$, case 16a, | $\tilde{A}_E$, case 16a, |
| $A_N$, case 16b, | $A_E$, case 16b, |
| $A_N-\tilde{A}_N=0.039\pm0.005$ (with correlated sampling), $\pm0.009$ (without correlated sampling), | $A_E-\tilde{A}_E=-0.0012\pm0.0016$ (with correlated sampling), $\pm0.0033$ (without correlated sampling), |
| Correlated sampling increases effective sample size by factor 2.9, | Correlated sampling increases effective sample size by factor 3.9, |
| Correlation coefficient $\rho=0.664$, | Correlation coefficient $\rho_E=0.771$. |
| Maximal correlation coefficient $\rho_{max}=0.853$, | |

## 7.8. Low-Energy End of the Spectrum

Details of the low-energy part of the spectrum were obtained as a byproduct of the detailed information obtained for the statistical analysis of the correlated calculations at 14 Mev. Figure 13 shows a plot of the spectrum on a logarithmic scale which emphasizes the low energies. The spectral shape at low energies is quite similar to that obtained by Spinney [5] who calculated by age theory the albedo for 2-Mev neutrons incident on concrete. This suggests that computations of the spectrum down to very low energies could advantageously be done by a combination of Monte Carlo and age theory, with Monte Carlo covering the energy region not very far below the source energy in which age theory does not apply.

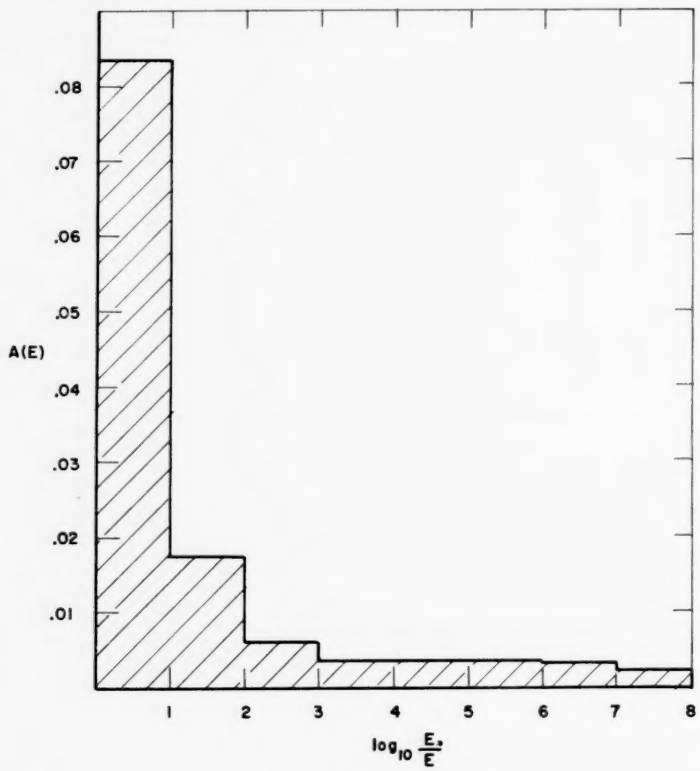


FIGURE 13. *Energy spectrum of reflected neutrons on semilog scale.*
Source energy 14 Mev, perpendicular incidence.

## 7.9. Slab Albedo

The deeper a neutron penetrates into the medium, the smaller is its chance of returning. Therefore, the collisions leading to reflection take place rather close to the surface of the medium, and thin slabs have nearly the same reflecting power as a semi-infinite medium. This is shown by the results in figure 14 pertaining to the reflection of 3-Mev neutrons incident on slabs with thicknesses of 2, 5, 10, and 20 cm. (These thicknesses are to be compared with the transport mean-free path in water at 3 Mev which is 5.1 cm.) The dependence of the number albedo on the slab thickness is similar to that found by Foderaro and Obenshain [6] at 0.89 Mev. The energy albedo reaches a limiting value at an even smaller slab thickness than the number albedo, because the energy degradation in successive collisions makes it necessary for a neutron to be reflected very early in its history if it is to carry back an appreciable amount of energy.

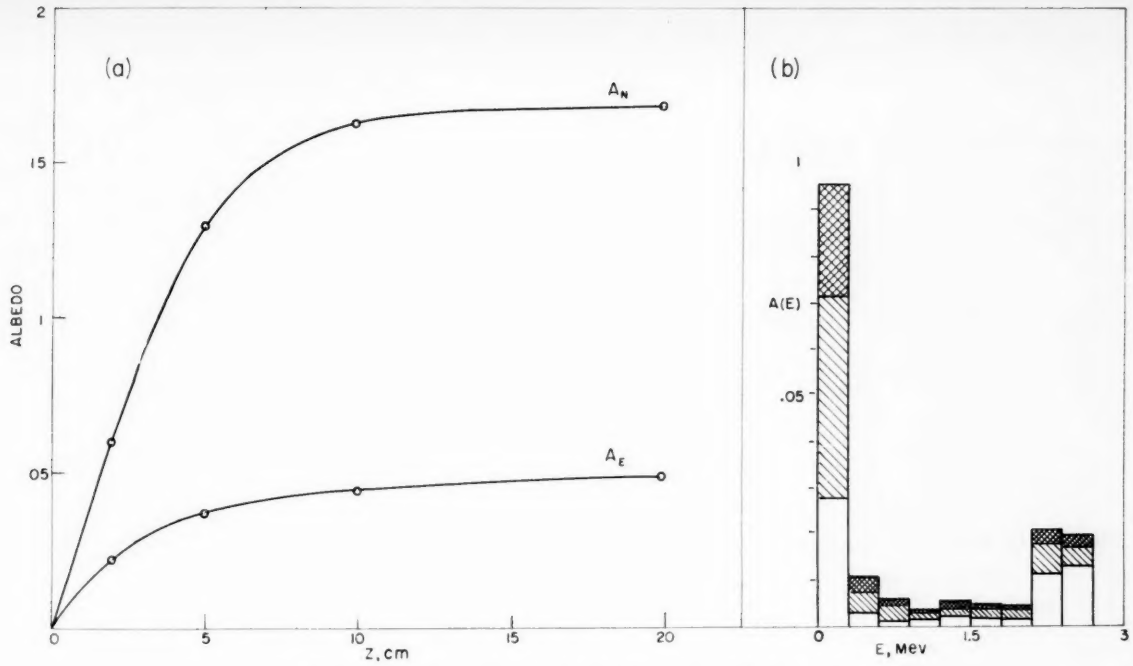


FIGURE 14. *Dependence of slab albedo on slab thickness.*
Source energy 3 Mev, perpendicular incidence. a. Number and energy albedo and b. Energy spectrum.

## 8. Appendix A. Integrals Over the Differential Single-Scattering Albedo

### 8.1. Energy Spectrum

The evaluation of (4.15) leads to the following expression for the energy spectrum of neutrons reflected from a semi-infinite medium after exactly one collision:

$$A^{(1)}(E;E_0,\theta_0)=\sum_{j=1}^{3}p_j(E_0)F_j(E;E_0)\{U(a_j,b_j)-kV(a_j,b_j)\}, \tag{A.1}$$

where

$$\begin{aligned} a_j&=\cos\,(\alpha_j+\theta_0)\\ b_j&=\cos\,(\alpha_j-\theta_0)\\ k&=(\lambda_0/\lambda)\,\cos\,\theta_0, \end{aligned} \tag{A.2}$$

and where $U(a_j,b_j)$ and $V(a_j,b_j)$ are defined as follows:

(1) If $E_0\left[\dfrac{\sqrt{M_j^2K_j^2-\cos^2\theta_0}+\sin\,\theta_0}{M_j+1}\right]^2\leq E\leq E_0$,

$$U(a_j,b_j)=V(a_j,b_j)=0. \tag{A.3}$$

(2) If $E_0\left[\dfrac{\sqrt{M_j^2K_j^2-\cos^2\theta_0}-\sin\,\theta_0}{M_j+1}\right]^2\leq E\leq E_0\left[\dfrac{\sqrt{M_j^2K_j^2-\cos^2\theta_0}+\sin\,\theta_0}{M_j+1}\right]^2$,

$$U(a_j,b_j)=\frac{1}{2}-\frac{1}{\pi}\sin^{-1}\frac{b_j+a_j}{b_j-a_j}, \tag{A.4}$$

$$\left.\begin{aligned}
&\text{if } k<b_j,\quad V(a_j,b_j)=\frac{1}{\pi\sqrt{(b_j-k)(k-a_j)}}\{\log(b_j-a_j)k-\log[(b_j+a_j)k-2a_jb_j\\
&\qquad\qquad -2\sqrt{a_jb_j(b_j-k)(a_j-k)}]\};\\
&\text{if } k=b_j,\quad V(a_j,b_j)=\frac{2}{\pi(b_j-a_j)}\sqrt{\frac{-a_j}{b_j}};\\
&\text{if } k>b_j,\quad V(a_j,b_j)=\frac{1}{\sqrt{(k-b_j)(k-a_j)}}\left\{\frac{1}{2}-\frac{1}{\pi}\sin^{-1}\left[\frac{(b_j+a_j)k-2a_jb_j}{(b_j-a_j)k}\right]\right\}.
\end{aligned}\right\} \tag{A.5}$$

(3) If $E_0\left[\frac{M_jK_j-1}{M_j+1}\right]^2\leq E\leq E_0\left[\frac{\sqrt{M_j^2K_j^2-\cos^2\theta_0}-\sin\theta_0}{M_j+1}\right]^2$

$$U(a_j,b_j)=1 \tag{A.6}$$

$$V(a_j,b_j)=\frac{1}{\sqrt{(k-b_j)(k-a_j)}} \tag{A.7}$$

(4) If $E\leq E_0\left[\frac{M_jK_j-1}{M_j+1}\right]^2$

$$U(a_j,b_j)=V(a_j,b_j)=0. \tag{A.8}$$

In certain limiting cases, the formula for the energy spectrum becomes much simpler than the above expressions. For perpendicular incidence, the energy must lie in the range

$$E_0\left[\frac{M_jK_j-1}{M_j+1}\right]^2\leq E\leq E_0\frac{M_j^2K_j^2-1}{(M_j+1)^2}, \tag{A.9}$$

and the spectrum is

$$A^{(1)}(E;E_0,0)=\sum_{j=1}^{3}p_j(E_0)F_j(E;E_0)\frac{1}{1-\frac{\lambda_0}{\lambda\cos\alpha_j}}. \tag{A.10}$$

For grazing incidence ($\theta_0\to\pi/2$), the energy range is

$$E_0\left[\frac{M_jK_j-1}{M_j+1}\right]^2\leq E\leq E_0\left[\frac{M_jK_j+1}{M_j+1}\right]^2 \tag{A.11}$$

and the spectrum is

$$A^{(1)}\left(E;E_0,\frac{\pi}{2}\right)=\sum_{j=1}^{3}p_j(E_0)\frac{1}{2}F_j(E;E_0). \tag{A.12}$$

Figure 15 shows energy spectra of neutrons reflected after a single scattering from a semi-infinite medium of pure oxygen ($E_0=1$ Mev, $\theta_0=0°$, 45°, and 90°). These spectra were obtained by numerical evaluation of the factor

$$F_2(E;E_0)\{U(\alpha_2,b_2)-kV(\alpha_2,b_2)\}$$

in (A.1). They are characterized by a peak at the low-energy limit which is rather independent of the source obliquity $\theta_0$. In addition there is another peak at the high-energy limit in the case of grazing incidence.

For perpendicular and grazing incidence the spectrum for reflection from water can be derived very simply from the corresponding spectrum for oxygen. For $\theta_0=0°$, reflection from hydrogen is impossible after one scattering, and it is sufficient to renormalize the oxgyen spectrum in figure 15, multiplying it by $p_2(E_0)=0.485$. For $\theta_0=90°$, one must not only normalize the oxygen contribution but also add a hydrogen contribution which is energy-independent and has the value $p_1(E_0)\frac{1}{2}F_1(E;E_0)=0.515\ (1/2E_0)=0.2575$.

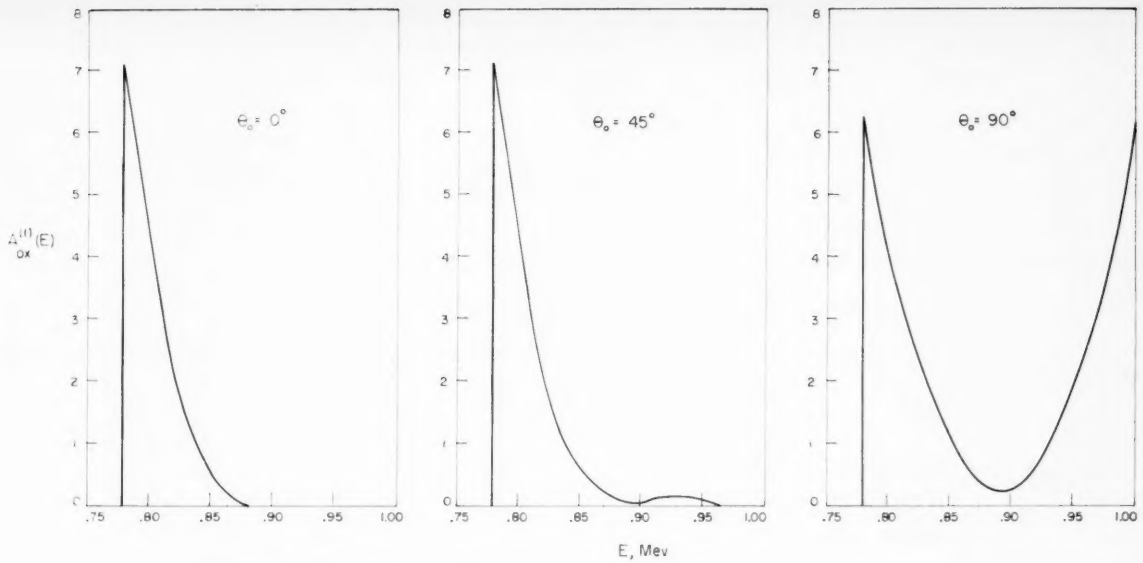


FIGURE 15. *Energy spectrum of neutrons reflected after one collision.*
Source energy 1 Mev, oxygen medium.

## 8.2. Angular Distribution

The angular distribution of neutrons reflected after one collision is even more complicated than their energy spectrum. We shall confine ourselves to the discussion of some limiting cases. The characteristics of the angular distribution are expressible in terms of the integrals

$$h_j(\theta;E_0,\theta_0)=\int \frac{H_j(E,\theta;E_0,\theta_0)\cos\theta}{\cos\theta-(\lambda_0/\lambda)\cos\theta_0}\,dE \tag{A.13}$$

which are needed for the evaluation of (4.16). The angular distribution of reflected energy, $A_E^{(1)}(\theta;E_0,\theta_0)$, depends on the integrals

$$h_{Ej}(\theta;E_0,\theta_0)=\int \frac{H_j(E,\theta,E_0;\theta_0)\cos\theta}{\cos\theta-(\lambda_0/\lambda)\cos\theta_0}\,E\,dE. \tag{A.14}$$

The integrations in (A.13) and (A.14) are facilitated by changing the variable of integration from $E$ to $\cos\alpha_j$, noting that

$$E=E_0\left[\frac{\cos\alpha_j+\sqrt{\cos^2\alpha_j+M_j^2K_j^2-1}}{M_j+1}\right]^2 \tag{A.15}$$

and that

$$\frac{dE}{d\cos\alpha_j}=\frac{2E_0}{(M_j+1)^2}\left\{2\cos\alpha_j+\sqrt{M_j^2K_j^2-\sin^2\alpha_j}+\frac{\cos^2\alpha_j}{\sqrt{M_j^2K_j^2-\sin^2\alpha_j}}\right\}. \tag{A.16}$$

We now take up limiting cases, and drop the index $j$ for simplicity.

CASE (1): Heavy nucleus, $M\gg 1$
Perpendicular incidence, $\theta_0=0°$
Elastic scattering, $K=1$.

Note that

$$\left.\begin{aligned} &E\approx E_0, \quad \lambda\approx\lambda_0, \\ &\frac{dE}{d\cos\alpha}\approx\frac{2E_0}{M}, \\ &\Theta_c\approx\alpha, \quad F(E;E_0)\approx\frac{M}{2E_0}f(\alpha;E_0) \end{aligned}\right\} \tag{A.17}$$

Substituting expression (4.13) for $H(E,\theta;E_0,0)$, we find that

$$h(\theta;E_0,0)\approx\frac{\cos\theta f(\alpha;E_0)}{\cos\theta-1}, \tag{A.18}$$

and that

$$h_E(\theta;E_0,0)\approx E_0 h(\theta;E_0,0) \tag{A.19}$$

Case (2): Heavy nucleus, $M\gg1$
Grazing incidence, $\theta_0=90°$
Elastic scattering, $K=1$.

The approximations (A.17) may again be used. For $H\left(E,\theta;E_0,\frac{\pi}{2}\right)$ we substitute expression (4.14), the result being

$$h\left(\theta;E_0,\frac{\pi}{2}\right)=\frac{1}{\pi}\int_{-\sin\theta}^{\sin\theta}\frac{f(\alpha;E_0)\,d\cos\alpha}{\sqrt{\sin^2\theta-\cos^2\alpha}}. \tag{A.20}$$

Assuming for $f(\alpha;E_0)$ a Legendre expansion of the type (3.9), with expansion coefficients $fl\,(E_0)$, we can integrate (A.20) and find that

$$h\left(\theta;E_0,\frac{\pi}{2}\right)=\sum_{l=0}^{\infty}\frac{4l+1}{2}f_{2l}(E_0)\,(-1)^e\frac{(2l)!}{2^{2e}l!\,l!}P_{2l}(\cos\theta), \tag{A.21}$$

and that

$$h_E\left(\theta;E_0,\frac{\pi}{2}\right)\approx E_0 h\left(\theta;E_0,\frac{\pi}{2}\right). \tag{A.22}$$

Case (3): Hydrogen nucleus, $M=1$
Grazing incidence, $\theta_0=90°$.

We have $f(\Theta_c;E_0)=1/2$ and $0\leq\alpha\leq\pi/2$. Using (A.14), (A.15), and (A.16), we find that

$$h\left(\theta;E_0,\frac{\pi}{2}\right)=\frac{2}{\pi}\int_0^{\sin\alpha}\frac{\cos\alpha d\cos\alpha}{\sqrt{\sin^2\theta-\cos^2\alpha}}=\frac{2}{\pi}\sin\theta, \tag{A.23}$$

and that

$$h_E\left(\theta;E_0,\frac{\pi}{2}\right)=\frac{2E_0}{\pi}\int_0^{\sin\theta}\frac{\cos^3\alpha d\cos\alpha}{\sqrt{\sin^2\theta-\cos^2\alpha}}=\frac{4E_0}{3\pi}\sin^3\theta. \tag{A.24}$$

## 9. Appendix B. Pseudorandom Numbers Generated by Congruential Multiplication

### 9.1. Proof of Their Uniform Distribution

We consider the pseudorandom number sequence $\{\xi_n=2^{-35}x_n\}$ $(n=0,1,\ldots,2^{33}-1)$ derived from a sequence of integers $\{x_n\}$ which is generated according to (5.4) or by the equivalent rule

$$x_n=c5^{kn} \bmod 2^{35}, \tag{B.1}$$

where $c$ and $k$ are odd integers. The sequence $\{\xi_n\}$ consists of $2^{33}$ different numbers which are distributed with uniform density over the interval (0,1). This can be proved with the use of standard number-theoretical results [17]. However, Dr. Morris Newman[24] has given a simple proof proceeding from first principles which we reproduce here in a somewhat amplified form.

The uniformity of the distribution of the pseudorandom numbers obtained by congruential multiplication is a consequence of the following theorem.

THEOREM: *The sequence of integers*

$$\{x_0, x_1, x_2, \ldots, x_2^{33}-1\} \tag{B.2}$$

*generated according to* (B.1), *is a permutation of the sequence*

$$\{1, 5, 9, \ldots, 2^{35}-3\} \tag{B.3}$$

*or of the sequence*

$$\{3, 7, 11, \ldots, 2^{35}-1\} \tag{B.4}$$

*depending on whether the starting number $x_0=c$ has remainder 1 or 3 when divided by 4.*

The proof of this theorem is based on the following lemma:

*The integer $5^{k2^M}-1$ is divisible by $2^{M+2}$ but by no higher power of 2, if* k *is an odd integer.*

To see this we consider the factorization

$$5^{k2^M}-1=(5^{k2^{M-1}}+1)(5^{k2^{M-1}}-1)=(5^{k2^{M-1}}+1)(5^{k2^{M-2}}+1)\ \ldots\ (5^k+1)(5^k-1). \tag{B.5}$$

The factor

$$5^k-1=(1+4)^k-1=4k+\sum_{j=2}^{k}\binom{k}{j}4^j \tag{B.6}$$

is divisible by 4 but by no higher power of 2. The other factors in (B.5) have the form

$$5^{k2^m}+1=(1+4)^{k2^m}+1=2+\sum_{j=1}^{k2^m}\binom{k2^m}{j}4^j, 0\leq m\leq M-1 \tag{B.7}$$

and are each divisible by 2 but by no higher power of 2. By combining all the factors we obtain the lemma.

We now consider the sequence $\{c5^{kn}\}$, $n=0,1, \ldots 2^{33}-1$. The difference between any two terms in this sequence, say $c5^{k(n+n')}$ and $c5^{kn}$, can be expressed as

$$\Delta(n,n')=c5^{kn}(5^{kn'}-1). \tag{B.8}$$

We may set

$$n'=2^a b, \tag{B.9}$$

where $a$ is an integer $<2^{33}$, and where $b$ is an odd integer. By application of the lemma it follows that $5^{kn'}-1$, and therefore $\Delta(n,n')$, is divisible only by powers of 2 smaller than $2^{35}$. This implies that the integers $x_n$ in the sequence (B.2) are all different from each other.

It can be seen from (B.8) that the differences between the $x_n$'s are all multiples of 4. Thus two different sequences $\{x_n\}$ can be formed, one of which is a permutation of (B.3) and the other of (B.4), depending on the starting number $c$. Each of the two sequences contains $2^{33}$ numbers, and there is no overlap between them, so that together they exhaust the $2^{34}$ odd integers $<2^{35}$. This completes the proof of the theorem. Finally, we note that by computing the $x_n$'s modulo $2^N$ rather than modulo $2^{35}$, and by using a starting number $c$, that is not odd but contains a factor $2^\gamma$, one would obtain a sequence of $2^{N-2-\gamma}$ different numbers.

[24] Informal memorandum, Applied Mathematics Laboratory, NBS, Oct. 27, 1951.

### 9.2. Statistical Indications of Their Randomness

In order to be acceptable as a source of random numbers for a Monte Carlo calculation, the pseudorandom number sequence $\{\xi_n\}$ must fulfill the following requirements:

(1) In any subsequence of reasonable length, such as would be used in generating neutron histories, the $\xi_n$'s must be distributed with uniform density in the interval (0,1).

(2) Successive $\xi_n$'s must be uncorrelated.

These two conditions cannot be satisfied rigorously, but empirical statistical tests indicate that they are satisfied in very good approximation. For example, elaborate tests on 16,384 pseudorandom numbers have been reported in the memorandum mentioned in footnote 24.

We have made some rough-and-ready statistical tests on 237,000 pseudorandom numbers that were used to generate a set of 3,000 neutron histories.[25] These numbers were divided into three sets, corresponding to the three types of pseudorandom number sequences (primary, secondary, and tertiary) described in section 5.4. Set $P$ includes the numbers in the primary sequence, set $S$ the numbers in all the secondary sequences, and set $T$ the numbers in all the tertiary sequences. Separate tests were applied to each set. In order to gauge the uniformity of the distribution of the numbers, we computed the averages $\overline{\xi_n}$ and $\overline{\xi_n^2}$. In order to check on the lack of correlation between successive pseudorandom numbers we computed the mean square difference of successive numbers, $\overline{(\xi_{n+1}-\xi_n)^2}$. As a further test of possible correlation, the algebraic sign of the differences between successive pseudorandom numbers was examined, and an index $t$ was computed which was defined as the excess of positive over negative signs. Table B.1 compares the actual values of all these quantities with the values that one would expect if the pseudorandom numbers were truly random. We infer from the table that the pseudorandom numbers are sufficiently random for our purpose.

TABLE B.1. *Analysis of the randomness of the pseudorandom numbers*

In order to indicate the significance of the deviations of the empirical from the expected values of the various statistics, the standard deviations of the empirical values are given. The pseudorandom numbers were obtained by starting a primary sequence with the initial value $c=16{,}743{,}785{,}845$. The number of pseudorandom numbers in each set is indicated within brackets.

| Statistic | Expected value | Empirical value | | |
|---|---|---|---|---|
| | | Set $P$ [3,000] | Set $S$ [220,776] | Set $T$ [13,384] |
| $\overline{\xi_n}$ | $\frac{1}{2}$ | 0.49402±0.00527 | 0.49955±0.00061 | 0.50233±0.00250 |
| $\overline{\xi_n^2}$ | $\frac{1}{3}$ | .32937± .00544 | .33359± .00064 | .33580± .00258 |
| $\overline{(\xi_{n+1}-\xi_n)^2}$ | $\frac{1}{6}$ | .16743± .00360 | .16579± .00042 | .16461± .00171 |
| $t$ | 0 | 28 ±55 | −638 ±470 | 34 ±116 |

## 10. Appendix C. Tables of Differential Albedo

The following tables are indexed by table 6.1 and described in section 6.2 of the text.

TABLE 1.

cos $\theta$

| $E$ \ $i$ \ $k$ | 1 | 2 | 3 | 4 | 5 | 6 | 7 | 8 | 9 | 10 | Sum |
|---|---|---|---|---|---|---|---|---|---|---|---|
| 1 | | | | | | | | | | | 0 |
| 2 | 3 | 7 | 4 | 8 | 12 | 14 | 14 | 6 | | | 68 |
| 3 | 1 | 2 | 1 | 3 | 1 | 5 | 1 | 3 | 15 | 18 | 50 |
| 4 | | | 2 | 1 | 2 | | 1 | 2 | 3 | 3 | 14 |
| 5 | | | | | | 3 | | 3 | 1 | 3 | 10 |
| 6 | | | | | 2 | 5 | 4 | 2 | 5 | 7 | 25 |
| 7 | | | | | 1 | 4 | 5 | 2 | 3 | 3 | 18 |
| 8 | | | | 1 | 2 | 1 | 3 | 2 | 2 | 2 | 13 |
| 9 | 1 | | 1 | 2 | 4 | 5 | 6 | 6 | 4 | 6 | 35 |
| 10 | | 10 | 16 | 49 | 48 | 75 | 91 | 101 | 124 | 142 | 656 |
| Sum | 5 | 19 | 24 | 64 | 72 | 112 | 125 | 127 | 157 | 184 | 889 |

[25] This set of numbers was used repeatedly for most of our calculations.

TABLE 2a.

$\cos\theta$

| $E$ | $i$ \ $k$ | 1 | 2 | 3 | 4 | 5 | 6 | 7 | 8 | 9 | 10 | Sum |
|---|---|---|---|---|---|---|---|---|---|---|---|---|
| | 1 | | | 1 | | | | | | | | 1 |
| | 2 | 5 | 10 | 16 | 20 | 32 | 37 | 48 | 30 | 3 | | 201 |
| | 3 | | | | 7 | 4 | 7 | 4 | 14 | 40 | 41 | 117 |
| | 4 | 1 | 1 | 2 | 2 | 2 | 4 | 3 | 3 | 3 | 5 | 26 |
| | 5 | | 2 | 1 | 1 | 5 | 3 | 5 | 4 | 2 | 5 | 28 |
| | 6 | | 1 | | 3 | 2 | 4 | 5 | 2 | 11 | 5 | 33 |
| | 7 | | | 2 | 1 | 5 | 9 | 8 | 3 | 9 | 6 | 43 |
| | 8 | | 1 | 2 | 1 | 1 | 5 | 5 | 7 | 3 | 10 | 35 |
| | 9 | 1 | 1 | | 3 | 5 | 4 | 6 | 15 | 11 | 10 | 56 |
| | 10 | 3 | 10 | 17 | 43 | 52 | 48 | 52 | 94 | 102 | 123 | 544 |
| | Sum | 10 | 26 | 41 | 81 | 108 | 121 | 136 | 172 | 184 | 205 | 1,084 |

TABLE 2b.

$\cos\theta$

| $E$ | $i$ \ $k$ | 1 | 2 | 3 | 4 | 5 | 6 | 7 | 8 | 9 | 10 | Sum |
|---|---|---|---|---|---|---|---|---|---|---|---|---|
| | 1 | | | | | | | | | | | 0 |
| | 2 | 1 | | 5 | 10 | 21 | 32 | 46 | 56 | 1 | | 172 |
| | 3 | 1 | 2 | 2 | 5 | 6 | 5 | 12 | 34 | 86 | 113 | 266 |
| | 4 | | | | 2 | 5 | 3 | 3 | 6 | 8 | 12 | 39 |
| | 5 | | 1 | | | 3 | 5 | 5 | 11 | 3 | 7 | 35 |
| | 6 | | 1 | 2 | | 1 | 4 | 4 | 8 | 7 | 7 | 34 |
| | 7 | | 1 | | 3 | 7 | 5 | 1 | 4 | 7 | 4 | 32 |
| | 8 | | | 3 | 8 | 5 | 10 | 2 | 5 | 8 | 11 | 52 |
| | 9 | 2 | 5 | | 4 | 4 | 5 | 11 | 5 | 9 | 10 | 55 |
| | 10 | 4 | 7 | 22 | 37 | 49 | 51 | 51 | 64 | 86 | 88 | 459 |
| | Sum | 8 | 17 | 34 | 69 | 101 | 120 | 135 | 193 | 215 | 252 | 1,144 |

TABLE 2c.

$\cos\theta$

| $E$ | $i$ \ $k$ | 1 | 2 | 3 | 4 | 5 | 6 | 7 | 8 | 9 | 10 | Sum |
|---|---|---|---|---|---|---|---|---|---|---|---|---|
| | 1 | | | | | | | | | | | 0 |
| | 2 | 1 | | 4 | 9 | 19 | 31 | 42 | 56 | | | 162 |
| | 3 | | | | | | | | 21 | 68 | 88 | 177 |
| | 4 | | | | | | | | | | | 0 |
| | 5 | | | | | | | | | | | 0 |
| | 6 | | | | | | | | | | | 0 |
| | 7 | | | | | | | | | | | 0 |
| | 8 | | | | | | | | | | | 0 |
| | 9 | | | | | | | | | | | 0 |
| | 10 | | | | | | | | | | | 0 |
| | Sum | 1 | 0 | 4 | 9 | 19 | 31 | 42 | 77 | 68 | 88 | 339 |

TABLE 3a.

$\cos\theta$

| $F$ | $i$ \ $k$ | 1 | 2 | 3 | 4 | 5 | 6 | 7 | 8 | 9 | 10 | Sum |
|---|---|---|---|---|---|---|---|---|---|---|---|---|
| | 1 | 1 | 2 | 1 | 3 | 2 | | | | | | 9 |
| | 2 | 4 | 4 | 13 | 9 | 16 | 11 | 17 | 21 | 18 | 37 | 150 |
| | 3 | 1 | 11 | 14 | 18 | 32 | 21 | 33 | 49 | 47 | 45 | 271 |
| | 4 | 1 | 1 | 2 | 7 | 7 | 6 | 7 | 10 | 6 | 8 | 55 |
| | 5 | 1 | 4 | 1 | 3 | 4 | 10 | 9 | 2 | 4 | 4 | 42 |
| | 6 | 1 | | 2 | 2 | 2 | 7 | 8 | 7 | 10 | 7 | 46 |
| | 7 | 1 | 10 | 2 | 3 | 5 | 2 | 5 | 3 | 9 | 4 | 44 |
| | 8 | 1 | 4 | 9 | 6 | 12 | 10 | 7 | 6 | 14 | 9 | 78 |
| | 9 | 2 | 5 | 9 | 7 | 3 | 9 | 10 | 12 | 10 | 19 | 86 |
| | 10 | 8 | 11 | 24 | 42 | 56 | 62 | 59 | 84 | 100 | 123 | 569 |
| | Sum | 21 | 52 | 77 | 100 | 139 | 138 | 155 | 194 | 218 | 256 | 1,350 |

TABLE 3b.

$\cos\theta$

| | i \ k | 1 | 2 | 3 | 4 | 5 | 6 | 7 | 8 | 9 | 10 | Sum |
|---|---|---|---|---|---|---|---|---|---|---|---|---|
| | 1 | 1 | 2 | 1 | 2 | | | | | | | 6 |
| | 2 | 4 | 3 | 10 | 6 | 12 | 10 | 16 | 18 | 16 | 37 | 132 |
| | 3 | | 7 | 6 | 9 | 22 | 14 | 22 | 31 | 35 | 27 | 173 |
| | 4 | | | | | | | | | | | 0 |
| E | 5 | | | | | | | | | | | 0 |
| | 6 | 1 | | | | | | | | | | 1 |
| | 7 | | 4 | | | | | | | | | 4 |
| | 8 | 1 | | 5 | | | | | | | | 6 |
| | 9 | | 1 | 4 | 5 | 1 | | | | | | 11 |
| | 10 | | | | 2 | 6 | 1 | | | | | 9 |
| | Sum | 7 | 17 | 26 | 24 | 41 | 25 | 38 | 49 | 51 | 64 | 342 |

TABLE 4a.

$\cos\theta$

| | i \ k | 1 | 2 | 3 | 4 | 5 | 6 | 7 | 8 | 9 | 10 | Sum |
|---|---|---|---|---|---|---|---|---|---|---|---|---|
| | 1 | 6 | 10 | 6 | 9 | 8 | 7 | 2 | | 1 | | 49 |
| | 2 | 5 | 8 | 7 | 18 | 10 | 15 | 16 | 13 | 22 | 44 | 158 |
| | 3 | 4 | 14 | 19 | 27 | 19 | 38 | 46 | 41 | 35 | 18 | 261 |
| | 4 | 2 | 4 | 9 | 4 | 6 | 6 | 9 | 6 | 3 | 9 | 58 |
| E | 5 | 1 | 10 | 8 | 6 | 11 | 10 | 5 | 8 | 2 | 5 | 66 |
| | 6 | 1 | 3 | 12 | 5 | 5 | 7 | 8 | 10 | 7 | 1 | 59 |
| | 7 | 2 | 2 | 4 | 12 | 7 | 6 | 4 | 9 | 5 | 4 | 55 |
| | 8 | 1 | 4 | 8 | 12 | 9 | 13 | 11 | 6 | 9 | 13 | 86 |
| | 9 | 1 | 9 | 12 | 3 | 19 | 17 | 13 | 12 | 15 | 19 | 120 |
| | 10 | 7 | 15 | 29 | 55 | 43 | 79 | 84 | 85 | 119 | 121 | 637 |
| | Sum | 30 | 79 | 114 | 151 | 137 | 198 | 198 | 190 | 218 | 234 | 1,549 |

TABLE 4b.

$\cos\theta$

| | i \ k | 1 | 2 | 3 | 4 | 5 | 6 | 7 | 8 | 9 | 10 | Sum |
|---|---|---|---|---|---|---|---|---|---|---|---|---|
| | 1 | 6 | 9 | 5 | 7 | 6 | 5 | | | | | 38 |
| | 2 | 4 | 6 | 2 | 14 | 9 | 13 | 12 | 12 | 21 | 43 | 136 |
| | 3 | 3 | 8 | 13 | 21 | 9 | 25 | 27 | 28 | 21 | 3 | 158 |
| | 4 | 1 | | | | | | | | | | 1 |
| E | 5 | 1 | 5 | 3 | | | | | | | | 9 |
| | 6 | 1 | 2 | 7 | 1 | | | | | | | 11 |
| | 7 | | 2 | 3 | 7 | 3 | | | | | | 15 |
| | 8 | 1 | 2 | 2 | 2 | 3 | 4 | | | | | 14 |
| | 9 | | 5 | 1 | 1 | 7 | 11 | 2 | | | | 27 |
| | 10 | | 2 | 2 | 1 | 2 | 4 | 4 | 2 | | | 17 |
| | Sum | 17 | 41 | 38 | 54 | 39 | 62 | 45 | 42 | 42 | 46 | 426 |

TABLE 5a.

$\cos\theta$

| | i \ k | 1 | 2 | 3 | 4 | 5 | 6 | 7 | 8 | 9 | 10 | Sum |
|---|---|---|---|---|---|---|---|---|---|---|---|---|
| | 1 | 6 | 24 | 26 | 21 | 18 | 12 | 11 | 7 | 1 | 1 | 127 |
| | 2 | 12 | 20 | 23 | 19 | 11 | 15 | 17 | 26 | 35 | 23 | 201 |
| | 3 | 10 | 22 | 37 | 41 | 41 | 38 | 34 | 31 | 10 | 10 | 274 |
| | 4 | 3 | 4 | 16 | 16 | 9 | 6 | 5 | 8 | 2 | 7 | 76 |
| E | 5 | 4 | 8 | 9 | 13 | 20 | 10 | 10 | 4 | 4 | 3 | 85 |
| | 6 | | 4 | 9 | 7 | 20 | 13 | 10 | 12 | 4 | 2 | 81 |
| | 7 | 1 | 5 | 8 | 9 | 11 | 18 | 16 | 7 | 8 | 3 | 86 |
| | 8 | 5 | 5 | 17 | 10 | 14 | 14 | 10 | 21 | 8 | 15 | 119 |
| | 9 | 2 | 4 | 18 | 12 | 12 | 7 | 27 | 22 | 25 | 12 | 141 |
| | 10 | 3 | 18 | 27 | 47 | 56 | 86 | 87 | 90 | 137 | 116 | 667 |
| | Sum | 46 | 114 | 190 | 195 | 212 | 219 | 227 | 228 | 234 | 192 | 1,857 |

TABLE 5b.

$\cos\theta$

| | i \ k | 1 | 2 | 3 | 4 | 5 | 6 | 7 | 8 | 9 | 10 | Sum |
|---|---|---|---|---|---|---|---|---|---|---|---|---|
| | 1 | 6 | 21 | 23 | 20 | 16 | 9 | 9 | 5 | | | 109 |
| | 2 | 12 | 17 | 13 | 14 | 10 | 9 | 11 | 25 | 35 | 21 | 167 |
| | 3 | 8 | 16 | 27 | 22 | 25 | 27 | 18 | 17 | | | 160 |
| | 4 | 3 | | 13 | 11 | | | | | | | 27 |
| $E$ | 5 | 2 | 2 | 4 | 6 | 12 | | | | | | 26 |
| | 6 | | | 1 | 3 | 10 | 6 | | | | | 20 |
| | 7 | | 3 | 1 | 3 | 6 | 9 | 5 | | | | 27 |
| | 8 | 2 | 2 | 6 | 2 | 6 | 4 | 6 | 5 | | | 33 |
| | 9 | 2 | 3 | 6 | 3 | 2 | 2 | 15 | 10 | 4 | | 47 |
| | 10 | | 1 | 1 | 4 | 1 | 1 | 3 | 9 | 4 | | 24 |
| | Sum | 35 | 65 | 95 | 88 | 88 | 67 | 67 | 71 | 43 | 21 | 640 |

TABLE 6a.

$\cos\theta$

| | i \ k | 1 | 2 | 3 | 4 | 5 | 6 | 7 | 8 | 9 | 10 | Sum |
|---|---|---|---|---|---|---|---|---|---|---|---|---|
| | 1 | 111 | 84 | 61 | 41 | 52 | 42 | 30 | 19 | 15 | 3 | 458 |
| | 2 | 45 | 33 | 41 | 56 | 20 | 30 | 35 | 30 | 24 | 8 | 322 |
| | 3 | 47 | 53 | 57 | 43 | 57 | 38 | 9 | 8 | 4 | 3 | 319 |
| | 4 | 11 | 13 | 18 | 14 | 20 | 24 | 5 | 4 | 7 | 4 | 120 |
| $E$ | 5 | 11 | 11 | 18 | 15 | 15 | 13 | 22 | 2 | 1 | 1 | 109 |
| | 6 | 8 | 5 | 13 | 10 | 8 | 11 | 18 | 20 | 2 | 1 | 96 |
| | 7 | 4 | 11 | 15 | 11 | 9 | 17 | 18 | 26 | 8 | 1 | 120 |
| | 8 | 9 | 6 | 9 | 16 | 16 | 15 | 11 | 21 | 14 | 4 | 121 |
| | 9 | 7 | 6 | 11 | 14 | 17 | 10 | 13 | 21 | 30 | 17 | 146 |
| | 10 | 7 | 15 | 28 | 36 | 42 | 57 | 67 | 75 | 78 | 85 | 490 |
| | Sum | 260 | 237 | 271 | 256 | 256 | 257 | 228 | 226 | 183 | 127 | 2,301 |

TABLE 6b.

$\cos\theta$

| | i \ k | 1 | 2 | 3 | 4 | 5 | 6 | 7 | 8 | 9 | 10 | Sum |
|---|---|---|---|---|---|---|---|---|---|---|---|---|
| | 1 | 107 | 80 | 58 | 39 | 48 | 39 | 29 | 18 | 14 | 3 | 435 |
| | 2 | 41 | 30 | 39 | 52 | 17 | 24 | 34 | 28 | 21 | 7 | 293 |
| | 3 | 44 | 46 | 47 | 37 | 48 | 29 | 1 | | | | 252 |
| | 4 | 9 | 11 | 12 | 8 | 18 | 21 | 2 | | | | 81 |
| $E$ | 5 | 9 | 8 | 13 | 8 | 8 | 10 | 20 | | | | 76 |
| | 6 | 2 | 4 | 8 | 4 | 5 | 6 | 12 | 15 | | | 56 |
| | 7 | 3 | 7 | 9 | 5 | 6 | 10 | 8 | 20 | 3 | | 71 |
| | 8 | 7 | 3 | 6 | 9 | 7 | 7 | 5 | 11 | 11 | | 66 |
| | 9 | 6 | 5 | 7 | 6 | 8 | 4 | 8 | 16 | 19 | 11 | 90 |
| | 10 | 4 | 3 | 2 | 4 | 5 | 4 | 8 | 5 | 12 | 12 | 59 |
| | Sum | 232 | 197 | 201 | 172 | 170 | 154 | 127 | 113 | 80 | 33 | 1,479 |

TABLE 7a.

$\cos\theta$

| | i \ k | 1 | 2 | 3 | 4 | 5 | 6 | 7 | 8 | 9 | 10 | Sum |
|---|---|---|---|---|---|---|---|---|---|---|---|---|
| | 1 | | | | | | | | | | | 0 |
| | 2 | 1 | 2 | 2 | 6 | 4 | 8 | 8 | 7 | | | 38 |
| | 3 | | | | | 2 | 2 | 1 | 3 | 13 | 14 | 33 |
| | 4 | | | | | 2 | | | 2 | | | 4 |
| $E$ | 5 | | | | 1 | | | 2 | | | 2 | 5 |
| | 6 | | 1 | | 1 | | 3 | 1 | | | | 6 |
| | 7 | | 1 | | | | | 1 | 1 | 1 | | 4 |
| | 8 | | | | | 1 | | | 1 | 1 | | 3 |
| | 9 | | | | | 2 | 1 | | 1 | 3 | | 7 |
| | 10 | | 5 | 1 | 4 | 7 | 7 | 13 | 19 | 13 | 14 | 83 |
| | Sum | 1 | 9 | 3 | 12 | 16 | 21 | 26 | 34 | 31 | 30 | 183 |

## Table 7b.

$\cos\theta$

| $E$ | $i$ \ $k$ | 1 | 2 | 3 | 4 | 5 | 6 | 7 | 8 | 9 | 10 | Sum |
|---|---|---|---|---|---|---|---|---|---|---|---|---|
| | 1 | | | | | | | | | | | 0 |
| | 2 | 1 | 2 | 2 | 8 | 5 | 11 | 14 | 9 | | | 52 |
| | 3 | | | | 1 | | 3 | 1 | 6 | 19 | 24 | 54 |
| | 4 | | | | | 3 | 1 | | 4 | 1 | 1 | 10 |
| | 5 | | | | 1 | | 2 | 3 | 1 | 1 | 2 | 10 |
| | 6 | | 1 | | 2 | 1 | 3 | 2 | | 1 | 1 | 11 |
| | 7 | | 1 | | | 1 | 2 | 1 | 2 | 1 | | 8 |
| | 8 | | | | | 2 | 1 | 1 | 3 | 4 | 2 | 13 |
| | 9 | | | 1 | | 3 | 2 | 3 | 5 | 4 | 3 | 21 |
| | 10 | 1 | 8 | 6 | 10 | 13 | 18 | 29 | 42 | 38 | 48 | 213 |
| | Sum | 2 | 12 | 9 | 22 | 28 | 43 | 54 | 72 | 69 | 81 | 392 |

## Table 7c.

$\cos\theta$

| $E$ | $i$ \ $k$ | 1 | 2 | 3 | 4 | 5 | 6 | 7 | 8 | 9 | 10 | Sum |
|---|---|---|---|---|---|---|---|---|---|---|---|---|
| | 1 | | | | | | | | | | | 0 |
| | 2 | 1 | 2 | 2 | 8 | 7 | 12 | 14 | 11 | | | 57 |
| | 3 | | | | 1 | | 4 | 2 | 6 | 20 | 27 | 60 |
| | 4 | | | | 1 | 3 | 1 | | 5 | 1 | 2 | 13 |
| | 5 | | | | 1 | | 2 | 3 | 2 | 1 | 3 | 12 |
| | 6 | | 1 | | 2 | 1 | 3 | 2 | 1 | 3 | 2 | 15 |
| | 7 | | 1 | | | 1 | 3 | 1 | 2 | 1 | | 9 |
| | 8 | | | | 1 | 2 | 2 | 1 | 3 | 5 | 3 | 17 |
| | 9 | | | 1 | 1 | 3 | 2 | 4 | 6 | 5 | 6 | 28 |
| | 10 | 1 | 9 | 9 | 12 | 15 | 24 | 41 | 51 | 51 | 64 | 277 |
| | Sum | 2 | 13 | 12 | 27 | 32 | 53 | 68 | 87 | 87 | 107 | 488 |

## Table 8a.

$\cos\theta$

| $E$ | $i$ \ $k$ | 1 | 2 | 3 | 4 | 5 | 6 | 7 | 8 | 9 | 10 | Sum |
|---|---|---|---|---|---|---|---|---|---|---|---|---|
| | 1 | | | | | | | | | | | 0 |
| | 2 | 2 | 5 | 5 | 7 | 13 | 18 | 15 | 10 | | | 75 |
| | 3 | | 1 | | 2 | 1 | 3 | 1 | 5 | 18 | 22 | 53 |
| | 4 | | | 2 | 2 | 1 | | | 2 | 2 | 2 | 11 |
| | 5 | | | | | 1 | 3 | 1 | 3 | 3 | 3 | 14 |
| | 6 | | 1 | | | 2 | 2 | 5 | 1 | 5 | 2 | 18 |
| | 7 | | | 1 | | | 5 | 3 | 3 | 3 | 4 | 19 |
| | 8 | | | | 2 | 3 | 2 | 1 | 1 | 5 | 3 | 17 |
| | 9 | | | 1 | 2 | 2 | 3 | 8 | 6 | 7 | 5 | 34 |
| | 10 | | 10 | 11 | 17 | 23 | 27 | 49 | 50 | 48 | 59 | 294 |
| | Sum | 2 | 17 | 20 | 32 | 46 | 63 | 83 | 81 | 91 | 100 | 535 |

## Table 8b.

$\cos\theta$

| $E$ | $i$ \ $k$ | 1 | 2 | 3 | 4 | 5 | 6 | 7 | 8 | 9 | 10 | Sum |
|---|---|---|---|---|---|---|---|---|---|---|---|---|
| | 1 | | | | | | | | | | | 0 |
| | 2 | | 2 | 6 | 4 | 11 | 10 | 16 | 9 | | 1 | 59 |
| | 3 | | | 1 | 1 | 1 | 1 | 2 | 6 | 11 | 22 | 45 |
| | 4 | 1 | | | 2 | 1 | 2 | 2 | 2 | 1 | 3 | 14 |
| | 5 | | | | | 2 | 2 | 3 | 4 | 1 | 1 | 13 |
| | 6 | | | 1 | 1 | 4 | 1 | 1 | 4 | 4 | 1 | 17 |
| | 7 | | | | | 1 | 1 | 2 | 1 | 4 | 3 | 12 |
| | 8 | | | 1 | 1 | 3 | 3 | 1 | 1 | 3 | 6 | 19 |
| | 9 | | 1 | 1 | 2 | 3 | 2 | 4 | 3 | 5 | 9 | 30 |
| | 10 | 1 | 5 | 10 | 16 | 22 | 30 | 49 | 41 | 53 | 66 | 293 |
| | Sum | 2 | 8 | 20 | 27 | 48 | 52 | 80 | 71 | 82 | 112 | 502 |

TABLE 8c.

$\cos\theta$

| | i \ k | 1 | 2 | 3 | 4 | 5 | 6 | 7 | 8 | 9 | 10 | Sum |
|---|---|---|---|---|---|---|---|---|---|---|---|---|
| | 1 | | | | | | | | | | | 0 |
| | 2 | | 2 | 5 | 4 | 11 | 10 | 16 | 8 | | | 56 |
| | 3 | | | | | | | | 3 | 8 | 17 | 28 |
| | 4 | | | | | | | | | | | 0 |
| $E$ | 5 | | | | | | | | | | | 0 |
| | 6 | | | | | | | | | | | 0 |
| | 7 | | | | | | | | | | | 0 |
| | 8 | | | | | | | | | | | 0 |
| | 9 | | | | | | | | | | | 0 |
| | 10 | | | | | | | | | | | 0 |
| | Sum | 0 | 2 | 5 | 4 | 11 | 10 | 16 | 11 | 8 | 17 | 84 |

TABLE 9a.

$\cos\theta$

| | i \ k | 1 | 2 | 3 | 4 | 5 | 6 | 7 | 8 | 9 | 10 | Sum |
|---|---|---|---|---|---|---|---|---|---|---|---|---|
| | 1 | 1 | 1 | 2 | 1 | 2 | | | | | | 7 |
| | 2 | | 2 | 5 | 4 | 8 | 4 | 6 | 7 | 8 | 11 | 55 |
| | 3 | | 1 | 1 | 2 | 6 | 4 | 2 | 15 | 10 | 9 | 50 |
| | 4 | 1 | | | 2 | 5 | | | 3 | 1 | 3 | 15 |
| $E$ | 5 | 1 | 3 | 1 | 2 | 1 | 4 | 2 | | 4 | 2 | 20 |
| | 6 | 2 | | 2 | 3 | 1 | 4 | 4 | 3 | 4 | 2 | 25 |
| | 7 | | 2 | 1 | | 3 | 1 | 4 | 3 | 6 | 2 | 22 |
| | 8 | 1 | 4 | 9 | 3 | 7 | 5 | 3 | 4 | 9 | 2 | 47 |
| | 9 | 1 | 2 | 5 | 7 | 9 | 8 | 7 | 10 | 6 | 11 | 66 |
| | 10 | 4 | 8 | 17 | 26 | 36 | 38 | 45 | 56 | 82 | 78 | 390 |
| | Sum | 11 | 23 | 43 | 50 | 78 | 68 | 73 | 101 | 130 | 120 | 697 |

TABLE 9b.

$\cos\theta$

| | i \ k | 1 | 2 | 3 | 4 | 5 | 6 | 7 | 8 | 9 | 10 | Sum |
|---|---|---|---|---|---|---|---|---|---|---|---|---|
| | 1 | 1 | 1 | 2 | 1 | 2 | | | | | | 7 |
| | 2 | | | 3 | 2 | 6 | 2 | 5 | 6 | 8 | 11 | 43 |
| | 3 | | | | 1 | 2 | 3 | 1 | 10 | 7 | 6 | 30 |
| | 4 | | | | | | | | | | | 0 |
| $E$ | 5 | | | | | | | | | | | 0 |
| | 6 | 1 | | | | | | | | | | 1 |
| | 7 | | 1 | | | | | | | | | 1 |
| | 8 | 1 | 1 | 6 | | | | | | | | 8 |
| | 9 | | | 3 | 2 | 1 | | | | | | 6 |
| | 10 | | 1 | | 2 | 6 | | | | | | 9 |
| | Sum | 3 | 4 | 14 | 8 | 17 | 5 | 6 | 16 | 15 | 17 | 105 |

TABLE 10a.

$\cos\theta$

| | i \ k | 1 | 2 | 3 | 4 | 5 | 6 | 7 | 8 | 9 | 10 | Sum |
|---|---|---|---|---|---|---|---|---|---|---|---|---|
| | 1 | 3 | 6 | 5 | 5 | 4 | 6 | 3 | 1 | | | 33 |
| | 2 | 3 | 1 | 6 | 4 | 5 | 6 | 4 | 8 | 10 | 15 | 62 |
| | 3 | 2 | 1 | 5 | 5 | 4 | 6 | 11 | 12 | 7 | 5 | 58 |
| | 4 | 2 | 3 | 4 | 1 | 3 | 2 | 1 | | 4 | 3 | 23 |
| $E$ | 5 | | 8 | 6 | 3 | 5 | 5 | 3 | 4 | 1 | 2 | 37 |
| | 6 | 2 | 2 | 14 | 5 | 3 | 5 | 5 | 5 | 3 | 2 | 46 |
| | 7 | 2 | 3 | 5 | 9 | 7 | 1 | 4 | 5 | 4 | 3 | 43 |
| | 8 | 1 | 5 | 8 | 8 | 12 | 13 | 10 | 9 | 9 | 5 | 80 |
| | 9 | | 3 | 2 | 6 | 10 | 10 | 9 | 10 | 17 | 16 | 83 |
| | 10 | 2 | 14 | 18 | 27 | 34 | 54 | 70 | 77 | 92 | 92 | 480 |
| | Sum | 17 | 46 | 73 | 73 | 87 | 108 | 120 | 131 | 147 | 143 | 945 |

TABLE 10b.

$\cos\theta$

| | i \ k | 1 | 2 | 3 | 4 | 5 | 6 | 7 | 8 | 9 | 10 | Sum |
|---|---|---|---|---|---|---|---|---|---|---|---|---|
| | 1 | 3 | 5 | 5 | 3 | 4 | 6 | 2 | 1 | | | 29 |
| | 2 | 2 | 1 | 2 | 3 | 3 | 3 | 3 | 6 | 10 | 15 | 48 |
| | 3 | 2 | | 1 | 3 | | 6 | 9 | 7 | 2 | 1 | 31 |
| | 4 | 2 | | | | | | | | | | 2 |
| $E$ | 5 | | 4 | 3 | | | | | | | | 7 |
| | 6 | 1 | 2 | 8 | 3 | | | | | | | 14 |
| | 7 | 1 | 2 | 2 | 7 | 2 | | | | | | 14 |
| | 8 | 1 | 3 | 3 | 3 | 5 | 4 | | | | | 19 |
| | 9 | | 2 | | 2 | 5 | 7 | 1 | | | | 17 |
| | 10 | | 1 | | 2 | 3 | 3 | 5 | 2 | | | 16 |
| | Sum | 12 | 20 | 24 | 26 | 22 | 29 | 20 | 16 | 12 | 16 | 197 |

TABLE 11a.

$\cos\theta$

| | i \ k | 1 | 2 | 3 | 4 | 5 | 6 | 7 | 8 | 9 | 10 | Sum |
|---|---|---|---|---|---|---|---|---|---|---|---|---|
| | 1 | 5 | 9 | 12 | 14 | 10 | 10 | 5 | 6 | 5 | | 76 |
| | 2 | 10 | 13 | 10 | 10 | 7 | 9 | 5 | 12 | 18 | 13 | 107 |
| | 3 | 4 | 12 | 20 | 9 | 11 | 11 | 6 | 9 | 6 | 4 | 92 |
| | 4 | 2 | 2 | 12 | 22 | 6 | 4 | 2 | 2 | 1 | 3 | 56 |
| $E$ | 5 | 1 | 4 | 4 | 10 | 22 | 6 | 7 | 3 | 3 | 2 | 62 |
| | 6 | | 11 | 7 | 7 | 22 | 13 | 10 | 5 | 4 | 4 | 83 |
| | 7 | | 5 | 9 | 8 | 7 | 19 | 10 | 9 | 5 | 5 | 77 |
| | 8 | 1 | 5 | 17 | 10 | 19 | 18 | 17 | 20 | 11 | 10 | 128 |
| | 9 | 3 | 2 | 9 | 14 | 7 | 14 | 31 | 29 | 14 | 19 | 142 |
| | 10 | 1 | 11 | 28 | 46 | 42 | 66 | 74 | 92 | 119 | 115 | 594 |
| | Sum | 27 | 74 | 128 | 150 | 153 | 170 | 167 | 187 | 186 | 175 | 1,417 |

TABLE 11b.

$\cos\theta$

| | i \ k | 1 | 2 | 3 | 4 | 5 | 6 | 7 | 8 | 9 | 10 | Sum |
|---|---|---|---|---|---|---|---|---|---|---|---|---|
| | 1 | 5 | 9 | 11 | 13 | 9 | 7 | 5 | 6 | 4 | | 69 |
| | 2 | 10 | 10 | 3 | 3 | 6 | 3 | 3 | 12 | 16 | 12 | 78 |
| | 3 | 3 | 12 | 18 | 5 | 8 | 7 | 2 | 3 | | | 58 |
| | 4 | 2 | 1 | 10 | 18 | | | | | | | 31 |
| $E$ | 5 | 1 | 2 | 4 | 5 | 13 | | | | | | 25 |
| | 6 | | 1 | 2 | 5 | 16 | 8 | | | | | 32 |
| | 7 | | 3 | 1 | 3 | 5 | 11 | 6 | | | | 29 |
| | 8 | 1 | 1 | 6 | 3 | 7 | 4 | 10 | 5 | | | 37 |
| | 9 | 1 | 2 | 4 | 4 | 1 | 4 | 13 | 7 | 1 | | 37 |
| | 10 | | 3 | 1 | 2 | 2 | 3 | 4 | 12 | 7 | | 34 |
| | Sum | 23 | 44 | 60 | 61 | 67 | 47 | 43 | 45 | 28 | 12 | 430 |

TABLE 12a.

$\cos\theta$

| | i \ k | 1 | 2 | 3 | 4 | 5 | 6 | 7 | 8 | 9 | 10 | Sum |
|---|---|---|---|---|---|---|---|---|---|---|---|---|
| | 1 | 81 | 62 | 50 | 26 | 29 | 25 | 10 | 15 | 10 | 8 | 316 |
| | 2 | 38 | 30 | 38 | 57 | 19 | 13 | 16 | 16 | 14 | 11 | 252 |
| | 3 | 19 | 23 | 22 | 30 | 46 | 18 | 3 | 3 | 4 | 3 | 171 |
| | 4 | 17 | 20 | 19 | 16 | 26 | 38 | 7 | | 2 | | 145 |
| $E$ | 5 | 16 | 20 | 19 | 22 | 17 | 20 | 29 | 2 | 1 | 1 | 147 |
| | 6 | 7 | 12 | 15 | 12 | 10 | 14 | 33 | 25 | 5 | 2 | 135 |
| | 7 | 7 | 17 | 19 | 12 | 15 | 22 | 17 | 36 | 7 | 2 | 154 |
| | 8 | 11 | 9 | 13 | 19 | 21 | 18 | 19 | 28 | 20 | 2 | 160 |
| | 9 | 13 | 10 | 16 | 11 | 20 | 11 | 23 | 28 | 38 | 18 | 188 |
| | 10 | 4 | 19 | 23 | 38 | 44 | 52 | 73 | 71 | 93 | 99 | 516 |
| | Sum | 213 | 222 | 234 | 243 | 247 | 231 | 230 | 224 | 194 | 146 | 2,184 |

## TABLE 12b.

$\cos\theta$

| $E$ | $i$ \ $k$ | 1 | 2 | 3 | 4 | 5 | 6 | 7 | 8 | 9 | 10 | Sum |
|---|---|---|---|---|---|---|---|---|---|---|---|---|
| | 1 | 77 | 60 | 50 | 26 | 27 | 25 | 10 | 15 | 10 | 8 | 308 |
| | 2 | 34 | 27 | 35 | 53 | 18 | 8 | 13 | 14 | 13 | 10 | 225 |
| | 3 | 18 | 20 | 20 | 29 | 45 | 17 | 1 | | | | 150 |
| | 4 | 15 | 17 | 15 | 15 | 25 | 37 | 5 | | | | 129 |
| | 5 | 14 | 17 | 16 | 14 | 11 | 15 | 29 | | | | 116 |
| | 6 | 6 | 9 | 10 | 6 | 7 | 9 | 25 | 21 | | | 93 |
| | 7 | 5 | 10 | 15 | 9 | 10 | 14 | 8 | 31 | 5 | | 107 |
| | 8 | 9 | 3 | 8 | 8 | 10 | 10 | 9 | 19 | 17 | | 93 |
| | 9 | 11 | 8 | 10 | 6 | 9 | 6 | 14 | 20 | 28 | 11 | 123 |
| | 10 | 2 | 6 | 4 | 8 | 6 | 7 | 12 | 9 | 20 | 21 | 95 |
| | Sum | 191 | 177 | 183 | 174 | 168 | 148 | 126 | 129 | 93 | 50 | 1,439 |

## TABLE 13.

$\cos\theta$

| $E$ | $i$ \ $k$ | 1 | 2 | 3 | 4 | 5 | 6 | 7 | 8 | 9 | 10 | Sum |
|---|---|---|---|---|---|---|---|---|---|---|---|---|
| | 1 | 5 | 15 | 6 | 8 | 5 | 6 | 5 | 2 | 1 | 3 | 56 |
| | 2 | 6 | 5 | 7 | 13 | 5 | 10 | 10 | 6 | 12 | 21 | 95 |
| | 3 | 5 | 10 | 9 | 11 | 9 | 5 | 9 | 6 | 5 | 10 | 79 |
| | 4 | 1 | 3 | 8 | 3 | 6 | 6 | 2 | 3 | | 1 | 33 |
| | 5 | 2 | 7 | 3 | 5 | 9 | 4 | 4 | 2 | 2 | 4 | 42 |
| | 6 | 2 | 6 | 7 | 6 | 5 | 14 | 12 | 8 | 6 | 4 | 70 |
| | 7 | 1 | 3 | 8 | 7 | 11 | 10 | 10 | 9 | 6 | 7 | 72 |
| | 8 | 2 | 7 | 3 | 10 | 9 | 15 | 20 | 10 | 7 | 4 | 87 |
| | 9 | 3 | 4 | 5 | 6 | 13 | 19 | 7 | 18 | 10 | 13 | 98 |
| | 10 | 6 | 10 | 24 | 21 | 38 | 59 | 62 | 57 | 98 | 106 | 481 |
| | Sum | 33 | 70 | 80 | 90 | 110 | 148 | 141 | 121 | 147 | 173 | 1,113 |

## TABLE 14a.

$\cos\theta$

| $E$ | $i$ \ $k$ | 1 | 2 | 3 | 4 | 5 | 6 | 7 | 8 | 9 | 10 | Sum |
|---|---|---|---|---|---|---|---|---|---|---|---|---|
| | 1 | | | | | | | | | | | 0 |
| | 2 | 3 | 3 | 11 | 5 | 15 | 16 | 15 | 11 | 3 | | 82 |
| | 3 | 1 | | 1 | 1 | 3 | 2 | 2 | 8 | 13 | 23 | 54 |
| | 4 | | | 1 | 1 | | 2 | 4 | 3 | 2 | 3 | 16 |
| | 5 | | | | 1 | 2 | 1 | 2 | 2 | 1 | 2 | 11 |
| | 6 | | 1 | 1 | 1 | 5 | 2 | 1 | 7 | 1 | 4 | 23 |
| | 7 | | | | 2 | 3 | 1 | 3 | 1 | 3 | 5 | 18 |
| | 8 | | | 2 | 2 | 2 | 3 | 1 | | 5 | 3 | 18 |
| | 9 | | 1 | | 2 | 2 | 4 | 6 | 3 | 5 | 7 | 30 |
| | 10 | 2 | 4 | 6 | 10 | 14 | 22 | 30 | 31 | 50 | 50 | 219 |
| | Sum | 6 | 9 | 22 | 25 | 46 | 53 | 64 | 66 | 83 | 97 | 471 |

## TABLE 14b.

$\cos\theta$

| $E$ | $i$ \ $k$ | 1 | 2 | 3 | 4 | 5 | 6 | 7 | 8 | 9 | 10 | Sum |
|---|---|---|---|---|---|---|---|---|---|---|---|---|
| | 1 | | | | | | | | | | | 0 |
| | 2 | 4 | 3 | 12 | 6 | 16 | 18 | 16 | 17 | 3 | | 95 |
| | 3 | 1 | | 1 | 1 | 3 | 4 | 2 | 10 | 16 | 28 | 66 |
| | 4 | | | 1 | 1 | | 2 | 4 | 3 | 2 | 3 | 16 |
| | 5 | | | | 1 | 2 | 1 | 2 | 2 | 1 | 3 | 12 |
| | 6 | | 1 | 1 | 1 | 5 | 2 | 3 | 7 | 2 | 4 | 26 |
| | 7 | | 1 | | 2 | 3 | 1 | 3 | 3 | 3 | 5 | 21 |
| | 8 | | | 2 | 2 | 3 | 3 | 1 | 1 | 5 | 3 | 20 |
| | 9 | | 1 | | 3 | 3 | 4 | 6 | 3 | 5 | 8 | 33 |
| | 10 | 2 | 4 | 7 | 10 | 14 | 22 | 31 | 33 | 51 | 51 | 225 |
| | Sum | 7 | 10 | 24 | 27 | 49 | 57 | 68 | 79 | 88 | 105 | 514 |

TABLE 15a.

$\cos\theta$

| | i \ k | 1 | 2 | 3 | 4 | 5 | 6 | 7 | 8 | 9 | 10 | Sum |
|---|---|---|---|---|---|---|---|---|---|---|---|---|
| | 1 | | | | | | | | | | | 0 |
| | 2 | | 2 | 2 | 3 | 4 | 2 | 5 | 3 | 2 | | 23 |
| | 3 | | | 2 | 3 | | | | 1 | 6 | 21 | 33 |
| | 4 | | 1 | 1 | | 1 | | 2 | 2 | 2 | 4 | 13 |
| $E$ | 5 | | | | | 2 | | | 3 | 1 | 2 | 8 |
| | 6 | | 1 | 3 | | 2 | 3 | | 2 | 4 | 1 | 16 |
| | 7 | | | 1 | | 1 | 3 | 3 | 1 | 3 | 1 | 13 |
| | 8 | | 1 | | 4 | 1 | 7 | 3 | 3 | 3 | | 22 |
| | 9 | | | | 1 | 2 | 3 | 5 | 3 | 9 | 10 | 33 |
| | 10 | 2 | 5 | 6 | 14 | 17 | 26 | 17 | 23 | 28 | 21 | 159 |
| | Sum | 2 | 10 | 15 | 25 | 30 | 44 | 35 | 41 | 58 | 60 | 320 |

TABLE 15b.

$\cos\theta$

| | i \ k | 1 | 2 | 3 | 4 | 5 | 6 | 7 | 8 | 9 | 10 | Sum |
|---|---|---|---|---|---|---|---|---|---|---|---|---|
| | 1 | | | | | | | | | | | 0 |
| | 2 | 1 | 2 | 3 | 5 | 8 | 2 | 5 | 6 | 3 | 1 | 36 |
| | 3 | | 1 | 2 | 4 | 1 | 1 | | 2 | 11 | 27 | 49 |
| | 4 | | 1 | 1 | | 1 | 3 | 4 | 4 | 2 | 4 | 20 |
| $E$ | 5 | | | | 2 | 4 | 1 | 3 | 3 | 2 | 4 | 19 |
| | 6 | | 1 | 3 | 1 | 4 | 3 | | 3 | 4 | 1 | 20 |
| | 7 | | | 2 | | 2 | 4 | 4 | 1 | 3 | 2 | 18 |
| | 8 | | 1 | 1 | 4 | 1 | 7 | 3 | 4 | 3 | 2 | 26 |
| | 9 | | | | 3 | 3 | 3 | 6 | 3 | 10 | 12 | 40 |
| | 10 | 2 | 6 | 7 | 19 | 18 | 29 | 20 | 24 | 30 | 27 | 182 |
| | Sum | 3 | 12 | 19 | 38 | 42 | 53 | 45 | 50 | 68 | 80 | 410 |

TABLE 15c.

$\cos\theta$

| | i \ k | 1 | 2 | 3 | 4 | 5 | 6 | 7 | 8 | 9 | 10 | Sum |
|---|---|---|---|---|---|---|---|---|---|---|---|---|
| | 1 | | | | | | | | | | | 0 |
| | 2 | 3 | 4 | 4 | 6 | 8 | 2 | 5 | 7 | 4 | 1 | 44 |
| | 3 | | 1 | 2 | 5 | 1 | 2 | 1 | 4 | 14 | 33 | 63 |
| | 4 | | 1 | 1 | | 1 | 3 | 4 | 5 | 2 | 3 | 20 |
| $E$ | 5 | | 1 | | 3 | 4 | 1 | 3 | 3 | 3 | 3 | 21 |
| | 6 | | 1 | 3 | 2 | 4 | 3 | | 3 | 4 | | 20 |
| | 7 | | | 2 | | 2 | 4 | 4 | 2 | 3 | 2 | 19 |
| | 8 | | | 1 | | 1 | 3 | 1 | 4 | 3 | 2 | 15 |
| | 9 | | | | 2 | 3 | 2 | 4 | 2 | 5 | 7 | 25 |
| | 10 | 2 | 7 | 6 | 14 | 15 | 30 | 18 | 21 | 28 | 24 | 165 |
| | Sum | 5 | 15 | 19 | 32 | 39 | 50 | 40 | 51 | 66 | 75 | 392 |

TABLE 16a.

$\cos\theta$

| | i \ k | 1 | 2 | 3 | 4 | 5 | 6 | 7 | 8 | 9 | 16 | Sum |
|---|---|---|---|---|---|---|---|---|---|---|---|---|
| | 1 | | | | | | | | | | | 0 |
| | 2 | | 3 | 4 | 4 | 6 | 3 | 1 | 2 | 1 | | 27 |
| | 3 | | | | 3 | | 1 | | 1 | 7 | 21 | 33 |
| | 4 | | | | | | | 3 | 1 | | 2 | 6 |
| $E$ | 5 | | | | | 1 | 1 | 1 | 1 | 1 | 1 | 6 |
| | 6 | 2 | 1 | 3 | 8 | 10 | 10 | 9 | 16 | 14 | 7 | 80 |
| | 7 | | | 1 | 1 | 4 | 6 | 5 | 8 | 8 | 11 | 44 |
| | 8 | | 1 | 1 | 2 | 2 | 1 | 5 | 2 | 4 | 5 | 23 |
| | 9 | 1 | | 1 | 3 | 2 | 5 | 5 | 5 | 4 | 6 | 32 |
| | 10 | 1 | 3 | 2 | 11 | 14 | 15 | 15 | 13 | 25 | 22 | 121 |
| | Sum | 4 | 8 | 12 | 32 | 39 | 42 | 47 | 49 | 64 | 75 | 372 |

## Table 16b.

$\cos\theta$

| $E$ | $i$ \ $k$ | 1 | 2 | 3 | 4 | 5 | 6 | 7 | 8 | 9 | 10 | Sum |
|---|---|---|---|---|---|---|---|---|---|---|---|---|
| | 1 | | | | | | | | | | | 0 |
| | 2 | 1 | 6 | 10 | 7 | 16 | 10 | 13 | 13 | 2 | | 78 |
| | 3 | | | | | 3 | 1 | 2 | 7 | 13 | 13 | 39 |
| | 4 | 1 | | | 1 | | 2 | | 1 | 2 | 1 | 8 |
| | 5 | | 1 | | | | | 4 | 1 | 2 | | 8 |
| | 6 | 2 | 1 | 3 | 8 | 9 | 7 | 8 | 17 | 13 | 10 | 78 |
| | 7 | | | 2 | 4 | 2 | 9 | 6 | 10 | 5 | 14 | 52 |
| | 8 | | | 1 | 6 | 3 | 2 | 6 | 7 | 4 | 6 | 35 |
| | 9 | 1 | | | 5 | 6 | 6 | 6 | 1 | 4 | 9 | 38 |
| | 10 | 2 | 4 | 3 | 12 | 11 | 23 | 20 | 23 | 27 | 28 | 153 |
| | Sum | 7 | 12 | 19 | 43 | 50 | 60 | 65 | 80 | 72 | 81 | 489 |

## Table 16c.

$\cos\theta$

| $E$ | $i$ \ $k$ | 1 | 2 | 3 | 4 | 5 | 6 | 7 | 8 | 9 | 10 | Sum |
|---|---|---|---|---|---|---|---|---|---|---|---|---|
| | 1 | | | | | | | | | | | 0 |
| | 2 | 5 | 8 | 11 | 12 | 14 | 6 | 13 | 13 | 4 | 2 | 88 |
| | 3 | | 1 | 3 | 9 | 4 | 3 | 5 | 14 | 34 | 56 | 129 |
| | 4 | 2 | 1 | | | 3 | 1 | 8 | 5 | 2 | 4 | 26 |
| | 5 | | 1 | | 3 | 2 | 3 | 4 | 3 | 4 | 4 | 24 |
| | 6 | | 2 | | 2 | 2 | 4 | 3 | 4 | 10 | 1 | 28 |
| | 7 | | | | 2 | 3 | 4 | 4 | 2 | 4 | 4 | 23 |
| | 8 | | | 2 | 1 | 3 | 4 | 3 | 1 | 5 | 4 | 23 |
| | 9 | 1 | | 2 | 2 | 3 | 5 | 2 | 4 | 8 | 9 | 36 |
| | 10 | 2 | 1 | 2 | 13 | 10 | 15 | 22 | 15 | 21 | 16 | 117 |
| | Sum | 10 | 14 | 20 | 44 | 44 | 45 | 64 | 61 | 92 | 100 | 494 |

## Table 16d.

$\cos\theta$

| $E$ | $i$ \ $k$ | 1 | 2 | 3 | 4 | 5 | 6 | 7 | 8 | 9 | 10 | Sum |
|---|---|---|---|---|---|---|---|---|---|---|---|---|
| | 1 | | | | | | | | | | | 0 |
| | 2 | | 3 | 4 | 4 | 6 | 3 | 4 | 2 | 1 | | 27 |
| | 3 | | | | 3 | | 1 | | 1 | 7 | 21 | 33 |
| | 4 | | | | | | | 3 | 1 | | 2 | 6 |
| | 5 | | | | | 1 | 1 | 1 | 1 | 1 | 1 | 6 |
| | 6 | | 1 | | 1 | 1 | 3 | 1 | 2 | 3 | 1 | 13 |
| | 7 | | | | | 1 | 2 | | 1 | 2 | 2 | 8 |
| | 8 | | | | 1 | 2 | 1 | 1 | | | 1 | 6 |
| | 9 | 1 | | | | 1 | 3 | 1 | 1 | 4 | 3 | 14 |
| | 10 | 1 | 1 | 1 | 8 | 9 | 11 | 14 | 8 | 15 | 11 | 79 |
| | Sum | 2 | 5 | 5 | 17 | 21 | 25 | 25 | 17 | 33 | 42 | 192 |

## 11. References


[1] O. Halpern, R. Lueneburg, and O. Clark, Phys. Rev. **53.** 173 (1938).
[2] E. Fermi, Ricerca sci. **7**(2), 13 (1936).
[3] C. C. Grosjean, Geneva Conference, July 1958, Paper 1692 (preprint).
[4] S. Chandrasekhar, Radiative Transfer, Oxford (1950).
[5] K. T. Spinney, The energy spectrum of neutrons reflected from a moderator, Atomic Energy Research Establishment, Harwell Rep. AERE T/M–120 (1955).
[6] A. Foderaro and F. Obenshain, Neptune, Westinghouse Atomic Power Div. Rept. WAPD–TN–517.
[7] H. Goldstein, The attenuation of gamma rays and neutrons in reactor shields, Addison-Wesley (1958).
[8] D. Hughes and R. Schwartz, Neutron cross sections, Brookhaven Natl. Lab. Rept., BNL–325 (1958).
[9] H. Lustig, H. Goldstein, and M. Kalos, An interim report on the neutron cross sections of oxygen, Nuclear Develop. Corp. of Am. Rept., NDA–086–2 (1958).
[10] H. Goldstein, P. Zweifel, and D. Foster, The slowing down of neutrons in hydrogeneous media—status of theory and experiment, Geneva Conference, July 1958, Paper 2375 (preprint).
[11] F. Ajzenberg and T. Lauritsen, Revs. Mod. Phys. **27.** 135 (1955).
[12] H. Bethe, Revs. Mod. Phys. **9**(2), 132 (1937).
[13] a. U. Fano, L. V. Spencer and M. J. Berger, Penetration and diffusion of X Rays, Encyclopedia Phys. **38.** pt. 2, Springer-Verlag (1959).
b. Monte Carlo Method (Proc. of a Symposium held in 1949), NBS Applied Math. Series No. 12 (1951).
c. Monte Carlo Methods, Proc. of a Symposium held in 1954 (H. A. Meyer, New York, N.Y., Wiley 1956).
d. G. Goertzel and M. H. Kalos, Monte Carlo Methods in Transport Problems, Prog. in Nuclear Energy, ser. I, vol. II (Pergamon Press, 1958).
[14] H. Cramer, Mathematical methods of statistics, Princeton (1946).
[15] F. Obenshain, A. Eddy and H. Kuehn, Polyphemus, A Monte Carlo study of neutron penetrations through finite water slabs, Westinghouse Atomic Power Div. Rept., WAPD–TM–54 (1957).
[16] T. Strickler, H. Gilbert, and J. Auxier, J. Nuc. Sci. Eng. **3.** 11 (1957).
[17] M. Juncosa, Random number generation on the BRL high-speed computing machines, Ballistic Research Lab. Aberdeen, Md., Rept. BRL 855.



Washington, D.C. (Paper 63A2–6)

Journal of Research of the National Bureau of Standards—A. Physics and Chemistry
Vol. 63A, No. 2, September–October 1959

# Some Vibrational-Rotational Bands of Deuterated Methanes[1]

Harry C. Allen, Jr., and Earle K. Plyler

(June 17, 1959)

A parallel band at 2,200 $cm^{-1}$ and a perpendicular band at 2,780 $cm^{-1}$ of $CH_3D$ have been observed under high resolution and analysed. The analysis of the perpendicular band revealed the presence of l-type doubling in the doubly degenerate excited state. From the analysis of the parallel band it is found that $B_0=3.880$ $cm^{-1}$. A hybrid band of $CD_3H$ has been observed near 2,600 $cm^{-1}$. Both active components, $A$ and $E$ are observed and analysed. The ground state $B_0$ value found from this analysis is in good agreement with previous determinations.

## 1. Introduction

A study of the spectra of deuterated methanes was undertaken as part of a program for studying the spectra of deuterated molecules. In spite of the apparent simplicity of the $CH_3D$ and $CD_3H$ molecules, both being symmetric tops, very little work has been done on their spectra. Early work on the spectra of these molecules was done at rather low resolution [1,2].[2] More recently one band of each molecule has been studied under somewhat higher resolution by Thompson and his coworkers [3,4]. Two bands of $CD_3H$ have been studied in the photographic infrared [5] and the overtone of the C—H stretch, $\nu_1$, has been studied with high resolution [6]. A complete study of the spectra of the two molecules has been made using prism instruments by Wilmshurst and Bernstein [7].

The resolution available with the instruments of the Radiometry Section made it feasible to study several bands of these molecules between 3 and 6 $\mu$ in greater detail than had been possible before. No perpendicular band of either molecule had previously been studied with high resolution. In this work a perpendicular band of $CH_3D$ was observed and analysed. Likewise a hybrid band of $CD_3H$ was observed and analysed, one component of which obeys the selection rules of a perpendicular type band.

## 2. Experimental Method

The spectra were recorded on a 2.35-m grating spectrometer. For the wavelengths shorter than 4 $\mu$ the spectrometer was equipped with a 10,000 lines/in. grating which was double-passed, and a cooled PbS detector. Higher orders of the grating were eliminated by using a cut-off filter that started transmitting at 2.7 $\mu$. The resolution in this region is 0.02 to 0.03 $cm^{-1}$. For the $CH_3D$ band at 2,200 $cm^{-1}$ the spectrometer was equipped with a PbTe detector and the grating was not double-passed. The resolution in this band was $\sim$0.05 $cm^{-1}$. The spectra were measured by using the fringes of a Fabry-Perot interferometer as previously described [8].

The $CH_3D$ and $CD_3H$ were obtained from Merck and Co., Ltd., and had a stated purity of 98 percent. The gases were used without further purification and no troublesome impurities were found. The gas was placed in a cell with a pathlength of 6 m and the gas pressures used ranged from a few millimeters to a few centimeters of Hg.

Two regions of absorption of $CH_3D$ were studied in detail. The parallel band at 2,200 $cm^{-1}$ which is, in Herzberg's notation [9], $\nu_2$, and a perpendicular combination band near 2,780 $cm^{-1}$ which has the excited state $\nu_3+\nu_5$. Recorder traces of the observed spectra of $CH_3D$ are shown in figures 1 and 2.

One region of $CD_3H$ was studied in detail. This region is of particular interest since the absorption arises from a hybrid band. Both infrared active components of this band are resolved. The observed absorption is shown in figures 3 and 4.

## 3. $CH_3D$

*Parallel band.* The absorption in the 2,200 $cm^{-1}$ region is clearly that arising from a typical parallel band. Unfortunately the short wavelength portion of the absorption is masked by the absorption of atmospheric $CO_2$. In spite of this handicap it is possible to identify transitions as high as $R(10)$, although some of the $K$- components are not observed because of the atmospheric absorption. The observed wave numbers and quantum number assignments are given in table 1. Some of the assignments are indicated on figure 1. The intensity alternation of the $K$-components arising from the nuclear spin statistics of the three identical H-atoms is clearly seen in figure 1. The statistical weights of the $A$ and $E$ rotational levels are in the ratio 2:1, and the observed intensity alternation simplifies the process of assigning quantum numbers. The rotational-vibrational energy levels of a symmetric rotor in a nondegenerate vibrational state are given by

$$F(J,K)=BJ(J+1)+(A-B)K^2 + D_JJ^2(J+1)^2+D_{JK}J(J+1)K^2+D_KK^4. \quad (1)$$

[1] The work reported herein was supported by the U.S. Atomic Energy Commission.

[2] Figures in brackets indicate the literature references at the end of this paper.

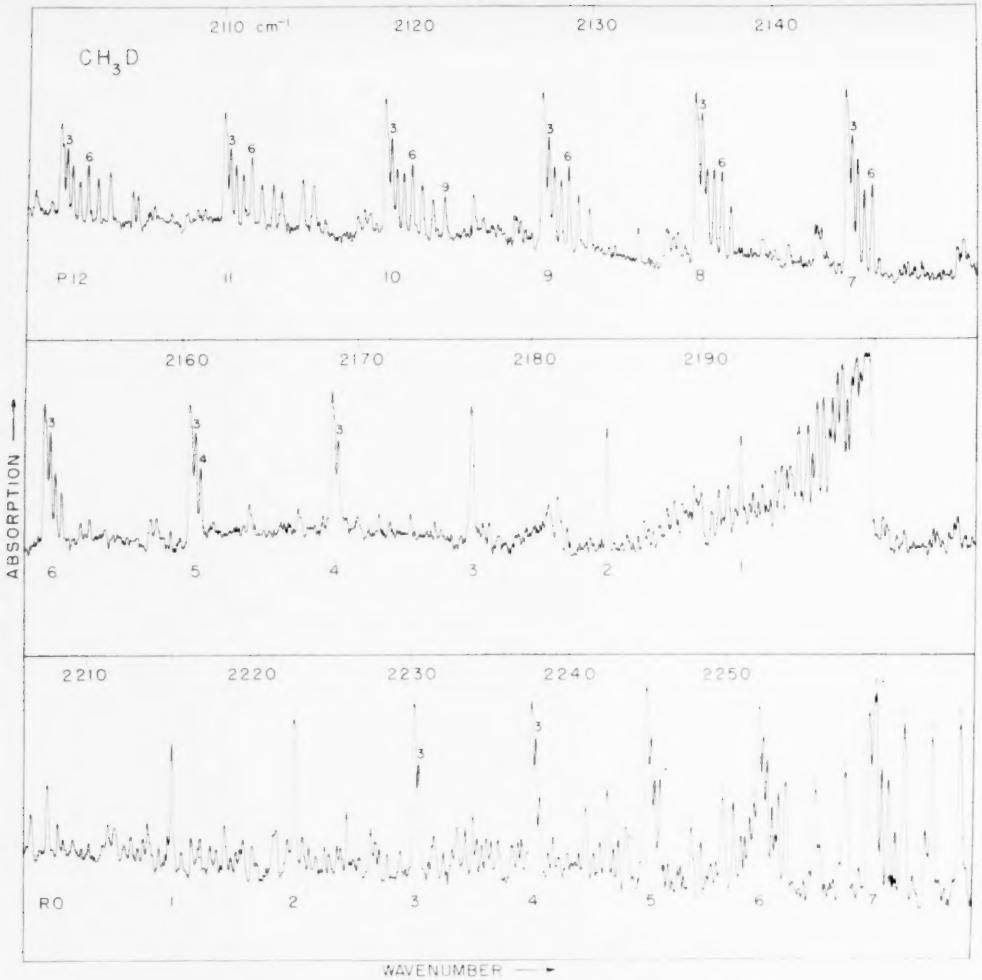


FIGURE 1. *The parallel band, $\nu_2$, of* $CH_3D$ *at 2,200 cm*$^{-1}$.

This energy expression together with the selection rules

$$\Delta J=0,\pm1 \qquad \Delta K=0 \qquad K\neq0$$
$$\Delta J=\pm1 \qquad \Delta K=0 \qquad K=0$$

enables the calculation of the difference relations involving only the ground state energies.

$$\Delta F''_2=\frac{R(J-1,K)-P(J+1,K)}{(2J+1)}=(2B''-3D''_J) -4D''_J\left(J+\frac{1}{2}\right)^2-4D''_{JK}K^2, \qquad (2)$$

and a similar one involving only excited state energies,

$$\Delta F'_2=\frac{R(J,K)-P(J,K)}{(2J+1)}=(2B'-3D'_J) -4D'_J\left(J+\frac{1}{2}\right)^2-2D'_{JK}K^2, \qquad (3)$$

which were used to determine the B's and centrifugal distortion constants. Since the transitions in the P- and R-branches with $K=0$, 1, 2 were not resolved these transitions were not used in the calculations. Thus 35 equations of type (2) and 29 equations of type (3) with $K\geq3$ were solved by the method of least squares for the best estimates of the constants. The combination sum,

$$R(J-1, K)+P(J, K)=2\nu_0+2[(A'-B') -(A''-B'')]K^2+2(D'_K-D''_K)K^4+2[(B'-B'') +(D'_{JK}-D''_{JK})K^2]J^2+2(D'_J-D''_J)J^2(J+1)^2, \qquad (4)$$

was used to determine the band center. The results of these determinations are given in table 2. These molecular constants compare favorably with previous results [4] although a different method of analysis was used here. The present results are believed to be more precise and are more complete than those reported previously for this band. Earlier workers neglected the effect of $D_{JK}$ which accounts for the apparently different values of $(A'-B')-(A''-B'')$

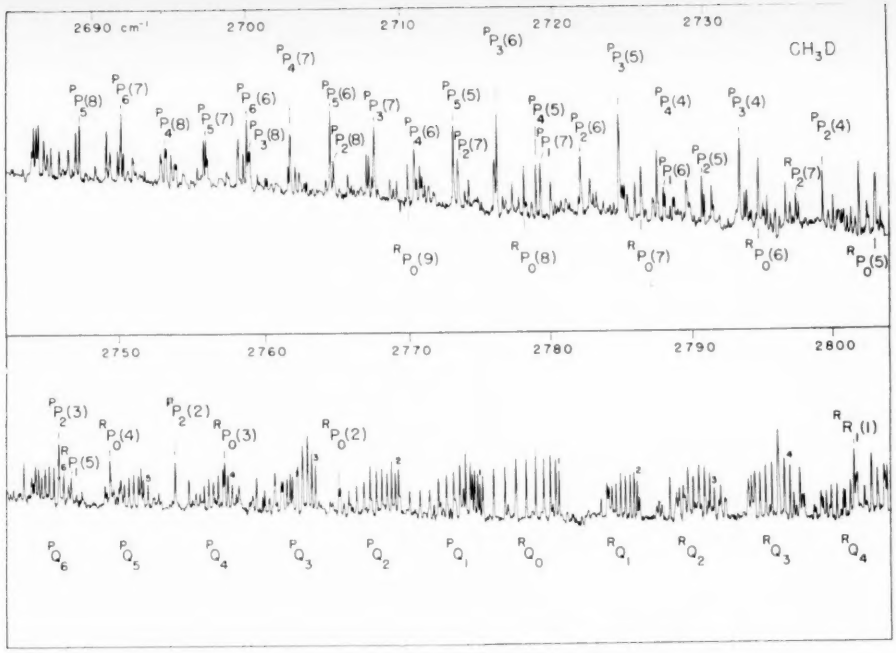


FIGURE 2. *The perpendicular band, $\nu_3+\nu_5$ of* $CH_3D$.

The transitions have been designated by the notation suggested by Herzberg. The presuperscript $P$ or $R$ means $\Delta K=-1$ or $\Delta K=+1$ respectively. The basic symbol $P$, $Q$, or $R$ has the usual meaning $\Delta J=-1$, 0, $+1$. The subscript gives the $K$ value of the ground state level of the subband while the number in parenthesis gives the $J$ value of the ground state.

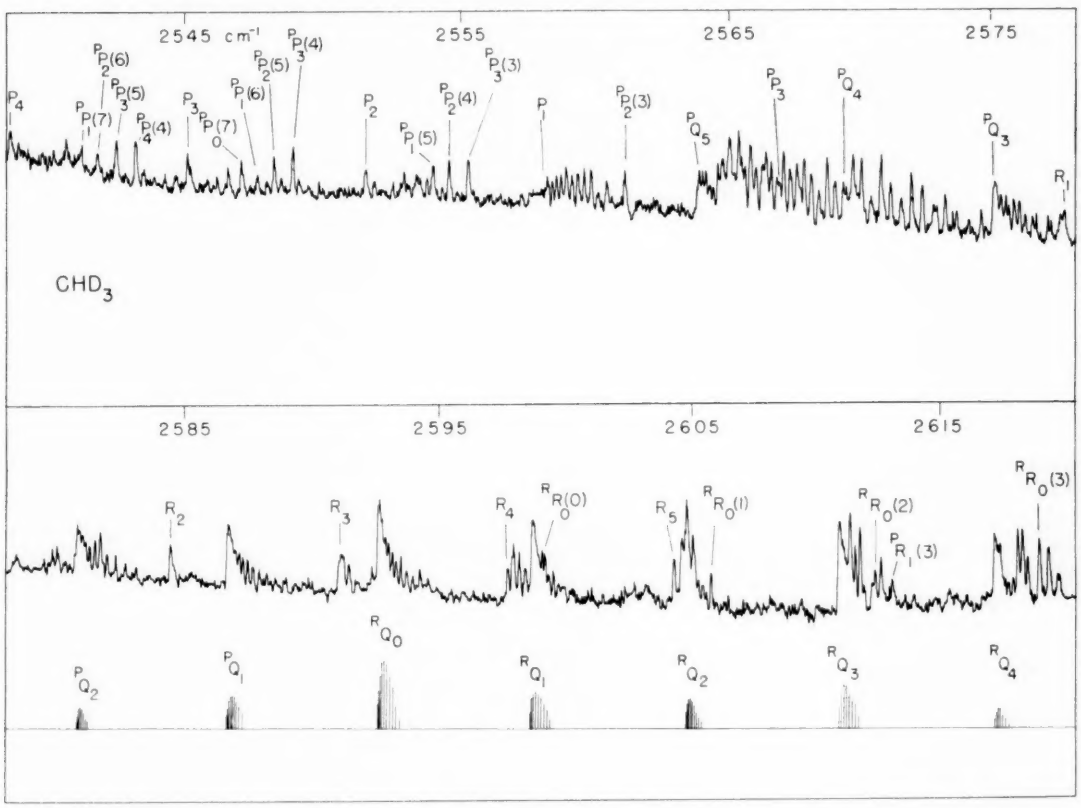


FIGURE 3. *A portion of the $2\nu_5$ band of* $CD_3H$ *showing the Q-branch and low J-, P-, and R-branch transitions of the A-component.*

The $Q$-branches of the $E$-component are also clearly evident in the lower panel.

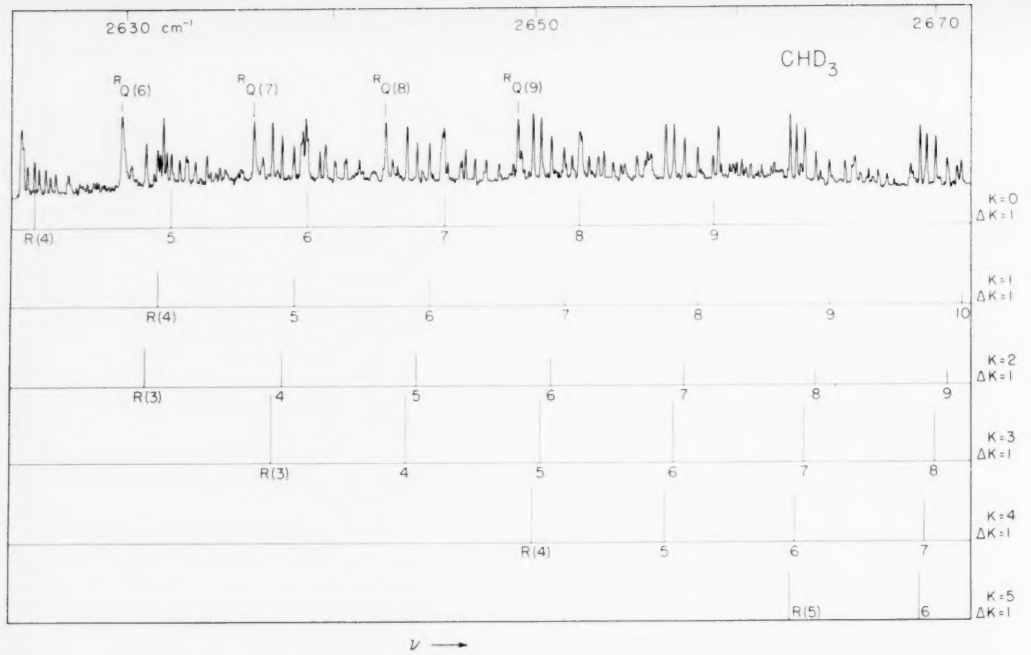


FIGURE 4. *The* $^{R}R_{K}$ *branches of the* E*-component of the* $2\nu_5$ *band of* $CD_3H$.

TABLE 1. *Observed wave numbers of 2,200 cm*$^{-1}$ *band of* $CH_3D$

| $J_K$ | $R$ | $P$ | $J_K$ | $R$ | $P$ |
|---|---|---|---|---|---|
| $0_0$ | 2,207.70 | | $8_8$ | 2,267.18 | 2,137.10 |
| | | | $8_7$ | 2,267.66 | 2,137.61 |
| $1_0$ | | 2,192.29 | | | |
| $1_1$ | 2,215.32 | | $9_{0,1}$ | 2,272.75 | 2,127.29 |
| | | | $9_2$ | 2,272.85 | 2,127.41 |
| $2_{0,1}$ | 2,222.82 | 2,184.45 | $9_3$ | 2,273.05 | 2,127.63 |
| $2_2$ | 2,222.93 | | $9_4$ | 2,273.31 | 2,127.92 |
| | | | $9_5$ | | 2,128.28 |
| $3_{0,1}$ | 2,230.23 | 2,176.53 | $9_6$ | 2,274.00 | 2,128.72 |
| $3_2$ | 2,230.35 | 2,176.63 | $9_7$ | 2,274.47 | 2,129.25 |
| $3_3$ | 2,230.54 | | $9_8$ | 2,274.99 | 2,129.83 |
| $4_{0,1}$ | 2,237.56 | 2,168.50 | $10_{0,1}$ | 2,279.48 | 2,118.83 |
| $4_2$ | 2,237.66 | 2,168.63 | $10_2$ | 2,279.58 | 2,118.95 |
| $4_3$ | 2,237.86 | 2,168.84 | $10_3$ | 2,279.80 | 2,119.16 |
| $4_4$ | 2,238.13 | | $10_4$ | 2,280.04 | 2,119.44 |
| | | | $10_5$ | | 2,119.80 |
| $5_{0,1}$ | 2,244.78 | 2,160.44 | $10_6$ | 2,280.75 | 2,120.26 |
| $5_2$ | 2,244.89 | 2,160.55 | $10_7$ | 2,281.21 | 2,120.78 |
| $5_3$ | 2,245.09 | 2,160.77 | $10_8$ | | 2,121.38 |
| $5_4$ | 2,245.34 | 2,161.04 | $10_9$ | | 2,121.99 |
| $5_5$ | 2,245.68 | | | | |
| | | | $11_{0,1}$ | | 2,110.27 |
| $6_{0,1}$ | 2,251.94 | 2,152.26 | $11_2$ | | 2,110.40 |
| $6_2$ | | 2,152.39 | $11_3$ | | 2,110.60 |
| $6_3$ | 2,252.23 | 2,152.59 | $11_4$ | | 2,110.90 |
| $6_4$ | 2,252.48 | 2,152.87 | $11_5$ | | 2,111.26 |
| $6_5$ | 2,252.80 | 2,153.23 | $11_6$ | | 2,111.70 |
| $6_6$ | 2,253.21 | | $11_7$ | | 2,112.23 |
| | | | $11_8$ | | 2,112.84 |
| $7_{0,1}$ | 2,258.97 | 2,144.02 | $11_9$ | | 2,113.30 |
| $7_2$ | 2,259.05 | 2,144.13 | $11_{10}$ | | 2,114.33 |
| $7_3$ | 2,259.31 | 2,144.35 | | | |
| $7_4$ | | 2,144.63 | $12_{0,1}$ | | 2,101.62 |
| $7_5$ | 2,259.84 | 2,144.98 | $12_2$ | | 2,101.77 |
| $7_6$ | 2,260.25 | 2,145.42 | $12_3$ | | 2,101.97 |
| $7_7$ | 2,260.71 | | $12_4$ | | 2,102.27 |
| | | | $12_5$ | | 2,102.65 |
| $8_{0,1}$ | 2,260.90 | 2,135.68 | $12_6$ | | 2,103.10 |
| $8_2$ | 2,266.02 | 2,135.81 | $12_7$ | | 2,103.62 |
| $8_3$ | 2,266.20 | 2,136.03 | $12_8$ | | 2,104.25 |
| $8_4$ | 2,266.47 | 2,136.31 | $12_9$ | | 2,105.48 |
| $8_5$ | | 2,136.37 | $12_{10}$ | | 2,105.75 |

in the $P$- and $R$-branches, a result they noticed but did not explain. Starting at P(10) there is a perturbation which affects the $K=9$ component. This arises from an interaction of the excited state with another higher vibrational level of $CH_3D$. Some of the transitions to this other level can be seen in figure 1. Unfortunately not enough of this overlapping band can be identified to enable a complete understanding of this perturbation. However such a perturbation cannot have any effect on the ground state constants as determined by the method outlined here. The perturbed levels were not used in determining the excited state constants.

TABLE 2. *Constants of* $CH_3D$ *from* $\nu_2$ *at 2,200 cm*$^{-1}$

| | Excited | Ground |
|---|---|---|
| $B'$ | 3.837$_8$ cm$^{-1}$ | 3.880$_0$ cm$^{-1}$ |
| $C'_J$ | 0.00005$_8$ | 0.00005 |
| $D'_{JK}$ | .00012 | .00012 |

$(A'-B')-(A''-B'')=0.03858$ $\quad \nu_0=2200.03$.

*Perpendicular band.* The absorption near 2,780 cm$^{-1}$ arises from the perpendicular band $\nu_3+\nu_5$, and is shown in figure 2. The excited state of this band is doubly degenerate and the rotational contribution is not given by the simple expression (1). The levels are perturbed by the interaction of rotation and vibration which leads to an additional term in the energy, thus,

$$F(J,K)=BJ(J+1)+(A-B)K^2\mp 2A\zeta K + \text{centrifugal terms.} \qquad (5)$$

For a perpendicular transition the selection rules on $K$ are somewhat relaxed,

$$\Delta J=0, +1 \qquad \Delta K=\pm 1.$$

The overall band is thus made up by a series of subbands. [9, pp. 425 and 431] The prominent feature of the overall band is the series of $Q$-branches of the subbands whose spacing is approximately $2[A'(1-\zeta)-B']$.

The series of $Q$-branches characteristic of a perpendicular band are clearly evident in the 2,780 $cm^{-1}$ region. Again the nuclear spin statistics provide the clue which enables the assignment of $K$-values to the $Q$-branches. Those $Q$-branches with ground state $K$'s a multiple of three are stronger due to the nuclear spin statistics and this intensity pattern is clearly evident in the figure. This is the first perpendicular band to be observed in which all the individual $Q$-branch transitions are resolved. Once the quantum numbers have been assigned in the Q-branches, each subband can be considered separately and effective constants can be calculated from the $Q$-branch using formulas applicable to linear molecules, i.e.,

$$\nu=\nu_{sub}+(B'-B'')J(J+1)+(D'_J-D''_J)J^2(J+1)^2. \quad (6)$$

These effective constants together with the ground state constants determined from the parallel band can then be used to calculate the $P$- and $R$-branches of the subband associated with the particular $Q$-branch in question by using

$$\nu=\nu_{sub}+(B'+B'')m+(B'-B'')m^2+2(D'_J+D''_J)m^3+(D'_J-D''_J)m^4, \quad (7)$$

with $m=-J$ for the $P$-branch and $m=J+1$ for the $R$-branch.

It should be remembered that in a given subband the branch in which $\Delta J=\Delta K$ is the stronger and becomes very much stronger than the branch with $\Delta J\neq\Delta K$ as $K$ increases. In this manner assignments could be made for all the subbands except that for which $K=0$. The observed wave numbers and quantum number assignments made in this manner are given in table 3. Unfortunately the short wavelength end of the band is overlapped by a much stronger band of $CH_3D$ so the weaker perpendicular band could not be analyzed in this region. The $P$- and $R$-branch transitions of the $K=0$ subband were located by a trial and error procedure. Since both branches are fairly strong in this molecule they could be picked out with a minimum of difficulty.

Ground state constants and band centers were determined using equations (2) and (4) with $K=0$. The $\nu_0$ found from (4) agreed exactly with that found from (6) but the values of $B'-B''$ were different by nearly a factor of 3, that found using (6) being larger. This behavior is reminiscent of the behavior of a perpendicular transition of a linear molecule where the levels of the degenerate state have the so-called l-type doubling, one component of the doublet being accessible from the ground state with $\Delta J=0$, and the other component being accessible from the ground state when $\Delta J=\pm 1$,

TABLE 3. *Subbands of* $CH_3D$ *perpendicular band at 2,780 cm*$^{-1}$

| J | K=0 | K=1 | | K=2 | | K=3 | | K=4 | K=5 | K=6 |
|---|---|---|---|---|---|---|---|---|---|---|
| | ΔK=1 | ΔK=1 | ΔK=−1 | ΔK=1 | ΔK=−1 | ΔK=1 | ΔK=−1 | ΔK=−1 | ΔK=−1 | ΔK=−1 |
| ΔJ=0: | | | | | | | | | | |
| 1 | 2,780.42 | | 2,774.85 | | | | | | | |
| 2 | 2,780.20 | 2,785.96 | 2,774.70 | | 2,769.15 | | | | | |
| 3 | 2,779.82 | 2,785.74 | 2,774.48 | 2,791.43 | 2,768.91 | | 2,763.40 | | | |
| 4 | 2,779.35 | 2,785.44 | 2,774.19 | 2,791.11 | 2,768.64 | 2,796.86 | 2,763.14 | 2,757.66 | | |
| 5 | 2,778.78 | 2,785.11 | 2,773.85 | 2,790.75 | 2,768.33 | 2,796.44 | 2,762.82 | 2,757.38 | 2,751.91 | 2,746.15 |
| 6 | 2,778.13 | 2,784.78 | 2,773.45 | 2,790.34 | 2,767.98 | | 2,762.47 | 2,757.04 | 2,751.59 | 2,745.85 |
| 7 | 2,777.40 | 2,784.43 | 2,773.00 | 2,789.95 | 2,767.60 | 2,795.54 | 2,762.09 | 2,756.71 | 2,751.27 | 2,745.50 |
| 8 | 2,776.61 | | 2,772.52 | 2,789.57 | 2,767.18 | 2,795.11 | 2,761.64 | 2,756.37 | 2,750.92 | 2,745.19 |
| 9 | 2,775.82 | | 2,771.95 | 2,789.23 | 2,766.73 | 2,794.70 | 2,761.14 | 2,756.05 | 2,750.61 | 2,744.90 |
| 10 | 2,775.04 | | 2,771.32 | | 2,766.23 | | 2,760.58 | | 2,750.30 | |
| ΔJ=+1: | | | | | | | | | | |
| 0 | 2,788.27 | | | | | | | | | |
| 1 | 2,795.99 | 2,801.48 | | | | | | | | |
| 2 | 2,803.64 | 2,809.00 | 2,797.76 | 2,814.70 | 2,792.19 | | | | | |
| 3 | 2,811.28 | 2,816.47 | 2,805.26 | 2,822.15 | 2,799.68 | 2,827.87 | 2,794.16 | | | |
| 4 | 2,818.93 | 2,823.89 | 2,812.65 | 2,829.51 | 2,807.12 | 2,835.20 | 2,801.62 | | | |
| 5 | 2,826.61 | 2,831.35 | 2,820.00 | 2,836.85 | 2,814.50 | 2,842.51 | 2,809.00 | | | |
| 6 | 2,834.32 | 2,838.71 | 2,827.29 | 2,844.20 | 2,821.83 | | 2,816.29 | | | |
| ΔJ=−1: | | | | | | | | | | |
| 1 | | | | | | | | | | |
| 2 | 2,764.99 | | 2,759.33 | | 2,753.76 | | | | | |
| 3 | 2,757.15 | | 2,751.44 | | 2,745.85 | | 2,740.35 | | | |
| 4 | 2,749.35 | 2,754.70 | 2,743.47 | | 2,737.91 | | 2,732.39 | 2,726.91 | | |
| 5 | 2,741.47 | 2,746.67 | 2,735.43 | 2,752.36 | 2,729.89 | 2,758.13 | 2,724.40 | 2,718.91 | 2,713.46 | |
| 6 | 2,733.63 | 2,738.61 | 2,727.34 | 2,744.27 | 2,721.83 | 2,749.96 | 2,716.34 | 2,710.89 | 2,705.43 | 2,700.03 |
| 7 | 2,725.85 | 2,730.54 | 2,719.20 | 2,736.12 | 2,713.76 | 2,741.78 | 2,708.27 | 2,702.85 | 2,697.39 | 2,691.97 |
| 8 | 2,718.12 | | 2,711.05 | 2,727.97 | 2,705.64 | 2,733.63 | 2,700.14 | 2,694.77 | 2,689.32 | 2,683.91 |
| 9 | | | | | | | | | 2,681.27 | |
| 10 | | | | | | | | | 2,673.17 | |

thus leading to a different effective $B'$ value for the $Q$-branch than for the $R$- and $P$-branches.

The possibility of this type of behavior in symmetric top molecules was first suggested by Wilson [9, 10]. The interaction to a second order approximation has been worked out by Nielsen [11] who has found that for molecules with $C_{3v}$ symmetry the interaction matrix elements are of the form

$$(v_i,l_i,K|H_2'|v_i,l_i\pm 2,K\pm 2=q\{[(v_i\mp l_i)(v_i\pm l_i+2)]$$
$$\times[J(J+1)-K(K\pm 1)][J(J+1)-K(K\pm 1)(K\pm 2)]\}^{\frac{1}{2}} \quad (7)$$

As can be seen levels are mixed pair-wise by this interaction but only the levels $K=1$, $l=1$; $K=-1$, $l=-1$ are actually split. All other levels are merely shifted in position by this interaction to this approximation. For $K=1$, $l=1$, (7) reduces to

$$q[v+1]\ J(J+1) \quad (8)$$

which is the same as the expression for a linear molecule. The actual splitting is twice the quantity given in (8). Since the interaction in the $K=0$ subband varies as $J(J+1)$ it has the effect of producing two effective $B'$ values in the subband. Thus from the two effective $B'$s found for the excited state with $K=1$ it is possible to evaluate $B'-B''$ and $q$ for this state. These results are included in table 5.

Sufficient lines in the $P$- and $R$-branches of 6 subbands were observed to enable a determination of subband centers from the transitions using the relation

$${}^RR_K(J-1)+{}^RP_K(J)=2\nu_{\text{sub}}$$
$$+(B'-B'')J^2+(D'-D'')J^4 \quad (9)$$

since $K$ is a constant for each subband. The highest value of $K$ for any subband is 3. Similarly the band centers of the same subbands can be determined from (6). The $\nu_0$'s obtained by these two methods agree within the experimental error and are compared in table 4.

These subband centers may then be used to determine the quantities in the relation

$$\nu_{\text{sub}}=\nu_0+[A'(1-2\zeta)-B']\pm 2$$
$$[A'(1-\zeta)-B']K+[(A'-B')-(A''-B'')]K^2 \quad (10)$$

This relation neglects the effect of centrifugal distortion but this should not cause serious error since only values of $K\leq 3$ are used. The main error will arise because nowhere is $D_{JK}'$ considered. However since no high quantum numbers could be used in the analysis there was no good way to determine this constant with any precision for the excited state.

In view of the perturbation in the excited state, the usual combination relations among the transitions of a perpendicular band could not be used in the analysis of this band [12]. However, if the perturbation discussed above is the only perturbation present, the combination relation

TABLE 4. *Subband centers of* $\nu_3+\nu_5$ *band of* $CH_3D$

| $K$ | $\Delta K$ | $Q$-branch | $R$- and $P$-branches |
|---|---|---|---|
| 0 | 1 | 2,780.55 | 2,780.55 |
| 1 | 1 | 2,786.15 | 2,786.17 |
| 1 | −1 | 2,774.90 | 2,774.88 |
| 2 | 1 | 2,791.90 | 2,791.90 |
| 2 | −1 | 2,769.33 | 2,769.31 |
| 3 | 1 | 2,797.73 | ---------- |
| 3 | −1 | 2,763.76 | 2,763.75 |
| 4 | −1 | 2,758.30 | ---------- |
| 5 | −1 | 2,752.77 | ---------- |

$$[{}^PQ(J_K)+{}^RQ(J_K)]/2=\nu_0+[A'(1-2\zeta)-B']$$
$$+(B'-B'')J(J+1)+(D'-D'')J^2(J+1)^2, \quad (11)$$

$K$ constant, averages out this perturbation and if for each $K$ one plots

$$[{}^PQ(J_K)+{}^RQ(J_K)]/2-(D'-D'')J^2(J+1)^2$$
versus $J(J+1)$

a straight line should result. Such a plot for three values of $K$ gives good straight lines and hence seems to rule out any further perturbations.

The value of $q$ obtained from the $K=0$ subband does not appear to be entirely satisfactory for the other subbands. However, not enough transitions in the other subbands are observed to enable one to make meaningful higher order corrections. The constants derived from the analysis of this band are collected in table 5. Unfortunately the inadequacy of the data makes these constants subject to uncertainties which are larger than would be normal for measurements of this precision. The strong overlapping in the high frequency portion of the absorption sharply limits the number of ${}^RR$ and ${}^PR$ lines which can be assigned and the general weakness of the ${}^RP$ and ${}^PR$ lines makes it impossible to assign many of these transitions. However it is felt that the analysis is correct in all essential features and that only the evaluation of the small higher order corrections needs improvement.

TABLE 5. *Derived constants from the* $\nu_3+\nu_5$ *band of* $CH_3D$

| | | $cm^{-1}$ |
|---|---|---|
| $\nu_0+[A'(1-2\zeta)-B']$ | = | 2,780.55 |
| $A'(1-\zeta)-B'$ | = | 2.82 |
| $(A'-B')-(A''-B'')$ | = | 0.02 |
| $B''$ | = | 3.88 |
| $B'-B''$ | = | −0.041 |
| $D_J'-D_J''$ | = | .00011 |
| $q$ | = | .011 |

If $A''$ is calculated from the methane geometry, it is then possible to evaluate $\zeta$ and $\nu_0$. Using $A=5.24$ $cm^{-1}$ one finds $\zeta=-0.26$. Simple theory predicts [13] that the $\zeta$ of this band should be the same as for the fundamental $\nu_5$. Herzberg [9] has estimated $\zeta_5=-0.27$, in remarkable agreement. However, it is felt that this may be in large measure fortuitous. The above figures lead to a value of $\nu_0=2{,}776.33$ $cm^{-1}$.

## 4. $CD_3H$

*Hybrid band.* Only the absorption of $CD_3H$ near 2,600 $cm^{-1}$ was studied in detail. This region has more than usual interest. The main absorption here is due to the first overtone of $\nu_5$. $\nu_5$ is a degenerate fundamental and its first overtone has the components $A_1$ and $E$ [9,14].

The electric dipole moment selection rules allow transitions from the ground state to both the $A_1$ and $E$ components of this overtone level. Thus one would expect the absorption in this region to show the features of both a parallel and a perpendicular case. This is, indeed, the case as can be seen in figures 3 and 4. There is a collected $Q$-branch near 2,565 $cm^{-1}$ which is characteristic of a parallel type band. It is possible to identify the $P$- and $R$-branch transitions of this band and they are labelled in figures 3 and 4. Unfortunately the absorption is very weak so the $K$-components of the $P$- and $R$-branch transitions could not be identified but only the general absorption peak representing the aggregate absorption of all the $K$-components. Thus precise molecular constants could not be determined for this component of the overtone. The band center of this component is 2,564.6 $cm^{-1}$. The $B_0$ value is compatible with the previously determined values, 3.278 $cm^{-1}$ and the $B'-B''$ value is about 0.01 $cm^{-1}$.

The series of $Q$-branches of the subbands belonging to the $E$-component are clearly evident in figure 3, the strongest being near 2,590 $cm^{-1}$. This strongest $Q$-branch belongs to the $K=0$ subband, and the other $K$-numbering follows automatically, since again for this molecule the subbands with $K$ a multiple of 3 are strong due to nuclear spin statistics. In this case the ratio is 11:8. Unfortunately the structure of these $Q$-branches cannot be resolved well because the band is very weak, and if the pressure in the absorption cell is increased the pressure broadening eliminates the fine structure. Also the quantity $(B'-B'')$ is very small in this transition $\sim 0.007$ $cm^{-1}$.

The assignments of the $P$- and $R$-branch transitions were made by calculating the approximate line positions using the relation

$$\nu_0=\nu_{sub}\pm[A'(1-\zeta)-B']K+[(A'+B')-(A''-B'')]K^2\pm(B'+B'')m+(B'-B'')m^2 \qquad (12)$$

Here the negative sign of the $K$ dependent term applies for $\Delta K=-1$ and $m=-J$ for the $P$-branch and $m=J+1$ for the $R$-branch. The coefficients of $K$ and $K^2$ were estimated from the $Q$-branch positions and the coefficients of $m$ and $m^2$ were estimated from previous work on this molecule [5, 6]. The resulting assignments are given in table 6 and shown in figures 3 and 4. Assignments could be made in 11 subbands. Unfortunately, due to weakness of the absorption only lines in the branches $\Delta K=\Delta J$ could be assigned with any degree of assurance and are the only ones given in the table and the only ones used in subsequent calculations. In the $K=0$ subband most of the $P$-branch lines were masked by other absorption and could not be uniquely assigned to absorption peaks. The measurements could not be extended to longer wavelengths because of the weakness of the absorption and the fact that the sensitivity of the PbS detector falls off rapidly beyond 3.5 $\mu$. Since the $Q$-branch transitions were not resolved and since, in general, only the stronger

TABLE 6. *Subband assignments for the* E*-component of the hybrid band of* $CD_3H$

| $J$ | $K=0$ | $K=1$ | | $K=2$ | | $K=3$ | | $K=4$ | | $K=5$ | | $K=6$ |
|---|---|---|---|---|---|---|---|---|---|---|---|---|
| | | $\Delta K=+1$ | $\Delta K=-1$ | $\Delta K=1$ | $\Delta K=-1$ | $\Delta K=1$ | $\Delta K=-1$ | $\Delta K=1$ | $\Delta K=-1$ | $\Delta K=1$ | $\Delta K=-1$ | $\Delta K=1$ |
| $\Delta J=+1$: | | | | | | | | | | | | |
| 0 | 2,599.19 | | | | | | | | | | | |
| 1 | 2,605.76 | | | | | | | | | | | |
| 2 | 2,612.36 | | | | | | | | | | | |
| 3 | 2,618.98 | | 2,613.06 | 2,624.40 | | | | | | | | |
| 4 | 2,625.58 | | 2,619.70 | 2,630.39 | | 2,637.12 | | | | | | |
| 5 | 2,632.20 | 2,631.57 | 2,626.33 | 2,637.59 | | 2,643.70 | | 2,649.89 | | | | |
| 6 | 2,638.84 | 2,638.16 | | 2,644.19 | | 2,650.29 | | 2,656.48 | | 2,662.74 | | |
| 7 | 2,645.52 | 2,644.79 | | 2,650.81 | | 2,656.89 | | 2,663.06 | | 2,669.31 | | 2,675.64 |
| 8 | 2,652.17 | 2,651.43 | | 2,657.41 | | 2,663.48 | | 2,669.64 | | 2,675.86 | | 2,682.18 |
| 9 | | 2,658.07 | | 2,664.03 | | 2,670.08 | | 2,676.21 | | 2,682.42 | | 2,688.71 |
| 10 | | 2,664.72 | | 2,670.66 | | 2,676.69 | | 2,682.80 | | 2,688.99 | | 2,695.27 |
| 11 | | 2,671.38 | | 2,677.31 | | 2,683.32 | | 2,689.39 | | 2,695.55 | | 2,701.80 |
| 12 | | 2,678.07 | | 2,683.98 | | 2,689.93 | | 2,695.97 | | 2,702.12 | | 2,708.36 |
| 13 | | | | | | 2,696.55 | | 2,702.58 | | 2,708.67 | | 2,714.90 |
| 14 | | | | | | 2,703.19 | | 2,709.18 | | | | 2,721.42 |
| 15 | | | | | | 2,709.83 | | | | | | 2,727.99 |
| $\Delta J=-1$: | | | | | | | | | | | | |
| 1 | | | | | | | | | | | | |
| 2 | | | | | | | | | | | | |
| 3 | 2,572.99 | | 2,567.08 | | 2,561.21 | | 2,555.42 | | | | | |
| 4 | | 2,572.45 | 2,560.58 | | 2,554.71 | | 2,548.94 | | 2,543.21 | | | |
| 5 | 2,559.98 | 2,565.96 | 2,554.09 | | 2,548.24 | | 2,542.48 | | 2,536.74 | | 2,531.09 | |
| 6 | | 2,559.50 | 2,547.62 | | 2,541.80 | | 2,536.06 | | 2,530.28 | | 2,524.63 | |
| 7 | | | 2,541.21 | | 2,535.39 | | | | 2,523.86 | | 2,518.19 | |
| 8 | | | 2,534.83 | | | | | | | | 2,511.78 | |
| 9 | | | | | | | | | | | 2,505.39 | |

Lines not listed are obscured by other absorption in this band.

branch of the subbands could be observed it was not possible to use the usual combination relations for a perpendicular band in the analysis. Thus an alternate and less desirable method of deriving the molecular constants had to be used. This method involved the use of an expression for the line position deduced from the energy expression for the two energy levels in the transition. In order to include the effects of centrifugal distortion an expression of thirteen terms had to be used. One would expect to fit almost any set of observations with this many disposable constants and the use of this expression is justified only by the results obtained. The expression used is

$$\nu=\nu_0+[A'(1-2\zeta)-B']+bK+cK^2+dK^3+eK^4$$
$$+fm+gm^2+hm^3+im^4+jmK+kmK^2+lm^2K+nm^2K^2 \quad (13)$$

in which the coefficients are readily related to the molecular constants from the expressions for the vibrational rotational terms, (1) and (5). Eighty-one equations of type (13) were fit by the method of least squares. The resulting values of the molecular constants, where they can be compared, are in remarkable agreement with those determined previously [5, 6]. The agreement between observed and calculated frequencies about 0.01 $cm^{-1}$, and the uncertainties in the constants are very small. The derived constants are given in table 7. The size of the higher order terms indicates that there is no l-type doubling interaction in the excited state of this band. Using the methane geometry it is possible to calculate a value for the ground state $A$ of this molecule, $A=2.628$ $cm^{-1}$. With this value of $A''$ and the constants in table 7 one finds a value $\zeta=0.89$. Thompson [4] has estimated $\zeta_5$ from the fundamental to be 0.67. Simple theory predicts the $\zeta$ here should be twice the $\zeta$ of the fundamental; however, it is thought that the $\zeta$ value from the fundamental band is not sufficiently precise to justify comparisons at this time.

TABLE 7. *Molecular constants of* $CD_3H$ *derived from the E-component of the hybrid band near 2,600* $cm^{-1}$

| | |
|---|---|
| $A'(1-\zeta)-B'$ | $=2.977\pm.002$ $cm^{-1}$ |
| $(A'-B')-(A''-B'')$ | $=0.0379\pm0.0018$ |
| $B''$ | $=3.278\pm0.001$ |
| $B'$ | $=3.285\pm0.001$ |
| $D_J''-D_J'$ | $=5.0\pm0.8\times10^{-5}$ |
| $D_{JK}''$ | $=4\times10^{-5}$ |
| $D_{JK}'$ | $=1\times10^{-5}$ |
| $D_K'\sim D''\sim$ | $\sim0$ |
| $\nu_0+[A'(1-2\zeta)-B']$ | $=2592.637\pm0.005$ |

The band center, $\nu_0$, becomes 2,592.64 if one uses the above values of $A'$ and $\zeta$. The separation of these two components is given by $g_{55}[(l+2)^2-l^2]$, with $l=0$ in this case. Thus from the component separation $g_{55}=8.05$ $cm^{-1}$.

---

The authors express their appreciation to Carroll Dannemiller and Joseph Cameron for carrying out the least squares estimates on the 704 computer and to E. D. Tidwell and Jessie Kirkland for considerable help in obtaining and reducing the data.

## 5. References

[1] N. Ginsberg and E. F. Barker, J. Chem. Phys. **3,** 668 (1935).
[2] W. S. Benedict, K. Morikawa, R. B. Barnes, and H. S. Taylor, J. Chem. Phys. **5,** 1 (1937).
[3] D. R. J. Boyd and H. W. Thompson, Proc. Roy. Soc. London [A] **216,** 143 (1953).
[4] D. G. Rea and H. W. Thompson, Trans. Faraday Soc. **52,** 1,304 (1956).
[5] L. H. F. Bovey, J. Chem. Phys. **21,** 830 (1953).
[6] Wiggins, Shull, Bennett, and Rank, J. Chem. Phys. **21,** 1,940 (1953).
[7] J. K. Wilmshurst and H. J. Bernstein, Can. J. Phys. **35,** 226 (1957).
[8] E. K. Plyler, L. R. Blaine, and E. D. Tidwell, J. Research NBS **55,** 279 (1955).
(9) G. Herzberg, Infrared and Raman Spectra (D. Van Nostrand Co., Inc., New York, N.Y., 1945).
[10] E. B. Wilson, Jr., J. Chem. Phys. **3,** 818 (1935).
[11] H. H. Nielsen, Phys. Rev. **77,** 130 (1950); Rev. Mod. Phys. **23,** 90 (1951).
[12] W. S. Benedict, E. K. Plyler, and E. D. Tidwell, J. Chem. Phys. **29,** 829 (1958).
[13] D. R. J. Boyd and H. C. Longuet-Higgins, Proc. Roy. Soc. London [A] **213,** 55 (1952).
[14] E. B. Wilson, Jr., J. C. Decius, and P. C. Cross, Molecular Vibrations (McGraw-Hill Book Co., Inc., New York, N.Y., 1955).

WASHINGTON, D.C. (Paper 63A2-7)

Journal of Research of the National Bureau of Standards—A. Physics and Chemistry
Vol. 63A, No. 2, September–October 1959

# Precise Coulometric Titration of Acids and Bases

John K. Taylor and Stanley W. Smith[1]

(May 25, 1959)

Apparatus and techniques are described for the titration of acids and bases by constant-current coulometry. The precision and accuracy of the method are indicated by titrations of benzoic acid, potassium acid phthalate, adipic acid, hydrochloric acid, and sodium carbonate. Standard deviations of ±0.003 percent have been obtained which indicate that the reliability of the method is equal to or exceeds that of classical analytical procedures.

## 1. Introduction

In coulometric analysis, the laws of electrolysis are applied to analytical chemistry. The material to be analyzed is placed in an electrolytic cell and is neutralized, oxidized, reduced, or precipitated, as the case may be, by a measured quantity of electricity. From this measurement, Faraday's laws are used to determine the amount of chemical substance originally present.

While this technique has been used only for the past 20 years, and particularly in the past decade, numerous procedures have been developed, especially in microchemical analysis, where coulometry has definite experimental advantages over conventional volumetric methods [1, 2, 3].[2]

With the evaluation of the faraday constant with ever-increasing precision, by purely physical methods, coulometry offers the attractive possibility of permitting chemical standardizations to be made directly with reference to fundamental electrical constants. In fact, a proposal has been made to the International Union of Pure and Applied Chemistry to accept the electron as a fundamental chemical standard [4].

The National Bureau of Standards has had a continuing interest in developing analytical methods of the highest accuracy for the determination of the purity of materials suitable for chemical standards. Because they differ so much from conventional procedures, the precision and accuracy of coulometric methods are being extensively investigated. A preliminary report on this program was presented to the National Academy of Sciences at its meeting in Washington in November 1956 [5]. The present paper is a detailed account of the apparatus and techniques developed for coulometric titrations of high precision. It is shown that the reliability of the results obtained is equal to or exceeds that of the most careful determinations made by classical analytical methods.

## 2. General Considerations

### 2.1. Classification of Methods

Coulometric titrations may be classified according to whether the electrode process directly or indirectly influences the composition of the solution. Acidimetric titrations in which hydrogen ion is reduced at the cathode are examples of the former type, while the precipitation of halide ion by coulometrically generated silver ion is an example of the latter type.

A further classification may be made on the basis of the type of current control. Controlled-potential coulometry consists in maintaining the electrode potential at a selected value that produces only a desired electrode reaction. In this case, the current decreases continuously and exponentially during the electrolysis, and asymptotically approaches zero or some small constant value. The current is integrated during the course of the electrolysis, and is discontinued when it does not differ significantly from this terminal value.

Constant-current coulometry is based on the maintenance of an accurately measured current and the determination of the time required to complete the desired reaction. Integration is not required, but the electrolysis must be discontinued at the end point of the desired reaction. End-point determination may be made by conventional methods such as potentiometric, colorimetric, amperometric, or thermometric techniques, depending on the particular reaction.

### 2.2. Advantages of Coulometric Titrations

In addition to the possibility of making determinations based on physical standards, coulometric measurements have several obvious advantages. Electrochemical reactions may be considered as titrations with electrons, a universal "reagent." This reagent may be added uniformly at any desired rate by methods more convenient than those required to dispense conventional chemical substances. Uncertainties in composition of standard solutions are eliminated as are volumetric errors. The high precision with which electrical measurements can be

[1] Present address: Delco-Remy Division, General Motors Corporation, Anderson, Ind.

[2] Figures in brackets indicate the literature references at the end of this paper.

made is a distinct advantage in coulometric methods. Methods for the control of electrical circuits are well-developed, so that coulometric titrations are especially adaptable for automatic operation.

### 2.3. Sources of Error

It is of prime importance that the stoichiometry of the electrode process and any of its indirect reactions be completely defined. Any uncertainty in the current-chemical reaction relationship will result in a direct error in the determination. In general, reactions which proceed with less than 100-percent current efficiency are not useful.

In many cases, the reverse of the desired reaction occurs at the second electrode, or the product of the reaction at this electrode may interfere with the reaction of primary interest. Accordingly, it is frequently necessary to isolate the second electrode in a separate compartment that is in electrolytic contact with the electrolysis chamber. In such cases, it is necessary to minimize losses due to diffusion or to bulk transfer of the solution. A further source of error may arise from ionic migration from the electrolysis chamber. The familiar technique of addition of a supporting electrolyte will minimize this error.

Errors, both accidental and systematic, can arise in the determination of the end point as in conventional titrations. Errors can arise from faulty calibration of the apparatus used for the measurement of the current and the time.

## 3. Apparatus and Procedure

### 3.1. Apparatus

The acidimetric titrations to be described were made by the method of constant-current coulometry. The cell consists of a platinum cathode and a silver anode, with an alkali chloride solution as the supporting electrolyte. The cell reaction results in the reduction of one equivalent of hydrogen ion (liberation of one equivalent of hydrogen gas) at the cathode, and the formation of one equivalent of silver chloride at the anode for each faraday of electricity.

Because of the small but finite solubility of silver chloride in the electrolyte, a small amount of silver is reduced and deposited on the cathode when a single compartment cell is used. To overcome this source of error, the titration cell shown in figure 1 was designed. The cathode chamber, *C*, contains the platinum-gauze cathode and also the glass and calomel electrodes to indicate the end point *p*H of the solution. An encapsulated magnet bar is used to stir the solution. A tube is provided to admit nitrogen to the cell to remove carbon dioxide. The compartment is sealed with a rubber stopper and a bubble trap to exclude air.

The anode compartment, *A*, contains a silver anode of large area so that the anode reaction results only in the precipitation of silver chloride on its surface, no acid being formed. It is fabricated

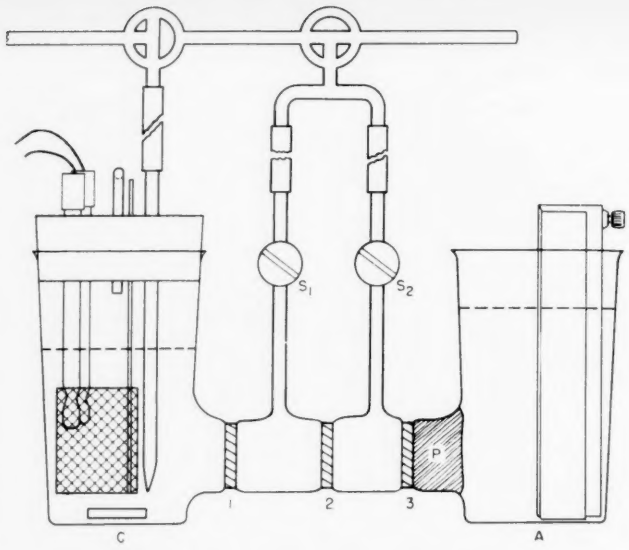


FIGURE 1. *Coulometric titration cell.*

from a sheet of silver 7.6 by 15 by 0.065 cm in thickness. This is corrugated and placed as far as possible from the connecting port, to assure large current capacity and good current distribution. Such an electrode has a capacity of more than 1,500 coulombs and can be regenerated by electrolytic reduction of the silver chloride. More conveniently, however, the electrode may be renewed by chemical solution of the chloride in ammonia.

The actual compartments are 400-ml beakers of the electrolytic type, without lip. They are connected by a 35-mm tube, approximately 125 mm in length, in which are sealed sintered glass disks as shown in the figure. Sintered disks 1 and 2 are of medium porosity while 3 is of fine porosity. For convenience, this bridge is made from commercially available "sealing tubes." Each of the center compartments has a tube attached to permit emptying and filling under nitrogen pressure as will be described. A plug of agar gel, *P* (3 percent agar-agar in 1 *N* potassium chloride) is placed at the anode side of disk 3 to prevent liquid transfer into or from this compartment.

The circuit used for the maintenance of the constant current is shown in figure 2. A storage battery, $B_1$, of 48 v serves as the current source. It permits a high-resistance circuit so that small changes in cell resistance (voltage drop across the cell) during the course of the electrolysis will have a proportionally smaller effect on the current. A voltage dropping resistor, $R_1$, is immersed in an oil bath to aid in heat dissipation and stabilize its resistance during a measurement. The combination, $R_5R_6$, consists of a fixed resistance and a carbon-compression resistor in parallel. It has an overall variation of about 20 ohms and is adjusted continuously during the measurement to maintain the current constant. Resistance $R_4$ is used for coarse adjustment of the current.

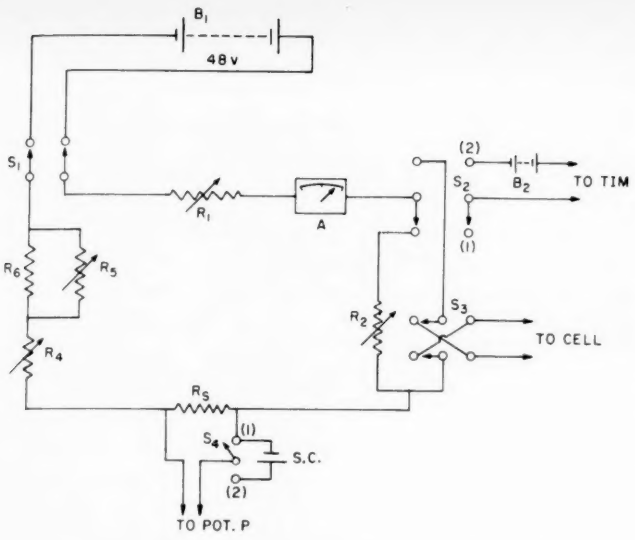


FIGURE 2. *Electrical circuit diagram for coulometric titrations.*

A variable resistor, $R_2$, is adjusted to have, within narrow limits, the same resistance as the cell. The switch $S_2$ when in position (1), permits the current to flow through this "dummy" resistor for preliminary adjustment. Ammeter $A$ is used to facilitate the initial adjustment of the current. Switch $S_2$, when thrown to position (2), causes the current to flow through the cell and simultaneously triggers the timing device.

The current is measured by the voltage drop across the standard resistor, $R_s$, a 5- or a 10-ohm precision resistor, depending on the value of the current. These resistors are placed in a constant-temperature oil bath. Saturated standard cells, suitably thermostated, serve as the primary reference of voltage. The voltage drop across $R_s$ is compared with the voltage of the standard cell, any difference being measured by potentiometer $P$.

During a titration, the current is maintained constant by manually adjusting it in the following manner. By preliminary trials, it is possible to adjust the value of the dummy resistor to approximately that of the cell. Accordingly, when the switch is thrown to the "electrolysis" position, potentiometer $P$ can be adjusted quickly to correspond to the cell current. The potentiometer key is then locked in the closed position. Any change in the current causes the galvanometer to deflect from the null position, and this is immediately corrected by adjustment of resistor $R_5$.

Initially, the time interval was determined by means of an electric clock, driven by a tuning-fork regulated constant-frequency device, capable of a precision of one part in a hundred thousand. To secure higher precision in timing, and to eliminate errors due to clutch slippage in the clock, a quartz crystal-controlled time-interval meter (TIM) was used in later experiments. The meter is compared occasionally with NBS standard time signals to check its performance. It is capable of an accuracy of one part in a million, and has never differed from the time signal by this amount.

The $p$H measurements, on which the end point determination is based, are made with conventional glass electrodes and a line-operated indicator. A suitable resistance is connected in series with the meter of the instrument and the voltage drop across this is measured (14.5 mv per $p$H unit). This effectively expands the scale of the instrument since this voltage can be readily measured to a few hundredths of a millivolt with an ordinary potentiometer. The stability of the $p$H meter during the period of a determination of the end point is sufficient to warrant this procedure.

All apparatus for making the electrical measurements, including standard cells, standard resistors, and potentiometers, was calibrated by the electrical division of this Bureau. The value for the faraday constant used was 96,495.6 coulombs [7].

### 3.2. General Procedure

A 1 $N$ solution of potassium chloride is added to the anode compartment of the cell. A weighed portion of solid potassum chloride is placed in the cathode compartment and, after flushing with nitrogen, freshly boiled distilled water is added in sufficient quantity to make the resulting solution 1 $N$. Pure nitrogen is then introduced through the connecting tube and into the solution to remove dissolved carbon dioxide. To insure that the electrolyte is sufficiently acid to facilitate this operation, a few drops of acid are intentionally added to bring the electrolyte to a $p$H of 5.

After purging is complete, the added acid is neutralized as follows. Stopcocks $S_1$ and $S_2$ are opened to the atomsphere to permit the solution to flow into the connecting tube to a depth of about 2 mm. A current of 10 ma is passed until the glass electrode indicates a $p$H value of 7.0.[3] Nitrogen is then admitted into the side tube to "blow" the contents back into the cathode compartment. This procedure is repeated until no further change in $p$H results on mixing and the $p$H remains at 7.00.

By appropriate manipulation of the stopcocks, the connecting tube is then filled with neutralized catholyte. The stopper is momentarily removed to introduce the acid to be titrated.

The current is then adjusted to a value of 200 ma and the solution is electrolyzed until the glass electrode indicates a value very close to the end point. At this rate of electrolysis, the acidity of the electrolyte in the vicinity of the end point changes more rapidly than the glass electrode can respond. Accordingly, some experience may be required to insure that the end point is not overrun. Nitrogen pressure is then used to push the contents of the connecting tube into the cathode compartment for mixing.

[3] No appreciable error is incurred by assuming the neutral point of the solution to be that of pure water.

The connecting tube is then filled with electrolyte to a depth of 2 mm, as previously described, and the solution is electrolyzed at a current of 10 ma to within about 0.5 $p$H unit of the end point. At this current, the glass electrode follows the change of $p$H very closely so that there is little danger of overrunning the desired value.

Electrolysis is then carried out, stepwise, for convenient time intervals and the $p$H is recorded for each interval. From these data, a conventional differential potentiometric plot is constructed to determine the end point. The connecting tube is then flushed several times with catholyte until no further change in $p$H results. From the change in $p$H resulting from this flushing, and the titration curve, a small correction is made to the end-point time already determined.

A typical end-point determination is shown in figure 3. Curve $P$ represents the plot of the potential of the glass electrode indicator as a function of the elapsed time. Curve $D$ is the differential plot used to locate the end point, identified as point $C$. The tolerance limits for the location of the end point that would correspond to an error of $\pm 0.002$ percent in the titration are indicated. Point $A$ represents the time at which electrolysis was discontinued, while point $B$ indicates the final $p$H value for the solution, after rinsing was completed. The corrected end point is then time $C+$(time $A-$time $B$).

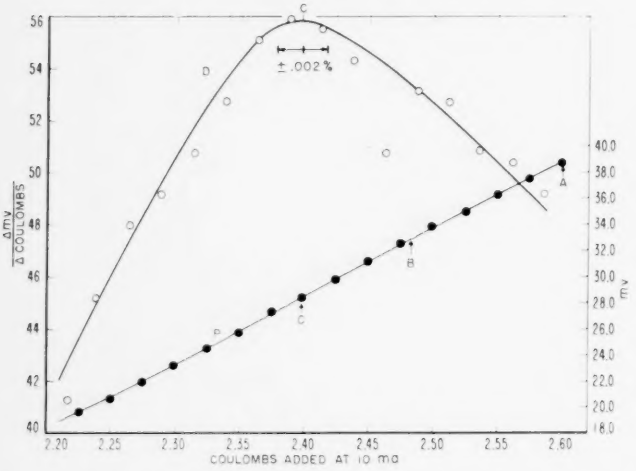


FIGURE 3. *Typical end-point determination.*

## 4. Titration of Potassium Hydrogen Phthalate

### 4.1. Procedure

The potassium hydrogen phthlate used in these experiments was NBS Standard Sample 84d. Small amounts (15 to 20 g) were crushed in a mortar and dried at 120° C for 2 to 3 hr. The samples were stored in a desiccator until used.

After removal of carbon dioxide from, and neutralization of the supporting electrolyte, the rubber stopper was removed momentarily, and the acid (2 g), weighed to 0.01 mg, was dumped into the cell from a weighed platinum boat. Reweighing of the boat gave the amount of acid introduced into the cell.

The acid was then electrolyzed at a current rate of 200 ma and finally at a rate of 10 ma, as described above.

### 4.2. Results

The results obtained for a number of titrations of standard sample 84d are given in columns 2 and 3 of table 1. The values given represent the purity found for the sample on the basis of an equivalent weight of 204.216. The electric clock was used for measurement of time in the case of the first group while the time-interval meter was used in the second series.

Although separated by a period of time of about 1 year, and determined by slightly different techniques, the agreement of the averages for the two series is excellent and shows the high precision of coulometric titrations.

On the basis of very careful titrations by conventional methods, sample 84d was indicated originally as having an assay of 100.04 percent. Subsequently, Bates and Wichers [6] compared this material with specially purified benzoic acid by differential titration and reported an assay of 99.987 percent ($\sigma = 0.002$). The agreement of the values of table 1 with this latter value is confirmation that the coulometric method is one of high accuracy.

TABLE 1. *Summary of results*

| Determination number | Potassium hydrogen phthalate [a] | Potassium hydrogen phthalate [b] | Benzoic acid [a] | Benzoic acid [b] | Hydrochloric acid [a, c] | Adipic acid [a, d] | Adipic acid [b, e] | Sodium carbonate [a] |
|---|---|---|---|---|---|---|---|---|
| | assay | assay | assay | assay | assay | assay | assay | assay |
| | % | % | % | % | % | % | % | % |
| 1 | 99.976 | 99.979 | 99.985 | 99.991 | 99.982 | 99.935 | 99.985 | 99.909 |
| 2 | 99.980 | 99.976 | 99.991 | 99.993 | 100.004 | 99.937 | 99.987 | 99.901 |
| 3 | 99.978 | 99.981 | 99.989 | 99.996 | 100.014 | 99.937 | 99.980 | 99.915 |
| 4 | 99.970 | 99.976 | 100.001 | 99.991 | 100.003 | 99.947 | 99.981 | 99.910 |
| 5 | 99.974 | 99.974 | 99.985 | 99.986 | 100.002 | 99.942 | 99.989 | 99.920 |
| 6 | | | | 99.998 | 99.989 | 99.955 | | |
| 7 | | | | | 99.990 | 99.951 | | |
| 8 | | | | | | 99.948 | | |
| Mean | 99.976 | 99.977 | 99.990 | 99.994 | 99.999 | 99.945 | 99.984 | 99.911 |
| Standard deviation | 0.004 | 0.003 | 0.006 | 0.004 | 0.010 | 0.007 | 0.004 | 0.007 |

[a] Timed by electric clock.
[b] Timed by time interval meter.
[c] Assay based on calculated acidity by the pressure-distillation method.
[d] Once recrystallized from melt.
[e] Twice recrystallized from melt.

## 5. Titration of Benzoic Acid

### 5.1. Procedure

The benzoic acid used was prepared at NBS for use as a calorimetric standard. The acid was a coarse, crystalline material and has been shown by other investigators [5] not to take up water under conditions prevailing in this locality. Accordingly, it was used without further purification or drying.

After preparation of the cell as described previously, a 1-g sample was weighed in a platinum boat and transferred to the cathode compartment. A period of about 30 min was allowed before starting the electrolysis, to permit a substantial amount of the acid to dissolve. Additional acid dissolves during the initial reduction period. When the reaction is approximately 98 percent complete, the current is discontinued, the connecting tube is blown dry, and sufficient time is allowed for the solution of the remainder of the sample (about 20 to 30 min). The titration is then completed with a current of 10 ma as already described. A final rinsing of the cell walls and stopper is accomplished with 15 percent, carbon dioxide free ethanol, to insure solution of residual traces of the acid.

### 5.2. Results

The results obtained in two independent series of measurements with different timing techniques are shown in columns 4 and 5 of table 1. The values reported represent the assay of the acid on the basis of an equivalent weight of 122.112.

By the differential method already referred to, Bates and Wichers [6] found the assay of this acid to be 99.996 percent ($\sigma$=0.001).

## 6. Titration of Hydrochloric Acid

### 6.1. Procedure

A solution of hydrochloric acid was prepared by weight dilution of constant-boiling acid. Based on the pressure during the distillation of the starting material and the dilution data, the acid was calculated to have a concentration of $0.11485_2$ milliequivalents per gram of solution [8].

After the usual preparation of the cell, 50 g of the acid was added from a weight buret. Electrolysis was started immediately and continued to about 99.8 percent of completion. The connecting tube was then rinsed and the neutralization was completed at the 10-ma rate as described previously. In this case, it was not necessary to prepare an end point curve, due to the rapid change in $p$H at the end point. Thus, a difference in $p$H of 0.1 unit at the end point corresponded to 0.005 coulombs (0.5 sec at the 10-ma rate). It was only necessary to attain the same end point obtained in the preliminary conditioning of the cell, a value easily determined within 0.02 $p$H units.

### 6.2. Results

The results of seven coulometric titrations of this acid are given in column 6 of table 1. The reported value is the "purity" of the acid on the basis of its calculated concentration from pressure-distillation data. Expressed in other terms, the solution was found to have a concentration of 0.114850 milliequivalents per gram, as compared with the calculated value of $0.11485_2$ indicated in section 6.1.

While the agreement with the calculated value is satisfactory, the precision of the determination is disappointing. On the basis of uncertainty of the end point, a reproducibility of at least 1 part in 100,000 would be expected. Undoubtedly, some of the error is that inherent in the dispensing of liquid samples. In order to estimate the magnitude of such errors, a series of measurements were made in which 50-g samples of water were dispensed from a weight buret into tared weighing bottles. The difference between the weight of water dispensed and the contents of the weighing bottles showed a variation of 3.6 parts in 100,000. If all of this were reflected in the uncertainty of the weight of the sample, the larger average deviation found in these measurements would be partially explained.

## 7. Titration of Adipic Acid

### 7.1. Procedure

The adipic acid used was reagent grade material which had been further purified by filtration and crystallization from the melt by Delmo Enagonio of the Bureau. The material was estimated to have an assay of 99.9+ percent. The titration procedure used was the same as that followed in the case of potassium acid phthalate, and the results are reported merely to show the adaptability of the method to a variety of acids.

### 7.2. Results

The results of a series of titrations to determine the purity of this sample of adipic acid are given in column 7 of table 1. The material was further recrystallized and the purity was found to be higher, as recorded in column 8. The smaller value for the standard deviation indicated that the homogeneity of the sample was also improved by the second purification.

## 8. Titration of Sodium Carbonate

### 8.1. Procedure

These experiments were performed to extend the method to the titration of bases. The sodium carbonate was reagent grade material which had been heated in a platinum dish for several hours at a temperature of 350° to 400° C. The assay was not determined by an independent method.

The electrolyte used was 1-$M$ sodium sulfate, since chlorides would be oxidized at the anode if

present in the solution. The agar plug was also made with 1-*M* sodium sulfate.

The solution was preconditioned as described previously. After addition of the base, the platinum electrode was made the anode and electrolysis was continued until approximately 99 percent of the base had been neutralized. The titration was completed at the 10-ma rate as before. Sufficient time must be allowed near the end point for the removal of carbon dioxide.

### 8.2. Results

The results of a series of five titrations of this material are given in column 9 of table 1. The precision obtained is comparable to that found with the acids determined by this method.

## 9. Discussion

This investigation shows that the coulometric method is capable of a high degree of precision. In view of the results obtained for benzoic acid and potassium acid phthalate, for which the assay is known, there is substantial evidence that the method is also capable of a high degree of accuracy.

The attainment of precision and accuracy of the order indicated by the data requires careful control over several sources of error. These may be discussed best by a division into errors of procedure and of measurement.

Errors may arise as a result of the pretreatment of the acid to be determined, in its introduction into the cell, and as a result of losses during the titration.

Errors associated with the preparation of the sample are frequently overlooked. In the case of the phthalate, for example, the procedure for drying the sample is critical. It is important that only small quantities be crushed preliminary to drying, in order to release microamounts of entrapped mother liquor from the crystals. Furthermore, the crushing must be done gently, to avoid generation of appreciable heat in localized areas which might result in decomposition of a part of the sample. Also, the sample should be spread out to facilitate the drying process.

To minimize errors associated with the transfer of the sample into the cell, it has been found advantageous to stop the flow of nitrogen during this process. This assures that fine spray will not deposit on the platinum dish to cause an error in weight and also prevents spray losses of material from the cathode compartment.

After the sample has been introduced into the cell, it can be lost only through transfer of solution into the anode compartment, or escape as spray through the nitrogen exit tube. The former is effectively prevented by the agar plug in the connecting tube. The latter is minimized by maintaining only sufficient flow of nitrogen during the titration to guarantee a positive pressure of nitrogen in the cell.

It is very important to remove residual amounts of strong acids from the cell, such as would be introduced during a cleaning operation. This is accomplished by drawing large quantities of hot distilled water through the frits. The effectiveness of the cleaning procedure can be checked when the solution is brought to neutrality at the start of a titration. Prolonged downward drift of *p*H on standing and continuing change of *p*H on rinsing the connecting tube indicate the presence of acid in the frits. Should this situation arise, it is necessary to discard the solution and to rinse the cell further with hot distilled water.

Errors associated with the electrical measurements are easily made much smaller than other errors. Standard resistors, certified to a few parts in a million, are readily obtained, and normal temperature control is all that is required to assure maintenance of their calibration to this accuracy. Calibrated potentiometers permit measurement of the voltage drop, and hence the current, to better than one part in ten thousand. For current measurements of the highest precision, the arrangement used here is preferred, in which the potentiometer measures only the difference between the voltage drop across the resistor and that of a saturated standard cell. This differential method permits measurements with a precision of a few parts in a million.

No difficulties have been experienced in maintaining the current constant to better than one part in a hundred thousand. The galvanometer used to indicate potentiometric balance had a sensitivity of 0.3 $\mu$v/mm. Accordingly, a deflection of 3 mm from the null position corresponded to only 1$\mu$v, or 1 ppm with reference to variation in the current.

It was possible to maintain balance within a few millimeters throughout a determination, provided the variable resistor used for current control had a smooth response. In this connection, a carbon compression resistor, spring-loaded and mounted vertically, is much superior to multiturn potentiometers which have a tendency to become "noisy" with use.

For accurate measurements, it is imperative to insure that the current through the standard resistor is actually that through the cell. While this may seem an obvious condition, the possibilities of extraneous connection to ground ("ground loops"), even though of high resistance, must be considered.

Timing errors should not seriously affect the precision or accuracy of coulometric titrations. For samples of the order of about 10 milliequivalents, approximately 1,000 coulombs are needed, requiring about 5,000 sec at the 200-ma rate of electrolysis. Electric clocks, driven by frequency-controlled power supplies, are inexpensive timing devices which provide measurements reliable to a few parts in a hundred thousand. Perhaps the largest source of error associated with their use is the so-called clutch error involved in starting and stopping, which may amount to a few hundredths of a second per operation. The crystal-controlled electronic time interval meter used here is reliable to a part in a million. Both techniques require that the timing switch operate in close synchronization with the current switch.

Errors arising from the determination of the end point depend on the slope of the *p*H curve in this

region, as well as the sensitivity of the *p*H indicating device. In the case of the weak acids used in this investigation (*p*K values, 4.5 to 5.5), the uncertainty of the end point is about 8 millicoulombs, corresponding to errors of less than 10 ppm. For strong acids the end point error is much smaller than this, due to the greater slope of the end point curve, and depends largely on the reliability of the *p*H indication.

Errors in accuracy arise from the deviation of the inflection point in a potentiometric titration from the stoichiometric equivalence point. According to Roller's equations [9], errors from this source should be less than 0.001 percent. There is some evidence to indicate that the experimental deviations are somewhat greater than the calculated values [6]. However, insufficient work has been done to justify the assignment of corrections to the values reported in this paper.

## 10. Summary

This investigation has shown that coulometric acidimetric titrations can be made with a precision and accuracy equal to or exceeding that obtainable by the most careful conventional chemical methods of analysis. Furthermore, reliable results are less dependent upon the manipulative skill of the analyst than are classical methods. The method has the further advantage of being absolute in the sense that the results are based on electrical standards and no assumptions as to the purity of chemical primary standards are involved. Titrations reliable to a few hundredths of a percent for both strong and weak acids can be readily obtained. The method is equally well-adapted to the titration of bases.

## 11. References

[1] J. J. Lingane, Electroanalytical Chemistry (Interscience Publishers, Inc., New York, N.Y., 1953).
[2] J. J. Lingane, Anal. Chem. **30,** 1716 (1958).
[3] F. Cuta, Anal. Chim. Acta **18,** 45 (1958).
[4] P. S. Tutundzic, Anal. Chim. Acta **18,** 60 (1958).
[5] J. K. Taylor and S. W. Smith, Science. **124,** 940, (1956).
[6] R. G. Bates and E. Wichers, J. Research NBS **59,** 9 (1957) RP2769.
[7] E. R. Cohen and J. W. Du Mond, Phys. Rev. Letters **1,** 283 (1958).
[8] C. W. Foulk and M. Hollingsworth, J. Am. Chem. Soc. **45,** 1220, (1923).
[9] P. S. Roller, J. Am. Chem. Soc. **54,** 3485 (1932).

Washington, D.C. (Paper 63A2–8)

Journal of Research of the National Bureau of Standards—A. Physics and Chemistry
Vol. 63A, No. 2, September–October 1959

# Heat of Formation of Titanium Tetraiodide

W. H. Johnson, A. A. Gilliland, and E. J. Prosen

(May 6, 1959)

The heat of formation of titanium tetraiodide was determined relative to that of titanium tetrabromide by comparison of their heats of hydrolysis in dilute sulfuric acid. The difference in the heats of formation may be expressed by the equation:

$$TiI_4(c) + 2Br_2(liq) = TiBr_4(c) + 2I_2(c),$$

$$\Delta H(25^\circ\ C) = -230.91 \pm 0.75\ kj/mole\ (-55.19 \pm 0.18\ kcal/mole).$$

By taking the heat of formation of $TiBr_4(c)$ as $-616.72 \pm 4.60$ kj/mole, the heat of formation of $TiI_4(c)$ is calculated to be $-385.81 \pm 4.64$ kj/mole ($-91.21 \pm 1.11$ kcal/mole). The heats of hydrolysis of $TiBr_4$ and $TiCl_4$ were similarly measured; the value obtained for the difference (186.77 $\pm$1.34 kj/mole) is in good agreement with the difference between the directly determined heats of formation (187.11 $\pm$5.35 kj/mole).

## 1. Introduction

There are no experimental values available in the literature for the heat of formation of titanium tetraiodide. Brewer, Bromley, Gilles, and Lofgren [1] [1] calculated the heat of formation from estimated heats of solution and lattice-energy calculations. They obtained $-101 \pm 10$ kcal/mole for the heat of formation of $TiI_4$ at 25° C.

The direct combination of elemental titanium with gaseous iodine is not feasible because of the low vapor pressure of iodine at ordinary temperatures; at higher temperatures, the tetraiodide tends to decompose into $TiI_2$ and $TiI_3$ [2].

The heats of formation of titanium tetrachloride and titanium tetrabromide have recently been determined by the direct combination of the elements in a calorimeter [3, 4].

It is possible to hydrolyze $TiI_4$, as well as $TiCl_4$ and $TiBr_4$, in dilute sulfuric acid. We can assume that the final state of the $Ti^{4+}$ ion is the same in each case and that the differences in the heats of hydrolysis are measures of the differences in the heats of formation. We may, therefore, compare the heats of hydrolysis of $TiI_4$ and $TiBr_4$ and obtain the heat of formation of $TiI_4$ relative to that of $TiBr_4$. We may also compare the heats of hydrolysis of $TiBr_4$ and $TiCl_4$ and obtain the difference between their heats of formation. This value should agree with the difference between the directly determined heats of formation.

The present investigation is comprised of two parts. The first part consists of the measurement of the heats of hydrolysis of $TiI_4$ and $TiBr_4$ and the calculation of the heat of formation of $TiI_4$ relative to that of $TiBr_4$. The second part includes the measurement of the heats of hydrolysis of $TiBr_4$ and $TiCl_4$ and the comparison of the difference between these heats of hydrolysis with the difference between the heats of formation.

## 2. Source and Purity of Samples

The $TiCl_4$, $TiBr_4$, and $TiI_4$ were prepared by the Inorganic Chemistry Section of the Chemistry Division. The purity of the $TiCl_4$ and $TiBr_4$ was determined to be 99.999 and 99.998 mole percent, respectively, from calorimetric freezing-point measurements conducted by George T. Furukawa of the Thermodynamics Section of the Heat Division. The purity of the $TiI_4$ was determined by analysis to be 99.91 mole percent; this analysis was performed by the Inorganic Chemistry Section of the Chemistry Division.

The 1–*N* sulfuric acid solution used as the calorimetric fluid for the hydrolysis experiments was prepared from concentrated, reagent-grade acid.

The hydrobromic and hydriodic acids were redistilled from reagent-grade solutions; the constant-boiling fractions were collected under nitrogen and stored in darkness in completely filled, glass-stoppered bottles. The hydrochloric acid was taken directly from a fresh bottle of reagent-grade acid.

The $TiCl_4$ and $TiBr_4$ were distilled in vacuum into Pyrex glass bulbs, and the bulbs sealed. Soft glass bulbs were filled with the solid $TiI_4$ in a helium atmosphere. The bulbs were then fitted with polyethylene caps, removed from the helium atmosphere, cooled in ice, and sealed. The hydrochloric, hydrobromic, and hydriodic acid solutions were placed in soft glass bulbs by means of a funnel drawn down to a capillary. They were then cooled in ice and sealed.

The quantity of each of the titanium tetrahalide samples was determined by weighing the bulbs before and after filling. The quantities of the hydrobromic and hydriodic acid samples were determined from the mass of the sample and the concentration of the stock solution. The quantities of the hydrochloric acid samples were determined by analysis of the resulting calorimetric solution.

[1] Figures in brackets indicate the literature references at the end of this paper.

## 3. Apparatus and Procedure

The calorimeter used for measurement of the heats of hydrolysis and dilution is shown in figure 1. It consists of a glass vessel having a silvered, evacuated jacket, a glass-enclosed manganin heating coil, a glass stirrer, a glass bulb-crusher, and a glass-enclosed platinum resistance thermometer. The upper part of the vessel consists of a 60/35 standard-taper joint; the volume of the enlarged portion is approximately 500 ml.

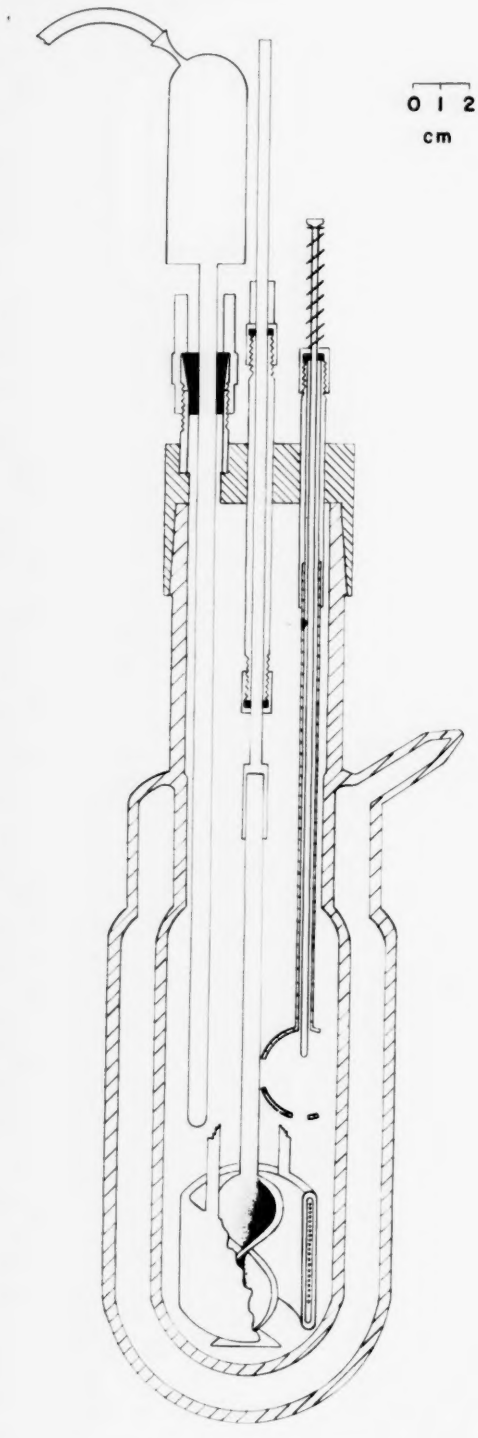


FIGURE 1. *Glass calorimeter.*

The heating coil, stirrer, bulb-crusher, and platinum thermometer are all supported by the brass head. The resistance of the heating coil is 124.33 ohms. The heater leads, which pass through the supporting tubes, have branch points, similar to a 4-lead thermohm, located approximately midway between the calorimeter and jacket boundaries. The stirrer shaft is constructed of stainless steel and passes through a stainless steel tube fitted at both ends with Teflon gaskets which serve as bearings. The glass stirrer is sealed into a stainless steel cup welded to the stirrer shaft. The calorimetric assembly was immersed in a thermostatically-controlled water bath during each experiment.

The apparatus for measurement of calorimeter temperatures, for calibration with electrical energy, and the details of calorimetric procedures have been described in previous papers [3, 4].

In order to compare the heats of hydrolysis of $TiBr_4$ and $TiI_4$, it was necessary that the composition of the end solution be essentially the same in each case. For this reason 0.04 mole of hydriodic acid was added to the sulfuric acid solution for the $TiBr_4$ hydrolysis experiments, and 0.04 mole of hydrobromic acid was added to the solution for the $TiI_4$ hydrolysis experiments. A similar procedure was used in the determination of the heats of hydrolysis of $TiBr_4$ and $TiCl_4$.

The solutions resulting from the $TiI_4$ hydrolysis experiments were carefully removed from the calorimeter and neutralized with ammonium hydroxide solution. The solution was boiled to coagulate the precipitate which was then filtered and ignited to constant weight and weighed as $TiO_2$. The average ratio of the $TiO_2$ found to the theoretical quantity based upon the weight of sample was $1.0022 \pm 0.0028$.

The solutions resulting from the $TiI_4$ hydrolysis experiments and from the hydriodic acid dilution experiments varied in color from faintly amber to brown. After standing for a few hours they became noticeably darker in color, presumably because of oxidation of the hydriodic acid.

The solutions resulting from the $TiBr_4$ hydrolysis experiments and the hydrobromic acid dulition experiments were clear, but usually turned very faintly amber after standing, probably because of oxidation of the hydriodic and hydrobromic acids.

The solutions resulting from the $TiCl_4$ hydrolysis experiments were very slightly turbid, but they became clear after standing for a few hours. This was probably caused by the rapidity of the reaction which, for some unknown reason, varied considerably among experiments. In some cases the violence of the reaction caused liquid to be splashed on the calorimeter walls above the level of the solutions, which made it necessary to reject the experiment.

## 4. Experimental Results

### 4.1. Hydrolysis of $TiI_4$

The results of the electrical calibration experiments are given in table 1, where $E$ is the electrical energy, in joules, added to the system; $\Delta Rc$ is the corrected temperature rise in ohms; and $E_s$ the energy equivalent of the "standard" calorimetric system in joules per ohm.

TABLE 1. *Electrical calibration of the* $TiI_4$ *system*

| Experiment | $E$ | $\Delta Rc$ | $E_s$ |
|---|---|---|---|
| | *j* | *Ohm* | *j/ohm* |
| 1 | 4559.62 | 0.208827 | 21834.4 |
| 2 | 4554.26 | .208568 | 21833.3 |
| 3 | 4541.07 | .208038 | 21828.4 |
| 4 | 4591.31 | .210309 | 21831.3 |
| 5 | 4541.72 | .208048 | 21830.3 |
| Mean | | | 21831.5 |
| Standard deviation of the mean | | | ±1.1 |

The results of the $TiI_4$ hydrolysis experiments are given in table 2. The quantity $\Delta e$ is the deviation in joules per ohm of the electrical energy equivalent of the actual calorimetric system from that of the calibrated system. This deviation includes the heat capacity of the sample and of the glass bulb, less that of the empty bulb used in the calibration. The energy in joules, $q$, evolved by the process is obtained as the product of $\Delta Rc$ and the actual energy equivalent of the system. The heat of hydrolysis, $-\Delta H$ (27° C), is therefore the ratio of $q$ to the number of moles of sample. For these calculations the heat capacities of $TiI_4(c)$ and Pyrex glass were taken as 0.235 and 0.795 j/g°C, respectively. For conversion to the conventional thermochemical calorie, one calorie has been taken as equivalent to 4.1840 j.

The heat of hydrolysis obtained in table 2 corresponds to the process:

$$TiI_4(c)+[24H_2SO_4+4HBr+2600\ H_2O](soln)=$$
$$[Ti^{4+}+4I^-+4H^++4Br^-+24H_2SO_4+2600H_2O]$$
$$(soln), \quad (1)$$

$$\Delta H(27°C)=-217.81\ \pm 0.42\ \text{kj/mole}.$$

TABLE 2. *Results of the experiments on the hydrolysis of* $TiI_4$

| Experiment | $\Delta e$ | $\Delta Rc$ | $q$ | $TiI_4$ | $-\Delta H(27°C)$ |
|---|---|---|---|---|---|
| | *j/ohm* | *Ohm* | *j* | *Mole* | *kj/mole* |
| 1 | 24.9 | 0.073937 | 1616.00 | 0.00742699 | 217.58 |
| 2 | 27.5 | .082475 | 1802.82 | .00826689 | 218.08 |
| 3 | 29.4 | .082103 | 1794.84 | .00822223 | 218.29 |
| 4 | 26.5 | .071992 | 1573.60 | .00724680 | 217.14 |
| 5 | 29.9 | .100405 | 2194.99 | .01009720 | 217.39 |
| 6 | 25.0 | .065496 | 1431.51 | .00655530 | 218.37 |
| Mean | | | | | 217.81 |
| Standard deviation of the mean | | | | | ±0.21 |

### 4.2. Hydrolysis of $TiBr_4$ in Sulfuric Acid Solution Containing Hydriodic Acid

The results of the electrical calibration and hydrolysis experiments are given in tables 3 and 4, respectively. The heat capacity of crystalline $TiBr_4$ was taken as 0.358 j/g°C [5]. The resulting heat of hydrolysis corresponds to the process:

$$TiBr_4(c)+[24H_2SO_4+4HI+2600\ H_2O](soln)$$
$$=[Ti^{4+}+4I^-+4H^++4Br^-+24\ H_2SO_4$$
$$+2600\ H_2O](soln), \quad (2)$$

$$\Delta H(27°C)=-244.63\pm 0.20\ \text{kj/mole}.$$

TABLE 3. *Electrical calibration of* $TiBr_4$ *system*

| Experiment | $E$ | $\Delta Rc$ | $E_s$ |
|---|---|---|---|
| | *j* | *Ohm* | *j/ohm* |
| 1 | 2064.70 | 0.094642 | 21815.9 |
| 2 | 2460.74 | .112853 | 21804.8 |
| 3 | 2458.30 | .112683 | 21816.1 |
| 4 | 2459.08 | .112730 | 21813.9 |
| 5 | 2458.50 | .112733 | 21808.2 |
| Mean | | | 21811.8 |
| Standard deviation of the mean | | | ±2.2 |

TABLE 4. *Results of the experiments on the hydrolysis of* $TiBr_4$

| Experiment | $\Delta e$ | $\Delta Rc$ | $q$ | $TiBr_4$ | $-\Delta H(27°C)$ |
|---|---|---|---|---|---|
| | *j/ohm* | *Ohm* | *j* | *Mole* | *kj/mole* |
| 1 | 11.9 | 0.091141 | 1989.32 | 0.00812468 | 244.85 |
| 2 | 14.8 | .110283 | 2407.12 | .00984278 | 244.56 |
| 3 | 14.0 | .111086 | 2424.65 | .00992151 | 244.38 |
| 4 | 13.6 | .100716 | 2198.31 | .00898268 | 244.73 |
| Mean | | | | | 244.63 |
| Standard deviation of the mean | | | | | ±0.10 |

### 4.3. Heats of Dilution of Hydriodic and Hydrobromic Acids

The heats of dilution of the constant-boiling HI and HBr solutions in 1–$N$ sulfuric acid are given in tables 5 and 6. Because of the small amount of energy evolved in these experiments, the actual calorimetric system was calibrated just prior to each experiment. The quantity $E_a$ denotes the energy equivalent of the actual calorimetric system. The heats of dilution correspond to the following reactions:

$$[4HI+29.1\ H_2O](soln)+[24H_2SO_4+2600\ H_2O](soln)$$
$$=[4HI+24H_2SO_4+2629.1\ H_2O](soln), \quad (3)$$

$$\Delta H(27°C)=-11.256\pm 0.088\ \text{kj},$$

$$[4HBr+20.1\ H_2O](soln)+[24H_2SO_4$$
$$+2600\ H_2O](soln)$$
$$=[4HBr+24H_2SO_4+2620.1\ H_2O](soln), \quad (4)$$

$$\Delta H(27°C)=-31.97\pm 0.24\ \text{kj},$$

$$\Delta H(25°C)=-31.54\pm 0.25\ \text{kj}.$$

TABLE 5. *Heat of dilution of aqueous hydriodic acid in 1–N sulfuric acid*

| Experiment | $E_a$ | $\Delta Rc$ | $q$ | HI | $-\Delta H(27°C)$ |
|---|---|---|---|---|---|
| | *j/ohm* | *Ohm* | *j* | *Mole* | *kj/mole* |
| 1 | 22100.4 | 0.001374 | 30.37 | 0.0109470 | 2.774 |
| 2 | 21975.1 | .000824 | 18.11 | .0064166 | 2.822 |
| 3 | 22082.4 | .000776 | 17.14 | .0060461 | 2.835 |
| 4 | 22075.3 | .000572 | 12.63 | .0044313 | 2.850 |
| 5 | 20183.8 | .003105 | 62.67 | .022347 | 2.804 |
| 6 | 20097.1 | .003661 | 73.58 | .026262 | 2.802 |
| Mean | | | | | 2.814 |
| Standard deviation of the mean | | | | | ±0.011 |

TABLE 6. *Heat of dilution of aqueous hydrobromic acid in 1–N sulfuric acid*

| Experiment | $E_a$ | $\Delta Rc$ | $q$ | HBr | $-\Delta H(27°C)$ |
|---|---|---|---|---|---|
| | *j/ohm* | *Ohm* | *j* | *Mole* | *kj/mole* |
| 1 | 22098.7 | 0.005812 | 128.44 | 0.015962 | 8.047 |
| 2 | 22073.3 | .003218 | 71.03 | .0088925 | 7.988 |
| 3 | 20150.6 | .014119 | 284.51 | .036083 | [a](7.885) |
| 4 | 19801.4 | .012594 | 249.38 | .031394 | 7.944 |
| Mean | | | | | 7.993 |
| Standard deviation of the mean | | | | | ±0.030 |

[a] Experiment number 3 was performed at 25° C rather than at 27°C, and the value was not included in calculating the mean. The value at 25° C is required for calculations in sec. 5.2. of this paper. The value of $-\Delta H$ at 25° C was taken as 7.885 kj/mole (from experiment number 3). This value is in good agreement with that calculated from the mean value at 27° C, using an estimated $\Delta Cp$ correction.

### 4.4. Heat Capacity of Hydrobromic and Hydriodic Acid Solutions

Because of the lack of data on the heat capacities of aqueous solutions of hydrobromic and hydriodic acid, these values were determined in separate experiments. The effective heat capacity of the empty calorimeter was determined by measuring the heat capacity when filled with pure water, and subtracting the known heat capacity of the water from the observed energy equivalent. The calorimeter was then filled with the same volume of the hydrobromic acid solution, weighed, and the energy equivalent determined. By subtracting the heat capacity of the calorimeter from the observed energy equivalent, the heat capacity of the hydrobromic acid solution was determined. The same procedure was used for determination of the heat capacity of the hydriodic acid solution.

The mean heat capacities obtained for aqueous hydrobromic and hydriodic acid in the range from 25° to 27° C were found to be:

$$[HBr+5.0\ H_2O],\ \overline{Cp}=2.008\ j/g°C$$

$$[HI+7.3\ H_2O],\ \overline{Cp}=1.845\ j/g°C.$$

### 4.5. Heats of Dilution of Sulfuric Acid

The heats of dilution of the sulfuric acid solution by the water included in the aqueous halogen acids have been calculated from existing data [5]. The values obtained correspond to the following processes:

$$29.1\ H_2O(liq)+[24H_2SO_4+2600\ H_2O+4HI](soln)=[24H_2SO_4+2629.1\ H_2O+4HI](soln), \quad (5)$$

$$\Delta H(27°C)=-0.402\ \pm0.084\ kj,$$

$$20.1\ H_2O(liq)+[24H_2SO_4+2600\ H_2O+4HBr](soln)=[24H_2SO_4+2620.1\ H_2O+4HBr](soln) \quad (6)$$

$$\Delta H(25°C)=-0.301\ \pm0.084\ kj,$$

$$13.5\ H_2O(liq)+[24H_2SO_4+2600\ H_2O+4HCl](soln)=[24H_2SO_4+2613.5\ H_2O+4HCl](soln), \quad (7)$$

$$\Delta H(25°C)=-0.230\pm0.084\ kj.$$

### 4.6. Heat of Hydrolysis of $TiCl_4$

The results of the electrical calibration and $TiCl_4$ hydrolysis experiments are given in tables 7 and 8, respectively. The value obtained for the heat of hydrolysis corresponds to the process:

$$TiCl_4(liq)+[24H_2SO_4+2600\ H_2O+4HBr](soln)=[Ti^{4+}+4Cl^-+4H^++4Br^-+24H_2SO_4+2600\ H_2O](soln), \quad (8)$$

$$\Delta H(25°C)=-241.81\ \pm0.72\ kj/mole.$$

TABLE 7. *Electrical calibration of the* $TiCl_4$ *system*

| Experiment | $E$ | $\Delta Rc$ | $E_a$ |
|---|---|---|---|
| | *j* | *Ohm* | *j/ohm* |
| 1 | 2907.27 | 0.133216 | 21823.4 |
| 2 | 2909.58 | .133348 | 21819.5 |
| 3 | 2903.97 | .133034 | 21828.8 |
| 4 | 2910.32 | .133377 | 21820.3 |
| 5 | 2903.01 | .133112 | 21808.8 |
| 6 | 2900.78 | .133003 | 21809.9 |
| Mean | | | 21818.4 |
| Standard deviation of the mean | | | ±3.2 |

TABLE 8. *Results of the experiments on the hydrolysis of* $TiCl_4$

| Experiment | $\Delta e$ | $\Delta Rc$ | $q$ | $TiCl_4$ | $-\Delta H(27°C)$ |
|---|---|---|---|---|---|
| | *j/ohm* | *Ohm* | *j* | *Mole* | *kj/mole* |
| 1 | 12.5 | 0.087154 | 1902.65 | 0.0078529 | 242.29 |
| 2 | 15.7 | .113947 | 2487.93 | .0102626 | 242.43 |
| 3 | 20.7 | .146828 | 3206.59 | .0132998 | 241.10 |
| 4 | 23.0 | .162914 | 3558.27 | .0147774 | 240.79 |
| 5 | 12.8 | .089692 | 1958.08 | .0080773 | 242.42 |
| Mean | | | | | 241.81 |
| Standard deviation of the mean | | | | | ±0.36 |

### 4.7. Heat of Hydrolysis of $TiBr_4$ in Sulfuric Acid Solution Containing Hydrochloric Acid

The results of the electrical calibration and $TiBr_4$ hydrolysis experiments are given in tables 9 and 10,

respectively. The value obtained for the heat of hydrolysis corresponds to the process:

$$TiBr_4(c)+[24H_2SO_4+2600\ H_2O+4HCl](soln)$$
$$=[Ti^{4+}+4Br^-+4H^++4Cl^-+24H_2SO_4$$
$$+2600\ H_2O](soln), \quad (9)$$

$$\Delta H(25°C)=-240.80\pm0.62\ kj/mole.$$

### 4.8. Heat of Dilution of Hydrochloric Acid

The results of the hydrochloric acid dilution experiments are given in table 11. As in the case of the hydriodic and hydrobromic acid dilution experiments, the actual calorimetric system was calibrated electrically for each experiment. The quantity of hydrochloric acid was determined by analysis of the resulting solution after each experiment. The value obtained for the heat of dilution corresponds to the process:

$$[4HCl+13.5\ H_2O](soln)+[24H_2SO_4+2600\ H_2O](soln)$$
$$=[24H_2SO_4+2613.5\ H_2O+4HCl](soln), \quad (10)$$

$$\Delta H(25°C)=-54.241\pm0.320\ kj.$$

TABLE 9. *Electrical calibration of the* $TiBr_4$ *system*

| Experiment | $E$ | $\Delta Rc$ | $E_s$ |
|---|---|---|---|
| | *j* | *Ohm* | *j/ohm* |
| 1 | 2910.17 | 0.132706 | 21914.6 |
| 2 | 2907.41 | .132761 | 21899.6 |
| 3 | 2902.85 | .132508 | 21907.0 |
| 4 | 2902.56 | .132474 | 21910.4 |
| 5 | 2920.41 | .133284 | 21911.2 |
| Mean | | | 21908.6 |
| Standard deviation of the mean | | | ±2.5 |

TABLE 10. *Results of the experiments on the hydrolysis of* $TiBr_4$

| Experiment | $\Delta e$ | $\Delta Rc$ | $q$ | $TiBr_4$ | $-\Delta H(25°C)$ |
|---|---|---|---|---|---|
| | *j/ohm* | *Ohm* | *j* | *Mole* | *kj/mole* |
| 1 | 13.7 | 0.122050 | 2675.62 | 0.0111647 | 239.65 |
| 2 | 19.4 | .146890 | 3221.00 | .0133545 | 241.19 |
| 3 | 15.0 | .129186 | 2832.22 | .0117395 | 241.26 |
| 4 | 11.0 | .093681 | 2053.45 | .0085122 | 241.24 |
| 5 | 10.8 | .099166 | 2173.66 | .0090327 | 240.64 |
| Mean | | | | | 240.80 |
| Standard deviation of the mean | | | | | ±0.31 |

TABLE 11. *Heat of dilution of hydrochloric acid in* 1-*N sulfuric acid*

| Experiment | $E_s$ | $\Delta Rc$ | $q$ | HCl | $-\Delta H(25°C)$ |
|---|---|---|---|---|---|
| | *j/ohm* | *Ohm* | *j* | *Mole* | *kj/mole* |
| 1 | 22129.1 | 0.025049 | 554.31 | 0.041259 | 13.435 |
| 2 | 22125.3 | .024841 | 549.61 | .040435 | 13.592 |
| 3 | 22129.8 | .024867 | 550.30 | .040749 | 13.505 |
| 4 | 22110.0 | .022551 | 498.60 | .036502 | 13.659 |
| 5 | 22111.9 | .023629 | 522.48 | .038246 | 13.610 |
| Mean | | | | | 13.560 |
| Standard deviation of the mean | | | | | ±0.040 |

## 5. Heats of Formation

### 5.1. Titanium Tetraiodide Compared to Titanium Tetrabromide

Appropriate combination of eq (1), (2), (3), (4), (5), and (6) leads to the process:

$$TiI_4(c)+[4HBr+20.1\ H_2O](soln)+9H_2O(liq)$$
$$=TiBr_4(c)+[4HI+29.1\ H_2O](soln), \quad (11)$$

$$\Delta H(27°C)=+6.00\pm0.54\ kj.$$

The heat capacities of the aqueous hydrobromic and hydriodic acid solutions, for the range 25° to 27°C, have been taken as 2.008 and 1.845 j/g°C, respectively, from section 4.4 of this paper. The heat capacities of $TiBr_4$ and $TiI_4$ have been taken as 0.358 and 0.235 j/g°C, respectively. By means of these data we obtain for eq (11):

$$\Delta H(25°C)=+6.29\pm0.55\ kj.$$

The heat of formation of HI in $[HI+7.3\ H_2O](soln)$ was taken as $-50.66\pm0.04$ kj/mole [5], and of HBr in $[HBr+5.0\ H_2O](soln)$ as $-109.96\pm0.18$ kj/mole [5].

Thus, we obtain for the difference in heats of formation of $TiI_4$ and $TiBr_4$:

$$TiI_4(c)+2Br_2(liq)=TiBr_4(c)+2I_2(c), \quad (12)$$

$$\Delta H(25°C)=-230.91\pm0.75\ kj/mole$$
$$=-55.19\pm0.18\ kcal/mole.$$

Since the heat of formation of $TiBr_4(c)$ has been previously measured [4] by the direct reaction of titanium with bromine [$\Delta Hf(25°C)=-616.72\pm4.60$ kj/mole], we obtain the following value for the heat of formation of $TiI_4$:

$$Ti(solid)+2I_2(c)=TiI_4(c) \quad (13)$$

$$\Delta Hf°(25°C)=-385.81\pm4.64\ kj/mole,$$
$$=-92.21\pm1.11\ kcal/mole.$$

### 5.2. Titanium Tetrachloride Compared to Titanium Tetrabromide

The appropriate combination of eq (6), (7), (8), (9), (10), and (4) leads to the process:

$$TiBr_4(c)+[4HCl+13.5\ H_2O](soln)+6.6\ H_2O(liq)$$
$$=TiCl_4(liq)+[4HBr+20.1\ H_2O](soln), \quad (14)$$

$$\Delta H(25°C)=-21.76\pm1.04\ kj/mole.$$

The heat of formation of HCl in [HCl+3.4 $H_2O$] (soln) is taken as $-151.21 \pm 0.17$ kj/mole [5] and of HBr in [HBr+5.0 $H_2O$](soln) is taken as $-109.96 \pm 0.13$ kj/mole [5]. Thus, we obtain for the difference in heats of formation of $TiBr_4$ and $TiCl_4$:

$$TiBr_4(c) + 2Cl_2(g) = TiCl_4(liq) + 2Br_2(liq), \quad (15)$$

$$\Delta H(25°C) = -186.76 \pm 1.34 \text{ kj/mole},$$
$$= -44.64 \pm 0.32 \text{ kcal/mole}.$$

This value is in very good agreement with $-44.72 \pm 1.28$ kcal for the difference in the directly determined heats of formation of $TiBr_4$ ($\Delta Hf = -147.40 \pm 1.10$) and $TiCl_4$ ($\Delta Hf = -192.12 \pm 0.65$) [3, 4]. This gives added confirmation to the values obtained for the heats of formation of $TiCl_4$ and of $TiBr_4$.

Gross, Hayman, and Levi [6, 7] have also reported direct determinations of the heats of formation of $TiBr_4$($\Delta Hf = -148.10 \pm 0.25$ kcal/mole) and $TiCl_4$ ($\Delta Hf = -191.45 \pm 0.30$ kcal/mole). The difference between these values is $-43.35 \pm 0.35$ kcal/mole, which is in reasonably good agreement with the value obtained in the present investigation.

## 6. References


[1] L. Brewer, L. A. Bromley, P. W. Gilles, and N. L. Lofgren, Paper No. 6 in L. L. Quill, ed., Chemistry and metallurgy of miscellaneous materials, thermodynamics, National Nuclear Energy Series IV–19B (McGraw-Hill Book Company, Inc., New York, N.Y., 1950).

[2] J. D. Fast, Z. anorg. u. allgem. Chem. **241,** 42 (1939).

[3] W. H. Johnson, R. A. Nelson, and E. J. Prosen, J. Research NBS **62,** 49 (1959) RP2928.

[4] R. A. Nelson, W. H. Johnson, and E. J. Prosen, J. Research NBS **62,** 67 (1959) RP2932.

[5] F. D. Rossini, D. D. Wagman, W. H. Evans, S. Levine, and I. Jaffe, Selected Values of Chemical Thermodynamic Properties, NBS Circ. **500,** (U.S. Government Printing Office, Washington 25, D.C., 1952).

[6] P. Gross, C. Hayman, and D. L. Levi, Trans. Faraday Soc. **51,** 626 (1955).

[7] P. Gross, C. Hayman, and D. L. Levi, Trans. Faraday Soc. **53,** 1601 (1957).



WASHINGTON, D. C.



(Paper 63A2–9)

Journal of Research of the National Bureau of Standards—A. Physics and Chemistry
Vol. 63A, No. 2, September–October 1959

# Reactions of Pentafluorohalobenzenes [1, 2]

Walter J. Pummer and Leo A. Wall

(June 15, 1959)

Both pentafluorobromobenzene and pentafluoroiodobenzene are reactive intermediates and can be used to introduce the perfluorophenyl ($C_6F_5$—) group into a variety of new compounds. The chief methods used are the Grignard coupling or addition reaction as well as the Ullmann condensation reaction. Some of the new compounds prepared were pentafluorobenzonitrile, perfluorodiphenyl, pentafluorophenyl-$\alpha$-ethanol, and pentafluorostyrene.

## 1. Introduction

Pentafluorobromobenzene is obtained as one of the products from the synthesis of hexafluorobenzene by the pyrolysis of tribromofluoromethane [1].[3] The isolation of this material is complicated by the presence of various fluorobromo olefinic and saturated aliphatic compounds boiling in the same range. These undesirable components can be effectively eliminated by subjecting the residue (bp>110° C) from the initial pyrolysis to another pyrolysis. This procedure converts the contaminants to more hexafluorobenzene and to higher boiling analogs without any apparent destruction of the pentafluorobromobenzene. A relatively pure sample can then be obtained by simple fractionation. Pentafluorobromobenzene and pentafluoroiodobenzene can also be prepared by the bromination or iodination of pentafluorobenzene in 65 percent oleum.[4]

Pentafluorobromobenzene (I) and pentafluoroiodobenzene (III) are useful reactive intermediates Since they contain labile bromine or iodine atoms, these compounds can be used to synthesize numerous new aromatic fluorocarbons containing the perfluorophenyl grouping, $C_6F_5$—. The methods chiefly used are the Grignard coupling or addition reaction and the Ullmann-type condensation. The following scheme will serve to illustrate some of these reactions:

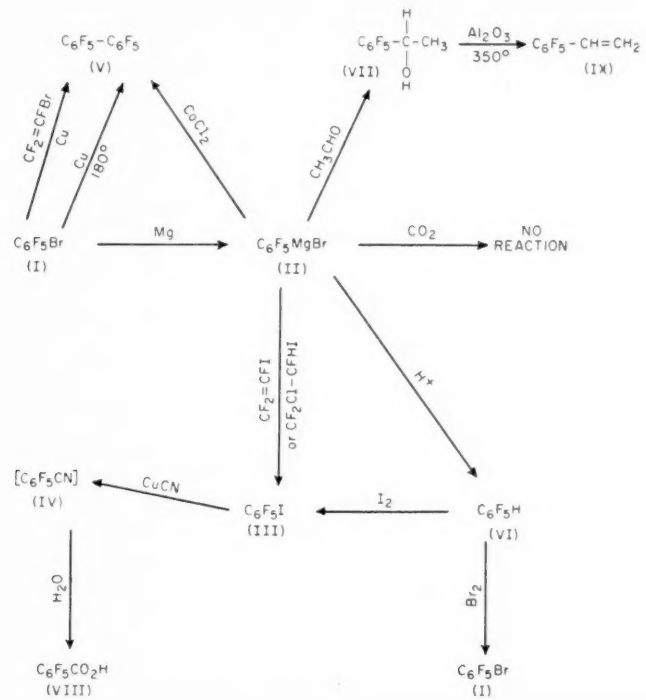


[1] This paper is based on work sponsored by the Bureau of Aeronautics and the Office of Naval Research, Department of the Navy, Washington, D.C.

[2] Presented as part of the Fluorine Symposium, Division of Industrial and Engineering Chemistry, 134th meeting of the American Chemical Society, Chicago, Ill., Sept. 1958.

[3] Figures in the brackets indicate the literature references at the end of this paper.

[4] Since the preparation of the article, work similar in part, has been published by E. Nield, R. Stephens, and J. C. Tatlow, J. Chem. Soc. **1959,** 166.

Perfluorodiphenyl (V) was obtained in good yields by the Ullmann condensation of pentafluorobromobenzene (I) in a sealed Pyrex tube at 180° C. The Grignard coupling method with cobalt chloride gave a low yield.

The preparation of perfluorobenzonitrile (IV) directly from pentafluorobromobenzene (I) following the Braun method [2], the use of pyridine and cuprous cyanide, gave unsatisfactory results. The reaction is extremely sensitive to heat, and after a short time at 138° C black insoluble solids appeared and no identifiable products could be obtained. The nitrile (IV) is also obtained from the reaction of (III) and cuprous cyanide. In this case the iodine is even more readily removed than the bromine, and once the reaction was initiated, the products were removed immediately by vacuum distillation. This procedure led to fair yields of pentafluorobenzonitrile (IV), based on its hydrolysis product, pentafluorobenzoic acid (VIII).

Pentafluorobromobenzene (I) readily forms a Grignard reagent, pentafluorophenylmagnesium bromide (II). Acidification of this reagent yields pentafluorobenzene (VI). The addition of acetaldehyde to (II) forms pentafluorophenyl-$\alpha$-ethanol (VII), which when dehydrated over alumina pellets at 350° C gave pentafluorostyrene (IX). Tarrant [3] employed the coupling of aromatic Grignard reagents and fluorochloro olefins to produce various styrenes halogenated in the side chain. Several attempts were made to utilize this concept for the synthesis of perfluorostyrene via the coupling of (II) and trifluoroiodoethene [4] or its precursor, 1,1,2-trifluoro-1-chloro-2-iodoethane. Instead of the desired coupling effect, an exchange reaction occurred, and pentafluoroiodobenzene (III) was obtained.

A similar attempt at preparing perfluorostyrene involved a mixed Ullmann reaction between pentafluorobromobenzene (I) and trifluorovinyl bromide. Only small amounts of perfluorodiphenyl (V) were isolated. No mixed coupling products were observed. Reactions involving the Grignard reagent (II) and tetrafluoroethylene are at present being explored.

Initial attempts to carbonate the reagent (II) by pouring it into an ether-solidified carbon dioxide slurry failed to produce any pentafluorobenzoic acid (VIII) after acidification. Only pentafluorobenzene (VI) was obtained. In this respect the Grignard reagent resembles pentachlorophenylmagnesium chloride in that it also failed to carbonate [5].

## 2. Experimental Procedures[5]

### 2.1. Pentafluorobenzene (VI)

To 1 g (0.041 g-atom) of magnesium turnings in 10 ml of anhydrous ether was added 1 ml of pentafluorobromobenzene (I) and a small crystal of iodine. Local heating was necessary to initiate the reaction. When the reaction was sufficiently in progress the flask was cooled in an ice-water bath and the remainder of compound (I) (total 10 g, 0.04 mole) was added over a half-hour period. The Grignard solution is dark brown in color. When all the magnesium appeared to have been consumed, the solution was allowed to come to room temperature and was stirred for an additional one-half hour. The Grignard solution was then poured on to 50 g of solidified carbon dioxide. After 1 hr, 100 ml of 10 percent hydrochloric acid was added. No pentafluorobenzoic acid (VIII) was observed, but there was obtained 3.5 g (51%) of pentafluorobenzene, bp 85° to 86° C; $n_D^{18.9}=1.3925$; reported bp 88° to 89°; $n_D^{18}=1.3931$ [6].

### 2.2. Pentafluoroiodobenzene (III)

To 200 g (1.5 moles) of iodine and 1 kg of 65 percent oleum, after stirring for 1 hr at room temperature, was added 255 g of reduced hexafluorobenzene (a mixture containing 45% of hexafluorobenzene, 40% of pentafluorobenzene, and 10% of tetrafluorobenzene) [7]. The mixture was stirred for 4 hr at 55° to 60° C. It was allowed to come to room temperature overnight. The flask was cooled in an ice bath, and gradually 1 liter of ice water was added. It was diluted further with another liter of ice water, then decolorized with aqueous sodium bisulfite, and the products (177 g) separated. After drying ($Na_2SO_4$) and distillation, there was obtained 82 g of unreacted hexafluorobenzene, 36 g of pentafluoroiodobenzene (bp 73° to 75°/35 mm, $n_D^{20}=1.4990$), and 48 g of higher iodinated fluorobenzenes. Analysis—calculated for $C_6F_5I$: C, 24.5; I, 43.1. Found: C, 24.7; I, 42.1.

### 2.3. Perfluorodiphenyl (V)—Ullmann Method

Five grams (0.02 mole) of pentafluorobromobenzene (I) and 2.5 g (0.039 g-atom) of activated copper powder [8] were sealed in an evacuated 5-mm Pyrex tube 20-cm long. The tube was placed in a furnace at 180° to 190° C for 48 hr. At the end of this period the temperature was slowly raised to 290° and held at this temperature for 6 hr. It was allowed to cool. Upon cooling, the contents solidified in long white needles. The tube was cooled in liquid nitrogen and opened. There was obtained 2.95 g (87%) of perfluorodiphenyl, mp 63° to 66° C. A recrystallization from methanol, followed by sublimation at 50°/1 mm afforded white plates, mp 67.5° to 68° C. Analysis—calculated for $C_{12}F_{10}$: C, 43.05. Found: C, 42.9.

### 2.4. Perfluorodiphenyl (V)—Grignard Coupling Method

The Grignard reagent, prepared from 10 g (0.04 mole) of compound (I), 1 g (0.04 g-atom) of magnesium turnings, and 25 ml of anhydrous ether, was filtered into a dropping funnel and added slowly to a refluxing mixture of 0.4 g (0.003 mole) of anhydrous cobalt chloride and 3 ml of ethyl bromide in 3 ml of anhydrous ether. The addition required 45 min. The mixture was then refluxed for 2 hr more, cooled, and acidified with 50 ml of 10 percent hydrochloric

[5] The boiling points given here are not corrected. Chemical analyses were performed by E. Deardorff of the Analytical Section, and the mass spectrometer analyses were obtained by Miss E. Quinn of the Mass Spectrometer Section of NBS.

acid. The ether layer was separated, dried ($Na_2SO_4$), and distilled. There was obtained 2.5 g (38%) of pentafluorobenzene, bp 84° to 86° C, and 0.5 g of perfluorodiphenyl (V) (15%), mp 67° to 68° C.

### 2.5. Pentafluorophenyl-α-Ethanol Alcohol (VII)

To the Grignard reagent, as prepared from 10 g of compound (I), was added rapidly at 0° C, 6.6 g (0.15 mole) of acetaldehyde. The solution was stirred at 0° C for 1 hr more, and finally decomposed by the addition of 50 ml of 6*N* hydrochloric acid. The ether layer was separated, dried ($Na_2SO_4$), and distilled. There was obtained 7 g (81%) of pentafluorophenyl-α-ethanol (VII), bp 80° to 82°/37 mm; $n_D^{20}=1.4426$. Analysis-calculated for $C_8H_5O_5F$: C, 45.3; H, 2.35. Found: C, 44.0; H, 2.30.

### 2.6. Pentafluorostyrene (IX)

Two grams of pentafluorophenyl-α-ethanol (VII) was passed through a 10-mm diameter by 20-cm glass tube containing 5 g of alumina pellets [9] at 345° to 350° C with the aid of nitrogen gas. The product (1.4 g) was caught in a solidified carbon dioxide trap and later distilled after drying ($Na_2SO_4$). There was obtained 0.6 g (33%) of pentafluorostyrene (IX), bp 140° to 141° C, $n_D^{20}=1.4414$. Mass spectrometer analysis of the product indicated a slight contamination with the starting material (VII).

### 2.7. Attempted Preparation of Perfluorostyrene

(a) The Grignard reagent (II) was prepared from 10 g (0.04 mole) of pentafluorobromobenzene (I), as described previously. To the refluxing Grignard solution was added 9.76 g (0.04 mole) of 1,1,2-trifluoro-1-chloro-2-iodoethane in 5 ml of anhydrous ether. No noticeable heat effect was observed. The solution was refluxed for 3 hr. At the end of this time a black solid appeared on the sides of the flask. The mixture was allowed to stand at room temperature overnight, and finally it was decomposed by addition of 50 ml of 6*N* hydrochloric acid. The ether layer was separated, dried ($Na_2SO_4$), and distilled. There was obtained 5.78 g (50%) of pentafluoroiodobenzene (III), bp 77° to 78°/35 mm, $n_D^{20}=1.4990$.

Mass spectrometer analysis of this product showed it to be 98 percent pure. Also, a carbonlike solid, which has not been characterized, was obtained.

(b) The Grignard reagent (II) was prepared from 10 g (0.04 mole) of pentafluorobromobenzene (I) in the usual fashion. To the Grignard solution, maintained at 0° C by means of an ice bath, was added 12.4 g (0.06 mole) of trifluoroiodoethene. The solution was stirred for 1 hr more and then refluxed for 2 hr. Decomposition was effected in the usual fashion. Distillation of the residue, after removal of the ether, afforded 2 g of pentafluorobenzene (VI), 1 g of pentafluoroiodobenzene (III), and 4.5 g of unreacted pentafluorobromobenzene (I).

(c) Two and one-half grams (0.01 mole) of compound (I), 3.71 g (0.06 mole) of activated copper, and 3.22 g (0.02 mole) of trifluorovinyl bromide were sealed in an evacuated 5-mm tube 25-cm long. The tube was placed in a furnace at 100° C, and the temperature was gradually raised to 200° C. This temperature was maintained for 5 hr. No apparent reaction was observed. The temperature was raised slowly to 260° to 270° C, and the tube was kept at this temperature for 15 hr. The copper became straw colored. The tube was cooled in liquid nitrogen and opened. The mixed Ullmann reaction produced only 0.1 g (2%) of perfluorodiphenyl (V). No mixed coupling products were observed.

### 2.8. Perfluorobenzonitrile (IV)

(a) From pentafluorobromobenzene (I), 5 g (0.02 mole) of compound (I), 3.58 g (0.02 mole) of cuprous cyanide, and 1.6 g (0.02 mole) of pyridine were refluxed together for 1 hr. The blackish mixture was cooled, and 50 ml of 6*N* hydrochloric acid was added. There was obtained a carbonlike insoluble solid, along with 30 percent (1.5 g) of recovered pentafluorobromobenzene (I). No pentafluorobenzonitrile (IV) was isolated.

(b) From pentafluoroiodobenzene (III), 5 g (0.017 mole) of compound (III), 1.6 g (0.009 mole) of cuprous cyanide, and 1.34 g (0.017 mole) of pyridine were placed in a small flask and gradually heated. The contents began to darken with increasing temperature. At 150° C the contents were a black viscous liquid. This temperature was maintained for 5 min more. The flask was allowed to cool to 100° C, and the apparatus was rearranged for distillation. The products were removed under reduced pressure obtained by a water aspirator. There was obtained 3.07 g of yellow liquid, bp 185° to 190° C, $n_D^{23.8}=1.4764$. The liquid, on standing, gradually turned brown and probably contained some unreacted starting material (III). To show that the pentafluorobenzonitrile (IV) had indeed formed, half of the above liquid, 1.5 g, was hydrolyzed with 75 percent sulfuric acid at 180° C. Upon pouring on ice, followed by an ether extraction and removal of the solvent, there was obtained 0.2 g (16%, based on reacted material) of pentafluorobenzoic acid (VIII), mp 101° to 103° C (reported mp 104° to 105°) [10]. There was obtained 0.4 g of unreacted starting material.

## 3. References


[1] M. Hellmann, E. Peters, W. J. Pummer, and L. A. Wall, J. Am. Chem. Soc. **79,** 5654 (1957)
[2] W. Braun and Karl Koeberle, U.S. Patent 2,195,076.
[3] P. Tarrant, University of Florida, private communication
[4] J. D. Park, R. J. Sefft, and J. R. Lacher, J. Am. Chem. Soc. **78,** 59 (1956).
[5] H. E. Ramdsen, A. E. Balint, W. R. Whitford, J. J. Walburn, and R. Cserr, J. Org. Chem. **22,** 1202 (1957).
[6] R. Stephens and J. C. Tatlow, Chemistry & Ind. (London) **1957,** 821.
[7] R. E. Florin, W. J. Pummer, and L. A. Wall, J. Research NBS **62,** 119 (1959) RP2940.
[8] A. I. Vogel, Textbook of practical organic chemistry, 188 (Longmanns, Green and Co., London, 1954).
[9] S. D. Ross, M. Markarian, and M. Nazzewski, J. Am. Chem. Soc. **69,** 1914 (1947).
[10] E. T. McBee and E. Rapkin, J. Am. Chem. Soc. **73,** 1366 (1951).



Washington, D.C. (Paper 63A2–10)

Journal of Research of the National Bureau of Standards—A. Physics and Chemistry
Vol. 63A, No. 2, September–October 1959

# Tritium-Labeled Compounds I. Radioassay of Tritium-Labeled Compounds in "Infinitely Thick" Films With a Windowless, Gas-Flow, Proportional Counter[1]

Horace S. Isbell, Harriet L. Frush, and Ruth A. Peterson

(May 5, 1959)

A simple, sensitive, and reliable technique has been devised for the radioassay of nonvolatile, water-soluble tritium compounds. The substance to be analyzed is dissolved in an aqueous solution of a thickening agent, preferably sodium *O*-(carboxymethyl)cellulose or sodium alginate. The solution is placed in a shallow planchet, and after evaporation of the water, the resulting film, which is "infinitely thick" to tritium *beta* particles, is counted with a $2\pi$, windowless, gas-flow, proportional counter. By means of an empirical factor, determined with a substance of known radioactivity, the counts are converted to microcuries. In a film having a thickness of 0.7 mg/cm$^2$, the counting efficiency is about 4 percent; the standard deviation from the mean, obtained in a series of routine measurements, was less than 2 percent. An assay can readily be made with tritium-containing material having 0.01 microcurie of radioactivity. The method, which is applicable to nonvolatile, water-soluble solids, solutions, or liquids, is suitable for routine analyses.

## 1. Discussion

Tritium is one of the cheapest and most versatile radioisotopes for use as a tracer in chemical reactions. However, its widespread use has been hampered by a lack of convenient methods of analysis. In connection with the development of methods for the preparation of position-labeled, radioactive carbohydrates containing tritium, a simple, rapid technique was needed for the assay of radioactivity of nonvolatile, tritium-labeled materials. Liquid scintillation counters [1],[2] although very satisfactory for assaying dissolved samples, are both expensive and unavailable to many workers. The conversion of materials to gases, for counting in ionization chambers [1] is laborious for routine analyses. Several workers have counted tritium-labeled materials from "infinitely thick" films with proportional counters [2 to 7]. A tritium-containing solid, if available in relatively large quantity, may be packed into a cupped planchet and counted [2, 3, 4]; this low-efficiency method has chiefly been used for comparisons, rather than for the determination of absolute activities. Alternatively, an infinitely thick film of a nonvolatile liquid has been employed [5], or a solid film has been deposited on a planchet by evaporation of the solvent from a solution [6, 7]. The last-mentioned method is probably the most versatile, but it suffers from the fact that crystallization on the planchet can render the surface area of the film uncertain and variable [5, 7], and may even cause contamination of the counter during flushing [6].

For routine radioassay of nonvolatile, water-soluble, tritiated materials in a windowless, gas-flow, proportional counter, a technique has been developed in this laboratory that avoids difficulty caused by crystallization and permits the counting, from uniform, infinitely thick films, of materials available in small quantity. The radioactive substance is dissolved in an aqueous solution of a thickening agent, preferably sodium *O*-(carboxymethyl)cellulose or sodium alginate.[3] The amount of sample and thickening solution are so adjusted that the thickness of the film formed on the planchet after evaporation of the water is more than the maximum range of the tritium *beta* particles, (infinitely thick, approximately 0.7 mg/cm$^2$ for the material used [9]). The films adhere well to the planchets, and the thickener prevents crystallization. The counts are converted to microcuries ($\mu$c) by means of an empirical factor determined under the same conditions with a sample of known radioactivity.[4] Although the counting efficiency of a film having a thickness of 0.7 mg/cm$^2$ is only about 4 percent, the reproducibility of the method corresponds to a standard deviation of less than 2 percent. A satisfactory determination can be made with as little as 0.01 $\mu$c of a tritium-labeled material on a 2-in. planchet. Because of its simplicity the method is suitable for routine analyses. The accuracy of the method depends on the absolute activity of the material used as standard. For the work reported here, D-glucose-*1-t* was standardized by comparing it with the NBS tritium oxide standard.

In the course of the work, a study was made with films of less than infinite thickness. Although high counting efficiencies can be obtained, uncertainty arising from uneven distribution of the sample makes counting from thin films less satisfactory than counting from infinitely thick films by the method described.

[1] Part of a project on the development of methods for the production of radioactive carbohydrates, sponsored by the Division of Research of the Atomic Energy Commission.

[2] Figures in brackets indicate the literature references at the end of this paper.

[3] A critical study of the energy loss and penetration range of *beta* particles is given in [8]. In general, the range increases with the atomic number of the material penetrated. In the film-counting method described here, the films are of organic materials, and have approximately the same elemental composition. In the presence of elements of higher atomic number, the greater depth of penetration would require a thicker film for infinite thickness, and use of a different factor for converting counts to microcuries.

[4] The counting of carbon-14 from thin films of agar has been reported by McCready [10]. See also a modification of the method [11].

## 2. Materials and Apparatus

### 2.1. Tritium-Labeled Materials

D-Glucose-1-*t* was prepared by sodium amalgam reduction of D-glucono-δ-lactone in tritiated water [12] in the presence of sodium acid oxalate [13]. The sample used as a tritium standard was assayed by comparing its activity in a phosphoric acid-phosphoric anhydride solution with that of the NBS standard tritium oxide sample No. 4926; the measurements were made with a proportional counter [14]. D-Mannitol-1-*t* was prepared by reducing D-mannose with tritiated lithium borohydride [14].

### 2.2. Solution of Sodium O-(Carboxymethyl)cellulose

The thickening agent was commercial, medium-viscosity sodium *O*-(carboxymethyl)cellulose, CMC-12MP, a product of Hercules Powder Company, Wilmington, Del. The CMC stock solution ordinarily used for the radioassay of solid samples was prepared by dissolving 1 g of CMC, 0.5 g of anhydrous D-glucose, and 10 mg of eosin[5] in sufficient water to give 100 ml of solution. The D-glucose serves as an organic "ballast" material and plasticizer. It was omitted entirely, or in part, in thickening solutions for use with large samples of weakly radioactive material. D-Glucitol has been used with equal success as ballast in place of D-glucose.

### 2.3. Solution of Sodium Alginate

The sodium alginate used was high-viscosity Algin, obtained from Kelco Company, San Diego, Calif. The stock solution was prepared from 0.5 g of Algin, 1 g of anhydrous D-glucose, 10 mg of eosin, and sufficient water to give 100 ml of solution.

### 2.4. Counting Equipment

Radioactivity measurements were made with a $2\pi$, windowless, gas-flow, proportional counter, Model PC–3, obtained from Nuclear Measurements Corp., Indianapolis, Ind.; the slide holder of the instrument had been modified by inserting tubes for water circulation [15]. Commercial gas, consisting of 90 percent of argon and 10 percent of methane, was used in the counter. The gas was dried by successive passage through soda-lime and anhydrous calcium sulfate. The 2-in., stainless-steel, cupped, flat-bottomed, counting planchets used in this work were also obtained from Nuclear Measurements Corp.; they have an effective area of 21.4 $cm^2$. Some of these planchets were modified by enclosing a 10-$cm^2$ area with a circular groove beyond which the solution did not spread.

[5] The dye serves to show the uniformity of the film.

## 3. Recommended Procedure for Radioassay of Tritium-Labeled Compounds in Infinitely Thick Films

The solution of the radioactive sample in the aqueous thickening agent can be prepared by any convenient method. Ordinarily, radioactive solids are weighed, and then dissolved in a known volume of the stock thickening solution. A radioactive liquid, usually less than 0.5 ml, is mixed with a measured amount of the thickening solution. However, if the liquid is sufficiently radioactive, it is measured in a dilution pipet and diluted to a definite volume with the thickening solution. Approximately 1 ml of the solution to be assayed is transferred to a clean,[6] 2-in. cupped planchet (or 500 microliters is transferred to the 10-$cm^2$ area of the planchet), which is then placed under an infrared lamp. After the solvent has evaporated, the planchet is kept for about 1 hr in a desiccator over a saturated solution of potassium acetate in contact with the solid phase. This rather unusual procedure gives films of reproducible moisture content, and does not lower the count substantially. The sample is then counted in the proportional counter for 3 periods, with a total of at least 10,000 counts. Before each period the counter is flushed with the counting gas for 30 sec. It occasionally happens that successive counts show a marked trend, presumably caused by the accumulation of a static charge on the film. If this occurs, the sample is removed to the desiccator for a short time, and then recounted. The background count is determined with a film-covered planchet placed in the counting chamber.

The voltage for optimum precision must be determined under the conditions used. The optimum voltage for assay of solid samples with the equipment used in the present study was approximately 2,050 volts.

## 4. Discussion of the Procedure and Results

The activity of tritium in the sample is given by the relationship:

$$\mu c = \frac{\text{dps}}{37{,}000} = \text{cps} \times m \times k \qquad (1)$$

where cps is the net count, $m$ is the total solids in a volume of solution containing the radioactive sample, and $k$ is a constant determined by the same method for a compound of known tritium content.

The value of $m$ must be determined accurately, although the exact amount of solution placed on the planchet is not critical if the film formed from it is infinitely thick. Because of hydration, the value of $m$ calculated from the ingredients in the formulation may differ slightly from that determined by weighing the film produced, under the conditions of

[6] Care must be used to obtain a grease-free surface on the planchet. In this laboratory the planchets are cleaned in a solution of sodium hydroxide or "Versene" immediately before use.

the method, from a definite volume of the solution. Determination of the weight of the film in each analysis is laborious. This step can be avoided by determining the weight of the film formed on a planchet from exactly 1 ml of the *stock solution* of CMC or Algin under the conditions of the analysis. Because of the viscosity of the solution, a pipet, calibrated to contain 1 ml, is employed, and the solution adhering to the pipet is carefully rinsed out and added to the planchet. The film, obtained after evaporation of the water, is conditioned in the usual manner and weighed. Several determinations are made, and the average value is used for calculating $m$, the weight of the film containing the radioactive substance, on the assumption that $m$ equals the weight of the film from the amount of stock solution used plus the weight of the radioactive sample. All nonvolatile matter in the formulation must be included in the calculation of $m$.

The value of $k$ depends on the surface area, backscattering, efficiency of the counter, geometry, and other factors; it has the dimension of weight$^{-1}$. To obtain accurate results in the analysis of a series of compounds, $k$ must be determined by assay of a standard tritium compound under the conditions used for the unknowns. With materials of similar character, the amount of radiation scattering is constant. Because scattering varies with the effective atomic number of the reflecting material, heavy elements such as barium increase internal scattering and may lead to small errors. These can be avoided by adding, to the standard, compounds of any heavy elements that may be present in the material to be assayed. Ions of certain metals, as, for example, lead, form insoluble compounds with both CMC and Algin. This undesirable effect can be overcome by adding Versene to the film-forming mixture.

Table 1 presents results obtained with two samples each of D-glucose-*1-t* and D-mannitol-*1-t*. The standard deviations are based on the deviations in counting rates for the separate planchets from the mean counting rate for the group of planchets. Sample $G_1$ was used as a standard, and its specific activity (0.0865 $\mu c$/mg) was carefully determined by the comparative method described under materials and apparatus. Use of this material as a control gave values of $k$ under various conditions, i.e., for CMC and Algin films and for the 10-cm² and 21.4-cm² (2-in.) planchets. By use of these constants, the specific activities of $G_2$, $M_1$, and $M_2$ were determined. The counting rates for films having thicknesses between 0.69 and 1.48 mg/cm² showed no significant differences.

## 5. Assay of Tritium Compounds in Films of Less Than Infinite Thickness

Table 2 and figure 1 show the relative counting rate of a preparation of D-glucose-*t* as a function of source thickness. Each sample was spread on a freshly cleaned, 2-in., stainless-steel planchet, and the solvent was evaporated under an infrared lamp. The planchet was cooled in a desiccator over anhydrous calcium chloride, and then counted with the equipment described before. The first seven determinations were made on films from solutions of D-glucose-*t* in water, and the last three on films from solutions of D-glucose-*t* containing sufficient Algin to give the weight recorded. The radioactivity in thin films can be estimated by use of the data of table 2 and figure 1.

## 6. Discussion of Absolute Radioactivity

The counting rate of a tritium source in an efficient, windowless, gas-flow, proportional counter can be represented by an equation of the type [6]:

TABLE 1. *Counting rates of tritium compounds in "infinitely thick" films*

| Sample | | Film | | | | Counting Data | | | Specific activity [d] of sample | k×10⁵ |
|---|---|---|---|---|---|---|---|---|---|---|
| Substance [a] | Weight [b] ($m'$) | Thickening agent | Area | Total solids ($m$) | Thickness | No. of planchets | Average count | Standard deviation [c] | | |
| | *mg* | | *cm²* | *mg* | *mg/cm²* | | *cps* | % | *μc/m'* | |
| $G_1$ | 0.435 | CMC | 10.0 | 7.7 | 0.77 | 5 | 50.1 | 1.04 | (0.0856) | 9.65 |
| $G_1$ | .87 | CMC | 21.4 | 15.4 | .72 | 5 | 108.7 | 0.86 | (.0856) | 4.45 |
| $G_1$ | .415 | Algin | 10.0 | 8.1 | .81 | 4 | 45.1 | .58 | (.0856) | 9.72 |
| $G_1$ | .83 | Algin | 21.4 | 16.2 | .76 | 5 | 95.3 | .87 | (.0856) | 4.60 |
| $G_2$ | .82 | CMC | 21.4 | 14.8 | .69 | 5 | 101.3 | .44 | .0814 | (4.45) |
| $G_2$ | 1.23 | CMC | 21.4 | 22.1 | 1.03 | 5 | 100.5 | .63 | .0804 | (4.45) |
| $G_2$ | 0.82 | CMC | 10.0 | 14.8 | 1.48 | 11 | 47.6 | 1.15 | .0829 | (9.65) |
| $G_2$ | .82 | Algin | 21.4 | 15.7 | 0.73 | 5 | 95.0 | 1.57 | .0837 | (4.60) |
| $G_2$ | 1.23 | Algin | 21.4 | 23.5 | 1.10 | 3 | 94.5 | 1.71 | .0831 | (4.60) |
| $M_1$ | 0.036 | CMC | 21.4 | 14.0 | 0.65 | 4 | 289.4 | 0.14 | 5.01 | (4.45) |
| $M_2$ | 2.50 | CMC | 21.4 | 16.7 | .78 | 5 | 34.1 | 1.40 | 0.010 | (4.45) |

[a] $G_1$ and $G_2$ are different preparations of D-glucose-*1-t*; $M_1$ and $M_2$ are D-mannitol-*1-t*.
[b] $m'$ is the weight of the radioactive sample contained in the film of weight $m$.
[c] $\sqrt{\frac{\Sigma d^2}{n-1}} \times 100$
[d] $\mu c = cps \times m \times k$. Values in parentheses were used as standards.

$$dps=\frac{cps}{f_g\times f_b\times f_s} \tag{2}$$

where dps is the activity of a source, and $f_g$, $f_b$, and $f_s$ are correction factors for the geometry of the detector, for backscattering, and for self-absorption, respectively. The geometry factor, $f_g$, with a flat planchet is approximately 0.5. The backscattering factor, $f_b$, is a function of the atomic weight of the backing material and depends somewhat on the character of the radiation and on the geometry of the counter [16]. But with an infinitely thick source, scattering from the backing material may be neglected because the only reflected radiation that reaches the counter originates in the source itself. With sources composed of carbon, hydrogen, and oxygen, the scattering factor is of the order of 5 percent, and can be neglected in obtaining an approximate estimate of the true activity. Prior workers have shown that the self-absorption factor, $f_s$, for the *beta* radiation is given by the relationship:

$$f_s=\frac{A_T}{A_0}=\frac{1-e^{-\mu T}}{\mu T}, \tag{3}$$

where $\mu$ is the self-absorption coefficient and $A_T$ is the radiation from a source containing a unit weight of the radioactive material with a thickness $T$; $A_0$ is the limiting value for $A_T$ as $T$ approaches zero. If the weight of the source is $m$ mg and the area is $a$ cm², $T=\frac{m}{a}$ and eq (3) can be rewritten:

$$f_s=\frac{A_T}{A_0}=\frac{1-e^{-\mu T}}{\frac{\mu m}{a}}. \tag{4}$$

When $T$ is infinite with respect to *beta* particles, as in the analytical method, $1-e^{-\mu T}=1$, and eq (4) becomes:

$$\frac{mA_T}{A_0}=\frac{a}{\mu}. \tag{5}$$

When $T$ aproaches zero, $f_s$ approaches 1, and from eq (2) and the definition of $A_0$:

$$A_0=\left(\frac{cps}{m}\right)_{f_s\to 1}=\frac{dps}{m}\times f_g\times f_b. \tag{6}$$

Since $mA_T$ is the cps of a source weighing $m$ milligrams, eq (5), by substitution for $mA_T$ and $A_0$ becomes:

$$\frac{a}{\mu}=\frac{cps}{\left(\frac{dps}{m}\right)\times f_g\times f_b}. \tag{7}$$

Assuming $2\pi$ geometry ($f_g=0.5$) and no backscattering ($f_b=1$), values of $1/\mu$ can be calculated from eq (7) for all of the measurements recorded in table 1. However, there is considerable uncertainty in the value of $a$ for determinations made with the 2-in., commercial, flat-bottomed planchets, because of the curved edge. Hence, the best value of $1/\mu$ is that obtained from the measurements for the standardized sample $G_1$ in the 10-cm² areas. In the first experiment of table 1, $a=10.0$, cps=50.1, and $(dps/m)\times f_g=(0.435\times 0.0856\times 37{,}000/7.7)\times 0.5$. From these values there is obtained:

$$\frac{1}{\mu}=0.0560 \text{ mg/cm}^2.$$

The value of $1/\mu$ can be used to obtain $T_{1/2}$ (the half-value thickness of the radiation) and $R$ (the

TABLE 2. *Counting rate of* D-*glucose-t as a function of film thickness*

| D-Glucose-*t* [a] | Volume of film-forming solution | Total solids | Film thickness | Average count [b] | Standard deviation | Counting efficiency cps/dps |
|---|---|---|---|---|---|---|
| *mg* | *ml* | *mg* | *mg/cm²* | *cps* | % | % |
| 0.02 | 0.02 | 0.02 | 0.000934 | 30.9 | 2.3 | 48.8 |
| .05 | .05 | .05 | .00234 | 74.3 | 2.9 | 46.9 |
| .10 | .10 | .10 | .00467 | 142.2 | 3.4 | 44.9 |
| .20 | .20 | .20 | .00934 | 232.7 | 5.7 | 36.7 |
| .50 | .50 | .50 | .0234 | 499 | 4.4 | 31.5 |
| 1.00 | 1.00 | 1.00 | .0467 | 750 | 4.0 | 23.7 |
| 2.00 | 2.00 | 2.00 | .0934 | 1103 | 3.4 | 17.4 |
| 1.00 | 1.00 | [c] 9.00 | 0.420 | [d] 1971 | 2.1 | 6.9 |
| 1.00 | 1.00 | 17.00 | .794 | 2108 | 2.0 | 3.9 |
| 1.00 | 1.00 | 25.00 | 1.170 | 2108 | 0.6 | 2.7 |

[a] The activity of the D-glucose-*t* was 0.0856 μc/mg. The "effective area" of the planchet was 21.4 cm².
[b] Average of three planchets, each counted to 10,000 counts.
[c] In the last three experiments, the amount of D-glucose-*t* was constant, and the weight of film was increased by use of an Algin solution.
[d] The observed cps and the total dps in the last three experiments were multiplied by the dilution ratio, i.e., by 9, 17, and 25, respectively, to reduce all results to a common specific activity.

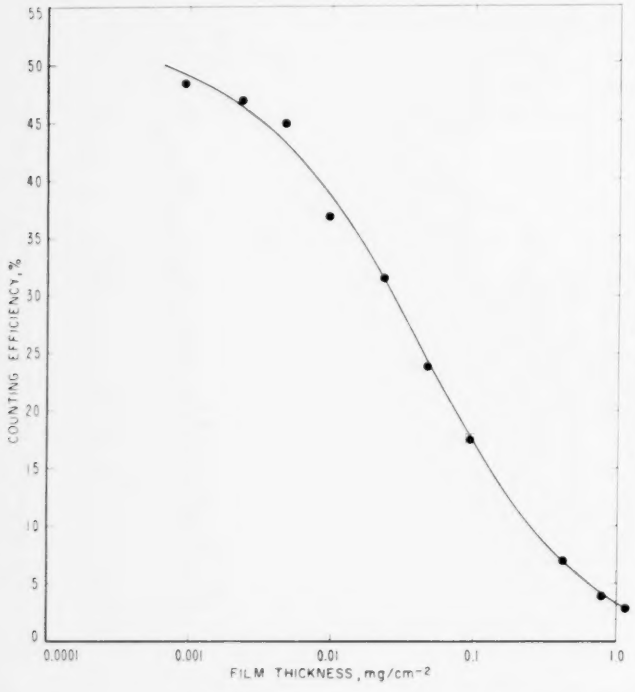


FIGURE 1. *Counting efficiency as a function of film thickness.*

range) from the relationships [9, 17] $T_{1/2}=0.693/\mu$ and $R=5/\mu$. With the above value of $1/\mu$, $T_{1/2}=0.039$ mg/cm$^2$ and $R=0.28$ mg/cm$^2$. This value of $R$ can be compared with experimental values, reported in the literature, of 0.23 mg/cm$^2$ [18], 0.5 mg/cm$^2$ [19],[7] 0.6 mg/cm$^2$ [6], and with the value of 0.7 mg/cm$^2$ based on an empirical energy-range relationship [9]. The variation in the results arises from experimental difficulties and from uncertainty in the absolute disintegration rate of the source.

It is of interest to note that extrapolation of the observed counting rates of figure 1 to zero thickness gave a value of approximately 50 percent of the absolute disintegration rate, based on the NBS tritium standard. With a stainless-steel planchet, under conditions somewhat comparable to those used here, Rydberg's data [6] for thin films indicate a backscattering factor of about 1.25. Thus the count would be expected to be approximately 62 percent of the absolute rate, with a stainless-steel planchet, $2\pi$ geometry, and no self-absorption. A low value might arise from unequal distribution of the material on the planchet. This factor is of no importance with thick samples, but could give rise to large errors with thin samples. Such errors make accurate assay of tritium materials in thin samples impracticable.

Assay of infinitely thick films is, however, highly satisfactory, and is recommended for routine, laboratory analysis. In eq (1), the empirical constant $k$ includes corrections for the area of the source, geometry of the counter, self-absorption, backscattering, and conversion of total $dps$ to microcuries. By use of eq (1) and (7), $k$ may be related to $a/\mu$ thus:

$$k=\frac{\mu}{a\times f_g\times f_b\times 37{,}000}$$

However, because of uncertainties in the values for $a$, $f_g$, and $f_b$, the constant $k$, for the calculation of absolute radioactivity from observed counts, should be experimentally determined under the conditions of use.

[7] Value derived from the average of two half-thickness values experimentally determined by Dorfman.

## 7. References


[1] Nucleonics **16,** No. 3, 62 (1958).
[2] W. A. Jenkins, Anal. Chem. **25,** 1477 (1953).
[3] T. E. Banks, J. C. Crawhall, and D. G. Smyth, Biochem. J. **64,** 411 (1956).
[4] W. A. Jenkins and D. M. Yost, J. Chem. Phys. **20,** 538 (1952).
[5] F. L. Jackson and H. W. Lampe, Anal. Chem. **28,** 1735 (1956).
[6] J. Rydberg, Acta Chem. Scand. **12,** 399 (1958).
[7] M. L. Eidenoff and J. E. Knoll, Science **112,** 250 (1950).
[8] A. T. Nelms, Energy loss and range of electrons and protons, NBS Circ. 577 (1956); Supplement (1958).
[9] L. E. Glendenin, Nucleonics **2,** No. 1, 12 (1948).
[10] C. C. McCready, Nature **181,** 1406 (1958).
[11] H. Campbell, H. A. Glastonbury, and M. D. Stevenson, Nature **182,** 1100 (1958).
[12] H. S. Isbell and coworkers (unpublished work).
[13] H. S. Isbell, J. V. Karabinos, H. L. Frush, N. B. Holt, A. Schwebel, and T. T. Galkowski, J. Research NBS **48,** 163 (1952) RP2301.
[14] H. S. Isbell and J. D. Moyer (unpublished work).
[15] A. Schwebel, H. S. Isbell, and J. D. Moyer, J. Research NBS **53,** 221 (1954) RP2537.
[16] W. B. Mann and H. H. Seliger, Preparation, maintenance, and application of standards of radioactivity, NBS Circ. 594 (1958).
[17] W. F. Libby, Anal. Chem. **19,** 2 (1947).
[18] S. C. Brown, Phys. Rev. **59,** 954 (1941).
[19] L. M. Dorfman, Phys. Rev. **95,** 393 (1954).



WASHINGTON, D.C. (Paper 63A2–11).

Journal of Research of the National Bureau of Standards—A. Physics and Chemistry
Vol. 63A, No. 2, September–October 1959

# Tritium-Labeled Compounds II. General-Purpose Apparatus, and Procedures for the Preparation, Analysis, and Use of Tritium Oxide and Tritium-Labeled Lithium Borohydride [1]

Horace S. Isbell and Joseph D. Moyer

(June 11, 1959)

A general-purpose manifold is described, which is useful for numerous procedures involving tritium gas and tritium-labeled materials.

Methods are given in detail for (a) converting tritium gas to tritium oxide, (b) preparing tritium-labeled lithium borohydride, and (c) conducting a variety of reactions in a closed system. Auxiliary equipment is shown, including water traps, reaction flasks, and apparatus for preparing solutions and making filtrations in closed systems. Methods are presented for assaying tritium-labeled water by (a) dissolving it in a phosphoric anhydride-sulfuric acid solution and counting in a windowless, gas-flow, proportional counter, or (b) converting it to hydrogen-*t* and assaying it in an ionization chamber. The use of tritium-labeled lithium borohydride is illustrated by the preparation of D-galactitol-*1-t* from D-galactose. Subsequent papers will describe the use of this apparatus in the synthesis of tritium-labeled carbohydrates. The detailed description of techniques and apparatus should be helpful to others who are interested in using tritium.

## 1. Introduction

In a program sponsored by the Division of Research of the Atomic Energy Commission at the National Bureau of Standards, efficient methods have been developed for the production of $C^{14}$-labeled carbohydrates [1 to 16].[2] Attention has now been directed to the development of methods for the synthesis, analysis, and study of tritium-labeled materials. As the first step in the program, a convenient method was developed for the assay of nonvolatile, water-soluble tritium compounds [17]. Undoubtedly, this and other improved methods of analysis [18 to 21] will lead to rapid expansion in the use of tritium compounds for research.[3]

The production of tritium-labeled carbohydrates required the development of apparatus and techniques for conducting a variety of operations in closed systems. These include: (a) Dilution of tritium with hydrogen, (b) removal of samples of gas for radioassay, (c) conversion of tritium to tritium oxide, (d) purification of materials by filtration and crystallization in closed systems, (e) exchange of tritium with hydrogen in solids, (f) recovery of hydrogen-*t* released in chemical reactions, and (g) circulation of hydrogen-*t*, in catalytic reductions. The following sections describe convenient equipment for conducting these and other procedures.

Detailed directions are given for the preparation of tritium-labeled lithium borohydride. This versatile reagent makes possible a wide variety of reactions for introducing tritium into specific positions in organic compounds. Use of tritium-labeled lithium borohydride is illustrated by the preparation of D-galactitol-*1-t* [4] from D-galactose. Other applications of the reagent will be described in future publications.

A convenient procedure is described for the radioassay of water-*t* in a proportional counter. The water-*t* is dissolved in a phosphoric anhydride-sulfuric acid solution and counted in a windowless, gas-flow, proportional counter in a manner similar to that used for assaying $C^{14}$-labeled compounds in solution [23].

## 2. Apparatus and Procedures

### 2.1. General-Purpose Manifold [5]

The general-purpose manifold shown in figure 1 is constructed from high-vacuum-grade ball-joints, stopcocks, and other parts. In figure 1, the stopcocks in the primary line are numbered; those connecting to auxiliary equipment are lettered. The commercial, automatic Toepler pump, *T*, is operated by an auxiliary pump activated by a lock-up or latch relay. A fritted-glass filter, just above the check valve on the pressure side of the Toepler pump, prevents entrainment of particles of mercury. To conserve space, the copper oxide furnace (for converting hydrogen-*t* to water-*t*) is placed above and behind the main line; it is kept in place, but is bypassed when not in use. Interchangeable, low-temperature traps (fig. 2) are used for collecting and storing water and other volatile liquids. Part (a)

[1] Project sponsored by the Division of Research of the Atomic Energy Commission.

[2] Figures in brackets indicate the literature references at the end of this paper.

[3] Published research on deuterium and tritium compounds prior to 1956 is listed in a series of annual bibliographies prepared by the Thermodynamics Section of NBS [22] under the auspices of the Atomic Energy Commission.

[4] The product is not a *meso* compound, but a true derivative of D-galactitol.

[5] The manifold and auxiliary equipment are more or less conventional, and ideas for their construction were drawn from many sources. Textbooks by Glascock [24] and by Sanderson [25] were particularly helpful.

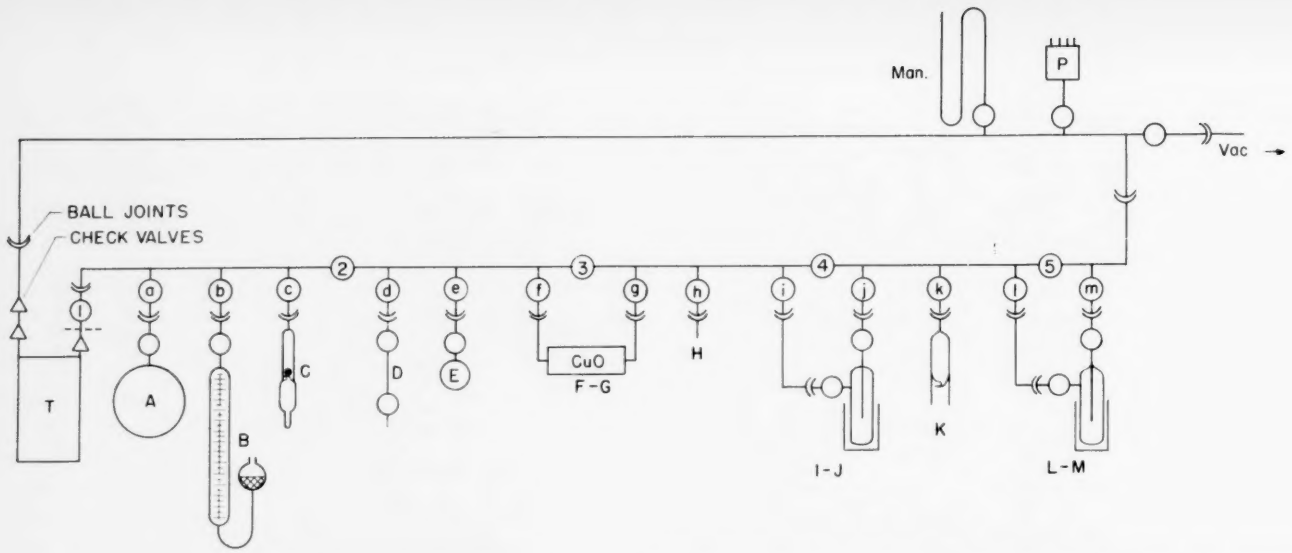


FIGURE 1. *General-purpose manifold.*

---- Sintered-glass filter.
*T* Automatic Toepler pump.
*P* Pirani vacuum gauge.
Man. Mercury manometer.
*A* Hydrogen-*t* storage flask.
*B* Gas buret.
*C* Tritium in break-seal tube.
*D* Gas-sampling tube. (See fig. 3).
*E* Water-storage flask.
*F–G* Copper oxide furnace.
*I–J* and *L–M* Cold traps. (See fig. 2).
*K* Break-seal receiving tube.

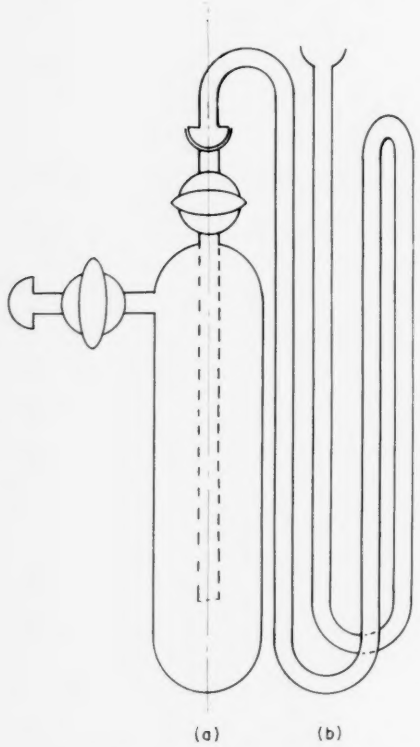


FIGURE 2. *Interchangeable traps.*

of this trap is ordinarily used alone, but for more efficient removal of condensable gases, a multiple trap (b) is included [26]. The two components are immersed in the same freezing bath, and can be used in combination (on the same outlets as a single trap). The traps are shown symbolically at (*I–J*) and (*L–M*) in figure 1. The gas buret, *B*, is used not only for measuring and dispensing hydrogen, but also for transferring gas to the reaction flasks. At the close of each preparation, hydrogen-*t* in the system is either converted to water-*t* in the copper oxide furnace (*F–G*), or is pumped into flask *A* attached to the manifold; any residual gas is stored in the Toepler pump. The arrangement given in figure 1 is used for the production of tritiated water. Other arrangements are used for special purposes; these will be described in subsequent reports on specific products.

### 2.2. Dilution of Tritium with Hydrogen

The apparatus of figure 1 is assembled, made vacuum-tight,[6] and evacuated. The system is then filled with dry hydrogen, introduced at *H*, and the quantity of hydrogen required for the desired dilution is drawn into gas buret *B*. The stopcock to *B* is closed and the system is evacuated to a pressure of less than 20 microns of mercury. With all stopcocks closed, the "break-seal" joint connecting the tritium sample, *C*, is ruptured by means of a steel ball operated by a magnet. Then, with stopcocks 1, 2, and *a* closed, the tritium and the hydrogen are mixed in *B* by opening stopcocks *b* and *c* and raising and lowering the leveling bulb containing mercury. Finally, the hydrogen-*t* is transferred to the evacuated reservoir *A* for storage, leaving any desired amount in *B*. Residual hydrogen-*t* in the line is drawn into the Toepler pump and held for future use. The empty tube, *C*, is removed and can be replaced by other apparatus.

[6] Stopcocks must be of high quality and carefully lubricated with vacuum grease. Ball-joints are sealed with vacuum-grade sealing wax.

### 2.3. Radioactivity Assay of Hydrogen-*t*

The gas in the manifold can be sampled at any desired time by means of the gas-sampling tube shown in figure 3(a). The tube is attached to the manifold at any available outlet. With the stopcock to the manifold closed and stopcock 1 of figure 3(a) open, the gas-sampling tube and connection are evacuated through stopcock 2 by an auxiliary pump. After stopcock 2 has been closed, the sample tube is filled with hydrogen-*t* from the manifold. The temperature and pressure are then measured. Next, 1 is closed (to trap a sample of the gas between 1 and 2). Residual gas in the line connecting the manifold is drawn into the Toepler pump, and the stopcock of the manifold is closed. Finally, the sample tube is removed from the manifold.

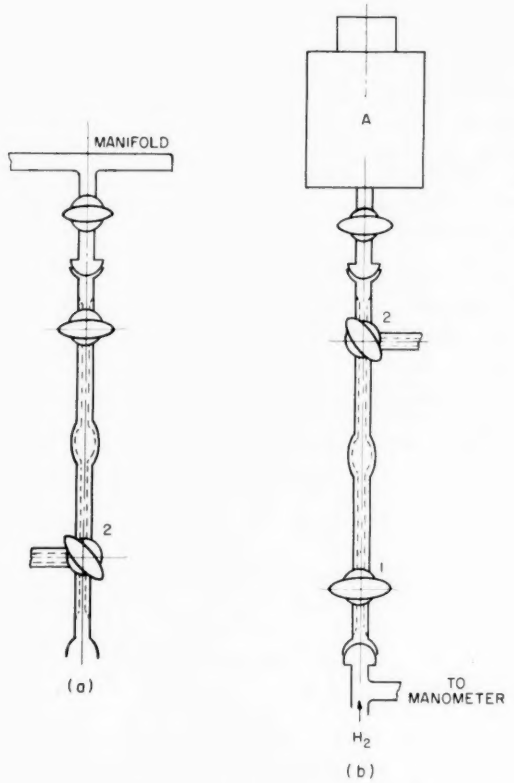


FIGURE 3. *(a) Gas sampling tube and (b) Tube connected for transfer of sample to ionization chamber.*

For radioassay, this gas is transferred to the ionization chamber with the apparatus of figure 3(b) in the following manner. The ionization chamber, *A*, is evacuated through stopcock 2. Then 2 is turned to allow gas from the sample tube to flow into the chamber. The line from a cylinder of hydrogen to 1 is first evacuated and then filled with hydrogen. Hydrogen is allowed to pass slowly, through 1 and the sample tube, into the ionization chamber, until atmospheric pressure is reached; then the stopcock on the ionization chamber is closed. The ion current arising from the sample in the ionization chamber is measured with a vibrating-reed electrometer in the customary manner [21]. The amount of tritium in the sample is calculated with a factor that is obtained by assaying hydrogen-*t* prepared from the NBS tritium oxide standard or from any source of known tritium content.

### 2.4. Conversion of Hydrogen-*t* to Water-*t*

To convert hydrogen-*t* to water-*t*, the copper oxide furnace (*F–G*) of figure 1 is heated to 500° C. The stopcocks are set so that hydrogen-*t* can pass from the gas buret *B* through the furnace and the water trap (*I–J*) (cooled by a dry-ice bath). The Toepler pump is started and the gas is circulated until the pressure in the system becomes constant. If desired, the water-*t* that collects in the trap can be diluted with water distilled from flask *E*. Finally, the trap containing the water-*t* is isolated by closing stopcocks *i* and *j* and opening stopcock 4. The water-*t* is stored in the trap until it is used. Any residual hydrogen-*t* in the system is diluted with hydrogen from *B*. The mixture is then oxidized by passing it through the copper oxide furnace and a second water trap (*L–M*) (cooled by a dry-ice bath). The gas is again circulated by the Toepler pump until the pressure in the system becomes constant. Finally, stopcocks *l* and *m* are closed and the water-*t* of low activity is stored in the trap until needed.

Water-*t* can be distilled from the trap into a receiver attached to the manifold at *k*. Water of high activity is collected and sealed in a break-seal receiving tube; it must be used in a closed system. Water of low activity is collected in a receiving flask such as *A* of figure 4. The receiving flask has a side arm closed with a rubber cap suitable for the addition or withdrawal of liquid by means of a hypodermic syringe. Under a suitable hood, samples of low-activity water can be withdrawn from the flask by a micropipet of the syringe type, and used as desired.

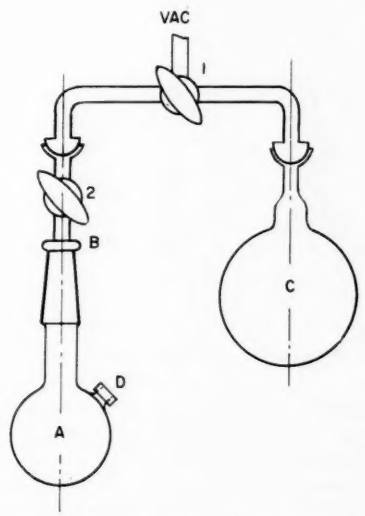


FIGURE 4. *Adapter and flask for use with injection technique.*

### 2.5. Assay of Water-*t* With a Proportional Counter

A definite quantity of water-*t*, less than 0.5 ml containing at least 10 $\mu$c of tritium, is placed in a 5-ml volumetric flask. The water-*t* is frozen, and the flask is partially filled with a solution prepared from 175 g of sulfuric acid and 25 g of phosphoric anhydride. The mixture is warmed to room temperature; the volume is adjusted to 5 ml with the sulfuric acid solvent, and the solution is mixed. Then approximately 1 ml of the solution is transferred to a stainless-steel cell and counted in a a $2\pi$, windowless, gas-flow, proportional counter. With the cell and equipment used for assay of carbon-14 [23], the counting rate was found to be 5.75 cps per $\mu$c of tritium per ml of solution. This corresponds to a counting efficiency of only about 0.0155 percent. The low efficiency limits the method to assay of relatively high-activity materials.

The phosphoric anhydride-sulfuric acid solvent can be used for assay of a variety of tritium compounds. To avoid absorption of moisture, the solution must be transferred to the counting cell quickly, and the counting gas must be dried with phosphoric anhydride.

### 2.6. Assay of Water-*t* as Hydrogen-*t* in an Ionization Chamber

Methods used for gas counting of tritium prior to 1958 are reviewed in [19]. In the present study, satisfactory results have been obtained with the apparatus of figure 5 and the procedure described below. This consists of diluting water-*t* with aqueous acid, and generating hydrogen-*t* by allowing the acid to react with metallic magnesium.

A definite volume, or weight, of water-*t*, containing about 3 $\mu$c of tritium, is diluted to 10 ml with 5-percent aqueous sulfuric acid and the solution is placed in flask *A* of figure 5. About 1 g of magnesium turnings is placed in flask *B*. Then the ionization chamber *E* and auxiliary apparatus are evacuated through stopcock 2 to a pressure of less than 0.1 mm of mercury. After the vacuum line has been closed, the tritiated aqueous acid is slowly added to *B*, until sufficient hydrogen-*t* has been generated to bring the system to atmospheric pressure. The pressure and temperature are read, and stopcock 3 is closed. Then the ionization chamber is connected to a vibrating-reed electrometer and the drift rate is measured in the customary manner. The radioactivity of the sample is evaluated by comparison of the drift rate with that in a control experiment run with a water sample of known tritium content (e.g., NBS Standard Sample 4926). The results are adjusted to correct for variation of temperature and pressure from standard conditions.

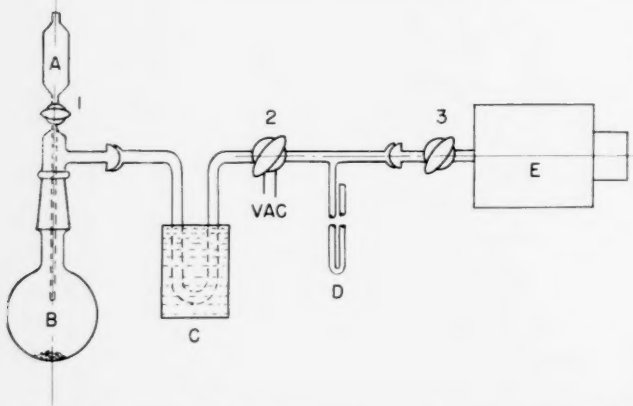


FIGURE 5. *Apparatus for preparation and assay of hydrogen-t.*

*A* Dropping funnel containing sample of water-*t* in 5-percent aqueous hydrochloric acid.
*B* Flask containing 0.1 g of magnesium turnings.
*C* Water trap cooled by dry-ice—ethyl alcohol bath.
*D* Manometer.
*E* Ionization chamber.

### 2.7. Apparatus for Dissolving, Filtering, and Freeze-drying Materials in a Closed System [7]

The apparatus of figure 6 can be used for a variety of operations. Flasks *A* and *B* are connected by a tube having a sealed-in, fritted-glass filter, *C*, and are joined to flask *E* through a 24/40 $ joint and a large-bore stopcock, *D*. In most applications, the material to be purified is placed in *A*, and the solvent in *E*. Flask *E* is cooled in liquid nitrogen and the system is evacuated through stopcock 1. After stopcock 1 is closed, sufficient solvent is distilled from *E* into *A* to dissolve the material. Stopcock *D* is closed, and the unit *A*–*B* is turned so that *A* is above *B*. Then *B* is cooled, and the solution passes from *A* through the filter to *B*. The residue on the filter is washed by placing a cork ring and a small quantity of powdered dry ice on the top of *A*; solvent condenses in *A* and ultimately drains back into *B*. After extraction of the material on the filter by this means, the solvent in *B* is transferred to *E* by distilling or freeze-drying. (For details, see the next section.) Such volatile solvents as ether, dioxane, liquid ammonia, liquid sulfur dioxide, and water may be used. Nonvolatile reagents may be placed in either *A* or *B*, and solvents and reagents may be distilled into either *A* or *B* from *E* or from sources attached at stopcock 2. Solutions may be stirred with a magnetic stirring bar, placed in either *A* or *B* before evacuation. The device may be attached to the general-purpose manifold at 2, and volatile substances may be introduced or removed at will.

### 2.8. Preparation of Lithium Borohydride-*t*

As shown by Brown, Kaplan, and Wilzbach [28], when lithium borohydride is heated with tritium gas at about 200° C, tritium-hydrogen exchange takes place and tritium-labeled lithium borohydride is formed. For efficient reaction, the lithium borohydride must be in a finely divided condition. Commercial lithium borohydride can be converted to a suitable powder with the apparatus of figure 6. To obtain dry ether about 0.2 g of lithium aluminum hydride and 100 ml of reagent-grade ether are placed in flask *E* of figure 6. When the evolution of hydro-

[7] An excellent review by R. S. Tipson [27] describes a variety of schemes for effecting crystallization and filtration in closed systems. Some of these are similar to, but not the same as, that described here.

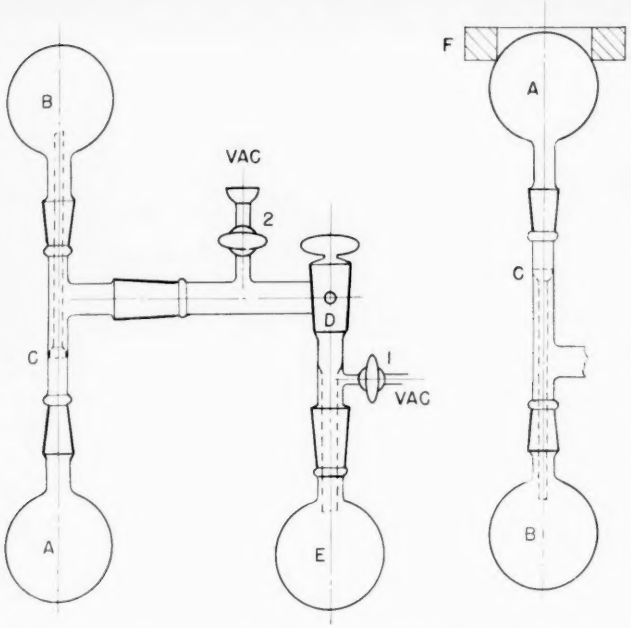


FIGURE 6. *Apparatus for preparing solutions of materials in a closed system.*

*A* and *B* $\overline{8}$ Flasks.
*C* Filter constructed from funnel and a 20-mm, sintered-glass filter disk.
*D* 10-mm Right-angle stopcock.
*E* 200-ml $\overline{8}$ Flask.
*F* Cork ring to hold dry ice in place.
1 and 2 Precision-grade stopcocks.

gen has subsided, 2 g of commercial lithium borohydride is transferred to *A* (in a dry box filled with nitrogen). Then the apparatus of figure 6 is assembled and is connected to a vacuum pump through stopcock 1 and a trap cooled by liquid nitrogen. The ether in *E* is frozen with liquid nitrogen, and the system is evacuated. The vacuum line is closed off, and the liquid-nitrogen bath is moved from *E* to *A*. The ether from *E* distills into *A*. When most of the ether has been transferred, stopcock *D* is closed and *A* is brought to room temperature. The lithium borohydride dissolves; the resulting solution is filtered to remove insoluble matter by turning the unit, carrying *A* and *B*, through 180° about the horizontal axis and then cooling *B*. This causes the liquid to drain from *A* into *B*. When the solution has collected in *B*, a cork ring and a few grams of dry ice are placed on *A*. Then ether distills from *B* into *A* and collects above the fritted-glass filter. When solvent sufficient for washing the residue on the filter has condensed, the cork ring and dry ice are removed and flask *B* is cooled. The solvent drains into *B*, washing the residue on the filter. Finally, the solvent is removed from *B* by opening stopcock *D*, cooling *E* with liquid nitrogen, and warming *B*. Care must be used to avoid bumping. When all of the solvent has been transferred to *E*, the last trace of solvent is removed through the vacuum line by heating *B* (in a silicone oil bath) to 200° C. Finally, stopcock *D* is closed and dry nitrogen is introduced through stopcock 2. The resulting product is a friable powder suitable for "labeling."

To make tritium-labeled lithium borohydride by tritium exchange [28], flask *B*, containing finely divided lithium borohydride, is connected to a source of tritium as shown in figure 7. The apparatus is attached to the general-purpose manifold (fig. 1 at *c*), made vacuum tight, and evacuated. Stopcock 1 and the stopcock to the manifold are closed, the break-seal to the tritium is broken, and flask *B* containing the lithium borohydride is heated in a silicone oil bath at 200° C. After 96 hr, the flask is opened to the manifold, and the hydrogen-tritium mixture in *B* is transferred by the Toepler pump to a receiver attached to the manifold. All traces of tritium are removed by introducing hydrogen from the manifold and re-evacuating. Finally, dry nitrogen is introduced into flask *B* from a source connected to the manifold. Then flask *B* is removed, stoppered, and kept in a dry box until the labeled lithium borohydride is to be used. The specific activity of the product depends on the relative proportions of tritium and lithium borohydride used. A preparation derived from 2 g of lithium borohydride and 4 curies of tritium gave a product having an activity of 2.94 curies. Thus, 73 percent of the tritium used was fixed in the hydride.

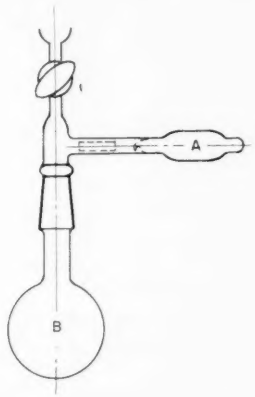


FIGURE 7. *Apparatus for treating solids with tritium gas.*

## 2.9. Preparation and Use of Solutions of Lithium Borohydride-*t*

Under nitrogen in a dry box, the desired amount of lithium borohydride-*t* (from flask *B*, described in the preceding section) is placed in flask *A* of figure 4. The flask is closed (in the dry box) with the adapter, *B*. The side arm of *A* is closed with a rubber stopper, *D*, suitable for perforation with a hypodermic needle. The flask and adapter are weighed before and after introduction of the lithium borohydride. The flask is then connected, as shown in figure 4, to flask *C*, containing tetrahydrofuran and sufficient lithium aluminum hydride to remove all moisture and other reactive contaminants. About 20 ml of tetrahydrofuran is used for each 100 mg of lithium borohydride in flask *A*. The tetrahydrofuran in *C* is frozen in liquid nitrogen, and the system

(including *A*) is evacuated. Then the tetrahydrofuran from *C* is distilled into *A*, by warming *C* and cooling *A*. After the solvent has been transferred to *A*, stopcock 2 is closed and *A* (including adapter *B*) is disconnected from *C*.

Reductions can be performed directly in flask *A*. A solution of the material to be reduced is added through the stopper *D* by means of a hypodermic syringe fitted with a stainless-steel needle. When reduction is complete, the reaction flask is connected to the manifold of figure 1 and any hydrogen-*t* present is transferred by the Toepler pump to a reservoir attached to the manifold. The nonvolatile product is isolated in a manner appropriate to the particular substance (see sec. 2.11). In the event that several reductions are to be performed, portions of the lithium borohydride solution in *A* are withdrawn with a graduated syringe and injected into several evacuated reaction flasks (like that shown by *A* of fig. 4) containing the material to be reduced.

### 2.10. Analysis of a Solution of Lithium Borohydride-*t*

For analysis, a known volume of the solution of lithium borohydride-*t* in tetrahydrofuran is injected into 5-percent aqueous hydrochloric acid contained in the gas buret of figure 8. The injection is made through a rubber cap, *D*, near the bottom of the buret. A small amount of mercury is placed in *D*, to prevent leakage. The hydrogen-*t* is collected in the gas buret, and the radioactivity is measured by transferring the gas from the gas buret to an evacuated ionization chamber, with the arrangements shown in figure 8. After introduction of the sample, the buret is flushed with hydrogen generated by injection of a solution of nonradioactive sodium borohydride at *D*. Finally, the ionization chamber, *C*, is filled to atmospheric pressure with hydrogen, and the radioactivity is measured with an electrometer in the conventional manner.

The specific activity of lithium borohydride-*t* can be estimated from the specific activity of a product made from it, as, for example, D-galactitol-*1-t* described in the next section. This method of analysis, although useful, is subject to error from isotope effects.

### 2.11. Preparation of D-Galactitol-*1-t*

A magnetic stirring bar, two millimoles of D-galactose, and one millimole of sodium carbonate are placed in a 50-ml flask of the type shown in figure 4. The flask is connected to the general-purpose manifold (fig. 1) and evacuated. Then the connection to the manifold is closed; the flask is cooled by an ice bath, placed on the driving mechanism of the stirrer. The stirrer is started, and 2 ml of ice water is added by injection with a hypodermic needle, through the rubber stopper of the flask. This is followed by addition, in the same manner, of 2 ml of a solution containing 12 mg of lithium borohydride-*t* (1.47 mc/mg) in dry tetrahydrofuran. Stirring is continued for about 1 hr at ice temperature, and then the solution is allowed to warm to

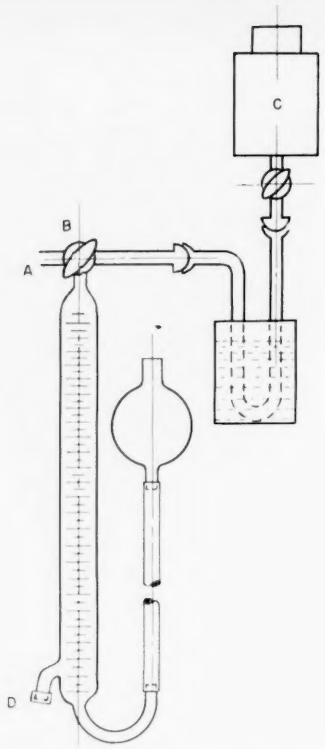


FIGURE 8. *Apparatus for assay of metal hydrides.*

room temperature. After 18 hr, 1 ml of 5-percent aqueous acetic acid is added to decompose any unreacted lithium borohydride; the solution is frozen in a liquid-nitrogen bath, and any hydrogen-*t* present is collected in the manifold. Finally, the connection to the manifold is closed and the flask is removed from the manifold. The solvent is removed by the freeze-drying technique, and, ultimately, transferred to a closed container used for disposal of radioactive waste. The residue containing the product is dissolved in 10 ml of water, and the solution is evaporated to dryness in a rotary still. The residue is dissolved in water and the solution is passed through a column containing 10 ml of a cation-exchange resin.[8] The effluent is evaporated to dryness on a vacuum rotary still; the residue is dissolved in 15 ml of methanol and the solvent is evaporated. Dissolution in methanol and evaporation are repeated 4 times to remove all of the boric acid as methyl borate. The residue consists of D-galactitol-*1-t* and a small quantity of unreacted D-galactose. It is recrystallized from 15 ml of hot ethanol. In a preparation conducted as described, the crude product contained 16 mc of tritium, and the yield of recrystallized D-galactitol-*1-t* was about 90 percent of the theroretical. The D-galactitol-*1-t* was assayed for radioactivity by the method of Isbell, Frush and Peterson [17]. A 0.00025-mg sample in a sodium *O*-(carboxymethyl) cellulose film weighing 19.8 mg gave 126 counts per second. This corresponds to an activity of 44 $\mu$c/mg.

[8] Amberlite IR-120-H, Rohm and Haas Co., Philadelphia, Pa.

## 3. References


[1] H. S. Isbell, J. V. Karabinos, H. L. Frush, N. B. Holt, A. Schwebel, and T. T. Galkowski, J. Research NBS **48,** 163 (1952), RP2301.

[2] H. S. Isbell and J. V. Karabinos, J. Research NBS **48,** 438 (1952), RP2334.

[3] H. L. Frush and H. S. Isbell, J. Research NBS **50,** 133 (1953), RP2400.

[4] H. L. Frush and H. S. Isbell, J. Research NBS **51,** 167 (1953), RP2446.

[5] H. L. Frush and H. S. Isbell, J. Research NBS **51,** 307 (1953), RP2458.

[6] H. S. Isbell, H. L. Frush, and N. B. Holt, J. Research NBS **53,** 217 (1954), RP2536.

[7] H. S. Isbell, H. L. Frush, and N. B. Holt, J. Research NBS **53,** 325 (1954), RP2550.

[8] H. S. Isbell, H. L. Frush, and R. Schaffer, J. Research NBS **54,** 201 (1955), RP2581.

[9] R. Schaffer and H. S. Isbell, J. Research NBS **56,** 191 (1956), RP2667.

[10] H. S. Isbell, N. B. Holt, and H. L. Frush, J. Research NBS **57,** 95 (1956), RP2697.

[11] H. S. Isbell and R. Schaffer, J. Am. Chem. Soc. **78,** 1887 (1956).

[12] J. D. Moyer and H. S. Isbell, Anal. Chem. **29,** 393 (1957).

[13] R. Schaffer and H. S. Isbell, J. Research NBS **57,** 333 (1956), RP2722.

[14] R. Schaffer and H. S. Isbell, J. Am. Chem. Soc. **79,** 3867 (1957).

[15] H. L. Frush and H. S. Isbell, J. Research NBS **59,** 289 (1957), RP2800.

[16] J. D. Moyer and H. S. Isbell, J. Research NBS **61,** 71 (1958), RP2886.

[17] H. S. Isbell, H. L. Frush, and R. A. Peterson, J. Research NBS **63A,** 171 (1959).

[18] J. R. Arnold, Symposium, Tritium tracer applications p. 12 (New England Nuclear Corp., Atomic Associates, Inc., Packard Instrument Co., Inc., New York, N.Y., 1957); see also Nucleonics **16,** No. 3, 62 (1958).

[19] See C. V. Robinson, Ref. 18, p. 17.

[20] J. Rydberg, Acta Chem. Scand. **12,** 399 (1958).

[21] B. M. Tolbert, Ionization chamber assay of radioactive gases, A.E.C. Report U.S.R.L.–3499 (Univ. of Calif., Berkeley, Calif., 1956).

[22] L. M. Brown, A. S. Friedman, and C. W. Beckett, Bibliography of research on deuterium and tritium compounds, NBS Circ. 562 (1956) (and annual supplements), U.S. Government Printing Office, Washington 25, D.C.

[23] A. Schwebel, H. S. Isbell, and J. D. Moyer, J. Research NBS **53,** 221 (1954), RP2537.

[24] R. F. Glascock, Isotopic gas analysis for biochemists (Academic Press Inc., New York, N.Y., 1954).

[25] R. T. Sanderson, Vacuum manipulation of volatile compounds (John Wiley & Sons, Inc., New York, N.Y., 1948).

[26] D. L. Buchanan and A. Nakao, J. Am. Chem. Soc. **74,** 2389 (1952).

[27] R. S. Tipson, Crystallization and recrystallization, in Technique of organic chemistry, vol. III, p. 395, 2d ed., A. Weissberger, ed. (Interscience Publishers, Inc., New York, N.Y., 1956).

[28] W. G. Brown, L. Kaplan, and K. E. Wilzbach, J. Am. Chem. Soc. **74,** 1343 (1952).



WASHINGTON, D.C. (Paper 63A3–12)

Journal of Research of the National Bureau of Standards—A. Physics and Chemistry
Vol. 63A, No. 2, September–October 1959

# Preparation of Trichloride and Tetrachloride of Molybdenum

Dwight E. Couch and Abner Brenner

(June 18, 1959)

Molybdenum trichloride was successfully prepared in quantity by the reduction of molybdenum pentachloride with hydrogen. The most satisfactory yields were obtained with a 4 to 5 mole excess of hydrogen at pressures of 100 psi or higher and at a temperature of 125°C.

Molybdenum tetrachloride was prepared by direct reaction of molybdenum trichloride with molybdenum pentachloride in a sealed tube or steel bomb maintained at 250° C. X-ray patterns of the various chlorides were obtained.

## 1. Introduction

Blomstrand [1] [1] prepared low-valence molybdenum halides by passing hydrogen over the pentachloride in a hot tube. The process has been modified many times. Liechti and Kempe [2] used a similar procedure and claimed to have prepared molybdenum tetrachloride by condensing the vapors resulting from the thermal decomposition of the trichloride. Michael and Murphy [3] prepared molybdenum tetrachloride and pentachloride by reacting the di- and trioxide with carbon tetrachloride at 250° C. Linder, Haller, and Helwig [4] prepared molybdenum dichloride by the reaction of molybdenum with phosgene at about 600° C. However, Biltz and Fendius [5] claimed that the tetrachloride had never been prepared. They prepared the dichloride by disproportionation of the trichloride. Wardlaw and Webb [6] studied molybdenum pentachloride in organic solvents and found that it reacted with dry pryidine to form pyridine-molybdenum tetrachloride, but they were not able to remove the pyridine from this salt completely. Forland [7] obtained a patent for the preparation of molybdenum chlorides by the direct chlorination of molybdenum disulfide.

Hellriegel [8] prepared molybdenum di- and trichloride from molybdenum and molybdenum pentachloride. Senderoff and Brenner [9] tried several reported methods in an effort to prepare the lower molybdenum chlorides. They found that the direct reduction of pentachloride by hydrogen [1] was very slow and gave only a small yield of molybdenum trichloride, and also reported the reaction between molybdenum and phosgene to be unsatisfactory. They prepared the trichloride by a procedure similar to that of Hellriegel [8] and also prepared the dichloride from the trichloride. Senderoff and Labrie [10] attempted to prepare molybdenum trichloride by reduction of the pentachloride with hydrogen, aluminum, and sodium, but failed to develop a suitable procedure. They prepared molybdenum tetrachloride containing organic material by heating molybdenum pentachloride with cetane or paraffin and obtained the trichloride by heating this product.

Since the tetrachloride and trichloride were required in moderate quantities for electrolytic studies, attention was directed toward the development of more convenient methods of making these compounds. As molybdenum pentachloride is now commercially available, it was used as the starting material. The trichloride was readily prepared by hydrogenation of the pentachloride under pressure at about 125° C. The reaction was unusual in that it proceeded to completion only with solid pentachloride. The tetrachloride was prepared by heating the trichloride and the pentachloride together in a sealed tube.

## 2. Preparation of Molybdenum Trichloride

Ordinary high pressure equipment was used for all hydrogen reductions discussed in this paper. It consisted of a stainless steel bomb equipped with glass liner. The bomb head was equipped with a pressure gauge and a three-way valve for evacuating the bomb and for subsequently adding the hydrogen. The bomb was heated with an external resistance furnace. All chemicals were handled in an inert atmosphere to prevent contamination of the molybdenum compounds with moisture and oxygen. After assembly, the bomb was evacuated, flushed once with hydrogen, refilled with hydrogen, and heated.

The determination of the yield of molybdenum trichloride was accomplished by mixing the reaction product with 1:1 hydrochloric acid-water solution in which the trichloride is insoluble, then filtering and drying the residue in a vacuum desiccator. This procedure gave the yield to within 2 percent, an accuracy sufficient for this work.

[1] Figures in brackets indicate the literature references at the end of this paper.

A few preliminary reductions of the pentachloride were made with an excess of hydrogen at a temperature of 200° C and a pressure of 5 to 10 atm (see table 1). An inspection of the reaction product indicated that only the upper surface of the pentachloride had reacted and a solid crust of molybdenum trichloride was formed on top of the liquid pentachloride. The reaction was slow because of the low rate of diffusion of hydrogen through this crust of molybdenum trichloride. Experiments 1 and 2, table 1, show that the procedures reported in the literature are not satisfactory for preparing molybdenum trichloride.

TABLE 1. *Preparation of molybdenum trichloride by reduction with hydrogen*

| Exp. | Temp | Time | $H_2$ pressure | Wt $MoCl_5$ used | Wt loss | Mole ratio $H_2$:$MoCl_5$ | $MoCl_3$ in product |
|---|---|---|---|---|---|---|---|
| | °C | hr | psi | g | g | | % |
| 1 | 125 to 160 | 4 | 14.7 | 50 | | | None |
| 2 | 250 to 275 | 12 | 14.7 | 200 | | | 5 |
| 3 | 200 | 65 | 1375 | 100 | | 25:1 | 79 |
| 4 | 145 | 1 | 90 | 211 | 13.5 | 0.4:1 | 4 |
| 5 | 135 | 0.5 | 1100 | 50 | 9.6 | 36:1 | 80 |
| 6 | 125 | 0.5 | 100 | 50 | 10.7 | 4:1 | 80 |
| 7 | 125 | 16 | 55 | 100 | 12 | 0.5:1 | 8 |
| 8 | 125 | 16 | 150 | 50 | 12 | 5:1 | 98 |
| 9 | 125 | 18 | 450 | 50 | 12 | 16:1 | 98 |
| 10 | 125 | 12 | 450 | 50 | 11 | 18:1 | 97 |
| 11 | 85 | 16 | 1600 | 50 | 0.5 | 58:1 | None |
| 12 | 25 | 16 | 1750 | 100 | None | 31:1 | None |

The reduction of pentachloride to trichloride was 98 percent complete after 16 hr at 125° C with a 5 to 1 mole ratio of hydrogen to pentachloride. The temperatures and pressures were not critical as long as there was an appreciable excess of hydrogen and the temperature was between 120° C and the melting point of molybdenum pentachloride, 190° C. Results of successive treatments with fresh hydrogen indicated that once the molybdenum trichloride had formed it was stable at the conditions used, 125° C, and was not reduced to the dichloride.

The last traces of molybdenum pentachloride and hydrogen chloride were removed from the trichloride by heating it in an inert atmosphere or in a vacuum after the reduction. Generally, this was accomplished by heating to 250° C under vacuum for about 15 min. Chemical analysis of a typical preparation gave 46 percent of molybdenum and 52 percent of chlorine. (Theoretical: 47.5 percent of molybdenum and 52.5 percent of chlorine.) The trichloride prepared in this way was practically insoluble in aqueous hydrochloric acid. However, if it was allowed to stand in contact with water for several hours, some oxidation took place as shown by the formation of a blue molybdenum solution. It also formed oxychlorides if allowed to remain in contact with moist air for several weeks. The trichloride was insoluble in dimethyl formamide, acetone, pyridine, acetic anhydride, ethyl alcohol, ethyl ether, and dimethyl cyanamide, but was soluble in ethyl pyridinium bromide at 110° C.

The molybdenum trichloride prepared by hydrogenation involved a solid phase reaction, and nonvolatile impurities remained in the product. It was desirable to purify molybdenum trichloride by sublimation to compare the properties of the solid-phase reaction product with that deposited from the gaseous phase. However, molybdenum trichloride decomposes on heating according to the reaction:

$$12\ MoCl_3 \xrightarrow{\text{heat}} Mo_6Cl_{12}(s) + 6\ MoCl_4(g)$$

and on cooling,

$$2\ MoCl_4(g) \xrightarrow{\text{cool}} MoCl_3(s) + MoCl_5(s)\text{[11]}$$

Three sections of glass tubing connected by 24/40 standard taper joints were used for preparing the molybdenum trichloride. One end, fitted with an inert gas inlet tube, was charged with molybdenum trichloride. The tube was then heated to about 500° C while a slow stream of dry helium passed through it. The molybdenum trichloride decomposed to yield a bright yellow residue of dichloride and a brown vapor. When allowed to cool, this vapor disproportionated to form a dark solid which was composed of trichloride and pentachloride. After the molybdenum trichloride was decomposed, the center section of the tube was heated to 300° C and the molybdenum pentachloride distilled into the third section. The apparatus was then placed in an inert atmosphere chamber and disassembled. In this way it was possible to isolate all three of the reaction products, molybdenum di-, tri-, and pentachlorides.

Excessive heating of the molybdenum dichloride did not contaminate the trichloride in the experiment since the dichloride also decomposes to the tetrachloride when heated above 700° C. In fact, both molybdenum trichloride and pentachloride can be prepared by heating the dichloride according to the following equations [11]:

$$2\ MoCl_2(s) \xrightarrow{700°} Mo(s) + MoCl_4(g)$$

$$2\ MoCl_4(g) \xrightarrow{\text{cool}} MoCl_3(s) + MoCl_5(s).$$

## 3. Preparation of Molybdenum Tetrachloride

The preparation of tetrachloride by the disproportionation of trichloride, as reported by Liechti and Kempe [2], was attempted. Chemical analysis of the sublimate from this reaction indicated that the product was not molybdenum tetrachloride; approximately one-half of it was insoluble in water and was found to be molybdenum trichloride. Thus, the material they prepared was apparently an equimolar mixture of trichloride and pentachloride.

Molybdenum tetrachloride prepared by the authors according to the procedure described by Senderoff and Labrie [10] was assayed for molybdenum trichloride. The product prepared with cetane at 165° C contained 40 percent of material insoluble in 1:1 HCl, assumed to be trichloride; that prepared with paraffin at 145° C contained only 6 percent of insoluble material. Both of these preparations contained organic contaminants. The tetrachloride prepared according to the procedure described by Michael and Murphy [3] contained no detectable trichloride, was completely soluble in 1:1 hydrochloric acid, and was slightly soluble in carbon tetrachloride.

An attempt was made to prepare tetrachloride by the controlled reduction of the pentachloride with hydrogen. With smaller amounts of hydrogen than are theoretically necessary to produce molybdenum tetrachloride (experiment 4, table 1), the product contained 4 percent trichloride, 36 percent of tetrachloride, and 60 percent of pentachloride. A second reduction (experiment 7, table 1) using the stoichiometric amounts of hydrogen needed to produce tetrachloride gave a mixture of halides containing 8 percent of trichloride, 74 percent of tetrachloride, and 18 percent of pentachloride. It was evident from these reactions that the molybdenum tetrachloride prepared in this way would always be contaminated with both trichloride and pentachloride.

Molybdenum tetrachloride was successfully prepared by direct reaction of pentachloride and trichloride in a sealed tube. This reaction was carried out by sealing about 5 g of the finely ground and mixed halides in a 14-mm ID gage-glass tube filled with helium or argon. All operations were performed in an inert atmosphere. The completeness of the reaction was determined by an assay for molybdenum trichloride based on its insolubility in 1:1 hydrochloric acid. Molybdenum tetrachloride and pentachloride are soluble. Table 2 shows the results of several different preparations. Experiments number 3 and 4, table 2, indicate that the reaction was more nearly complete at 250° C than at 400° C.

TABLE 2. *Preparation of molybdenum tetrachloride by direc reaction of the trichloride with pentachloride*

| Exp. | Mole ratio $MoCl_5/MoCl_3$ | Temp | Time | $MoCl_3$ in product |
|---|---|---|---|---|
| | | ° C | hr | % |
| 1 | pure $MoCl_3$ | 250 | 150 | 99 |
| 2 | 2.5:1 | 250 | 70 | trace |
| 3 | 2:1 | 400 | 20 | 9 |
| 4 | 2:1 | 250 | 20 | 3 |
| 5 | 1.5:1 | 150 | 150 | 14 |
| 6 | 1.5:1 | 250 | 150 | 2 |
| 7 | 1.2:1 | 250 | 70 | 5 |
| 8[a] | 1.2:1 | 250 | 150 | 3 |
| 9 | 1.2:1 | 250 | 500 | 4 |
| 10 | 1:1 | 250 | 40 | 10 |
| 11 | 1:1 | 250 | 70 | 7 |
| 12 | 1:1 | 250 | 150 | 4 |

[a] 100-g batch in a steel bomb.

The high yield of molybdenum tetrachloride is not entirely in agreement with the calculated data presented by Quill [11], according to which the tetrachloride is not stable when cooled from temperatures above 125° C. It is probable that the pressure in the tube and the excess of pentachloride shift the equilibrium in a favorable direction.

Since an excess of molybdenum pentachloride was required to convert all the trichloride to tetrachloride in a reasonable time, it was necessary to find a method of separating the pentachloride from the tetrachloride. A large number of anhydrous organic solvents were tested, but none was satisfactory. In fact, no solvent was found which would dissolve either halide in appreciable quantities without reacting with it.[2]

The products from the reaction of molybdenum pentachloride with molybdenum trichloride were subjected to vacuum sublimation at 120°C. The results showed that the pentachloride could be distilled out without causing any thermal decomposition of the tetrachloride. If any disproportionation was taking place during these sublimations, it would have been evident from the formation of the trichloride. However, an assay of both the sublimate, which was the pentachloride, and the residue, which was the tetrachloride, showed only traces of trichloriode. A chemical analysis of the residue from the sublimation showed that it contained 38 percent of molybdenum and 59 percent of chlorine. (Theoretical: 40.3 percent of molybdenum and 59.7 percent of chlorine.)

## 4. X-Ray Studies

Table 3 shows the *d* spacings and relative intensities of the molybdenum penta-, tetra-, tri-, and dichlorides. These data have not been reported previously. The molybdenum tetrachloride prepared by reacting the trichloride with the pentachloride and that prepared in accordance with Michael and Murphy [3] and Senderoff and Labrie [10] had similar patterns. Diagrams of the molybdenum trichloride prepared by hydrogen reduction and by thermal decomposition were identical. Furthermore, after the trichloride was washed with dilute hydrochloric acid and then dried in a vacuum desiccator, it still gave the same pattern showing that it was not affected by short-time treatments with dilute hydrchloric acid, but if allowed to stand in contact with moist air the pattern of trichloride was changed. The X-ray pattern of molybdenum dichloride which had been washed with dilute nitric acid or allowed to stand for a long period of time and dried, differed from that of the pure dichloride. This was rather surprising since the compound apparently did not take up moisture and showed no visible signs of reacting with the nitric acid.

[2] Roger J. Labrie of the NBS has recently found that titanium tetrachloride will dissolve molybdenum pentachloride but not molybdenum tetrachloride.

TABLE 3. *X-ray diffraction data on various molybdenum halides showing* d *spacing and relative intensities, taken with copper radiation, wavelength 1.5405 A (by Howard E. Swanson)*

| $MoCl_2$ | | $MoCl_3$ | | $MoCl_4$[a] | | $MoCl_5$ | | $MoCl_5$ (Continued) | |
|---|---|---|---|---|---|---|---|---|---|
| *d* | *I* | *d* | *I* | *d* | *I* | *d* | *I* | *d* | *I* |
| *A* | | *A* | | *A* | | *A* | | *A* | |
| 7.02 | 100 | 5.99 | 100 | 6.85 | 8 | 8.68 | 5 | 2.533 | 5 |
| 6.39 | 12 | 5.17 | 8 | 6.52 | 6 | 6.87 | 5 | 2.481 | 10 |
| 5.64 | 26 | 4.94 | 7 | 5.85 | 100 | 5.76 | 55 | 2.406 | 5 |
| 3.46 | 8 | 4.78 | 9 | 5.36 | 8 | 5.68 | 100 | 2.354 | 5 |
| 2.90 | 4 | 3.60 | 5 | 5.26 | 8 | 5.30 | 40 | 2.347 | 15 |
| 2.84 | 6 | 3.05 | 2 | 5.16 | 5 | 5.24 | 55 | 2.297 | 5 |
| 2.78 | 5 | 2.86 | 4 | 4.79 | 18 | 5.12 | 30 | 2.273 | 5 |
| 2.77 | 5 | 2.689 | 10 | 4.42 | 6 | 5.07 | 55 | 2.226 | 15 |
| 2.61 | 12 | 2.599 | 14 | 4.14 | 6 | 4.83 | 5 | 2.195 | 10 |
| 2.55 | 6 | 2.438 | 5 | 3.14 | 3 | 4.67 | 10 | 2.137 | 5 |
| 2.52 | 8 | 2.167 | 2 | 3.11 | 6 | 4.54 | 10 | 2.092 | 10 |
| 2.37 | 9 | 2.104 | 5 | 3.04 | 3 | 4.33 | 20 | 2.080 | 5 |
| 2.34 | 9 | 2.078 | 7 | 2.925 | 5 | 4.29 | 15 | 2.054 | 10 |
| | | 1.998 | 4 | 2.696 | 80 | 4.24 | 20 | 1.975 | 30 |
| 2.33 | 5 | 1.909 | 5 | 2.647 | 9 | 4.20 | 30 | 1.969 | 10 |
| 2.31 | 8 | 1.889 | 3 | 2.564 | 3 | 4.17 | 10 | 1.866 | 10 |
| | | 1.726 | 13 | 2.444 | 2 | 4.05 | 10 | 1.857 | 5 |
| 2.20 | 13 | 1.661 | 4 | 2.106 | 54 | 3.94 | 5 | 1.768 | 5 |
| 2.09 | 10 | 1.631 | 5 | 1.962 | 5 | 3.74 | 5 | 1.758 | 10 |
| 2.08 | 8 | 1.498 | 4 | 1.944 | 4 | 3.68 | 25 | 1.743 | 30 |
| 2.045 | 14 | 1.395 | 2 | 1.752 | 22 | 3.59 | <5 | 1.688 | 5 |
| 2.014 | 9 | 1.289 | 2 | 1.678 | 10 | 3.48 | 20 | 1.668 | 10 |
| 1.997 | 9 | 1.198 | 1 | 1.642 | 18 | 3.36 | 15 | 1.642 | 5 |
| 1.991 | 10 | ..... | ..... | 1.636 | 2 | 3.22 | 10 | ..... | ..... |
| 1.946 | 10 | ..... | ..... | 1.468 | 8 | 3.11 | 5 | ..... | ..... |
| 1.930 | 9 | ..... | ..... | 1.456 | 7 | 3.07 | 10 | ..... | ..... |
| 1.911 | 9 | ..... | ..... | 1.346 | 4 | 2.968 | 5 | ..... | ..... |
| 1.903 | 8 | ..... | ..... | 1.196 | 3 | 2.895 | 20 | ..... | ..... |
| 1.779 | 10 | ..... | ..... | 1.128 | 4 | 2.877 | 20 | ..... | ..... |
| 1.757 | 7 | ..... | ..... | 1.120 | 3 | 2.810 | 5 | ..... | ..... |
| 1.753 | 3 | ..... | ..... | ..... | ..... | 2.756 | 35 | ..... | ..... |
| 1.738 | 5 | ..... | ..... | ..... | ..... | 2.730 | 25 | ..... | ..... |
| 1.736 | 4 | ..... | ..... | ..... | ..... | 2.684 | 25 | ..... | ..... |
| 1.678 | 1 | ..... | ..... | ..... | ..... | 2.633 | 60 | ..... | ..... |
| 1.470 | 6 | ..... | ..... | ..... | ..... | 2.592 | 30 | ..... | ..... |

[a] Average of two patterns of $MoCl_4$, one prepared from $MoCl_3$+$MoCl_5$ and the other prepared from $MoO_2$+$CCl_4$.

The authors acknowledge the financial support of the Springfield Armory and the assistance of A. M. Brown, C. H. Schreyer, and W. H. Metzger, Jr., in making some of the preparations.

## 5. References

[1] C. W. Blomstrand, J. prakt. Chem. **71,** 453 (1857) and **77,** 97 (1859).
[2] L. P. Liechti and B. Kempe, Ann. Chem. Liebigs **169,** 350 (1873).
[3] A. Michael and A. Murphy, Jr., J. Am. Chem. Soc. **44,** 365 (1910).
[4] K. Linder, E. Haller and H. Helwig, Z. anorg. u. allgem. Chem. **130,** 209 (1923).
[5] W. Biltz and C. Fendius, Z. anorg. u. allgem. Chem. **172,** 385 (1928).
[6] W. Wardlaw and H. W. Webb, J. Chem. Soc. 2100 (1930).
[7] T. R. Forland, U.S. Patent 1,308,735 (July 1, 1919).
[8] W. Helriegel, German Patent 703,895 (March 19, 1941).
[9] S. Senderoff and A. Brenner, J. Electrochem. Soc. **101,** 28 (1954).
[10] S. Senderoff and R. J. Labrie, J. Electrochem. Soc. **102,** 77 (1955).
[11] L. L. Quill, The chemistry and metallurgy of miscellaneous material, Nuclear Ser. IV, 19B, 298 (McGraw Hill Book Co., New York, N.Y., 1950).

WASHINGTON, D.C. (Paper 63A–13).

Journal of Research of the National Bureau of Standards—A. Physics and Chemistry
Vol. 63A, No. 2, September–October 1959

# Infrared Spectra of Asphalts

Burton D. Beitchman

(March 18, 1959)

A procedure for preparing thin films of airblown asphalts and a spectroscopic study of such films throughout the infrared region of 2.5 to 15 microns are described. The relationship of transmittance of several absorption bands with the durability of the asphalt is discussed. Exposure to ultraviolet radiation produced changes in transmittance at four wavelengths which, in a series of asphalts studied, showed statistically significant correlations with durability.

## 1. Introduction

Roofing asphalts vary greatly in durability depending upon the source of the particular asphalt. One method for measuring durability that is currently being used is based upon the time required for development of cracks over 50 percent of the surface of an asphalt film when such a film is exposed to natural weathering conditions or to radiation from a carbon arc in an accelerated weathering test.[1]

Stewart [2] recently reported an infrared study of components from three asphalts before and after natural weathering. These asphalts varied in durability, and Stewart pointed out chemical properties in the components that might be associated with the durabilities of the asphalts.

An infrared study of the whole asphalt appeared desirable since the general characteristics of asphalts could be readily indicated without resorting to a fractionation procedure. The use of whole asphalt permits easy study of changes effected in the asphalt by exposure to heat, ultraviolet, and other forms of radiation.

Schweyer [3] has reported a study of films of asphalt residua. These films were too thick (0.1 mm) to permit study below 8 $\mu$ and he therefore resorted to solution techniques to obtain absorption data in this region.

The procedure described in this paper offers a simple means for studying whole asphalt.

## 2. Procedures

An infrared study was made of 28 airblown roofing asphalts from widely different sources. The softening points [4] of these asphalts ranged from 205° F to 241° F and the penetrations [5] at 77° F from 11 to 23.

Films of asphalt were prepared by placing a small drop of molten asphalt on a sheet of cellophane film. A second sheet of cellophane was placed over the asphalt, and the two sheets were then quickly placed in a hydraulic press in which the upper platen was maintained at approximately 90° C.[1,6] A pressure of 16,000 psi was applied to the sheets and maintained for about 20 sec. The sheets were removed from the press, and the thickness of the asphalt film and two cellophane sheets was measured with a dial-thickness gage having a foot about ¼ in. in diameter with which thickness could be estimated to the nearest 0.01 mil. By determining the thickness of the two cellophane sheets, the thickness of the asphalt film was obtained by difference. To ensure greater reproducibility of results, areas of nearly uniform thickness were predetermined and indicated by marking the boundaries of these areas on the cellophane film. The asphalt films were obtained in various thicknesses ranging from about 0.5 to 2.5 mils. By allowing the asphalt film and two sheets of cellophane to soak in distilled water for several minutes, one of the cellophane sheets could be removed easily. The asphalt film and the remaining cellophane sheet were soaked again in distilled water for several minutes in order to remove the second cellophane film. The asphalt film was mounted on a film support made of cardboard or plastic which had a rectangular opening, 1.4×3.5 cm. The predetermined area of nearly uniform thickness was placed over the opening. After allowing the asphalt films to dry, infrared spectra were taken.

The films prepared by this method were not perfectly uniform in thickness and thickness ranges have been recorded in this paper rather than average values. This must be considered a limitation where the transmittance ($\tau$)[7] of the unexposed films have been used for quantitative comparisons. The changes produced at four wavelengths by exposure to ultraviolet radiation did not appear to be dependent upon film thickness over the range of thickness employed. Thus, correlations which were made of changes in absorption with durability do not have this limitation imposed upon them.

[1] S. H. Greenfeld, ASTM Bull. **193**, 50 (1953).
[2] J. E. Stewart, J. Research NBS **58**, 265 (1957), RP2759.
[3] H. E. Schweyer, Anal. Chem., **30**, 205 (1958).
[4] ASTM Method D36–26.
[5] ASTM Method D5–52.

[6] S. H. Greenfeld reported the use of a press for making films with a range of 5 to 50 mils thickness, NBS Building Materials and Structures Report 147 (1956).
[7] The symbol $\tau$ has been used for optical transmittance in accordance with the publication ASA Z 10.6 (1948) of the American Society of Mechanical Engineers.

## 3. Results

The infrared spectra of films of asphalts obtained from widely different sources showed a marked similarity in their absorption characteristics. All the asphalts had absorption bands at the same or very nearly the same wavelengths and their spectra differed primarily in the transmittance values of some of these bands.

The structural groupings which appeared to be present in all the asphalts examined are hydroxyl, $—CH_2—$, $C—CH_3$, carbonyl, $—(CH_2)_4—$ and aromatic rings. There were also absorption bands which indicated aromatic substituents or fused rings. Other weak but reproducible bands were noted at 8.66 $\mu$ (1,155 $cm^{-1}$) and 9.71 $\mu$ (1,030 $cm^{-1}$). The structural assignments given to the various bands are listed in table 1. These are for the most part, the same groupings identified by Stewart [2] in fractions of three asphalts.

Figures 1 and 2 show representative spectra of two of the asphalt films. Table 1 gives values of log $1/\tau$, determined by the base-line method, for absorption bands from the spectra of seven asphalts. The less durable asphalts appear to have slightly more hydroxyl absorption than the more durable asphalts. The $C—CH_3$ band intensity at 7.25 $\mu$ (1,380 $cm^{-1}$) seems also to show a relationship to durability. Uncertainties in the average thickness produce corresponding uncertainties in the transmittance. In the case of the hydroxyl band at 2.91 $\mu$ (3,430 $cm^{-1}$), the uncertainties in average thickness do not invalidate the observed general correlation with durability. However, in the case of the band at 7.25 $\mu$ (1,380 $cm^{-1}$), uncertainties in the value of log $1/\tau$ may be sufficient to obscure any correlation with durability.

Duplicate samples of asphalts A and F are included in table 1 to demonstrate the reproducibility of the spectra. The relation of film thickness to absorption intensities appears to follow the Beer-Lambert Law as illustrated in figure 3.

Figures 4 and 5 show spectra of two asphalt films

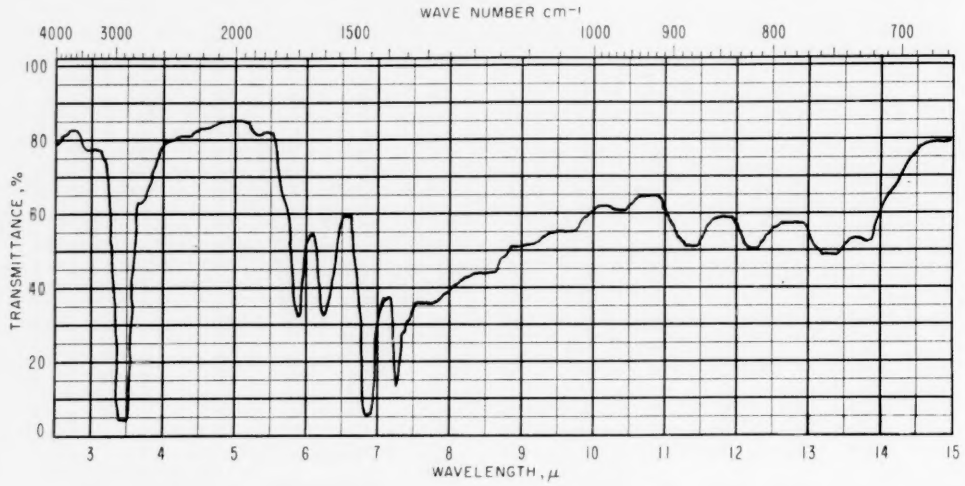


FIGURE 1. *Infrared spectrum of asphalt* D *(1.8 to 2.1 mils thick).*

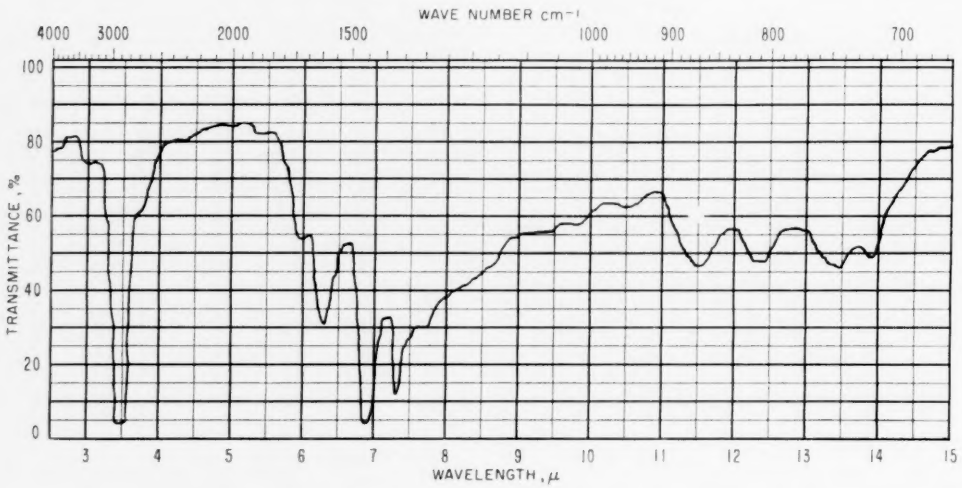


FIGURE 2. *Infrared spectrum of asphalt* B *(1.9 to 2.3 mils thick).*

TABLE 1. *Log 1/τ values obtained from the infrared spectra of asphalt films*

| Asphalt | Softening point [a] | Penetration at 77° F [a] | Durability [b] | Thickness of film | Log 1/τ values (determined by base-line method) | | | | | | | | | | | | |
|---|---|---|---|---|---|---|---|---|---|---|---|---|---|---|---|---|---|
| Frequency, $cm^{-1}$ | | | | | 3,430 | 2,960 | 1,700 | 1,600 | 1,470 | 1,380 | 1,155 | 1,030 | 961 | 866 | 811 | 750 | 720 |
| Wavelength, μ | | | | | 2.91 | 3.38 | 5.88 | 6.25 | 6.80 | 7.25 | 8.66 | 9.71 | 10.41 | 11.55 | 12.33 | 13.33 | 13.89 |
| Assigned structural groups | | | | | —OH | $-CH_2-$ C—$CH_3$ | C=O | Aromatic | $-CH_2-$ C—$CH_3$ | C—$CH_3$ | | C—O, S=O or SiO | Naphthenic | Aromatic substitution | | | $-(CH_2)_4-$ |
| | °F | | *Days* | *Mils* | | | | | | | | | | | | | |
| E | 231 | 18 | 23 | 1.8 to 2.0 | 0.065 | (c) | 0.127 | 0.206 | 0.948 | 0.518 | 0.034 | 0.021 | 0.020 | 0.061 | 0.066 | 0.110 | 0.072 |
| C | 230 | 18 | 45 | 1.7 to 1.9 | .050 | (c) | .059 | .153 | 1.040 | .542 | .034 | .024 | .016 | .039 | .060 | .114 | .079 |
| G | 226 | 13 | 51 | 1.7 to 1.9 | .041 | (c) | .074 | .200 | 1.040 | .478 | .042 | .026 | .019 | .096 | .068 | .116 | .080 |
| D | 216 | 12 | 66 | 1.8 to 2.1 | .019 | (c) | .305 | .240 | 1.102 | .476 | .044 | .030 | .019 | .085 | .062 | .024 | .131 |
| A | 220 | 13 | 73 | 1.6 to 1.8 | .030 | (c) | .071 | .171 | .942 | .415 | .035 | .012 | .017 | .078 | .070 | .117 | .100 |
| A | 220 | 13 | 73 | 1.6 to 1.8 | .032 | (c) | .071 | .166 | .977 | .409 | .028 | .018 | .013 | .072 | .060 | .101 | .089 |
| B | 229 | 14.5 | 73 | 1.5 to 1.9 | .025 | (c) | .074 | .200 | 1.182 | .411 | .026 | .026 | .012 | .100 | .061 | .108 | .115 |
| F | 221 | 19 | 75 | 1.7 to 2.0 | .033 | (c) | .036 | .192 | 1.068 | .458 | .038 | .020 | .020 | .083 | .068 | .114 | .108 |
| F | 221 | 19 | 75 | 1.7 to 2.0 | .031 | (c) | .038 | .208 | 1.064 | .480 | .036 | .014 | .020 | .082 | .076 | .123 | .100 |

[a] Data obtained from asphalt suppliers.
[b] Durability by accelerated weathering. Data obtained by J. Falzone and S. Ishihara, Research Associates for Asphalt Roofing Industry Bureau, NBS.
[c] Intense absorption.

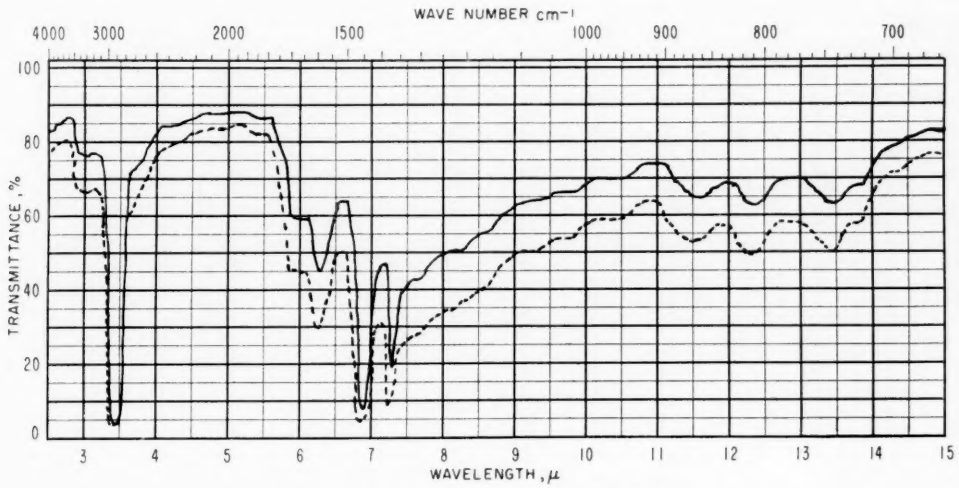


FIGURE 3. *Infrared spectra of asphalt* E.
—— 1.1 to 1.3 mils thick, - - - 1.8 to 2.0 mils thick.

before and after exposure to radiation from a carbon arc for 19.5 hr. These spectra show characteristic changes that were also observed in other asphalts. Table 2 shows some of the changes produced in the values of log $1/\tau$ of four asphalts. Changes in the values of log $1/\tau$ for bands at 3.38 μ (2,960 $cm^{-1}$) and 6.80 μ (1,470 $cm^{-1}$) are not shown in table 2 (the films used for illustrative purposes in this table were too thick to show the changes in these regions). All the asphalts increased in carbonyl and hydroxyl absorption and the less durable asphalts generally showed a greater increase in carbonyl and hydroxyl absorption and absorption at 8.66 μ (1,155 $cm^{-1}$) and 9.71 μ (1,030 $cm^{-1}$) than the more durable asphalts.

Plots of durability values versus changes in log $1/\tau$ at 5.88 μ (1,700 $cm^{-1}$), 2.91 μ (3,430 $cm^{-1}$), 8.66 μ (1,155 $cm^{-1}$), and 9.71 μ (1,030 $cm^{-1}$) appeared to show inverse relationships. Because of the small magnitude of these changes at the latter three wavelengths, statistical correlations based on their rankings were used rather than the actual values, and these were compared with the rankings of durabilities. On the basis of values obtained from spectra of 11 asphalts, Spearman's rank correlation coefficients were calculated for all four correlations of durability with changes in the value of log $1/\tau$ (table 3).

These correlation coefficients are significant at the 1 percent level for 9 degrees of freedom. As for the correlation of durability with changes in transmittance at 5.88 μ, a linear relation could be assumed to exist between durability and the reciprocal of changes in log $1/\tau$. The product-moment correlation coefficient was calculated to be 0.779, which is significant at the 1 percent level for the number of samples involved.

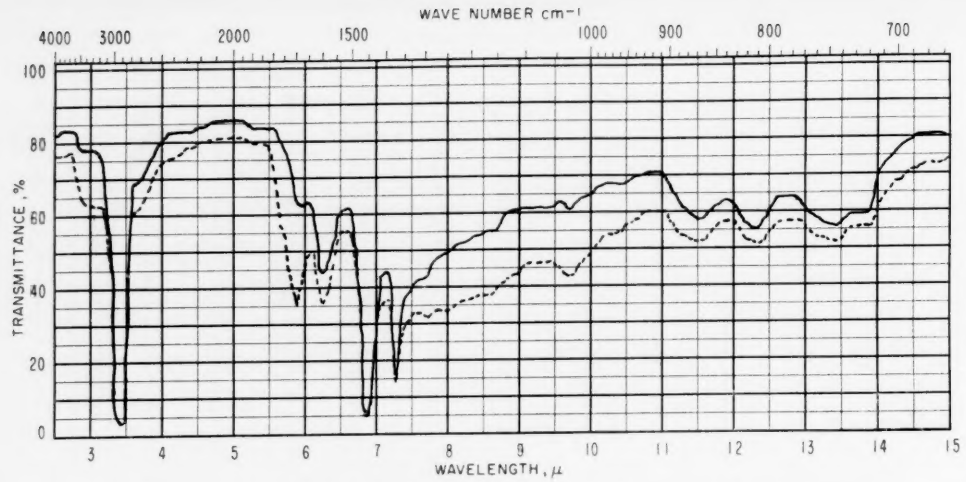


FIGURE 4. *Infrared spectra of asphalt* U *(1.15 to 1.55 mils thick).*

—— before exposure, - - - after exposure.

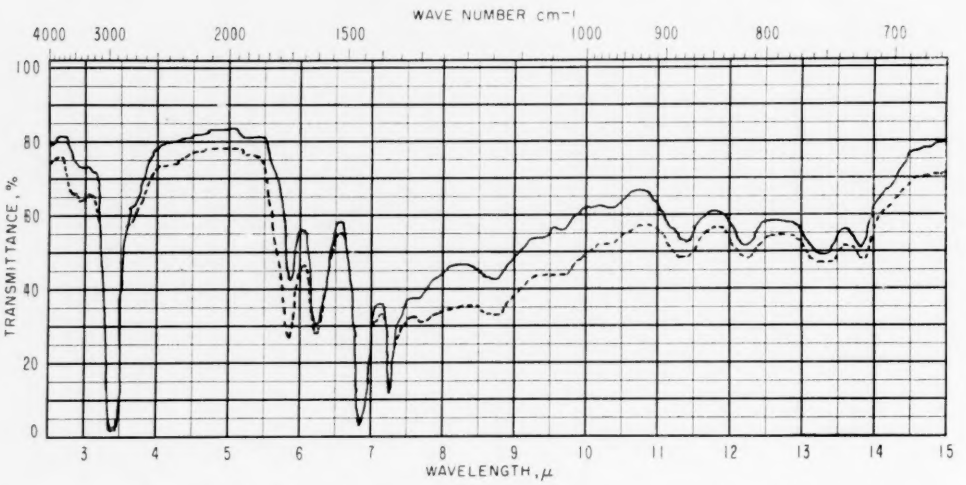


FIGURE 5. *Infrared spectra of asphalt* V *(1.81 to 2.09 mils thick).*

—— before exposure, - - - after exposure.

TABLE 2. *Changes produced in log 1/τ values of asphalts by ultraviolet exposure*

| | | | | | | | | | | | | |
|---|---|---|---|---|---|---|---|---|---|---|---|---|
| Frequency ..... cm⁻¹ | 3,430 | 1,700 | 1,600 | 1,380 | 1,155 | 1,030 | 961 | 866 | 811 | 750 | 720 |
| Wavelength ..... μ | 2.91 | 5.88 | 6.25 | 7.25 | 8.66 | 9.71 | 10.41 | 11.55 | 12.32 | 13.33 | 13.89 |
| Assigned structural groups | —OH | C=O | Aromatic | C—$CH_3$ | ..... | C—O, S=O, or SiO | Naphthenic | Aromatic substitution | | | —$(CH_2)_4$— |

| Asphalt | Softening point[a] | Penetration at 77° F[a] | Durability[b] | Thickness of film | Log 1/τ values (determined by base-line method) | | | | | | | | | |
|---|---|---|---|---|---|---|---|---|---|---|---|---|---|---|
| | ° F | | *Days* | *Mils* | | | | | | | | | | |
| Q | 227 | 18 | 35 | 2.2 to 2.6 | 0.055 | 0.262 | 0.421 | ..... | 0.036 | 0.028 | 0.008 | 0.071 | 0.084 | 0.096 | 0.101 |
| Q[c] | | | | 2.2 to 2.6 | .130 | .565 | .558 | ..... | .144 | .150 | .019 | .066 | .076 | .105 | .125 |
| R | 224 | 21 | 38 | 2.2 to 2.5 | .019 | .135 | .284 | 0.60 | .026 | .05 | .008 | .067 | .037 | .090 | .094 |
| R[c] | | | | 2.2 to 2.5 | .034 | .325 | .301 | .54 | .040 | .10 | .020 | .084 | .061 | .105 | .110 |
| S | 222 | 19 | 50 | 2.3 to 2.6 | .031 | .153 | .362 | .64 | .038 | .027 | .019 | .072 | .039 | .076 | .086 |
| S[c] | | | | 2.3 to 2.6 | .061 | .343 | .354 | .59 | .030 | .098 | .010 | .042 | .043 | .090 | .099 |
| T | 223 | 23 | 72 | 2.30 to 2.56 | .045 | .205 | .377 | .58 | .036 | .032 | .017 | .062 | .079 | .109 | .132 |
| T[c] | | | | 2.30 to 2.56 | .050 | .321 | .407 | .58 | .036 | .068 | .024 | .050 | .066 | .119 | .114 |

[a] Data obtained from asphalt suppliers
[b] Durability by accelerated weathering. Data obtained by J. Falzone and G. McDonald, Research Associates for Asphalt Roofing Industry Bureau, N.B.S.
[c] Exposed 19.5 hr.

TABLE 3. *Correlations of durability with changes in log $1/\tau$ at certain wavelengths*

| Wavelength (wave number) | Spearman's rank correlation coefficient |
|---|---|
| 5.88 $\mu$ (1,700 $cm^{-1}$) | 0.782 |
| 8.66 $\mu$ (1,155 $cm^{-1}$) | .945 |
| 9.71 $\mu$ (1,030 $cm^{-1}$) | .836 |
| 2.91 $\mu$ (3,430 $cm^{-1}$) | .815 |

## 4. Discussion of Results and Conclusions

A simple technique for studying the structure of whole asphalts by infrared spectroscopy has been developed. The use of this method on 28 asphalts, which come from widely different sources and which vary greatly in durability as roof coatings, showed the asphalts to be remarkably similar in absorption characteristics. In the unexposed asphalt the only absorption band that showed some degree of correlation with durability was that produced by hydroxyl absorption. In general, the less durable asphalts exhibited stronger hydroxyl absorption than the more durable asphalts. The intensities of the band at 7.25 $\mu$ (1,380 $cm^{-1}$) attributed to C–$CH_3$ absorption appeared to show some correlation with durability, but because of variations in film thickness, uncertainties existed which tended to obscure the significance of such a correlation.

The exposure of asphalt films to a carbon arc produced oxidative changes, which were largely the formation of carbonyl and hydroxyl groups and also changes in absorption at 9.71 $\mu$ (1,030 $cm^{-1}$) and 8.66 $\mu$ (1,155 $cm^{-1}$). The durabilities of the asphalts showed inverse relationships with changes in absorption at each of these wavelengths. By calculating Spearman's rank correlation coefficients, each of the correlations was shown to be statistically significant. A product-moment correlation coefficient was calculated for the correlation of durabilities with the changes of log $1/\tau$ at 5.88 $\mu$ (1,700 $cm^{-1}$). This correlation coefficient also indicated that the correlation was highly significant.

The absorption band near 9.71 $\mu$ (1,030 $cm^{-1}$) was observed in fractions of asphalt by Stewart.[2] Stewart considered C—O, S=O, or SiO as the most likely groups to be responsible for this absorption. He also observed that weakening of this band in exposed asphaltic fractions appeared to be consistent with oxidation of sulfoxides to sulfones. The asphalt films exposed to the carbon arc in this study, however, showed increases in the band near 9.71 $\mu$. The correlation of durabilities with changes in carbonyl and hydroxyl absorption and also with changes in values of log $1/\tau$ at 8.66 $\mu$ (1,155 $cm^{-1}$) and 9.71 $\mu$ (1,030 $cm^{-1}$) suggest that the changes at these wavelengths may have been caused by changes in concentration of C—O linkages.

---

The author is grateful for the assistance given by Victoria E. Sanchez and Dwight G. Moore, Jr., in obtaining spectra and thanks members of the Floor, Roof, and Wall Coverings Section for their cooperation. Statistical analyses of the correlations indicated in this paper were made by Hsien Hsiang Ku.

WASHINGTON, D.C. (Paper 63A2–14).

## Selected Abstracts

**A coulometric-titration coulometer,** S. W. Smith and J. K. Taylor, *J. Research NBS* **63C,** *No. 1, 65 (1959).*

A highly precise coulometer is described which permits integration of currents of 100 coulombs or more with a precision of about 1 part in 100,000. The current to be integrated oxidizes hydroquinone in an electrolysis cell, producing quinone and acid. The quinone is then reduced by constant-current coulometric-titration, the end point being indicated by *p*H measurements.

**A refined X-band microwave microcalorimeter,** G. F. Engin, J., *Research NBS* **63C,** *No. 1, 77 (1959).*

The microcalorimetric method for evaluation of the efficiency and substitution error of a bolometer mount proposed by Macpherson and Kerns has been the object of further study and refinement at the Boulder Laboratories of the National Bureau of Standards, and an improved instrument based on this technique has been recently placed in operation. The new microcalorimeter design features: (1) Greatly improved ambient temperature control, permitting higher sensitivity and resolution, (2) improved d-c instrumentation, (3) improved mechanical construction giving better repeatability, (4) relocation of the thermopile such that it is no longer attached directly to the bolometer mount, thus providing flexibility in the choice of termination, and (5) a more comprehensive treatment of this calorimetric substitution or equivalence error. These features permit the determination of the effective efficiency of a bolometer mount to an accuracy of better than 0.2 percent.

**A tilting air-lubricated piston gage for pressures below one-half inch of mercury,** U. O. Hutton, *J. Research NBS* **63C,** *No. 1, 47 (1959).*

A description is given of a tilting dead weight piston gage constructed at the National Bureau of Standards for ranges of differential pressure up to about 0.5 inch of mercury. A resolution of better than one part in a hundred thousand of full scale has been obtained by use of the toolmaker's sine bar method of angle measurement. The scale is a linear function of the sine. The instrument can be calibrated from basic measurements of length and weight, is rugged, and may be constructed in almost any laboratory mechanical shop. Sources of possible errors in reading are discussed in detail. Comparative tests with certain other gages or manometers are cited wherein linearity was found to be within one part in 10,000 and agreement within 2.5 parts in 10,000. The uses of the gage are briefly discussed.

**Compact multianvil wedge type high-pressure apparatus,** E. C. Lloyd, U. O. Hutton, and D. P. Johnson, *J. Research NBS* **63C,** *No. 1, 59 (1959).*

The paper describes apparatus for generating high pressures by application of anvil forces against each face of a solid polyhedron. The equipment constructed utilizes a tetrahedron of pyrophyllite and four tungsten carbide anvils as described earlier by H. T. Hall. External force is applied to one of the anvils and wedge reaction forces act on the other anvils, permitting the equipment to be used in a conventional hydraulic press. Examples of results of use of the equipment are given. Success of the design has been shown by the repeated generation of pressures in excess of 100,000 atmospheres (and higher pressures are anticipated), indicating that large existing presses might be used to generate pressures of this order in volumes of several cubic inches. For higher pressures a two-stage multianvil apparatus is proposed in which the second-stage anvils are embedded in a large pyrophyllite tetrahedron to obtain necessary supporting forces.

**Comparison of absolute intensities of [OI] 5577 in the auroral and subauroral zones,** F. E. Roach, J. W. McCaulley, and C. M. Purdy, *J. Research NBS* **63D,** *No. 1, 19 (1959).*

The distribution of 5577 zenith intensities is compared for Fritz Peak, Colorado, in the subauroral zone and Thule, Greenland, near the geomagnetic pole. At the Colorado station, the absolute intensity is bright enough to permit visual detection during 2 percent of the time; at the Greenland station 27 percent of the time. The distribution curves have a general similarity, suggesting a phenomenonological similarity in the excitation mechanisms at the two stations.

**Compressible turbulent boundary layers with heat transfer and pressure gradient in flow direction,** A. Walz, *J. Research NBS* **63B,** *No. 1, 53 (1959).*

Derivation of a method of approximate calculation using integral conditions obtained from basic partial differential equations for viscous compressible fluid. Generalization of semiempirical laws for turbulent wall friction and dissipation for application in the compressible case with heat transfer.

**Creep of cold-drawn nickel,** W. D. Jenkins and C. R. Johnson, *J. Research NBS* **63C,** *No. 1, 1 (1959).*

Creep tests were made in tension under constant loads at temperatures of 300°, 700°, 900°, and 1200°F on specimens of nickel initially cold-drawn 40-percent reduction in area. The relations between the experimental results and the equations proposed by other investigators are evaluated and discussed in some detail. None of these equations was found to be suitable to express or predict the creep-test results of this investigation with high accuracy as changes in structure accompanying the creep processes are inadequately described by these equations. However, conformance to the parabolic strain-time law was obtained over limited ranges of stresses and strains. The effects of cold-drawing on the creep properties are discussed, and certain etching techniques were employed that gave evidence of the presence and movement of dislocations in the structures.

**Current and potential relations for the cathodic protection of steel in a high resistivity environment,** W. J. Schwerdtfeger, *J. Research NBS* **63C,** *No. 1, 37 (1959).*

In order to evaluate criteria for the cathodic protection of bare low carbon steel in a high resistivity environment, specimens were exposed in the laboratory for a period of two months to a soil having a resistivity of about 20,000 ohm-cm. Emphasis was put on the protective potential criterion (−0.77 v with reference to a saturated calomel half-cell) with and without IR drop caused by the protective current included in the potential. A criterion based on current density indicated by the cathodic polarization curve was also studied. The current required for protection was about three times the magnitude of the corrosion current; therefore, the corrosion reaction was either under anodic control or an equivalent type of control which was caused by high resistance at anodic areas. The best degree of protection was achieved on the specimen controlled at −0.77 v without the IR drop. Applied current indicated by the break (change-in-slope) in the cathodic polarization curve agreed quite well with the actual current required to maintain polarization at −0.77 v.

**Diffraction of electromagnetic waves by smooth obstacles for grazing angles,** J. R. Wait and A. M. Conda, *J. Research NBS* **63D,** *No. 2, 181 (1959).*

The diffraction of electromagnetic waves by a convex cylindrical surface is considered. Attention is confined primarily to the region near the light-shadow boundary. The complex-integral representation for the field is utilized to obtain a correction to the Kirchoff theory. Numerical results are presented which illustrate the influence of surface curvature and polarization on the diffraction pattern. Good agreement with the experimental results of Bachynski and Neugebauer is obtained. The effect of finite conductivity is also considered.

**Effect of light and water on the degradation of asphalt,** L. R. Kleinschmidt and H. R. Snoke, *J. Research NBS* **63C,** *No. 1, 31 (1959).*

The effects of light only and of light and water on the degradation of asphalt by accelerated and outdoor exposures were determined. Specimens exposed to light only gained weight and developed a surface film of material insoluble in common asphalt solvents. Specimens exposed to light and water lost weight because of the leaching out of water-soluble degradation products. Since the loss in weight was greater for the thicker coatings, it was concluded that a migration of light degradable components occurred in specimens exposed to light and water.

**Electron beam magnetometer,** L. Marton, L. B. Leder, J. W. Coleman, and D. C. Schubert, *J. Research NBS* **63C,** *No. 1, 69 (1959).*

A theoretical investigation of the electron optics of an electron beam deflection method for detecting small magnetic fields is presented. It is shown that remarkably high sensitivity can be reached. A laboratory model of such a magnetometer was constructed, and it was demonstrated that the theoretical estimate of sensitivity $3\times10^{-5}$ amperes per oersted, could be attained in practice. A discussion of the possible improvements which could extend the sensitivity of the device is also given.

**Lens design: A new approach,** O. N. Stavroudis, *J. Research NBS* **63B,** *No. 1, 31 (1959).*

This paper is concerned with the problem of defining and calculating the aberrations of an optical system and their application to lens design. A method of defining total aberrations is presented which involves the derivatives of image space ray coordinates with respect to object space ray coordinates. Their calculation makes use of the properties of Jacobian matrices and Herzberger's fundamental optical invariant.

**Origin of [OI] 5577 in the airglow and the aurora,** F. E. Roach, J. W. McCaulley, and E. Marovich, *J. Research NBS* **63D,** *No. 1, 15 (1959).*

The distribution of 5577 zenith intensities at stations in the subauroral zone is found to be unimodal with no discontinuity at the visual threshold. This is interpreted as evidence that 5577 airglow and 5577 aurora may have a common origin.

**Relations between summation methods and integral transformations,** W. Greub, *J. Research NBS* **63B,** *No. 1, 1 (1959).*

Relations between the Lototsky method of summation and those of Borel, Euler, and Knopp are obtained by associating an integral transformation with the series transformation.

**Tables of transport integrals: A supplement,** W. M. Rogers, W. J. Hall, and R. L. Powell, *J. Research NBS* **63B,** *No. 1, 23 (1959).*

Tables of values of the transport integrals, defined by

$$J_n(x)=\int_0^x \frac{e^z z^n dz}{(e^z-1)^2},$$

were published in a previous National Bureau of Standards Circular for values of $n$ from 2 through 17. In this report values are given for the integrals where $n$ is 18 and 20 and where $x$ ranges from 0.2 to 50.0 in steps of 0.2.

**Transmission and reflection by a parallel wire grid,** M. T. Decker, *J. Research NBS* **63D,** *No. 1, 87 (1959).*

A comparison is made at X-band frequencies of the theoretical and measured transmission and reflection coefficients for a parallel wire grid. The methods used are applicable to the measurement of these factors for various building materials.

## Non-Bureau Publications

**An improved 8-hydroxyquinoline method for the determination of magnesium oxide in portland cement.** H. A. Berman, *ASTM Bull. No. 237, 51 (Apr. 1959).*

To determine MgO in portland cement, a rapid method (optional in Federal and ASTM Specifications) involves precipitation of the Mg salt of 8-hydroxyquinoline, which is then filtered, acidified, and titrated with $KBrO_3$. This method gives high results near the specification limit (4–5% MgO), poor operator reproducibility, and excessive specification "failures" which require time-consuming rechecks by the referee ammonium phosphate method. The high results are due to coprecipitation of excess 8-hydroxyquinoline with the Mg salt at high concentrations. Low results are obtained at low reagent or Mg concentrations (0–2% MgO). Precipitation conditions were studied. Although they can be adjusted to minimize the errors, this approach is not practicable when the MgO content of the sample is not known in advance. However, a double precipitation procedure with 8-hydroxyquinoline has been developed which is as accurate and reproducible as the ammonium phosphate method and considerably faster. A constant quantity of 8-hydroxyquinoline is added to a definite volume of solution containing the Mg (400 ml), the precipitate is filtered, redissolved, and reprecipitated with 1 ml. of the reagent solution. The improved procedure is proposed as a referee method. After separation of $SiO_2$, $Fe_2O_3$, $Al_2O_3$, $Mn_2O_3$ and CaO, six cement samples can be analyzed for MgO in 2.5 hours.

**Degradation of cellulose acetate films,** W. K. Wilson and B. W. Forshee, *SPE Journal* **15,** *No. 2. 146 (Feb. 1959).*

The degradation of several cellulose acetate film formulations has been studied in connection with a project on the development of specifications for a laminating film for the protection of archival documents. An unplasticized film and a typical plasticized film were studied over a temperature range from 60° C to 177° C in oxygen and in nitrogen. The degradation was principally oxidative in nature and was followed by measuring the change in intrinsic viscosity, which was correlated with changes in the stress-strain diagram. A study of the degradation of several commercial films at 124° C showed that they varied widely in their stability. For highest stability, plasticizers containing an aliphatic ether linkage should be avoided and acid acceptors and antioxidants should be incorporated into the film formulation.

**Formation of ozone from atomic oxygen at low temperatures,** R. A. Ruehrwein and J. S. Hashman, *J. Chem. Phys.* **30,** *No. 3, 823 (Mar. 1959).*

Oxygen was passed through an electrodeless discharge and was condensed, either alone or mixed with diluent gases, at liquid helium temperature. On warming through a temperature range of 13–30° K. the deposits darkened considerably in color (blue) and the amount of ozone formed was deter-

mined. From these observations it was concluded that about 11 percent is the maximum concentration of oxygen atoms that can be trapped in the solid and that the reaction $O+O_2=O_3$ has an activation energy of 1 kcal. At high concentrations of oxygen atoms in the discharged gas, ozone was formed upon condensation by the predominant reactions (1) $O+O=O_2$ and (2) $O+O_2=O_3$. The experimentally observed conversion to ozone of 58 percent agreed well with that calculated from a rate law with $K_1=K_2$.

**Note on measurement of sine-wave response of lenses,** R. E. Stephens, *J. Opt. Soc. Am.* **49,** *No. 4, 413 (Apr. 1959).*

In the procedure of Lamberts for measuring the sine-wave response of a lens the phase angle is measured by determining its cosine. For angles less than 45 degrees the precision achieved by measuring the cosine is less than is possible by measuring the sine. By displacing the scanning slit one-quarter wavelength transversely data for computing the sine of the phase angle may be obtained.

**Selection of glasses for three-color achromats,** R. E. Stephens, *J. Opt. Soc. Am.* **49,** *No. 4, 398 (Apr. 1959).*

If two thin lens elements of two different glasses are combined into a thin two-element system, then the chromatic properties of the system may be described by the effective values of $V[V=(N-1)/(N_F-N_C)]$, and $P[P=(\Delta N/N_F-N_C)]$. The effective value, $\overline{P}$, is a linear function of $\overline{V}$. On a graph of $P$ versus $V$, the straight line drawn through the points for two glasses is the locus of all possible effective values of $V$ and $P$ for combinations of these two glasses. By means of such a graph the effective value $\overline{P}$ for a combination of two glasses may be matched to $P$ of a third glass whose $V$ differs from $\overline{V}$ by a useful amount. An achromatic lens system of the three glasses may then be computed, which will have a common focal length for three wavelengths.

**Some radiological applications of gamma ray transport theory,** M. J. Berger and L. V. Spencer, *Radiation Research* **10,** *No. 5, 552 (May 1959).*

Gamma ray transport theory is applied to the calculation of energy dissipation in bounded water media under conditions approximating those found in radiological problems. A combination of analytical, numerical and random sampling techniques is used. Two typical situations are considered: a medium in which an isotropic source of radiation is distributed, and a medium irradiated by an external source consisting of a narrow pencil-beam. The spatial pattern of energy dissipation is worked out in detail for sources emitting 1.28-Mev photons.

**Thermal decomposition of poly(vinyl chloride),** R. R. Stromberg, S. Straus, and B. G. Achhammer, *J. Polymer Sci.* **35,** *No. 129, 355 (Mar. 1959).*

Poly(vinyl chloride) polymerized using gamma radiation, benzoyl peroxide, and 2,2′-azo-bis(isobutyronitrile) as initiators, was thermally decomposed in vacuo. The gaseous decomposition products as analyzed by mass spectrometry consist primarily of hydrogen chloride for decomposition temperatures below approximately 300° C. At temperatures approximating 400° C various hydrocarbons are evolved along with the hydrogen chloride. Energetic considerations are discussed and a temperature dependent activation energy is described. A free radical mechanism for the dehydrochlorination reaction that appears consistent with the reaction rate data is postulated.

## Other NBS Publications

**Journal of Research, Section 63B, No. 1, July–September 1959. 75 cents.**

Relations between summation methods and integral transformations. Werner Greub. (See above abstracts).

On a modification of Watson's lemma. F. Oberhettinger.

Principal submatrices of a full-rowed non-negative matrix. K. Goldberg.

Zeros of certain polynominals. A. J. Goldman.

Tables of transport integrals: A supplement. William M. Rogers, William J. Hall, and Robert L. Powell. (See above abstracts).

Lens design: A new approach. Orestes N. Stavroudis. (See above abstracts).

Analytical integration of the differential equation for water storage. Vujica M. Yevdjevich.

Compressible turbulent boundary layers with heat transfer and pressure gradient in flow direction. Alfred Walz. (See above abstracts).

**Journal of Research, Section 63C, No. 1, July–September 1959. 75 cents.**

Creep of cold-drawn nickel. William D. Jenkins and Carl R. Johnson. (See above abstracts).

Friction and endurance of prelubricated and unlubricated ball bearings at high speeds and extreme temperatures. Hobart S. White.

Effect of light and water on the degradation of asphalt. L. R. Kleinschmidt and H. R. Snoke. (See above abstracts).

Current and potential relations for the cathodic protection of steel in a high resistivity environment. W. J. Schwerdtfeger. (See above abstracts).

A tilting air-lubricated piston gage for pressures below one-half inch of mercury. U. O. Hutton. (See above abstracts).

Compact multianvil wedge type high-pressure apparatus. E. C. Lloyd, U. O. Hutton, and D. P. Johnson. (See above abstracts).

A coulometric-titration coulometer. Stanley W. Smith and John K. Taylor. (See above abstracts).

Electron beam magnetometer. L. Marton, Lewis B. Leder, J. W. Coleman, and D. C. Schubert. (See above abstracts).

A refined X-band microwave microcalorimeter. Glenn F. Engen. (See above abstracts).

**Journal of Research, Section 63D, No. 1, July–August 1959. 70 cents.**

Preliminary results of the National Bureau of Standards radio and ionospheric observations during the International Geophysical Year. David M. Gates.

Origin of [OI] 5577 in the airglow and the aurora. Franklin E. Roach, James W. McCaulley, and Edward Marovich. (See above abstracts).

Comparison of absolute intensities of [OI] 5577 in the auroral and subauroral zones. F. E. Roach, J. W. McCaulley, and C. M. Purdy. (See above abstracts).

Origin of "very low-frequency emissions." R. M. Gallet and R. A. Helliwell.

Climatology of ground-based radio ducts. Bradford R. Bean.

Power requirements and choice of an optimum frequency for a worldwide standard-frequency broadcasting station. A. D. Watt and R. W. Plush.

Measurments of phase stability over a low-level tropospheric path. M. C. Thompson, Jr. and H. B. Janes.

System loss in radio wave propagation. Kenneth A. Norton.

Mode expansion in the low-frequency range for propagation through a curved startified atmosphere. H. Bremmer.

Transmission and reflection by a parallel wire grid. Martin T. Decker. (See above abstracts).

Synoptic variation of the radio refractive index. B. R. Bean and L. P. Riggs.

Low-frequency propagation paths in arctic areas. A. D. Watt, E. L. Maxwell, and E. H. Whelan.

**Journal of Research, Section D. Radio Propagation, 63D, No. 2, September–October 1959. 70 cents.**

Stratification in the lower ionosphere. C. Ellyett and J. F. Watts.

Effect of small irregularities on the constitutive relations for the ionosphere. K. C. Budden.

Ionospheric investigations using the sweep-frequency pulse technique at oblique incidence. V. Agy and K. Davis.

Fields in electrically short ground systems: an experimental study. A. N. Smith and T. E. Devaney.

Diffraction of electromagnetic waves by smooth obstacles for grazing angles. J. R. Wait and A. M. Conda. (See above abstracts).

Very-low-frequency radiation spectra of lightning discharges. W. L. Taylor and A. G. Jean.

Radio-wave scattering by tropospheric irregularities. A. D. Wheelon.

Study at 1046 megacycles per second of the reflection coefficient of irregular terrain at grazing angles. R. E. McGavin and L. J. Maloney.

Synoptic study of the vertical distribution of the radio refractive index. B. R. Bean, L. P. Riggs, and J. D. Horn.

**Analytical integration of the differential equation for water storage,** V. M. Yevdjevich, *J. Research NBS* **63B,** *43* (*1959*).

**Climatology of ground-based radio ducts,** B. R. Bean, *J. Research NBS* **63D,** *29* (*1959*).

**Effect of small irregularities on the constitutive relations for the ionosphere,** K. G. Budden, *J. Research NBS* **63D,** *135* (*1959*).

**Fields in electrically short ground systems: an experimental study,** A. N. Smith and T. E. Devaney, *J. Research NBS* **63D,** *175* (*1959*).

**Fractional factorial experiment designs for factors at three levels,** W. S. Connor and M. Zelen, *NBS Applied Math. Series* **54** (*May 1959*).

**Tables of osculatory interpolation coefficients,** H. E. Salzer, *NBS Applied Math. Series* (*May 1959*).

**Friction and endurance of prelubricated and unlubricated ball bearings at high speeds and extreme temperatures,** H. S. White, *J. Research NBS* **63C,** *19* (*1959*).

**Ionospheric investigations using the sweep-frequency pulse technique at oblique incidence,** V. Agy and K. Davis, *J. Research NBS* **63D,** *151* (*1959*).

**Low-frequency propagation paths in arctic areas,** A. D. Watt, E. L. Maxwell, and E. H. Whelan, *J. Research NBS* **63D,** *99* (*1959*).

**Measurements of phase stability over a low-level tropospheric path,** M. C. Thompson, Jr., and H. B. Janes, *J. Research NBS* **63D,** *45* (*1959*).

**Mode expansion in the low-frequency range for propagation through a curved stratified atmosphere,** H. Bremmer, *J. Research NBS* **63D,** *75* (*1959*).

**Multi-factor experiments,** M. Zelen and W. S. Connor, *Ind. Quality Control* **15,** *No. 9, 1* (*Mar. 1959*).

**On a modification of Watson's lemma,** F. Oberhettinger, *J. Research NBS* **63B,** *15* (*1959*).

**On the theory of fading properties of a fluctuating signal imposed on a constant signal,** H. Bremmer, *NBS Circ.* **599** (*May 1959*).

**Origin of "very low-frequency emissions",** R. M. Gallet and R. A. Helliwell, *J. Research NBS* **63D,** *21* (*1959*).

**Power requirements and choice of an optimum frequency for a worldwide standard-frequency broadcasting station,** A. D. Watt and R. W. Plush, *J. Research NBS* **63D,** *35* (*1959*).

**Preliminary results of the National Bureau of Standards radio and ionospheric observations during the International Geophysical Year,** D. M. Gates, *J. Research NBS* **63D,** *1* (*1959*).

**Principal submatrices of a full-rowed nonnegative matrix,** K. Goldberg, *J. Research NBS* **63B,** *19* (*1959*).

**Radio-wave scattering by tropospheric irregularities,** A. D. Wheelon, *J. Research NBS* **63D,** *205 (1959).*

**Stratification in the lower ionosphere,** C. Ellyett and J. M. Watts, *J. Research NBS* **63D,** *117 (1959).*

**Study at 1046 megacycles per second of the reflection coefficient of irregular terrain at grazing angles,** R. E. McGavin and L. J. Maloney, *J. Research NBS* **63D,** *235 (1959).*

**Synoptic study of the vertical distribution of the radio refractive index,** B. R. Bean, L. P. Riggs, and J. D. Horn, *J. Research NBS* **63D,** *249 (1959).*

**Synoptic variation of the radio refractive index,** B. R. Bean and L. P. Riggs, *J. Research NBS* **63D,** *91 (1959).*

**System loss in radio-wave propagation,** K. A. Norton, *J. Research NBS* **63D,** *53 (1959).*

**The electromotive force method of determining ionization constants: Ionization of bisulfate ion,** W. J. Hamer, (**Book**) **The Structure of Electrolytic Solutions,** *edited by* W. J. Hamer (*John Wiley & Sons, Inc., New York, N.Y.*) *p. 236 (1959).*

**Transmission of power in radio propagation,** J. R. Wait, *Electronic and Radio Engr.* **36,** *No. 4, 146 (Apr. 1959).*

**Very-low-frequency radiation spectra of lightning discharges,** W. L. Taylor and A. G. Jean, *J. Research NBS* **63D,** *199 (1959).*

**Zeros of certain polynomials,** A. J. Goldman *J. Research NBS* **63B,** *21 (1959).*

UNITED STATES
GOVERNMENT PRINTING OFFICE
DIVISION OF PUBLIC DOCUMENTS
WASHINGTON 25, D.C.

OFFICIAL BUSINESS

PENALTY FOR PRIVATE USE TO AVOID
PAYMENT OF POSTAGE, $300
(GPO)

National Bureau of Standards Journal of Research
A. Physics and Chemistry

Vol. 63A, No. 2

September–October 1959

# Contents

Page

Reflection of fast neutrons from water. Martin J. Berger and John W. Cooper. 101

Some vibrational-rotational bands of deuterated methanes. Harry C. Allen, Jr., and Earle K. Plyler. 145

Precise coulometric titration of acids and bases. John K. Taylor and Stanley W. Smith. 153

Heat of formation of titanium tetraiodide. W. H. Johnson, A. A. Gilliland, and E. J. Prosen. 161

Reactions of pentafluorohalobenzenes. Walter J. Pummer and Leo A. Wall. 167

Tritium-labeled compounds I. Radioassay of tritium-labeled compounds in "infinitely thick" films with a windowless, gas-flow, proportional counter. Horace S. Isbell, Harriet L. Frush, and Ruth A. Peterson. 171

Tritium-labeled compounds II. General-purpose apparatus, and procedures for the preparation, analysis, and use of tritium oxide and tritium-labeled lithium borohydride. Horace S. Isbell and Joseph D. Moyer. 177

Preparation of trichloride and tetrachloride of molybdenum. Dwight E. Couch and Abner Brenner. 185

Infrared spectra of asphalts. Burton D. Beitchman. 189

Publications of the National Bureau of Standards. 195

For sale by the Superintendent of Documents, U.S. Government Printing Office, Washington 25, D.C. Price 70 cents (single copy). Subscription price: $4.00 a year; $0.75 additional for foreign mailing.

UNITED STATES GOVERNMENT PRINTING OFFICE, WASHINGTON: 1959